

Sheffield Hallam University

Modelling, simulation and performance evaluation: PEM fuel cells for high altitude UAS

SALAH, Ibrahim M. M.

Available from the Sheffield Hallam University Research Archive (SHURA) at:

<http://shura.shu.ac.uk/13602/>

A Sheffield Hallam University thesis

This thesis is protected by copyright which belongs to the author.

The content must not be changed in any way or sold commercially in any format or medium without the formal permission of the author.

When referring to this work, full bibliographic details including the author, title, awarding institution and date of the thesis must be given.

Please visit <http://shura.shu.ac.uk/13602/> and <http://shura.shu.ac.uk/information.html> for further details about copyright and re-use permissions.



Sheffield Hallam University

**Modelling, Simulation and Performance
Evaluation: PEM Fuel Cells
For High Altitude UAS**

By

Ibrahim M. M. Saleh

BSc, MSc

A thesis submitted in partial fulfilment of the requirements of
Sheffield Hallam University for the degree of
Doctor of Philosophy

**Materials and Engineering Research Institute
Faculty of Arts, Computing, Engineering and Sciences
Sheffield Hallam University – United Kingdom**

December 2015

Abstract

A fuel cell is a device that converts energy in the fuel and reactant into electrical DC power. Fuel cell powered aircraft are generally characterised by a low power to weight ratio (W/kg). The propulsion system of an unmanned aircraft needs a large range of power and fast response to fulfil the requirements of different flight phases and to balance the variations in the load demand.

A proton exchange membrane (PEM) fuel cell is considered as a potential power source for high altitude UAS (unmanned aircraft systems) operations. At altitudes in excess of 10 km, very low atmospheric temperatures and pressures, and unexpected variations in the load demand put severe stresses on the operation and performance of PEM fuel cells. A stable and robust controller and fuel supply system that can provide fast and sufficient flow of hydrogen and air/oxygen to the reaction of the fuel cell is one of the critical objectives.

In this research, a simplified mathematical model of the PEM fuel cell stack system is developed and validated with the commercially available 1 kW PEM fuel cell stack (H-1000) developed by Horizon Fuel Cell Technologies. Matlab-Simulink is used to implement the necessary design and simulations under various operational conditions.

The implications of high altitudes on the operation and performance of a PEM fuel cell stack are investigated, and a PID controller is adopted to efficiently optimise and provide a sufficient flow of hydrogen and air/oxygen to the stack, in particular maintaining the flow rates of the reactants was deemed most critical at high altitudes operation. Also, in order to store the required oxygen and hydrogen, the design of storage vessels is considered.

This research presents a design of a PEM fuel cell power system for unmanned aircraft systems with an integrated approach that enables estimation of required power for high altitudes UAS operation which is then used to determine the size and weight of the combined power-plant of fuel cell stack with hydrogen and air/oxygen vessels and the propulsion system of the UAS. This approach takes into the consideration the power capacity of fuel cell stack and the flight endurance as two main factors in designing the size and weight of storage vessels, and hence determining the overall weight of the UAS, which is a key requirement in the preliminary aircraft design phase.

One of the research outcomes shows a potential in extending the flying duration and altitude for more than five hours and a half, reaching up to 11 km altitude, for a UAS with an overall weight of 32 kg, including a payload capacity of 2 kg, based on a 1 kW PEM fuel cell propulsion system.

KEYWORDS: PEM Fuel Cell, Mathematical Modelling, Unmanned Aircraft Systems, High Altitude Operation, Performance and Evaluation, Pressure Vessel Design.

Declaration

I would like to confirm that the work presented in this thesis is my own work and an appropriate reference credit has been given to the work of others.

The intellectual property and copyrights of this thesis are retained by the author and Sheffield Hallam University. Therefore, any use of information or quotations, distribution or reproduction of this thesis is not permitted without proper acknowledgment and permission from the copyright holder.

Dedication

To

My Mother and Father

Acknowledgement

First and foremost, I am very grateful to his Almighty, the Most Merciful, for giving me the strength and motivation to undertake this research.

I would like to express my sincere gratitude and recognition to my principal supervisor Dr Rashid Ali, for his invaluable advice, guidance, and enthusiasm. His guidance and support was influential in every step of the research, and without this, this work would not have been possible. I would also like to thank my second supervisor, Dr Hongwei Zhang, for his help and concern.

Over the course of this project, I have had several academic supervisors and advisors; I would like to acknowledge my gratitude and appreciation to all of them: Dr George Pissanidis, Dr Z Peng, Dr Raj K Calay (now professor of Energy Technology at Narvik University College), and Professor Fateh Bhinder for his insightful advices and comments.

Special thanks are also due to Leonine Kunzwa from the School of Engineering and Technology at the University of Hertfordshire for allowing us to carry out the necessary experiments in their Fuel Cell Laboratory, also for their cooperation and technical support during the task of testing fuel cell stack.

Of course, thanks are due to the postgraduate research administrators Gail Hallewell, Corrie Houton, Rachael Toogood, and all other administrative and academic staff who supported me in any respect during the completion of my study.

Finally, my greatest thanks and gratitude go to my lovely family; I am sincerely indebted to my parents for their continuous support, encouragement, and supplications, my brother and sister for their eminent support, and certainly to my dearest wife for her patience and care during the years of my study.

Table of Contents

Contents

Abstract	II
Declaration	III
Dedication	IV
Acknowledgement	V
Table of Contents	VI
List of Figures	IX
List of Tables	XIII
Glossary and List of Abbreviations	XVI
Chapter One: Introduction	1
1.1 Overview	1
1.2 Types and Applications of Fuel Cells	3
1.3 Structure of a PEM Fuel Cell	5
1.4 Historical Background of Electrical Aircraft	8
1.5 Motivation of the Project.....	11
1.6 Aim and Objectives	12
1.7 Scope-Format, and Software Definition.....	13
1.8 Summary	14
Chapter Two: Literature Review	16
2.1 Introduction	16
2.2 Modelling of PEM Fuel Cells	18
2.3 Managing Operational Variables of PEM Fuel Cell	22
2.3.1 Managing the Flow Rate of Hydrogen.....	25
2.3.2 Managing the Flow Rate of Air/Oxygen.....	27
2.3.3 Managing Temperature	29
2.3.4 Managing Water.....	30
2.4 Managing and Controlling the Output Power of the Fuel Cell Stack	32
2.5 Fuel Cells as a Power Source for Aircraft and UAS Applications.....	35
2.5.1 Fuel Cells for Aircraft	38
2.5.2 Fuel Cells for UAS.....	40

2.5.3	High Altitude Long Endurance UAS	47
2.6	Other Applications for PEM Fuel Cells	51
2.7	Summary	52
Chapter Three: Modelling Voltages of the PEM Fuel Cell.....		55
3.1	Introduction	55
3.2	Principle of Electrochemical Reaction for the PEM Fuel Cell.....	56
3.3	Activation Losses and a Charged Double Layer	58
3.4	Ohmic Losses	61
3.5	Concentration Losses	63
3.6	Total Losses of PEM Fuel Cell	67
3.7	Summary	69
Chapter Four: Mathematical Modelling of Gases Flow in the PEM		
Fuel Cell		71
4.1	Introduction	71
4.2	System Description and Assumptions	72
4.3	Air Fan Flow Calculations	75
4.4	Thermodynamic Properties of Gases Flow in the PEM Fuel Cell	82
4.4.1	Cathode Flow Model.....	86
4.4.2	Membrane Hydration Model.....	92
4.4.3	Anode Flow Model	94
4.5	Summary	100
Chapter Five: Model Validation of the PEM Fuel Cell and Controller		
Design		103
5.1	Experimental Procedure and Validation of the Developed PEM Fuel Cell Model.....	103
5.1.1	First Test	107
5.1.2	Second Test	109
5.1.3	Third Test	111
5.1.4	Fourth Test	116
5.2	PID Controller for Air and Hydrogen Supply	118
5.3	Summary	126
Chapter Six: Implications of High Altitudes on the Operation of PEM		
Fuel Cell Based UAS		128
6.1	Introduction	128
6.2	Implications of High Altitudes on the Performance of the PEM Fuel Cell ...	129
6.3	Impact of High Altitude on the Air Consumption of the PEM Fuel Cell	133
6.4	Summary	142

Chapter Seven: Static Thrust for Unmanned Aircraft Systems 143

7.1	Introduction	143
7.2	Hydrogen Fuel for UAS Applications	145
7.3	Calculation of Required Thrust	148
7.4	Summary	157

Chapter Eight: Pressure Vessel Design and Power Plant Mass

Estimation Based UAS..... 159

8.1	Introduction	159
8.2	Pressure Vessel Design	162
8.3	Dimensions and Weight of Pressure Vessel.....	164
8.4	Hydrogen and Air-Oxygen Pressure Vessels	167
8.4.1	First Scenario: Pressure Vessel for Compressed Air	171
8.4.2	Second Scenario: Pressure Vessel for Compressed Oxygen	172
8.4.3	Third Scenario: Pressure Vessel for Limited Volume of Compressed Oxygen	176
8.4.4	Pressure Vessel for Compressed Hydrogen	179
8.5	Power Plant Mass Estimation for a PEM Fuel-Cell-Based UAS	185
8.6	Summary	191

Chapter Nine: Conclusion and Future Work..... 193

9.1	Conclusion.....	193
9.2	Future Work	198

References 201

Bibliography 212

Appendices 215

Appendix A	215
Appendix B	221
Appendix C	225
C.1 First Scenario: Pressure Vessel for Compressed Air	225
C.2 Second Scenario: Pressure Vessel for Compressed Oxygen	229
C.3 Third Scenario: Pressure Vessel for Limited volume of Compressed Oxygen.....	233
C.4 Pressure Vessel for Compressed Hydrogen.....	234

List of Figures

Figure 1.1: Schematic structure of a single PEM fuel cell.....	6
Figure 1.2: Different sizes of H-series 100W-5kW PEM fuel cell stacks produced by Horizon Fuel Cell Technologies (cited from[18])	7
Figure 3.1: Simulink block diagram of activation overvoltage	60
Figure 3.2: Simulink block diagram of ohmic overvoltage	63
Figure 3.3: Simulink block diagram of concentration overvoltage.....	67
Figure 3.4: Simulink block diagram of open circuit voltage for a PEM fuel cell.....	68
Figure 3.5: Simulink block diagram of voltage model for a single PEM fuel cell	68
Figure 4.1: Mechanical components and flow variables associated with the Horizon fuel cells stack system (H-1000) at sea level operation	73
Figure 4.2: Pressure-flow performance curve for the axial fan used by Horizon (H-1000) fuel cell stack.....	76
Figure 4.3: Hydrogen flow rate with respect to current for the Horizon (H-1000) stack.....	79
Figure 4.4: Air flow rate with respect to the current for the Horizon (H-1000) stack....	79
Figure 4.5: Simulink block diagram of the pressure of air at the supply manifold of cathode	80
Figure 4.6: Simulink block diagram of the required supply hydrogen to the fuel cell stack.....	81
Figure 4.7: Simulink block diagram of the required supply air to the fuel cell stack.....	81
Figure 4.8: Simulink block diagram of the mass flow rate of reacted oxygen and produced water in the cathode of the fuel cell stack	90
Figure 4.9: Simulink block diagram of the flow of air and partial pressure of oxygen in the cathode of the fuel cell stack.....	91
Figure 4.10: Simulink block diagram for the mass flow rate of water vapour across the membrane of the fuel cell stack	94

Figure 4.11: Simulink block diagram of the mass flow rate of reacted hydrogen in the anode of the fuel cell stack.....	97
Figure 4.12: Simulink block diagram of the flow and pressure of hydrogen in the anode of the fuel cell stack	98
Figure 4.13: Simulink block diagram of the integration and connections of all electrical and thermodynamic sub-models for the entire developed model of the PEM fuel cells	99
Figure 5.1: Block diagram configuration and bench layout of Horizon (H-1000) fuel cell stack configured with measuring and controlling devices, and a BLDC motor load ..	106
Figure 5.2: Output voltages for the Horizon (H-1000) fuel cell stack and mathematical developed model of the PEM fuel cell under various drawn load currents	108
Figure 5.3: Impact of drawn load current on the temperature of the Horizon (H-1000) fuel cell stack.....	110
Figure 5.4: Impact of operational duration at varied load current on the temperature of the Horizon (H-1000) fuel cell stack.....	110
Figure 5.5: Impact of drawn load current and operational duration on the temperature of the Horizon (H-1000) fuel cell stack.....	111
Figure 5.6: Output voltages and drawn currents for the Horizon (H-1000) fuel cell stack.....	112
Figure 5.7: Average of output voltages for each level of drawn current from the Horizon (H-1000) fuel cell stack.....	112
Figure 5.8: Output voltages of Horizon fuel cell stack test, and developed model of PEM fuel cell, under varied load currents and stack temperatures, and 85% tuning efficiency.....	114
Figure 5.9: Impact of drawn current on the temperature of the Horizon (H-1000) stack.....	114
Figure 5.10: Impact of operational duration at varied load current on the temperature of the Horizon (H-1000) fuel cell stack.....	115
Figure 5.11: Impact of drawn current and operational duration on the temperature of the Horizon (H-1000) fuel cell stack.....	115

Figure 5.12: Impact of constant drawn load current and operational duration on the temperature of the Horizon (H-1000) fuel cell stack	117
Figure 5.13: Output voltages for Horizon (H-1000) stack and the developed model of PEM fuel cell under the impact of constant drawn current and varied operating temperature.....	117
Figure 5.14: Response of developed PEM fuel cell model to the power demand for PID controller with time response setting at 1.35 second and integral value (1.4763).....	120
Figure 5.15: Responses of the developed PEM fuel cell model to the current demand varying from 1 A to 2 A, for PID controller with various time response settings	122
Figure 5.16: Responses of the developed PEM fuel cell model to the power demand varying from 58.2 W to 111 W, for PID controller with various time response settings	122
Figure 5.17: Simulink block diagram of the PID controller for the developed model of the PEM fuel cell stack system	124
Figure 5.18: Simulink block integration between the PID controller and the entire developed model of the PEM fuel cell stack system.....	125
Figure 6.1: Impact of high altitudes on the mass flow rates of consumed air at the reaction interface for a PEM fuel cell stack being supplied by fresh air	136
Figure 6.2: Mechanical components and flow variables associated with proposed model of fuel cells stack system operating at high altitudes.....	141
Figure 7.1: Power drawn by the BLDC motor with respect to the rotational speed of the propeller for three different sizes of propeller	154
Figure 7.2: Maximum static thrust with respect to the rotational speed of the propeller for three different sizes of propeller.....	155
Figure 7.3: Maximum permitted mass of the UAS with respect to the rotational speed of the propeller for three different sizes of propeller, at 0.4 static thrust to weight ratio..	155
Figure 7.4: Maximum permitted mass of the UAS with respect to the rotational speed of the propeller for three different sizes of propeller, at 0.2 static thrust to weight ratio..	156
Figure 8.1: Simulink block tools of pressure vessel design	166
Figure 8.2: Simulink block diagram configuration of pressure vessel design.....	167

Figure 8.3: Heights of air and oxygen cylindrical pressure vessels for one hour's operation, at a maximum current of 20 A, and power of 877 W	174
Figure 8.4: Masses of air and oxygen cylindrical pressure vessels for one hour's operation, at a maximum current of 20 A, and power of 877 W	174
Figure 8.5: Heights and masses of oxygen cylindrical pressure vessel for several hours of operation, at maximum current of 20 A, and power of 877 W, and for a limited volume of compressed oxygen up to 230 bar.....	178
Figure 8.6: Heights and masses of hydrogen cylindrical pressure vessel for several hours of operation, at maximum current of 20 A, and power of 877 W, and for limited volume of compressed hydrogen up to 175 bar at 15 °C ambient temperature	182
Figure 8.7: Flow rates of supply hydrogen based on the developed model of a PEM fuel cell stack, using limited flow rate of hydrogen (0.637 m ³ /hour), under various current load demand and up to five hours of operation.....	184
Figure 8.8: Flow rates of supply oxygen based on the developed model of a PEM fuel cell stack, using limited flow rate of oxygen (0.6 m ³ /hour), under various current load demand and up to five hours of operation.....	185
Figure A.1: Pressure-flow performance curve for Delta axial fan (cited from Delta Electronics [115])	218
Figure A.2: Voltage-Current and Power-Current for Horizon (H-1000) fuel cell stack, (cited from [81]).....	219
Figure A.3: Hydrogen and air flow rates for Horizon (H-1000) fuel cell stack, (cited from [81, 86]).....	220

List of Tables

Table 1.1: Basic details of different types of fuel cells.....	3
Table 4.1: Output power of Horizon (H-1000) fuel cell stack with respect to the flow rates of supply hydrogen and air	78
Table 5.1: Defined values of variables and constants for the operational parameters involved in the developed model of PEM fuel cell stack	107
Table 5.2: Supply air and hydrogen to the developed model of PEM fuel cell stack with current demand varies from 1 A at (58.2 W) to 2 A at (111 W), for various PID response tuning settings	123
Table 6.1: Supply of hydrogen and air to the fuel cell stack based on developed model of PEM fuel cell and PID controller at different altitudes under conditions of fixed hydrogen temperature at 15 °C, constant stack temperature at 27.73 °C, and maximum power output of stack at 877 W at 20 A current	138
Table 6.2: Supply of hydrogen and air to the fuel cell stack based on developed model of PEM fuel cell and PID controller at different altitudes under conditions of fixed hydrogen and ambient air temperature at 15 °C, constant stack temperature at 27.73 °C, and maximum power output of stack at 877 W at 20 A current	139
Table 6.3: Supply of hydrogen and air to the fuel cell stack based on developed model of PEM fuel cell and PID controller at different altitudes under conditions of fixed hydrogen and ambient air temperature at 20 °C, constant stack temperature at 27.73°C, and maximum power output of stack at 877 W at 20 A current	139
Table 7.1: Calculations of the power supplied to and produced from the BLDC motor, maximum static thrust produced, and maximum permitted mass of the UAS	154
Table 8.1: Dimensions and masses of air and oxygen cylindrical pressure vessels with two hemispherical ends for one hour's operation of a PEM fuel cell stack, at a maximum current of 20 A, and power of 877 W	173
Table 8.2: Dimensions and masses of air and oxygen cylindrical pressure vessels with two hemispherical ends for one hour's operation of a PEM fuel cell stack, at a	

maximum current of 20 A, power of 877 W, and compression pressure up to 300 bar at 15 °C	175
Table 8.3: Dimensions and masses of oxygen cylindrical pressure vessel with two hemispherical ends, using AK 2205 Duplex Stainless Steel with 2.29 mm metal thickness, for several hours of operation, at maximum current of 20 A, and power of 877W, and for a limited volume of compressed oxygen up to 230 bar at 15 °C	177
Table 8.4: Dimensions and masses of oxygen cylindrical pressure vessel with two hemispherical ends, using AK 2205 Duplex Stainless Steel with 2.29 mm metal thickness, for several hours of operation, at maximum current of 20 A, and power of 877W, for a limited volume of compressed oxygen up to 300 bar at 15 °C.....	179
Table 8.5: Dimensions and masses of hydrogen cylindrical pressure vessel with two hemispherical ends, using AK 2205 Duplex Stainless Steel with 2.29 mm metal thickness, for several hours of operation, at maximum current of 20 A, and power of 877W, for a limited volume of compressed hydrogen up to 175 bar at 15 °C	181
Table 8.6: Dimensions and masses of hydrogen cylindrical pressure vessel with two hemispherical ends, using AK 2205 Duplex Stainless Steel with 2.29 mm metal thickness, for several hours of operation, at maximum current of 20 A, and power of 877W, for a limited volume of hydrogen compressed up to 300 bar at 15 °C	183
Table 8.7: Volumes of supplied oxygen and hydrogen to the fuel cell stack according to the load demand and flying mode, based on the developed model of a PEM fuel cell stack and Simulink tools of pressure vessel design	187
Table 8.8: Volumes and masses of supply oxygen and hydrogen to the fuel cell stack according to the total flying hours, based on the developed model of a PEM fuel cell stack and Simulink tools of pressure vessel design	188
Table 8.9: Design specifications for the oxygen and hydrogen pressure vessels according to the desired flying hours, based on the developed model of a PEM fuel cell stack and Simulink tools of pressure vessel design	189
Table 8.10: Masses of the items and components used in the design of the power-plant system and propulsion system with the estimated mass of the UAS frame structure and carried payload for UAS applications	190
Table A.1: Values of specific gas constant for several gases	218

Table B.1: Output voltages for the first test of Horizon (H-1000) fuel cell stack, and the developed model of PEM fuel cell with different model tuning efficiencies	221
Table B.2: Second test for Horizon (H-1000) fuel cell stack under different levels of varying current load	222
Table B.3: Output voltages for third test of Horizon (H-1000) fuel cell stack, and the developed model of PEM fuel cell with different model tuning efficiencies	223
Table B.4: Fourth test of Horizon (H-1000) fuel cell stack and the developed model of PEM fuel cell, under impact of constant current load.....	224

Glossary and List of Abbreviations

Symbol	Description	Units
a	Water activity in the membrane	-
A	Flowing gas area	m^2
A	Rotational area of the propeller	m^2
A_{fc}	Membrane active area of the fuel cell	cm^2
F	Faraday's constant ($F = 96485$)	coulomb/mol
C_{O_2}	Concentration of oxygen at the catalyst interface	mol/cm^3
c_p	Specific heat of the fluid	$kJ/kg.K$
C_w	Molar concentration of water in the membrane	$kmol/m^3$
D_w	Diffusion coefficient of water molecules in the membrane	-
E	Weld joint efficiency code of the metal	-
h	Altitude	m, km
h	Specific enthalpy	kJ/kg
h_{shell}	Overall height of the cylindrical vessel	cm, m
h^o	Stagnation enthalpy	kJ/kg

I	Fuel cell current	Ampere (A)
i	Current density of fuel cell	mA/cm^2
i_m	Maximum current density of fuel cell	mA/cm^2
I_{st}	Current drawn from fuel cell stack	Ampere (A)
k	Constant of specific heat ratio	-
$K_{sm,out,an}$	Nozzle constant of supply manifold outlet of anode	$\text{kg}\cdot\text{s}^{-1}/\text{kPa}$
$K_{sm,out,ca}$	Nozzle constant of supply manifold outlet of cathode	$\text{kg}\cdot\text{s}^{-1}/\text{kPa}$
L	Thickness of membrane	cm
M_{air}	Molar mass of air	kg/kmol
m_{an}	Mass of hydrogen inside the anode	kg
m_{ca}	Mass of gas inside the cathode	kg
M_{H_2}	Molar mass of hydrogen	kg/kmol
$m_{H_2,rc}$	Mass of reacted hydrogen in the anode	kg
m_{O_2}	Mass of oxygen inside the cathode	kg
M_{O_2}	Molar mass of oxygen	kg/kmol
$m_{O_2,rc}$	Mass of reacted oxygen in the cathode	kg
m_{N_2}	Mass of nitrogen inside the cathode	kg

M_{N_2}	Molar mass of nitrogen	kg/kmol
M_{shell}	Mass of the cylindrical vessel	kg
m_w	Mass of water vapour inside the cathode	kg
M_w	Molar mass of water or water vapour	kg/kmol
$m_{w,gen}$	Mass of produced water in the cathode	kg
$m_{w,mbr}$	Mass of water vapour across electrolyte membrane	kg
$m_{w,out}$	Mass of water vapour exit the cathode	kg
n	Number of fuel cells in the stack	-
n_d	Electro-osmotic drag coefficient of water molecule	-
N	Number of moles in a volume of gas	-
P	Internal pressure of gas inside the vessel	psi
P_n	Pressure of denoted gas	kPa
$P_{an,in}$	Pressure of hydrogen enter the anode	kPa
$P_{an,out}$	Pressure of hydrogen exit the anode	kPa
$P_{ca,in}$	Pressure of air enter the cathode	kPa
$P_{ca,out}$	Pressure of air exit the cathode	kPa
P_d	Power delivered by the motor to the propeller	Watts (W)

P_{H_2}	Pressure of hydrogen in the anode	kPa
P_i	propeller induced power	Watts (W)
P_{O_2}	Partial pressure of oxygen in the cathode	kPa
P_r	Necessary power required by the propeller	Watts (W)
P_s	Electrical DC power supplied to the motor	Watts (W)
P_{sat}	Saturation pressure of water vapour	kPa
P_{sf}	Fan static pressure	kPa
$P_{sm,in,an}$	Pressure of supply H_2 to the supply manifold of anode	kPa
$P_{sm,in,ca}$	Pressure of supply air to the supply manifold of cathode	kPa
$P_{sm,out,an}$	Pressure of H_2 exit the supply manifold of anode	kPa
$P_{sm,out,ca}$	Pressure of air exit the supply manifold of cathode	kPa
P_t	Total pressure of fan air stream	kPa
P_o	Pressure of ambient air at sea level	kPa
P^o	Stagnation pressure of gas	kPa
r	Radius of the cylindrical shell	cm
R	Universal gas constant ($R = 8.31441$)	kJ/kmol.K kPa.m ³ /kmol.K
RD	Relative density of air at certain altitude	-

$R_{electrons}$	Electronic resistivity of fuel cell	Ohm (Ω)
r_i	Inner radius of the cylindrical shell	cm
R_{ions}	Ionic resistivity of fuel cell	Ohm (Ω)
R_m	Membrane specific resistivity	ohm.cm
r_o	Outer radius of the cylindrical shell	cm
R_s	Specific constant of the fluid	kJ/kg.K kPa.m ³ /kg.K
S	Allowable code stress of the metal	psi
S_y	Yield stress of the metal	psi
t	Thickness of the shell	cm
T	Temperature of ambient air	Kelvin (K)
T	Fuel cell temperature	Kelvin (K)
T	Required thrust produced by the propeller	Newton (N)
T_s	Static thrust produced by the propeller	Newton (N)
T_{sm}	Maximum static thrust produced by the propeller	Newton (N)
T_{st}	Stack temperature	Kelvin (K)
T_o	Temperature of ambient air at sea level	Kelvin (K)
T^o	Stagnation temperature of gas	Kelvin (K)

v	Velocity of the flowing gas in a section	m/s
v	Velocity of the stream air through the propeller	m/s
V	Volume of gas	m^3
V_{act}	Activation voltage losses of fuel cell	Volt (V)
V_{an}	Volume of fuel cell anode	m^3
V_{ca}	Volume of fuel cell cathode	m^3
V_{con}	Concentration voltage losses of fuel cell	Volt (V)
V_{OC}	Open circuit voltage of fuel cell	Volt (V)
V_{ohm}	Ohmic voltage losses of fuel cell	Volt (V)
V_{fc}	Fuel cell output voltage	Volt (V)
V_{shell}	Volume of the cylindrical vessel	m^3
V_o	Velocity of free-stream air far ahead from propeller	m/s
w	Propeller induced velocity	m/s
W	Mass flow rate of gas	kg/s
$W_{an,in}$	Mass flow rate of hydrogen enter the anode	kg/s
$W_{an,out}$	Mass flow rate of hydrogen exit the anode	kg/s
$W_{ca,in}$	Mass flow rate of air enter the cathode	kg/s

$W_{ca,out}$	Mass flow rate of air exit the cathode	kg/s
W_f	Volume flow rate of air through the fan of the stack	m ³ /minute
$W_{H2,rc}$	Mass flow rate of reacted hydrogen in the anode	kg/s
$W_{O2,in}$	Mass flow rate of oxygen enter the cathode	kg/s
$W_{O2,out}$	Mass flow rate of oxygen exit the cathode	kg/s
$W_{O2,rc}$	Mass flow rate of reacted oxygen in the cathode	kg/s
$W_{N2,in}$	Mass flow rate of nitrogen enter the cathode	kg/s
$W_{N2,out}$	Mass flow rate of nitrogen exit the cathode	kg/s
$W_{sm,in,an}$	Mass flow rate of H ₂ enter the supply manifold of anode	kg/s
$W_{sm,in,ca}$	Mass flow rate of air enter the supply manifold of cathode	kg/s
$W_{sm,out,an}$	Mass flow rate of H ₂ exit the supply manifold of anode	kg/s
$W_{sm,out,ca}$	Mass flow rate of air exit the supply manifold of cathode	kg/s
$W_{w,gen}$	Mass flow rate of produced water in the cathode	kg/s
$W_{w,mbr}$	Mass flow rate of water vapour across the membrane	kg/s
$W_{w,out}$	Mass flow rate of water vapour exit the cathode	kg/s
ζ_n	Empirical parametric coefficient of fuel cell	-
λ	Water content in the membrane	-

ρ	Density of gas	kg/m ³
ρ_m	Density of the material	g/cm ³
ρ_o	Density of air at sea level	kg/m ³
ρ^o	Stagnation density of gas	kg/m ³
ΔP_f	Rise in the pressure of air generated by the fan	kPa
ΔV	Change in fuel cell voltage	Volt (V)
Φ_{an}	Relative humidity in the anode	-
Φ_{ca}	Relative humidity in the cathode	-
η_m	Efficiency of the motor	-
σ_L	Stress applied in the longitudinal direction	psi
σ_t	Stress applied in the tangential direction	psi

Chapter One: Introduction

1.1 Overview

A fuel cell is a device which converts energy in the fuel and the reactant into direct current. Origins of the fuel cell can be traced to the early nineteenth century. William Grove demonstrated his fuel cell for the first time in 1839. However, it remained in an experimental state until 1932 when Francis Bacon manufactured the first prototype fuel cell [1].

The lack of advanced manufacturing technologies and the high prices of catalyst materials, such as platinum, along with readily available fossil fuels at low cost, have limited the interest in fuel cells as the main or auxiliary source of power. Consequently, commercial uptake in the technology has been low. But, with recent developments in manufacturing technologies of electrolyte membranes, electrode materials, effective use of catalyst materials, and with advances in solid state power electronics and control systems, these factors have rejuvenated the interest in the use of fuel cells as a prime source of power [2].

The increasing demand for electrical energy has resulted in increased production which in turn has increased harmful emissions. Natural reserves of fossil fuels are being depleted at an accelerated rate. Awareness of global warming, and the need for alternative sources of energy that are reliable, safe and environmentally clean with low cost has led to accelerated research [3, 4].

The efficiency of energy conversion-production for a fuel cell is comparatively higher than combustion engines, both internal and gas turbines, because there is no intermediate thermal conversion process that converts heat energy to mechanical motion, which is ultimately used to drive electrical generators [5].

The pollutants such as carbon dioxide, nitrous oxides, and sulphur dioxide which are produced from combusting hydrocarbon fuels are eliminated when using fuel cells. Also, the absence of the intermediate mechanical conversion process makes a fuel cell a quiet device [3].

Compared to conventional storage elements such as lead acid, and some other forms of batteries, fuel cells produce higher energy density. In practical applications, batteries need to be charged, and this process is time consuming. In contrast, recharging of the fuel cell reactants, namely oxygen and hydrogen, is a quick process [2].

Fuel cells are deployed in many industries such as transportation, aviation, navy, microelectronics, and combined heat and power (CHP) applications, and their applicability in diverse application areas is on the increase [6]. However, fuel cells are characterised as highly energy dense devices, but with low power density, therefore a heavy and large size of stack is required to fulfil an application with a high power demand [7].

Furthermore, fuel cells respond slowly to sudden changes in power demands which limit their dynamic performance. Thus, to enhance the performance of the power source using a fuel cell system, an electric storage device, such as rechargeable batteries or super capacitors, must be connected in parallel with the fuel cell stack in order to boost and improve the transient behaviour of the fuel cell system [8, 9].

1.2 Types and Applications of Fuel Cells

Fuel cells are usually classified according to the type of the electrolyte that has been deployed, the reactants, or the operating temperature [3]. Commonly there are six types of fuel cells, as presented in Table 1.1 below [1]:

Table 1.1: Basic details of different types of fuel cells			
Fuel Cell Type	Mobile Ion	Operating Temperature, °C	Applications
Direct Methanol Fuel Cell	H ⁺	20-90	Suitable for portable electronic systems running a slow and steady low power consumption for long periods.
PEM Fuel Cell	H ⁺	30-100	Vehicles, mobile application, and for low power CHP systems.
Alkaline Fuel Cell	OH ⁻	50-200	Used in space shuttles (Apollo).
Phosphoric Acid Fuel Cell	H ⁺	~ 220	Large numbers of 200 kW CHP systems.
Molten Carbonate Fuel Cell	CO ₃ ²⁻	~ 650	Suitable for medium to large scale CHP systems up to MW capacity.
Solid Oxide Fuel Cell	O ²⁻	500-1000	Suitable for all sizes of CHP systems, 2 kW to multi MW.

The proton exchange membrane (PEM) fuel cell, also known as a polymer electrolyte membrane fuel cell requires a high purity of hydrogen fuel and operates at low temperatures ranging between 30 °C and 100 °C. One of the alternative solutions to replacing the use of pure hydrogen in the PEM fuel cell is to supply the fuel cell directly

with liquid menthol, such a fuel cell is called a direct menthol fuel cell (DMFC), where the hydrogen is extracted from menthol. The problem of a slow reaction rate is avoided by using an alkaline fuel cell (AFC) which has the ability to operate at high pressures and temperatures of about 200 °C, AFC requires pure oxygen and hydrogen [1].

The phosphoric acid fuel cell (PAFC) operates at a fairly high temperature 220 °C, which results in an increased reaction rate. The issue of hydrogen fuelling is solved by reforming natural gas (mostly methane) to hydrogen and carbon dioxide, but this process adds more cost, size and complexity to the fuel cell. PAFC can operate for long periods with very minor maintenance and high reliability, with an opportunity to be integrated to the combined heat and power (CHP) systems [1].

Molten carbonate fuel cells (MCFC) operate at temperatures of around 650 °C and require carbon dioxide in the air in order to operate. While solid oxide fuel cells (SOFC) operate at temperature levels of 500-1000 °C and can be supplied with low purity hydrogen (i.e. hydrogen containing carbon monoxide). These high temperatures offer high reaction rates without the need to use an expensive catalyst. Hydrocarbon fuel such as propane, kerosene, methane, and coal gas can be used after a reforming process. Reforming and filtering processes work to break the bonds between the molecules of hydrocarbon fuel in order to separate hydrogen molecules from carbon monoxide and carbon dioxide molecules in order to produce the desired purity level of hydrogen. However, this technique introduces extra costs, complexity, weight and volume to the system. Moreover, as they operate at very high temperatures, the costs of heat tolerant materials and the associated cooling system costs make the system very expensive and complex [1, 10].

PEM fuel cells and SOFCs are currently attracting the greatest interest and development. SOFCs offer higher overall system efficiency but lower power density and lower load dynamic responses in comparison with PEM fuel cells. SOFCs take a

longer time to reach high operational temperatures, which make these more convenient for stationary power generation applications [10].

When compared with other types of fuel cells, PEM fuel cells have several features, such as high power density, high conversion efficiency, long operational life hours, low corrosion, low weight and compact size, low operational temperature, and faster transient response, which makes PEM fuel cells suitable for transport and can also be used in stationary applications. Therefore, research and development are on-going in academia and industry in order to produce commercially viable PEM fuel cell systems for different applications [11-14].

Despite increased efforts to develop PEM fuel cells technology, durability and cost remain the major barriers against PEM fuel cell commercialisation and exploitation. The target of the US Department of Energy toward fabrication cost and operational lifetime of a PEM fuel cell for transportation applications is \$30/kW and 5000 hours by 2015, in order to compete effectively with the conventional technology of internal combustion engines [15].

1.3 Structure of a PEM Fuel Cell

A PEM fuel cell is an electrochemical device where hydrogen is fed to the anode, and air/oxygen is fed to the cathode. In the most elemental state, the fuel cell consists mainly of one electrolyte and two electrodes. But practically a fuel cell may consist of more than these two components in order to increase its efficiency and output power, which makes the fuel cells commercially viable. A schematic structure of a single PEM fuel cell is shown as Figure 1.1. It consists of a membrane electrode assembly (MEA) sandwiched by two parallel flow field plates called bipolar plates, which serve as current collectors and to connect cells in series for greater stack voltage. The MEA consists of three layers, (1) polymer electrolyte membrane layer (i.e. proton exchange

membrane), (2) catalyst layer and, (3) gas diffusion layer (GDL). The electrolyte is a proton conduction polymer, bonded by a catalysed porous electrode on each side. The anode, electrolyte, and cathode are assembled as one very thin piece. Usually, these components are manufactured individually and then pressed together at high temperature and pressure [16].

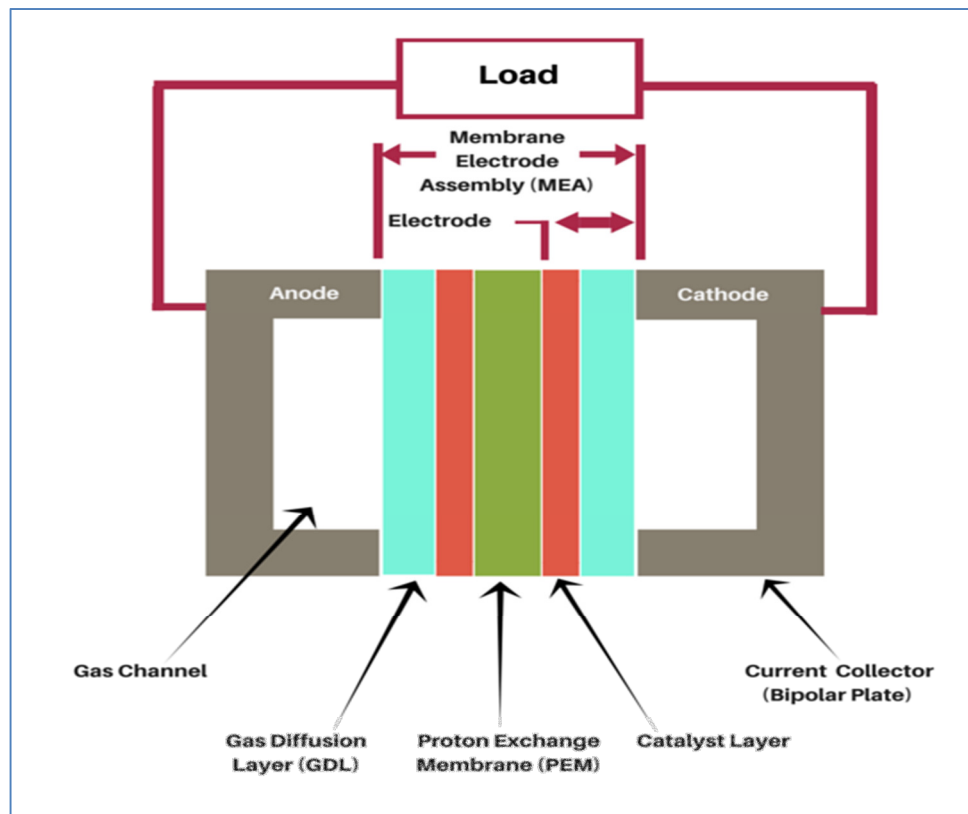


Figure 1.1: Schematic structure of a single PEM fuel cell

The electrolyte plays an important role in a PEM fuel cell, as it conducts protons from the anodic electrode catalyst layer to the cathode one while blocking electrons. The electrical ohmic resistance properties and the protonic conductivity of the membrane has a great impact on the voltage and performance of a PEM fuel cell [17].

As a result of continuous development, in the late 1960s, a new polymer membrane Nafion® (registered trademark of Dupont) became a standard electrolyte membrane for

a PEM fuel cell [1]. Development of catalysts, membrane electrolyte assembly (MEA) components, and bipolar plates are vital for overcoming the concerns of cost and durability. Materials with higher degradation and corrosion resistance and low platinum loading are essential to achieve lifetime and cost targets. Improvement and optimisation of the materials used in the gas diffusion layer (GDL) and gas flow channel (GFC) interfaces are also important, so as to provide efficient water removal and flow of gases and to avoid flow maldistribution, hence achieving and maintaining high fuel cell performance [15]. Figure 1.2 shows different sizes of H-series 100W-5kW PEM fuel cell stacks produced by Horizon Fuel Cell Technologies.



Figure 1.2: Different sizes of H-series 100W-5kW PEM fuel cell stacks produced by Horizon Fuel Cell Technologies (cited from[18])

1.4 Historical Background of Electrical Aircraft

Aviation transportation was recently noted to have contributed 4.2% toward global CO₂ emissions and the rate is expected to have increased to approximately 5.7% by the end of 2015 due to growing demand on global travel [19]. Boeing Research and Technology Europe, in collaboration with other industrial partners, are working towards reducing airplane emissions, not only through investing in and developing an efficient fuel for aircraft, but also through developing propulsion systems and power generating technologies that are environmentally friendly, by accepting the possibility of integrating fuel cell systems and batteries in aerospace applications [20].

Typically, control surfaces on aircraft are actuated using servo hydraulic actuators. The hydraulic fluid is pressurised using engine driven pumps. The power required places an additional burden on the engine, which requires hydro-carbon fuels, thus increasing emissions. One of the specific characteristics of the electric aircraft is that it deploys electric motors and local electro-hydraulic actuators. All electric aircraft employ brushless DC motors instead of internal combustion engines. Different technologies are used to supply power to the electric motors, such as electrical generators, fuel cells, solar cells, and batteries and ultra-capacitors. Electric aircraft can be mainly divided into two main categories: the all-electric aircraft (AEA), where electricity produced from different power systems is the only driving power for the aircraft, and more-electric aircraft (MEA), where a combination of an internal combustion engine with other electrical power supply systems is most likely used on board the aircraft, with increasing roles of electrical systems on board among the other systems employed in the aircraft [21].

However, an increase in the payload capacity and/or the increase in the flight duration (range) impose several challenges, and necessitate an increase in the power and energy densities of the on-board power system. Hence, MEA can be considered to make an

attempt to overcome the challenges associated with AEA. It has been estimated that MEA technology is capable of reducing the empty weight of a typical airliner by about 10%. A reduction of moving parts also reduces maintenance costs and increases the overall reliability of the system [21].

An electrical propulsion exhibits high efficiency and reliability, low noise and heat radiation, and low cost compared to the small internal combustion engines typically used for small unmanned aircraft [8]. Also, using induction motors to drive the propellers contributes toward elimination of sparks [21].

The first electrical airplane propulsion system using poly-phase synchronous generators, and a number of poly-phase motors driving a number of propellers, was proposed in 1943 [21].

In the seventies, NASA and AeroVironment, Inc. initiated the first research programme into a solar-powered electric airplane, and the first test flight was made in 1974 as the world's first solar-powered airplane. The first official manned flight of a solar-powered aircraft deploying solar cells, batteries, an electric motor and a propeller was made in 1980. About a decade later, the U.S. Government launched a programme of high altitude solar energy (HALSOL) to explore the feasibility of solar-electric flight above 65,000 ft., which contributed to the first unmanned aircraft that was able to fly to altitudes of 50,500 ft., reaching an altitude of 71,530 ft. in 1997. However, NASA's solar-powered aircraft research was only a fraction of the extensive research work carried out worldwide for this aim [21].

Interest prevails in the research community to investigate the design methods for fuel cell powered aircraft in order to determine the design trade-off and to characterise the optimum configurations of fuel cell power-plant, and also to identify appropriate techniques for developing and improving the performance of unmanned aerial vehicles

(UAV). Naturally, the benefits need to be seen in comparison with conventional aircraft [22].

The replacement of conventional power units with a fuel cell power system offers several advantages for aircraft applications, such as: reducing noise and harmful emissions, reducing ground support and maintenance, on-board water generation, and further weight reduction [23].

Leading commercial aircraft manufacturing companies, such as Boeing and Airbus, have started significant research into the use of fuel cells as an alternative source of electric power to drive several systems, for example the nose-wheel undercarriage system and also to provide on-board water production facilities. However, in recent years, small-powered airplanes have successfully been flown using fuel cells as the primary source of power [9].

The first use of fuel cells as an auxiliary power source device was in the 1960s. The device was used in the Gemini space flights programme directed by NASA. In particular, PEM fuel cells were developed and deployed for this programme [16]. Early fuel cells proposed to produce electricity as an alternative technology for the electric aircraft were suggested in 1974, where the configuration employed fuel cells and batteries for driving the motors of propellers [21].

The first fuel cell powered aircraft was built and tested by AeroVironment, Inc. in 2003, using PEM fuel cells run by hydrogen extracted from sodium borohydride. It had a very short flying endurance of less than 15 minutes. Then, in 2005, AeroVironment, Inc. demonstrated a second version of UAV using PEM fuel cells operated by liquefied hydrogen; this had an endurance of about 2.4 hours. A solid oxide fuel cell powered UAV using propane fuel was constructed in 2006 by Advanced Materials, Inc. with a flying endurance of about 4 hours. However, since 2003, a significant increase has been observed in the research and investigations into the use of fuel cells in aviation [22, 24].

In the literature, the acronym UAV is an abbreviation for unmanned aircraft/aerospace/aerial vehicles. However, the aviation industry has now adopted UAS rather than UAV as a preferred acronym for unmanned aerial/aircraft systems, “as UAS encompasses all aspects of deploying these aircraft and not just the platform itself” [25].

1.5 Motivation of the Project

Fuel cell powered aircraft are generally characterised by low specific power (power to weight ratio W/kg), where the power to weight ratio is an important indicator of aircraft performance, leading to several limitations between the power consumption and the total weight of the aircraft [26].

The propulsion system of the UAS is required to have a large range of power in addition to a fast response, in order to fulfil the requirements of different flight phases and to balance the variations in load demand.

PEM fuel cells suffer from limited power density and slow dynamic responses when a sudden change in power demand is presented, which limits their performance particularly for high altitude long endurance (HALE) UAS applications, where a very low atmospheric temperature and pressure, altitude turbulences, and unexpected variations in the load demand put severe stresses on the operation and performance of PEM fuel cells. A stable and robust controller which can optimise PEM operation and provide fast and sufficient flow of hydrogen and air/oxygen to the reaction chamber of the fuel cell is one of the critical objectives [8, 27].

In order to supply sufficient hydrogen and oxygen to the PEM fuel cell when operating at high altitudes, fuel and reactant need to be stored in pressurised cylinders. The size and weight of the storage vessels play an important role in determining the endurance of the UAS flight [28].

However, in the published literature to date, there appears to be no particular study that determines or specifies the size and weight of the combined power-plant of the fuel cell stack with hydrogen and air/oxygen vessels and the propulsion system of UAS for high altitude flight operation; or takes into consideration the power capacity of the fuel cell stack and the flight endurance as the main factors in designing the size and weight of the storing vessels, and hence determining the overall weight of the UAS.

The weight of the power-plant has a direct impact on the wing loading (W/S), and that in turn determines the wing area, and technologies needed to produce a structure capable of being produced [28, 29].

1.6 Aim and Objectives

The aim of this project is to develop and design a PEM fuel cell power system for high altitudes UAS operation; and to determine the overall weight of the UAS based on determining the size and weight of the combined power-plant of the fuel cell stack with hydrogen and air/oxygen vessels, and the propulsion system. The objectives can be summarised as follows:

1. To carry out a critical literature review of the relevant published literature relating to using fuel cells as a power source for aircraft and UAS applications, and the techniques of managing and controlling output power of the fuel cell stack, and managing operational variables of PEM fuel cells under load variations.
2. To develop a mathematical model for the PEM fuel cell stack, and using Matlab-Simulink to implement the necessary design and simulations.
3. To validate and tune the developed mathematical model of the stack with the commercially available 1 kW PEM fuel cell stack (H-1000) developed by Horizon Fuel Cell Technologies. Where, simulations will be applied to examine

all of the operational and performance variables under various operational conditions, and fuel cell losses are considered as well.

4. To investigate the implications of high altitudes on the operation and performance of the PEM fuel cell stack.
5. To propose and examine a controller that can efficiently optimise and supply a sufficient flow of hydrogen and air/oxygen to the PEM fuel cell stack.
6. To develop and design a technique that can determine the size and weight of the combined power-plant of the fuel cell stack with hydrogen and air/oxygen vessels and the propulsion system of the UAS for high altitude operation. Taking into consideration the power capacity of the fuel cell stack and the flight endurance as the main factors in designing the size and weight of the storing vessels, and hence determining the overall weight of the UAS.

1.7 Scope-Format, and Software Definition

Related literature about the developed models of PEM fuel cells associated with managing and controlling their operation and performance, and the use of fuel cells for aircraft and UAS applications, will be presented in Chapter Two of this thesis. In Chapter Three, the thesis will look at modelling voltages of PEM fuel cells. Chapter Four will examine mathematical modelling of gases flow in PEM fuel cells, while Chapter Five will validate the PEM fuel cell and controller design models. Chapter Six will examine the implications of high altitudes on the operation of PEM fuel-cell-based UAS and then Chapter Seven will discuss hydrogen fuel and static thrust for UAS. Chapter Eight examines pressure vessel design and power-plant mass estimation, and finally, Chapter Nine presents the conclusion and discusses future work.

However, some important related literature will be specifically presented in each chapter separately based on the related work of concern. Also, any findings and

contributions to the body of knowledge proposed in this research will be highlighted in *bold-italic* font.

Matlab and Simulink are registered trademarks of The MathWorks, Inc. Matlab is a high level language and interactive environment used by scientists and engineers for technical computing integrates computation, programming, and visualisation where problems and solutions are expressed in a familiar mathematical form. “Simulink is a block diagram environment for multi-domain simulation and model-based design. It supports system-level design, simulation, automatic code generation, and continuous test and verification of embedded systems. It provides a graphical editor, customisable block libraries, and solvers for modelling and simulating dynamic systems. Simulink is integrated with Matlab, enabling to incorporate Matlab algorithms into models and export simulation results to Matlab for further analysis” [30].

LabVIEW program is a registered trademarks of National Instruments and is described as a virtual instruments software because their operation and appearance and imitate sort of physical instruments, such as multi-meters and oscilloscopes. LabVIEW consist of a set of comprehensive tools for acquiring, displaying, storing, and analysing data, as well as tools to help the user to troubleshoot the codes.

1.8 Summary

This chapter presented a historical overview relating to the use and development of fuel cells. A summary of the major six types of fuel cells and their applications in different fields of stationary and transportation sectors was demonstrated. The structure of the PEM fuel cell, along with the materials used in manufacturing of such a device, was also discussed. Furthermore, a historical background regarding the use and development of electrical aircraft was presented.

Fuel cell powered aircraft are generally characterised by a low power to weight ratio (W/kg). The propulsion system of an unmanned aircraft needs a large range of power and fast response to fulfil the requirements of different flight phases and to balance the variations in the load demand. PEM fuel cells suffer from limited power density and slow dynamic responses when a sudden change in power demand is presented, which limits their performance particularly for high altitude long endurance (HALE) UAS applications, where a very low atmospheric temperature and pressure, altitude turbulences, and unexpected variations in the load demand put severe stresses on the operation and performance of PEM fuel cells. A stable and robust controller and fuel supply system that can provide fast and sufficient flow of hydrogen and air/oxygen to the reaction of the fuel cell is one of the critical objectives.

In the next chapter, the literature relating to many developed models of PEM fuel cells, different techniques of managing and controlling the output power of a fuel cell stack, and managing the operational variables of PEM fuel cells under steady and transient states of load variations will be reviewed and presented. Also, the deployment of fuel cells as primary or auxiliary power sources for aircraft and UAS applications will be presented and critically discussed.

Chapter Two: Literature Review

2.1 Introduction

Many researchers and development programmes have carried out extensive investigations in order to develop fuel cells. Material characteristics, design and implementation, performance and control of the fuel cells have been studied. Some researchers have focused on the geometrical design parameters and their impact on the performance of the fuel cell. Others have focused on the operational parameters and variables and their relations to the performance and output power of the fuel cell.

The power generated by the PEM fuel cell is a function of the size of the fuel cell stack, while the energy capacity is a function of the availability and storage capacity of hydrogen and oxygen vessels [31].

Also, Barbir et al. [31] reported that the efficiency of the fuel cell is related to its size, for two different sizes of fuel cells to generate the same level of power, the fuel cell which has a larger total active area is more efficient than a fuel cell with a smaller active area. A larger active area leads to lowering the current density and hence increases the cell potential, which is directly proportional to the fuel cell efficiency. Thus, maximum stack efficiency leads to a heavier stack weight.

Steady state performance of fuel cells is usually presented in the form of a polarisation curve (V-I curve) which specifies the relation between the fuel cell stack output voltage and stack output current. The relationship between the air supply, water management and cooling process leads to a non-linear relationship in the stoichiometry of air in the

cathode, membrane humidification, and stack temperature which is reflected in the performance of the polarisation curve [8].

Pukrushpan et al. [32] reported that a fuel cell control system could be subdivided into three main subsystems that deal with:

- Regulation of the supply of air and hydrogen.
- Management of the produced water.
- Management of heat produced from the reaction.

Larminie and Dicks [1] proposed many ways to overcome the slow reaction rates that can lead directly or indirectly to improving the performance of the fuel cell operation by one or more of the following methods:

- Using catalysts such as platinum.
- Raising the reaction temperature.
- Increasing the electrode contact area with the reactants.
- Adjusting the flow rate and/or pressure of the fuel and reactant.

Improvement of the transient response performance and synchronisation of the power output of the fuel cell to the power demand could be achieved by the following [33-35]:

- managing the operational variables and parameters such as pressures and concentrations, mass flow rate of the fuel and reactant, temperature of the fuel cell, and water content in the membrane, or
- managing the DC output power of the fuel cell stack via controlling the power conversion unit (PCU) and associated energy storage device (ESD) such as battery or super-capacitor.

Bordons et al. [13] proposed a constrained model predictive control, in order to control the operational process of the fuel cell to fulfil one of three main objectives individually:

- Achieving maximum efficiency.
- Controlling fuel cell voltage.
- Preventing oxygen starvation.

In the next sections, the literature review relating to many developed models for PEM fuel cells is presented. In particular, the following aspects will be presented and critically discussed:

- Management of the operational variables of PEM fuel cells under steady and transient states.
- Management and control of the output power of fuel cells, and their operation under load variations.
- Deployment of fuel cells as primary or auxiliary power sources for aircraft and UAS applications.

2.2 Modelling of PEM Fuel Cells

The steady state behaviour of the PEM fuel cell can be predicted through estimating the equilibrium cell voltage for a particular set of operating conditions, such as concentration of gases, associated pressures, operating temperatures, and the drawn current. Transient behaviour is an important aspect, particularly when operating conditions change with time; such as starting up or shutting down, or when there is a large sudden change in the load current accompanied with changes in the cell temperature or gas concentration on the surface of electrodes [36].

Amphlett et al. [36] developed a model that predicts the transient response of a fuel cell stack based on adopting the steady-state electrochemical model previously developed by a group of developers [37-39] for 5 kW Ballard Mark V stack fuel cell. By coupling the steady state model and the thermal model, the transformed integrated model was used to

determine the transient cell voltage as a complex function to the operating current, stack temperature, flow rates and partial pressures of oxygen and hydrogen.

Pathapati et al. [11] devised a novel dynamic model, incorporating the capacitive impact of a charged double layer to the electrochemical model of the group of Ballard developers [36-39], in order to simulate and predict the transient response of cell voltages, flow rates of hydrogen and oxygen, temperature of the cell, and temperatures/pressures of the anode and cathode channels under sudden changes in the load current of the PEM fuel cell.

Mann et al. [40] reported that a steady-state electrochemical model (SSEM) developed by group of developers [37-39] is specific to the Ballard Mark IV and Mark V that were developed between 1988 and 1990. By adopting the SSEM to modify and develop a generic model (GSSEM), it is possible to not only accept operating variables such as cell temperature, current density, pressure and flow rates of the reactants, but also to extend this model to accept higher current densities above 500 mA.cm^{-2} . New parameters such as dimensions of the electrolyte membrane, water content level in the membrane, and the level of aging and degradation of the membrane with operating time were also included in the model. However, based on the electrochemical reaction theories and proposed model by Amphlett et al. and Berger [38, 41], the equations of activation overvoltage and the empirical parametric coefficient values for the generic steady-state electrochemical model have been derived by Mann et al [40]. Also, by adopting the recommendations of Springer et al. [42] and data given by Büchi and Scherer [43], it was possible to develop an empirical relationship of membrane protonic resistivity as a function to the characteristics of the membrane, temperature, water contents and its distribution in the membrane, and current density.

Seyezhai and Mathur [44] developed a mathematical model for a 750 W PEM fuel cell to predict the behaviour of fuel cells under steady-state and transient conditions. The

dynamics of the charged double layer capacitance, dynamics of anode and cathode channel are all integrated into a single model and the transient responses of the PEM fuel cell model under a resistive load and for short-long operation times are analysed.

Yuan et al. [45] developed a three-dimensional multi-phase fuel cell model to predict the impacts of operating parameters such as operating pressure and temperature of the fuel cell, relative humidity of reactant gases, and air stoichiometric ratio on the performance of PEM fuel cells operating under steady-state conditions.

A dynamic model for a 1.2 kW PEM fuel cell that can be used for optimal operational strategies development and control design of fuel-cell-based power systems was developed by del Real et al.[46]. The model parameters are adjusted and validated with the 1.2 kW Ballard fuel cell stack, the proposed model allows prediction of both steady and transient behaviour due to variable loads, and also the impact of water flooding and purging of hydrogen.

A non-linear dynamic model of PEM fuel cells was proposed by Pukrushpan et al. [2, 32] to examine the behaviour associated with the flow of oxygen, using electrochemical-thermodynamics and zero-dimensional fluid mechanics principles (i.e. the anodes and cathodes of the stack are lumped as one anode volume and one cathode volume, respectively, and similarly for the supply and return manifolds of the stack, hence the dimensions of the stack have no impact on changing the properties of the flowing fluids).The output voltage of the stack is modelled based on load current, fuel cell operating temperatures, air pressure and partial pressure of oxygen, and humidity of the membrane.

Park and Choe [47] presented a new dynamic model of a stack comprising 20 cells, that considers the impact of temperature and the two phases of water (gas and liquid) in the gas diffusion layer. This layer plays a significant role in the transportation of water and gases. The model revealed the starting up and transient behaviour under different

conditions of load current, temperature, and coolant flow rate. The transient analyses of the model considered the dynamics of vapour and oxygen concentration in the gas diffusion media, liquid water saturation, temperature, and the changes of water content in the membranes at multistep load variations.

Youssef et al. [48] proposed a lumped model for PEM fuel cells based on zero-dimensional linear algebraic equations to determine the impact of various operating and design parameters such as input temperature, pressure, stoichiometric ratio, thickness of membrane and gas diffusion layer on the performance of the fuel cell. The published experimental results were used to validate the developed model.

Rowe and Li [49] developed a non-isothermal one-dimensional model of PEM fuel cells in order to investigate and examine the effect of design and operating conditions upon the performance, water management, and thermal response of PEM fuel cells.

Pasricha and Shaw [50] proposed a simple dynamic electrical model of PEM fuel cells by extending the steady state current-voltage behaviour of the model to incorporate the impact of temperature on the performance of the fuel cell. The model performance has been validated using experimental data of a 500 W commercial PEM fuel cell stack.

Golbert and Lewin [5] adopted the model developed by Yi and Nguyen [51] in order to produce a time dependent model for a fuel cell. The model details the heat transfer between the fuel cell body, gas channels, cooling water, condensation and evaporation, the water content and water through the membrane and, water at the cathode. Dynamics of the electrochemical and the transient response of fluids in the anode, cathode and coolant channels are assumed to be instantaneously related to the thermal transient response of the cell core, while all other parts of the entire system are considered in the quasi steady state. Hence, the complexity of the system is reduced to a one-dimensional model.

Springer et al. [42] developed a one-dimensional isothermal steady-state model for PEM fuel cells using the Nafion117 membrane, to determine the impact of water content on the performance of the fuel cell. The membrane conductivity is determined as a function of water content and current densities. While, Büchi and Scherer [43] carried out another attempt to determine the conductivity of the membrane as a function of drawn current densities under various pressures and temperatures.

Abul-Hawa et al. [35] presented a simplified model of relationships between the activation losses, ohmic losses, and concentration losses on one side and the operating temperature, pressure, and concentration of oxygen from another side, as determined for a PEM fuel cell. While, Mann et al. and Wang and Wang [40, 52] determined the impact of the water content of the electrolyte membrane and the membrane specific resistivity on the output power of the fuel cells.

2.3 Managing Operational Variables of PEM Fuel Cell

The response of the PEM fuel cell owing to the rapid changes in the current load demand tends to be slow. This is because operation of the PEM fuel cell depends on monitoring and controlling the flow rates and pressures of air and hydrogen, stack temperature, management of the produced heat and water as a result of the electrochemical reaction, and also maintaining of the proper hydration level of the membrane [35]. However, designing and implementing a control system that efficiently controls all these parameters and variables under a steady state and transient state of loads is a complex issue.

Furrutter and Meyer [53] reported that control of the flow rates of hydrogen and air has a significant impact on the performance of the fuel cell, particularly in self-humidified fuel cell systems, where the risk of under humidification is most likely to occur, particularly at low current densities as the amount of produced water in the cathode is

too small. Although a high flow rate of air leads to enhanced performance of the fuel cells, it would also contribute to removing the accumulated water or water vapour in the cathode side, which leads to an increased drying impact on the fuel cell. Thus, finding a balance in the flow rate of air and the fuel cell performance is a challenging issue.

When a fuel cell stack is supplied with dry gases, the level of membrane hydration depends on the production and evaporation rates of water inside the fuel cell, which are dependent on the load current, electrochemical reaction rate, operating temperature, and period of operation. Moreover, the fuel cell temperature affects the activity of the catalyst, the hydration level of the membrane, the saturation of the gas diffusion layers, and diffusion of gases through the membrane. Therefore, both the membrane humidification and stack temperature influence the dynamic performance of the fuel cell [8].

Two operational phenomena were reported by Bordons et al. [13] to adversely affect or even destroy the membrane of the fuel cell, namely: water flooding and reactant starvation. Water flooding is related to the temperature and humidity, while reactant starvation is the worst phenomenon and is related to the amount of oxygen in the cathode, particularly when the amount of oxygen drops below the certain limit.

Pukrushpan et al. and Bordons et al. [2, 13] reported that the issue of oxygen starvation cannot be controlled by only controlling the oxygen flow rate because the dynamics of the electrochemical reaction are much faster than the performances of fluid flow when a step change in current occurs. Therefore, an auxiliary storage device such as batteries or super-capacitors must be used to buffer the fuel cells system during the transient current demands. However, these additional components introduce additional weight, complexity and cost to the system. Meanwhile, Abul-Hawa et al. [35] reported that in order to prevent starvation, a PEM fuel cell is almost supplied with hydrogen and air or

oxygen higher than the level of the reaction rate. This would mean unreacted gases and therefore extra cost.

Abul-Hawa et al. and Amphlett et al. [35, 36] examined the performance of PEM fuel cells under different temperatures and pressures of oxygen, and they found that increasing either the temperature or pressure of oxygen will lead to reducing the activation losses via improving the exchange current density, and hence increasing the output power of the fuel cell. However, increasing the temperature of the fuel cell might not be the proper solution for improving its output power, because this will dehydrate the membrane. Also, increases in the pressure of the reactant inside the fuel cell must be determined during the design stage, as the high difference in pressures between cathode and anode will damage the membrane of the fuel cell.

Increasing the water content of the membrane to a certain limit was observed to reduce the value of membrane specific resistivity and hence increase the output power of the fuel cell [40, 52].

Barbir et al. [31] reported that there is a voltage gain when increasing the operating pressure of the fuel cell. Operating at high pressures can improve the diffusion of gases and reduce the concentration losses, but high pressure operation requires a thicker polymer membrane to avoid membrane damage, which leads to high ionic resistivity results due to the increase in the thickness of the membrane. They also reported [31] that using pure oxygen instead of air to feed the fuel cell stack leads to increasing the cell output voltage; this relates back to the fact that pressure and diffusion rates of pure oxygen in the cathodes are higher than the partial pressure and diffusion rate of oxygen in the mixture of nitrogen-oxygen of air. However, using pure oxygen is critical, as the entire system requires certain procedures in terms of maintenance and safety. Operating a fuel cell stack with air requires a pumping device such as a blower or a compressor,

resulting in further parasitic losses. Thus, the decision for using pure oxygen or air is debatable and dependent on the application.

Shih et al. [54] reported that there is a significant power increase of up to 32% from the fuel cell stack fed by pure oxygen in comparison with a stack fed by atmospheric air.

In a PEM fuel cell, the fuel (H_2) and reactant (O_2) are supplied by mechanical systems of pumps and valves. The mechanical adjustment time for these elements is comparatively longer than the reaction time. This mismatch between the two times causes a real shortage in the fuel and reactant (starvation of fuel and reactant), which consequently leads to a breakdown in the chemical reaction and to a rapid drop in the output power of the fuel cell. These problems have been addressed by researchers [12, 55] in the control models of fuel cell power systems for hybrid vehicles.

2.3.1 Managing the Flow Rate of Hydrogen

Thounthong et al. [55] reported that a flow of hydrogen must be maintained corresponding to the maximum rated current of the fuel cells stack, so that the fuel cells always have enough fuel, the flow is usually adjusted based on the feedback reference current signal which is varied according to the changes in load power. While Hauer et al. and Pukrushpan [56, 57] reported that the flow rate of fuel must be controlled simultaneously in reference to the drawn current from the fuel cell.

Hauer et al. [56] reported that a small fuel utilisation factor (~ 2) is necessary to be applied in order to ensure a faster and better response against sudden changes in the load demand, and also to reduce the size of the energy storage device. But, this will lead to extra hydrogen not being used in the reaction, which leads to more losses. Therefore, a compromise between the fuel utilisation factor and the size of the energy storage device must be considered.

El-Sharkh et al. [3] reported in their proposed dynamic model of 5 kW PEM fuel cell system, that a quick response of the fuel cell against step increases-decreases in the load current could be gained via controlling the mass flow of hydrogen.

Heinzel et al. [58] proposed that the unreacted hydrogen from the anode side can be reused in order to increase the gross efficiency of the combined reformer and fuel cell system by 30%. But, this increases both the cost and the consumed power, as the hydrogen has to be refined before it can be re-pumped back into the storage cylinder, which means extra cost and complications. This solution enhances the performance of the fuel cell partially, but it does not improve the responses of fuel cells towards sudden changes in the load demand.

Rodatz et al. [12] proposed a technique of powertrain in order to control the fuel cells in vehicles, mainly by controlling the mass flow rate of hydrogen. When the current is drawn from the fuel cell, voltages and currents are used in a feedback scheme and the controller determines the exact amount of fuel required by the reaction, and the mass flow rate is adjusted accordingly. Such a controller is quite complicated but it does provide efficient results.

Kim et al. [7] reported that in order to maintain stable stack performance, a fuel cell stack must be operated with closed ended anodes by using a purge valve instead of an open ended anode. A purging anode is important to maintain the internal pressure of hydrogen inside the anode of the fuel cell at appropriate levels, also to flush the anodes from residual unreacted hydrogen and any traces of formed water [8].

Semiz et al. [59] reported that the use of a hydrogen purge valve noticeably improved the performance of the fuel cell stack. When the valve is off, the pressure of hydrogen in the anode channel increases, which increases the concentration of hydrogen at the membrane electrode assembly surface and therefore increases the reaction rate, hence improving the performance of the fuel cell. The on and off periods of the purge valve

are optimised according to the size and power capacity of the fuel cell stack in order to achieve the highest performance.

Furrutter and Meyer [53] reported that in order to allow fresh hydrogen to enter the anode of the fuel cell, Horizon Fuel Cell Technologies used a purging technique for the H-100 PEM fuel cell stack that enables the hydrogen purging process to frequently take place every 10 seconds for a duration of 10 ms. However, this process has a negative impact on the performance of the fuel cell as this leads to a sharp drop in the output voltage, and hence power delivered by the fuel cell. Since the drop in voltage lasts for a very short period of time 10 ms, the controller is unable to cope with such a fast transition. A special controller was built by Horizon to switch the fuel cell stack on/off at almost every 10 seconds to overcome the issue of frequent purging of hydrogen, in order to maintain the maximum rated power from the fuel cell stack. However, the proposed controller technique might cause further problems as a continuous cycle of turning on/off for the stack, in a cycle of 10 seconds, would lead to unstable performance and in the worst-case scenario damage the stack after a period of continuous operation. It also might lead to further delay in the response of the stack toward the change in the load demand.

Verstraete et al. [8] reported that in order to prevent fuel cells from fuel starvation and membrane dehydration, the stack should be prevented from operating at levels of high concentration losses (i.e. high current demand), and the fuel utilisation of the stack set above 90% when the load varies from 25% to 100% of power capacity of the fuel cell stack.

2.3.2 Managing the Flow Rate of Air/Oxygen

Zhang et al. [60] reported that due to non-linear behaviour and time varying properties of the air supply subsystem, it is difficult to keep the oxygen excess ratio within the

required level, particularly during transitions. Therefore, an adaptive control algorithm is proposed which involves an estimation of time varying parameters and pole assignment of a closed loop system, in order to dynamically stabilise the excess ratio of oxygen. The operating points of the fuel cell system are adjusted via regulating the airflow and the stack current.

Pukrushpan et al. [2, 32] proposed a non-linear dynamic model of PEM fuel cells to examine and analyse the dynamic behaviour of a fuel cell, associated with the flow of oxygen, using electrochemical-thermodynamics and zero-dimensional fluid mechanics principles. Based on setting the instantaneous limit of the oxygen excess ratio ($\lambda_{O_2} = 2$), a combination of a non-linear feed-forward and linear-feedback controller was designed to determine and regulate the oxygen excess ratio during step changes in the current load demand based on:

1. Fuel cells stack current.
2. Pressure and humidity of the supplied oxygen.
3. Stack temperature.

This is primarily done to increase the controller robustness against device degradation and against uncertainty in ambient conditions. A non-linear feed-forward controller determines the input voltage of the compressor motor, this is done in order to control and maintain the required amount of oxygen in the cathode based on the drawn current from the fuel cell stack. This allows the desired net power output from the fuel cell stack to be maintained. The supplied hydrogen flow rate is regulated by using a high gain proportional control. The reference signal from the supply manifold pressure sensor is used in order to control the inlet valve of hydrogen and to retain a small pressure difference across the membrane. The operating temperature and humidity inside the cells are assumed to be efficiently controlled and literally considered constant. However, a high oxygen excess ratio improves the net power produced by the

fuel cell stack, but part of the produced power is used to derive the compressor motor, thus there is a trade-off between minimising the parasitic losses and providing fast airflow regulation, and these are considered conflict objectives.

Bradley et al. [26] proposed the use of two diaphragm compressors controlled by pulse-width modulation in order to manage and control the flow rate of the supplied air to the cathode. This involves turning off one compressor when a low flow rate is required at low current demand, and turning on two compressors when a high flow rate is required at high current demand. The cathode stoichiometric ratio between 2.0 and 3.0 is provided by the compressors as a function of stack current.

2.3.3 Managing Temperature

PEM fuel cells produce electrical power, water and heat as a result of the electrochemical reaction; released heat increases the temperature of the cell which leads to a reduction in water content in the membrane, hence reducing the conductivity of the membrane and increasing ohmic losses. Therefore, an adequate thermal management system plays a vital role in controlling the temperature of the stack, hence increasing and maintaining the performance and durability of the fuel cell stack [19].

It has been noticed that the fuel cells assembly stack has a non-homogenous temperature distribution as the temperature in the centre of the stack is higher than its ends, particularly in a cold operation environment [27].

A water cooling system shows a decent cooling performance in maintaining the performance of the fuel cell; however, it needs a coolant tank, pump and heat exchanger, which leads to an increase in the size, weight, and complexity of the entire system. Therefore, an air cooling system can be considered as an adequate alternative option for cooling a fuel cell stack [7].

Bégot et al. [27] reported that it is a complicated task to start-up and operate the fuel cell stack with sub-zero ambient temperatures, as the water produced in the cathode can turn to ice which can block the passage of the reactants to the reaction interface. The frozen water can change the conductive properties of the electrodes, membrane and in worst cases can damage the membrane. It was found that the formation of ice reduces the active surface of the electrode-catalytic layer which leads to a reduction in the rate of the electrochemical reaction, yielding a considerable drop in fuel cell output power.

Horizon Energy Systems developed a controller for a self-humidified PEM fuel cell stack, where the controller regulates the temperature of the stack by controlling the rotational speed of the cathode air supply fans, and also regulates the periodic purging process of the anode in order to maintain the pressure of hydrogen and to keep high levels of hydrogen utilisation in the anode, thus extending the stability of the stack performance [8, 61].

The performance evaluation of the fuel cell stack system presented by Kim and Kwon [24], showed that at a constant load, the temperature of the stack varied approximately between 22 °C and a maximum of 35 °C for the first 30 minutes of the stack's operation, and the controller of the fuel cell stack managed to maintain its stack temperature at around 35 °C for the remainder of the five hours test.

2.3.4 Managing Water

Van Nguyen and Knobbe [62] reported that the reactant gas (air or oxygen) and water management are the main factors in achieving a good performance for a PEM fuel cell stack. The gain in performance is due to managing the exhaust water control technique depending on the flow of reactant gas when removing the extra water from each individual cell, and separately from other cells in the stack. The experiment was applied on a stack of three cells operating at ambient pressure and temperature and the results

showed an improvement in peak power from 0.26 W/cm^2 per cell without exhaust control and up to 0.5 W/cm^2 per cell when using a sequential exhaust control technique. However, the design is good for a stack with a small number of cells and becomes more complicated for a high number of cells, because of the difficulty in establishing a uniform gas flow for each individual cell.

Santamaria et al. [63] reported that water management strategies are very important for the development of PEM fuel cell systems. Parallel and interdigitated are the most common types of gas flows for PEM fuel cell design, each of which have advantages and disadvantages depending on the operating conditions. Parallel flow depends mostly on the diffusion process to transport reactants and to remove water and other residual gases. While, an interdigitated flow relies on forcing the cross flow through porous gas diffusion layers, which has a significant water removal impact and leads to higher cell performance, but requires a high inlet pressure, several times greater in magnitude than that for a parallel flow, resulting in higher pumping losses.

Santamaria et al. [63] designed and tested a novel technique that is capable of providing efficient water removal and improving the performance and output power of a fuel cell through switching between parallel and interdigitated flows as a function of fuel cell current density, taking into account pumping losses. It has been found that at a certain flow rate, the parallel flow increases the system power output under low current density operation. This is due to the fact that there is less water is produced and hence no need for an interdigitated flow which is found to be very effective at higher current density, leading to maximising the output power and improving the performance of fuel cells.

2.4 Managing and Controlling the Output Power of the Fuel Cell Stack

To enhance the performance of the power source that uses a fuel cell system, an electric storage device such as rechargeable batteries or super-capacitors must be connected in parallel with the fuel cell stack, in order to boost and improve the output power of the fuel cell system [9]. In particular, at high levels of power demand, the battery plays a vital role in providing a substantial portion of the requested load and improving the stack's response to dynamic load changes and protecting fuel cells from fuel starvation and membrane dehydration [8].

Lithium-ion rechargeable batteries have high energy to weight ratio and the ability to maintain charge levels, even when left without use for a long period of time. These properties promote this type of battery for common use as an auxiliary power source with fuel cell applications [20].

In a hybrid power system, where the fuel cell stack and batteries, with their individual characteristics, are connected in parallel, the dynamic response of the fuel cell system which is relatively slower than the batteries, would lead to an imbalance in the load and the DC bus voltage. Therefore, a DC-DC convertor needs to be installed in series with the fuel cell stack in order to regulate the output voltage of the stack, hence achieving a power balance with the batteries and optimising the system weight and size [20].

The technique of combining power sources is adopted for solving the problem of limitations associated with the single power source, such as low power density or a slow dynamic response. Therefore, multi-source or hybrid power systems are very common for stationary and mobile power applications. Practically, the configuration of multiple power sources requires multi-converter systems to synchronise and regulate the flow of power amongst these sources. [64].

Nishizawa et al. [9] proposed a passive hybrid system based on a two diode configuration used to connect the PEM fuel cell stack and the storage device directly to the DC bus. The hybrid system does not use any DC-DC power convertor which reduces the cost of the entire system and minimises electrical losses when compared to using the DC-DC convertor in the active hybrid system. However, in the passive hybrid system, it is important to follow a special operating procedure in order to avoid inconsistencies in the current-voltage behaviour of the fuel cell and the storage devices, such as batteries or super-capacitors.

Rodatz et al. and Thounthong et al. [12, 55] proposed in their control models of fuel cell power systems for hybrid vehicles, that in order to overcome the problem of reactant starvation, fuel cells must run near steady state conditions. The dynamics of the load must be limited to a conservative 2.5 kW/s in order to limit the current of the fuel cell. These must be supplemented by using super-capacitors to match the extra demand for power during transient modes. By applying real time control on the power distribution between the fuel cells and power storage system with respect to the changes in the current load, the fuel cell runs as the primary source of power, while the super-capacitors are sized to the peak level of power in order to:

1. Support the fuel cells during the transient hard acceleration and to overcome the sudden change in load demand and also to avoid the impact of fast changes in fuel cell current.
2. To avoid the mechanical stresses of the fuel cell system.
3. And to increase the lifetime of the fuel cell stack.

Jiang et al. [65] reported that for power sharing between fuel cells and batteries, the current of the fuel cell must be limited to a safe level. The charging current of the batteries must be controlled in order to achieve maximum fuel cell power output and

maximum efficiency. While, Nishizawa et al. [9] reported that operating a fuel cell stack at a zero load current must be avoided because this tends to damage the fuel cells.

In order to manage and balance the flow of power between the power sources and the load, and also to overcome the issue of slow dynamic response of fuel cells, Lapena-Rey et al. [20] reported that a throttle control input can be used to ensure that the steady state electric motor power demand is not higher than the available power, by reducing the motor request commands through a slew ramp limiter, in order to ensure a smooth change in the demanded power rate.

Chen and Khaligh [66] proposed the use of a Proportional-Integral (PI) controller to control the flow of currents between the load, fuel cell/electrolyser stack, and the rechargeable batteries for a hybrid energy storage system involving a solar photovoltaic panel with fuel cell/electrolyser stack and rechargeable batteries for an unmanned aircraft system.

Golbert and Lewin [5] examined the impact of a step change in the fuel cell voltage upon the cell power density. Setting up a steady state gain ($\Delta P/\Delta V$) as a function to the average current density, a fixed gain integral controller is used to determine the sign change of the steady state gain from negative to positive. However, this method leads to difficulty in stabilising the controller, and in order to avoid using a fixed gain controller with integral action, two alternatives are proposed:

1. using an adaptive controller, or
2. using a non-linear model predict control system (MPC).

In the second approach, the system order can be reduced and optimised to predict the behaviour of the system with acceptable accuracy. This is done by predicting the effects of past inputs on future outputs, with multivariable control improving the performance. However, as an adaptive controller depends on many variables (flow rates,

temperatures, etc.), it is difficult to design and function all of these inputs instantaneously, leading to restricted performance and robustness of the controller.

Zhong et al. [67] proposed an adaptive controller, which can trace the locus of the unique maximum power point (MPP) when the internal impedance of the fuel cell is equal to the load impedance. It does this by estimating the real time of the MPP to maintain fuel cell operation at the MPP and to continuously deliver the highest power to the load under various operational conditions, which reduces the entire system efficiency.

Verstraete et al [8] reported that in order to increase the efficiency of a self-humidified PEM stack, the controller developed by Horizon Energy Systems is connected across the stack output terminals. The controller short circuits the stack output every 10 seconds through a solid-state switch. During the short-circuiting process, load is disconnected from the fuel cells stack for about 50 ms, terminating the power to the load or to the stack's controller. Alternatively, to ensure providing continuous power, a lithium polymer battery is incorporated in the circuit. The stack's controller has a built-in capacitor to smooth the output power, but its capacity is insufficient to completely bridge the gap of the 50 ms short-circuiting process to ensure a constant power output.

2.5 Fuel Cells as a Power Source for Aircraft and UAS Applications

Fuel cell power systems offer several advantages for aircraft applications, for instance reduction of noise and harmful emissions, reduced ground support and maintenance, on-board water generation, and potential weight reduction [23]. In comparison with gas turbine or internal combustion engines, fuel cells have advantages of high specific energy (Wh/kg), high efficiency, low noise, low cost and weight, low thermal radiation, and are friendly to the environment. They are associated with the capability to be integrated with an efficient electrical rechargeable storage system which has promoted

interest and concern for fuel cells in aviation applications, as power-plants for aircraft and small to large scales of unmanned aircraft systems (UAS) for a wide range of endurances [10, 22, 68].

However, despite the remarkable advantages of fuel cells, fuel cell powered aircraft are generally characterised by low specific power (power to weight ratio – W/kg). Power to weight ratio is an important indicator of aircraft performance, for instance an overweight aircraft which is underpowered will have severe limitations in its performance. Therefore, to improve the performance of the fuel cell powered aircraft, several design measures must be adopted, such as low weight fuselage structure, high efficiency of airframes, high efficiency of the power-plant system, and low power payloads [26].

The propulsion system of an aircraft mainly requires a large specific power (W/kg) of fuel, in addition to a fast response, in order to fulfil the requirements of different flight phases and to balance the variations in load demand. Fuel cells suffer from limited power density and slow dynamic responses due to sudden changes in power demand, which limit their performance, particularly for UAS applications [8]. Moreover, the difficult operational conditions of high altitude flights where the ambient temperature and pressure are very low leads to distress in the operation of fuel cells, hence special measures and procedures must be taken in order to preserve the performance of the fuel cells [27].

The low level of energy density of the available commercial batteries, in comparison with fuel cells, limits the endurance of the UAS, while the high power densities of these batteries are ideal for a short duration of peak power demand. Moreover, the high energy density of a fuel cell enables it to play a significant role in extending flight endurance. Therefore, a hybrid system in which a fuel cell stack is combined with rechargeable batteries associated with a sophisticated controller system can offer

advantages in operating and extending the endurance of an unmanned aircraft system [8, 53].

Barbir et al. [31] reported that the cycling efficiency of charging and discharging the existing rechargeable battery system is about 80%, while the achievable efficiency for a regenerative cycle of fuel cells (i.e. electricity and water to H_2/O_2 , and vice versa) is much lower than the battery system. The operating life of a battery is very limited under continuous daily usage; also a battery is a heavy component. Therefore, the use of batteries in aerospace applications is very limited, if the weight of the aircraft is an issue of interest. A regenerative fuel cell system can provide an alternative solution in achieving higher specific energy densities in comparison with rechargeable batteries.

Fuel cells can be used as a prime source of power for small-sized aircraft, and may also be used as an alternative reliable source of power to the auxiliary power unit APU (i.e. batteries) typically used on board large-sized aircraft. Reliability, performance, weight, and size reduction of the fuel cell system are very important factors for the operation and safety of electrical powered aircraft [19]. Solid oxide fuel cells (SOFCs) use hydrocarbon fuel at high temperatures to produce a power density higher than PEM fuel cells, which have an advantage of low operating temperatures, thus promoting PEM fuel cells to be widely used in aircraft and for long endurance UAS [24, 26].

Lucken et al. [23] recommended a parallel connection of several fuel cell stacks in order to maintain reliability and to increase power availability on the common electrical DC bus of the power system of the aircraft. This enables the controller to distribute the load demand equally among the fuel cell stacks, and to detect and reconfigure the failure among them, hence increasing the durability and reducing the maintenance cost. However, in order to integrate fuel cell power systems into the electrical network of modern aircraft, smart safety arrangements have to be developed to protect the entire network from power failure as a result of fuel cell system failure.

Most published work has focused on aircraft development and presented limited results on the flight test performance of propulsion systems. There is a lack of research in the investigations of the dynamic and steady state behaviour of the fuel cell power source and the performance of integrated hybrid power system of fuel cells and batteries for unmanned aircraft systems [8].

2.5.1 Fuel Cells for Aircraft

Nishizawa et al. [9] proposed a design method of a direct hybrid system to be used for aircraft applications. A direct hybrid system consists of a PEM fuel cell stack, Li-ion batteries and two diodes which offers the ability to directly connect the fuel cell stack with the batteries, and recharge the batteries without the need to use a DC-DC convertor. The first diode connected in series with the battery pack protects the batteries from reverse charging, while the second diode connected in series with the fuel cell stack in order to protect the stack from the reverse current produced by the potential difference on the load terminals. The steady state and dynamic behaviours of the hybrid system were monitored and indicated an increase in the operational efficiency of the system, while the delay in fuel cell output response in providing the required level of current was compensated directly through the batteries.

Lapena-Rey [20] developed a small manned airplane powered by two stacks of PEM fuel cells connected electrically in series to generate 200 V, 24 kW. This system drives a brushless DC motor and other support units such as an air compressor and humidifier. A 350 bar pressurised hydrogen tank is used to supply the required fuel, and air compressor to provide the required oxidant. During the cruise phase, the PEM fuel cells act as the only source of power, while during take-off and climbing the rechargeable Li-ion batteries act as an auxiliary power source to boost the generated power from the PEM fuel cells. A throttle control is used to manage and to balance the power flow

between the power sources and the load. This methodology also overcomes the issue of the slow dynamic response of fuel cells. The scheme also prevents the steady state electric motor power demand from being higher than the available power, by reducing the motor request commands through a slew ramp limiter in order to ensure smooth power change rates.

Correa et al. [19] presented an analytical model of a 20 kW PEM fuel cell power system for an ultra-light aircraft. The model predicts the temperature dynamics of the system as a function of ambient air temperature, and the generated heat by the stack which is a function of the electrical power demand. Uncertainty/sensitivity analysis is implemented in order to identify which components affect the reliability and the safety of the system, with a focus on evaluation of the system's uncertainty due to uncertain signals of temperature sensors, which are considered to be input parameters to the control system. Hence, any malfunction or error in one of these sensors will lead to instability in the control loops and cause damage to the fuel cell stack. Sensitivity analysis for the system shows that the sensor signal of the cathode inlet temperature has the highest impact on the stack temperature, while the sensor signal of the coolant inlet temperature to the stack shows the highest impact on the energy balance of the fuel cells, and therefore, a great influence on the stack temperature control.

Barbir et al. [31] proposed the use of a unitised regenerative PEM fuel cells system (URFC) using oxygen and pure hydrogen for aerospace applications. URFC can be operated as an alternative to the fuel cell to generate DC power, or as an electrolyser to produce hydrogen and oxygen and compress it to the storage tanks. The URFC system is integrated with a photovoltaic array. The performance and the efficiency of both the electrolyser and the fuel cell are determined according to their polarisation curves. Maximum roundtrip efficiency for the unitised regenerative fuel cell system is about 34% when the effect of the parasitic losses is considered, and 43% for an ideal case. The

efficiency for both the fuel cell and the electrolyser is a function of the size and weight. The analysis shows no significant advantages between a unitised regenerative fuel cell system and a separate regenerative fuel cell system (i.e. two stacks work individually, one as a fuel cell and a second as an electrolyser). The unitised design would offer lower stack weight, while a separate design would offer better stack efficiency.

Radmanesh et al. [6] proposed a hybrid power-plant system composed of a 240 W PEM fuel cell stack, DC-DC and DC-AC converters, ultra-capacitor, electrolyser and hydrogen tank, and multiple controllers. A PID controller is used to regulate the system; the output voltage is at 48 V via controlling the flow rate of hydrogen and oxygen. The proposed hybrid power system is intended to replace the auxiliary power supply generator for a C-130 Hercules aircraft that has several disadvantages of high cost, maintenance issues and a high rate of failure. The results showed that using fuel cells as an electrical backup system improves the reliability of the electrical system and the flight performance of the aircraft.

2.5.2 Fuel Cells for UAS

In the last few years, small numbers of successful flight tests of light unmanned aircraft systems (UAS) powered by fuel cells have been reported. However, most of these tests were restricted to short duration low altitude flights [28].

Bradley et al. [22] categorised the power supply system of UAS into fuel cell power-plant and fuel cell subsystem. A fuel cell power-plant consists of a fuel cell stack, air and hydrogen supply, regulating systems, and a cooling system. While, a fuel cell subsystem consist of an electrical distribution bus, and power management system.

Kim et al. [7] developed a hybrid power system that consisted of a 100 W PEM fuel cell (H-100) from Horizon Fuel Cell Technologies combined with a hydrogen generator system. The system also included a DC power management unit with auxiliary lithium

batteries in order to improve the flight endurance for a UAS. Hydrogen gas is produced from a catalytic hydrolysis of an alkaline solution of sodium borohydride (NaBH_4) and cobalt alumina as a catalysis. The proposed prototype small plane was designed to be launched by hand with a gross weight of 2.5 kg including fuel. The performance of the hybrid power system was evaluated in terms of measuring the performance of the hydrogen generation rate and the output power of the fuel cell. The performance of the UAS and power system was evaluated based on performing two and a half hours of ground flight tests and two hours of low altitude (30 m) flying test. It was found that the fuel cells system is more efficient in extending the endurance of the UAS in comparison with lithium batteries, and the fuel cell stack must be operated with dead-ended anodes using a purge valve to maintain stable stack performance, instead of open-ended anodes. Kim and Kwon [24] adopted the system of a PEM fuel cell combined with a hydrogen generator proposed by Kim et al. [7] as an alternative source of power to the existing batteries. About 42% of the weight of the fuel cell stack was reduced after certain modifications involving replacing the aluminium end plates with lighter materials. A steady state power output was at a constant load of 50 W for five hours. The total combined weight of the fuel cell stack and the hydrogen supply system was about 45.5% of total the aircraft's weight, which was 2.2 kg. However, the authors did not consider the impact of the temperature and air density changes due to the changes in altitude. Moreover, the process of extracting hydrogen was performed in the laboratory under normal room temperatures, where the impact of low pressure-temperature on the performance of the hydrogen generator was not considered.

Huang et al. [69] developed a design involving a 300 W PEM fuel cell stack integrated with a sodium borohydride (NaBH_4) based hydrogen generator. The stack of 15 cells, each of 140 cm^2 active reaction area, was built in a configuration of combined inlets of cathodes with two air fans for air supply and stack cooling and open-cathode outlets.

The reactant solution consisting of 20 wt.% NaBH₄ and 3 wt.% NaOH was pumped into the structured catalyst at a constant flow rate using a liquid pump. The conversion efficiency of the hydrogen generator was found to be 87%. It was found that the performance and power output of the fuel cell using hydrogen extracted from NaBH₄ hydrogen generator was the same as produced from a conventional pressurised hydrogen cylinder. The hydrogen produced from a sodium borohydride based hydrogen generator contains saturated water vapour, hence does not need further humidification before entering the fuel cell stack, which could offer a quick start-up in comparison with the dry hydrogen from a gas cylinder that requires humidification.

Semiz et al. [59] proposed performance optimisation for a manufactured air bearing PEM fuel cell producing 150 W for an unmanned aircraft system application. Air fans supplied the air to the cathode, while hydrogen gas was generated from the reaction between sodium borohydride and the catalyst. It was found that rate of hydrogen production depends mainly on the catalytic activity of the catalyst rather than the concentration of the sodium borohydride solution. However, there is a threshold catalyst concentration for the maximum available reaction rate; hence increasing the concentration of the catalyst above this threshold does not increase the hydrogen production. It was observed that the stack could provide 165 W continuously for four hours without any noticeable decline in its performance, which is considered an encouraging outcome in deploying PEM fuel cells as a prime power source for UAS applications. However, the fuel cell stack tests were carried out under normal room temperatures and pressure and did not consider the performance of a PEM fuel cell at high altitude operation.

Seo et al. [61] designed and developed an advanced ammonia borane-based hydrogen (NH₃BH₃) power pack to continuously drive an unmanned aircraft system, using a 200W PEM fuel cell stack. The power pack was developed to produce pure hydrogen

with an average flow rate of $3.8 \text{ L}\cdot\text{min}^{-1}$, auto-thermal H_2 released from ammonia borane with tetra ethylene glycol dimethyl ether as a promoter. During take-off, a hybrid power system consisted of the fuel cell stack, an auxiliary lithium-ion battery, and a controller used to supply the full power of 500 W to launch the UAS, having a maximum total weight of 7.5 kg. The fuel cell stack provided 180-200 W of the required power. The proposed UAS was flown up to 200 m altitude with cruising speed of 60 km/hour. The obtained results showed the ability of the power pack to continuously drive the UAS for 57 minutes. The fuel cell stack with the power pack production system was found to efficiently provide extra power to recharge the auxiliary battery during the cruising phase. The stack controller was responsible for controlling the rotational speed of the air fans and hydrogen purging valve, in order to manage the stack temperature and to build-up hydrogen pressure in the anode. However, the work ultimately focused on enhancing the continuity and the rate of hydrogen generation from the reactor for powering a 200 W PEM fuel cell stack.

Bradley et al. [26] proposed a 500 W, 32-cell self-humidified PEM fuel cell as the main and only source of power for an unmanned powered aircraft with a 310 bar compressed hydrogen tank, which provides 0.192 m^3 storage volume capacity. The power-plant for the aircraft is composed of a fuel cell stack, thermal management system, air and hydrogen management system, hydrogen storage, and controller units. The fuel cell stack provides power to the propulsion system through the DC bus. The propulsion system consists of an electric motor, motor controller, and a propeller. The performance of the entire system, using data captured from the flight and the laboratory tests, was analysed and indicated an improvement in the system performance. However, the proposed aircraft system was designed without consideration to the payload or endurance requirements. Also, to overcome the problem of a very low power to weight ratio for the fuel cell aircraft, when compared to conventionally powered small aircraft,

the entire proposed fuel cell powered aircraft is designed to be operated at a low speed, stable altitude flight level, with slow manoeuvrability. Moreover, the proposed aircraft was tested at 30 m maximum flying altitude, and for less than three minutes total flying time.

Furrutter and Meyer [53] proposed a design of a power-plant system as a prime source of power for a small-scaled fixed wing UAS, using a 100 W PEM fuel cell developed by Horizon Fuel Cell Technologies, to provide enough power to maintain a steady and stable flying level. The total weight of the demonstrated aircraft was 5.3 kg with 13 m/s maximum flight velocity. The lightweight aluminium vessel, weighing 0.255 kg, was filled with 30 bar pressurised hydrogen enough for nine minutes of flying time. The aircraft was tested at approximately 100 m cruising altitude, and the tests showed that the power delivered by the fuel cell stack was sufficient to maintain level flight at the required altitude with limited manoeuvrability.

Verstraete et al. [8] proposed an advanced hybrid AeroStack power system developed by Horizon Energy Systems; the power-plant system comprised a 200 W self-humidified PEM fuel cell stack and its controller, lithium-polymer battery, and power management board to enable higher endurance for a small electrical powered UAS. A series of tests were done to characterise the hybrid power-plant system. The results demonstrated a considerable difference between the dynamic and steady state performances of the fuel cell power system. At high power demand, the battery plays a vital role on the stack's response to the dynamic load changes and protects the fuel cells from fuel starvation and membrane dehydration, by providing a substantial portion of the requested load. The controller protects the stack from operating at levels of high concentration losses, and fuel utilisation of the stack was set above 90% when the load varied from 50 W to 200 W. Electrical efficiency of more than 50% was obtained for this power range.

Aguiar et al. [10] proposed a solid oxide fuel cell combined with gas turbine as an alternative power system for a high altitude long endurance (HALE) UAS. A liquid hydrogen tank was used to supply hydrogen in the form of gas to the fuel cell stack. Different system configuration models were investigated to improve the efficiency and reducing the fuel consumption to achieve a one-week operational endurance target. It was found that the configuration of connecting three separate fuel cell stacks in parallel and feeding fuel distribution in parallel, while the air is fed in series increases the system efficiency in comparison with a single stack configuration with the same power capacity. It was observed that a power system composed of a single stack has the ability to achieve efficiency of 54.4% (LHV) by using a large air compressor to cool the stack. System efficiency of 66.3% (LHV) was achieved for a three stacks system. This increase is primarily due to the use of air intercoolers between the three stacks system configuration which leads to a reduction in system losses and improves the overall efficiency.

Cooley et al. [64] explored and investigated the feedback control designs and the linearization of a converter for a hybrid solid oxide fuel cell stack for electrically propelled UAS. The technique of combining power sources was adopted for overcoming low power density or slow dynamic response power characteristics associated with a single power source. Therefore, multi-source or hybrid power systems are very common for stationary and mobile power applications. Practically, the configuration of multiple power sources requires a well-controlled multi-converter system to synchronise and regulate the flow of power amongst these sources. However, feedback regulated multi-converter systems impose several design challenges.

Chen and Khaligh [66] proposed a hybrid energy storage system, consisting of a solar photovoltaic panel with fuel cell/electrolyser stack and rechargeable batteries as an alternative power source to a conventional fuel-powered internal combustion engine, in

order to extend the endurance of UAS. During the day, the PV panels are the main source of power to drive both the UAS and the electrolyser. The produced hydrogen is stored in order to be consumed by the fuel cells during night operation. The rechargeable batteries compensate any fluctuations in the power demand of the hybrid power system during day and night operation. During night operation, air is extracted from the ambient source and fed to the electrochemical reaction of the fuel cell stack. It is considered that the peak load demand is more critical than expanding flight endurance, hence maintaining the full charge level of the batteries, particularly during day operation is a higher priority than supplying power to the electrolyser to generate sufficient hydrogen for night operation. A Proportional-Integral (PI) controller is used to control the flow of currents between the load, fuel cell/electrolyser stack, and the rechargeable batteries. The power demand of the load during steady state cruising is 500W, while the peak power demand for 2.5 hours for the taking off mode is 800 W. However, the proposed work did not determine by any means the implications of the volume and weight of hydrogen gas and its storage vessel, or the overall weight of the UAS with 8 m² of photovoltaic panels.

Verstraete et al. [70] presented a series of tests that are used to characterise the role of the battery and power-management system for a hybrid AeroStack Horizon Energy System, combining a battery and a fuel-cell-based propulsion system for small unmanned aircraft systems. The obtained results demonstrate that the battery plays a vital role on the response of the system to the dynamic changes of the load; the system response is highly influenced by the storage capacity of the battery and the rate of current. Also the results showed a limitation in the charging process of the battery, as the power-management board of the AeroStack can only recharges the battery to 70% of its capacity, for about 2 hours of a continuous charging. As the charging process

requires more fuel to be consumed by the fuel cells, a compromise is needed between the charging capacity of the battery and the whole endurance of the mission.

Omar [71] presented an experimental study to investigate the performance of the hybrid power system for low flying altitude of a small UAS PiperCub J3 aircraft. The power system consisting of a combined 1.2 kW Nexa PEM fuel cell stack and 12 volt rechargeable lead acid batteries, as a main source of power to drive an electric DC motor. The flight scenario was designed in order to enable the aircraft to climb to the altitude of 10 m and perform 30 m radial circling mission before landing, for a total flying time of 5 minutes. The results of the experiments revealed that the hybrid power system can fulfil the requirement of the power demand for different flight phases (take-off, climb, cruise, descent, and landing), with a fuel cell stack efficiency of 38% and total consumption of hydrogen of 48.5 litres, while a maximum power demand occurred during take-off and climb.

2.5.3 High Altitude Long Endurance UAS

Long endurance UAS has attracted more attention and interest among the aerospace community because of the capability to accomplish a variety of tasks and missions, such as surveillance and exploration, targeting and remote sensing for both commercial and military applications. In comparison to space satellites, unmanned aircraft systems exhibit lower costs, faster cycle times of missions, and high adoptability [22, 26].

A long endurance flight is identified as a main flight performance characteristic for a UAS [72]. However, in recent years, there has been an increase in focus on the design of a combined system of solar array and hydrogen fuel cells for very long endurance UAS applications [73].

Several restrictions and challenges exist in the use of small scale UAS, particularly for environmental remote sensing [74]:

- Structure of small scale aircraft.
- Low weight and narrow centre of gravity margins.
- Limited energy and power density of the on-board power sources.
- Harsh flying environment and safety regulations.

High altitude long endurance (HALE) unmanned aircraft systems are typically designed to fly at altitudes between 15 and 20 km, cruising at low speeds and circling the area of interest. They play a vital role in providing high-resolution surveillance due to their closeness to the earth. A HALE UAS needs to have a lightweight, high lift-low drag, low power consumption, and highly efficient propulsion and power system, in order to increase the mission endurance. Eliminating the mechanical couplings between the propulsion system and the power generation system would lead to enhancing the overall efficiency of the system and hence extending its endurance, as the privilege of deploying a fuel cell power system in comparison with turbo jet and combustion engines [10, 73].

Flight endurance is an important factor in improving the performance of the mission; higher energy density and efficiency of the power supply system are very important in increasing flight endurance of the UAS [7].

Due to the low efficiency of gas turbines and reciprocating engines, particularly for small scale UAS, batteries are used as a secondary power source. The energy density (i.e. energy capacity per unit volume or weight) of the available batteries is too low to power a small UAS to have long endurance. A lithium polymer battery can provide energy of (200 W-hr/kg), which can offer an endurance of 60-90 minutes for a small UAS. A hydrogen fuel cell system has high energy density and is more efficient in extending the endurance of a UAS in comparison with lithium batteries, hence can be considered as an ideal power alternative to existing batteries [7, 24, 53].

The UAS consumes more power during take-off and climb than in cruise mode. Combining fuel cells and rechargeable batteries in a configuration of hybrid propulsion systems offers a significant increase in the UAS endurance, where the fuel cell is normally used for cruise flight, while the auxiliary batteries provide the additional power required for taking-off, climbing, and the increase in power demand of transient loads [7, 68]. The take-off phase is considerably shorter than the cruise phase. The batteries can provide maximum power and then during cruise the fuel cell can recharge the batteries [9].

Romeo et al. [73] reported that continuous flight for several months is possible, using an integrated closed loop power system, composed of a solar array that is used during the day time to generate the required power to drive the plane's electric motors. Excess power is used to run the electrolysis unit that generates a sufficient amount of oxygen and hydrogen, in order to store it in pressurised form and re-use it during the night through the fuel cell stack. The water produced from the fuel cells is stored and re-used again during the day by the electrolyser.

Renau et al. [28] presented a study to determine the capability of a small UAS, under specific aerodynamic characteristics, powered by an electric motor and light PEM fuel cell stack with a power capacity of 650 W and current of 36.58 A, to reach a service ceiling of 10 km, carrying on-board the required amount of hydrogen and oxygen. A small and light UAS was used, with a total airframe mass of 3 kg, a 4 m wing span and 0.8 m² surface area, which offers a maximum UAS mass up to 16 kg, where 9 kg corresponds to the fixed elements and only 7 kg is available for the carried payload and oxygen-hydrogen storage cylinders. To simplify the calculations, the UAS is assumed to move along two axes only (x and z), in order to determine the minimum required power for the flight to fly at a certain horizontal altitude, where thrust is equal to the drag and lift is equal to the UAS weight. Moreover, due to the losses caused by the DC-DC

converter, electric motor, transmission, and the propeller, the total efficiency of the power-plant is assumed to be equal to 65%, hence net power of 422.5 W was supplied to the propeller. At a maximum power capacity of 650 W, the total consumption of hydrogen is (55 g/h) and oxygen is (436.7 g/h), as determined based on the theoretical specific reacted amount of hydrogen and oxygen per cell, which were found to be (0.0376 g/A.h) of hydrogen and (0.2985 g/A.h) of oxygen with respective stoichiometric factors of 1.0 and 1.2.

In order to ascend to 10 km, two different flight strategies were proposed by the authors [28]: first, an ascending strategy based on a constant climb rate of 0.88 m/s and variable power supply; hence the climb angle is decreased with altitude as the velocity increases due to the change in air density. Consequently, the required power of the propeller will increase from about 300 W at sea level to 422.5 W at maximum altitude. It has been observed that the task required 2.8 hours and energy of 1200 Wh with a fixed volume of hydrogen to reach a maximum altitude slightly below 9.5 km.

Second, an ascending strategy based on constant propeller power of 422.5 W and variable climb rate, which decreases with the climbing altitude from 1.5 m/s at sea level to 0.88 m/s at 10 km. It has been observed that the task required 2.2 hours and energy of 930 Wh for the same fixed volume of hydrogen as at a climbing rate of 0.88 m/s to reach above an altitude of 10 km. Hence, the required mass and volumes of hydrogen and oxygen for 2.2 hours of operation are determined to be equal to 121 g (1,346 L) of hydrogen (equivalent to 2.7 L under compression pressure up to 500 bar), and 960 g (672 L) of oxygen (equivalent to 1.34 L under compression pressure up to 500 bar).

A storing gas cylinder with dome ends, with filament winding and plastic liner wrapped with composites over the entire sidewall, is selected to store 500 bar pressurised gas. The hydrogen cylinder storing capacity is up to 4 L and has a gross weight of 1.91 kg.

The oxygen cylinder storing capacity is up to 2 L and has a gross weight of 1.84 kg (i.e. mass of empty oxygen cylinder is 0.88 kg).

However, from the presented results in [28]; it is clear that these calculations are valid for a fuel cell stack under the assumption of a theoretical reaction amount of hydrogen and oxygen, and no consideration has been given to the changes in the thermodynamic properties of the gases inside the stack and the manifolds upon the performance of the stack. Also, the proposed UAS is limited by specific aerodynamic characteristics (as the airplane is allowed to be displaced along only x and z axes, for a maximum mass of 16 kg with a maximum climb rate of 1 m/s), where any climb rate above this value will need further power from the propeller, which is higher than the power capacity of the fuel cell stack. Moreover, no valid justifications have been shown regarding the selection of a small mass of storing cylinders under the proposed high compression pressure of 500 bar, neither are there calculations to determine the total mass of UAS and the required volumes of hydrogen and oxygen for cruising operation.

Barroso et al. [75] proposed using a high temperature PEM fuel cell stack under operating temperatures above 140 °C for small and light UAS capable of ascending to an altitude of 10 km, in order to overcome the low atmospheric temperature (below -50 °C) at high altitudes. Heat transfer coefficients were determined in order to identify the optimal design of cooling system to cool the stack down to the recommended temperature of the manufacturer. However, the proposed cooling system will add extra weight and complexity to the entire system and will consume more power from the fuel cell power-plant.

2.6 Other Applications for PEM Fuel Cells

Shih et al. [54] proposed a hybrid PEM fuel cell stack with batteries as a prime and silent source of power for air-independent propulsion for an underwater vehicle for

naval operations. The power-plant system consists of a 1 kW fuel cell stack, oxygen and hydrogen cylinders, four lead-acid batteries, water cooler, pressure and temperature sensors, solenoid valves, and an operational controller. Results of the tests confirm the feasibility and the functionality of a PEM fuel cell power system for underwater vehicle operation with a maximum cruising speed up to 1.05 knots. Moreover, it has been found that there is a significant power increase of up to 32% from the fuel cell stack fed by pure oxygen in comparison with a stack fed by atmospheric air.

Khan and Iqbal [76] proposed and developed a model of a small wind-fuel cell hybrid power system, using a PID controller to control the fuel cell system. While, Kim et al. [77] designed and assembled an ultra-compact direct hydrogen PEM fuel cell system as an alternative power source for a Li-ion battery in a mobile phone. The fuel cell system consists of eight thin PEM fuel cells, and an air-breathing planar stack which has a total volumetric power density of 335 W/L. The hydrogen tank has a storage capacity of 4 L in an 8 ml tank volume, a tiny pressure regulator, and a high efficiency DC-DC voltage convertor circuit. The fuel cell system provides an estimated energy density of about 205 Wh/L which is sufficient to provide approximately six hours of continuous voice calling.

2.7 Summary

A critical review of the literature considering the related aspects took place in this chapter. Many developed models of PEM fuel cells reported in the existing literature were reviewed and presented. Operation of the fuel cell under steady and transient states of load variations was discussed. The effects of the flow rate of air-hydrogen, the pressure of the supplied fuel and reactant, the stack temperature, management of the produced heat and water as a result of the electrochemical reaction, and also proper hydration of the membrane were outlined and presented.

Different techniques for managing and controlling the output power of the fuel cell stack and managing operational variables of the PEM fuel cell were presented. Moreover, the deployment of fuel cells as primary or auxiliary power sources for aircraft and UAS applications was presented with a greater focus on UAS applications.

Although many of the fuel cell models are available in the literature, most of these models estimate the output voltage of the fuel cell for a particular set of operating conditions and some often for limited dynamic variations. But, developing a PEM fuel cell model that considers the major electric and thermodynamic variables and parameters involved in the operation, and taking into the consideration the impact of environmental conditions during fuel cell operation, is an important objective.

Most published work has focused on aircraft development and presented limited results on the flight test performance of propulsion systems. There is a lack of research in the investigations of the dynamic and steady state behaviour of the fuel cell power source and the performance of integrated hybrid power system of fuel cells and batteries for unmanned aircraft systems. Moreover, most of the research literature focuses on the design of hydrogen vessels for low altitude and low speed UAS applications, and for supplying air extracted directly from the surroundings, hence no oxygen pressure vessel has been used in the application. At a high altitude of 11 km (~36,000 ft.), atmospheric temperature, pressure and density of air are very low, these are severe conditions for a fuel cell to operate. Also, published experimental data for such operating conditions are very limited, therefore air or oxygen pressure vessel becomes a most vital issue relating to providing sufficient oxygen to the fuel cell power system.

Furthermore, in the published literature to date, there appears to be no particular study that determines or specifies the size and weight of the combined power-plant of the fuel cell stack with hydrogen and air/oxygen vessels and the propulsion system of UAS for high altitude flight operation; or takes into consideration the power capacity of the fuel

cell stack and the flight endurance as the main factors in designing the size and weight of the storing vessels, and hence determining the overall weight of the UAS.

In the next chapter, the principle of the electrochemical reaction and the mathematical modelling of voltages for a PEM fuel cell will be presented, along with all related parameters.

Chapter Three: Modelling Voltages of the PEM Fuel Cell

3.1 Introduction

The steady state behaviour of the PEM fuel cell can be predicted through estimating the equilibrium cell voltage for a particular set of operating conditions, such as concentration of gases, associated pressures, operating temperatures and the drawn current. Transient behaviour is an important aspect, particularly when operating conditions change with time; such as starting up or shutting down, or when there is a large sudden change in the load current, accompanied with changes in the cell temperature or gas concentration on the surface of electrodes [36].

The output power of a fuel cell can be determined by predicting the cell voltage as a function of the operating current, stack temperature, flow rate and partial pressures of oxygen and hydrogen, as proposed in the model of Amphlett et al. [36]. While Mann et al. [40] proposed using dimensions of the electrolyte membrane, level of water content in the membrane, and the level of aging and degradation of the membrane with operating time.

Pukrushpan et al. [2, 32] proposed modelling the output voltage of the PEM fuel cell stack based on the parameters proposed by Amphlett et al. and Mann et al. [36, 40], and considered the impact of the two phases of water (vapour and liquid) in the gas diffusion layer and their impacts on the transport of gases on the performance of the fuel cell.

The impact of the water content of the electrolyte membrane and the drawn current densities on the membrane specific resistivity and the conductivity of hydrogen ions, and hence on the output power of the fuel cells under various pressures and temperatures have been determined in various models [40, 42, 43, 52].

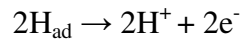
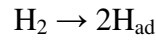
Although many of the fuel cell models are available in the literature, most of these models estimate the output voltage of the fuel cell for a particular set of operating conditions and some often for limited dynamic variations. But, developing a PEM fuel cell model that considers the major electric and thermodynamic variables and parameters involved in the operation, and taking into the consideration the impact of environmental conditions during fuel cell operation, is an important objective.

3.2 Principle of Electrochemical Reaction for the PEM Fuel Cell

A PEM fuel cell is a device that converts energy in the fuel and reactant into electrical DC power after a sequence of electrochemical reactions. When hydrogen and air (or oxygen) is continuously supplied to the fuel cell, the electrochemical reaction starts at the interfaces of the polymer electrolyte membrane [1]. At the anode side of the PEM fuel cell, hydrogen will be ionised in the existing platinum catalyst to release electrons and ions H^+ in a process called oxidation, each molecule of hydrogen H_2 will produce two free electrons and two positive ions (protons). The existence of the platinum catalyst is important to accelerate the reaction and reduce the activation energy. The mass of platinum in the electrode will not be depleted with time because it does not contribute to the reaction [16].

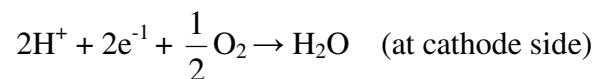
The protons and electrons are not produced immediately on the first instance of contact between hydrogen and the catalytic electrode. The process is more complicated and it passes through many stages. The H_2 molecule adsorbs on the surface of the electrode, the energy of the interaction between the hydrogen and platinum surface will contribute in

breaking the bonds between the hydrogen atoms. Hence, the hydrogen molecule is separated into two adsorbed hydrogen atoms (H_{ad}), and then each adsorbed atom will be dissociated into one electron and one proton, the equations below describe the adsorption and dissociation process [78].



The electrolyte membrane conducts protons to the cathode electrode, but it will not allow the electrons to be conducted through as the electrolyte has high resistivity toward electrons. Therefore, the electrons will flow as an electrical current to the connected load via the interconnections of bipolar plates [1].

At the cathode side, the oxygen reacts with the electrons and protons in the existing platinum catalyst to produce water in a process called a reduction [16]. The electrochemical reaction of the PEM fuel cell is exothermic and energy in the form of heat is released. The equations below represent the reaction.



The output power of the fuel cell depends on its current–voltage relationship at any operating point. The output voltage of the PEM fuel cell depends on the pressure and mass flow rates of fuel and reactant, operational temperature, relative humidity and concentrations of gases in the reaction interface, and on the level of water content in the electrolyte membrane. The output voltage drops when the current is drawn from the fuel cell, and also due to three main irreversible losses [5, 35]:

1. Activation losses.
2. Ohmic losses.
3. Concentration losses.

The magnitude of the output voltage of the fuel cell is less than the open circuit voltage due to the losses mentioned above.

Simplified models of relationships between the activation, ohmic, and concentration losses and the operating temperature, pressure, and concentration of oxygen are presented in various sources [35, 36].

It is important to understand the mechanisms of these losses and how they influence the design and operation of the fuel cell. There are various factors that can influence the output power of the PEM fuel cell. Amongst them is the design of an efficient stack system that maximises the output power for a range of operating conditions – a focus of much research.

3.3 Activation Losses and a Charged Double Layer

In electrochemical systems, the phenomenon of a charged double layer is fundamental. The charge layer builds up as a result of charge diffusion and charge collection, due to applied voltage across the fuel cell. Electrical voltage is generated due to the accumulation of electrons on the surface of the electrode and ions on the surface of the electrolyte. The rate of reaction is influenced by the density of the charges that are built. Thus, a part of the generated voltage will be lost in driving the electrochemical reaction responsible for moving the electrons to or from the electrodes [1].

The phenomenon of a charged double layer gives an explanation of why the activation overvoltage occurs. The collection of charges at the electrode/electrolyte interface forms a storage layer of electrical charges which act as an electrical capacitor and thus generate an electrical voltage. In this case, it is the activation overvoltage that results in slowing the electrochemical reaction at the electrodes surface. As a result of capacitive behaviour, if the drawn current from the fuel cell is increased, it will need more time to build up extra charge, and if the drawn current is reduced, it will take some time for the

charge (and its associated voltage) to dissipate. Therefore, activation overvoltage does not immediately follow the current in the way that the ohmic voltage drop does. The effect of this makes the voltage rise gently and smoothly, but fairly slowly to a new level in response to the change in current demand [1].

When a fuel cell is open circuit (i.e. no current drawn by the load), the rate at which electrons are being released at the anode and recombined with ions at the cathode will be the same, hence equilibrium occurs. The rate of the electron production at the anode or recombination at the cathode is called exchange current density. For a PEM fuel cell, the exchange current density at the cathode electrode is much smaller than its value at the anode electrode; sometimes 10^5 times smaller. Therefore, activation loss at the cathode is higher when compared with activation loss at the anode which can be ignored. Hence, a cathode's exchange current density is the most vital factor affecting activation losses. However, an efficient catalyst would increase the likelihood of a reaction, so that a higher current can flow without such a build-up of charges, and thus decreasing the activation loss [1].

In order to determine the impact of activation loss of cathode upon the output voltage of a PEM fuel cell, the empirical electrochemical relationship developed by Amphlett et al. and Mann et al. [36, 40] will be used, in order to determine the impact of temperature, concentration of oxygen, and the drawn current on the activation voltage loss, as presented by Equations (3.1) and (3.2).

$$V_{act} = \zeta_1 + \zeta_2 \cdot T + \zeta_3 \cdot T \cdot \ln(C_{O_2}) + \zeta_4 \cdot T \cdot \ln(I) \quad (3.1)$$

Where, T is the stack temperature in kelvin (K) which is nearly equal to cell temperature, I is the drawn current in ampere (A), C_{O_2} is the concentration of oxygen at the catalyst interface (mol.cm^{-3}), and ζ_n represents the empirical parametric coefficient based on the experimental data, which may vary from one stack to another, or one cell

to another, depending on the geometrical design and the materials used in the construction of a PEM fuel cell [35]. The values of ζ_n can be found from the experimentally determined data tables developed by Amphlett et al. and Mann et al. [36, 40].

$$\begin{aligned} \zeta_1 &= -0.944 \text{ V} & \zeta_3 &= 7.80 \times 10^{-5} \text{ V/K} \\ \zeta_2 &= 3.54 \times 10^{-3} \text{ V/K} & \zeta_4 &= -1.96 \times 10^{-4} \text{ V/K} \end{aligned}$$

The value of C_{O_2} in Equation (3.1) above can be determined based on Henry's Law [76].

$$C_{O_2} = \frac{P_{O_2}}{5.08 \times 10^6 \cdot \exp(-498/T)} \quad (3.2)$$

Where, P_{O_2} is the partial pressure of oxygen in the cathode of the fuel cell. The implementation of activation overvoltage in Simulink is shown in Figure 3.1.

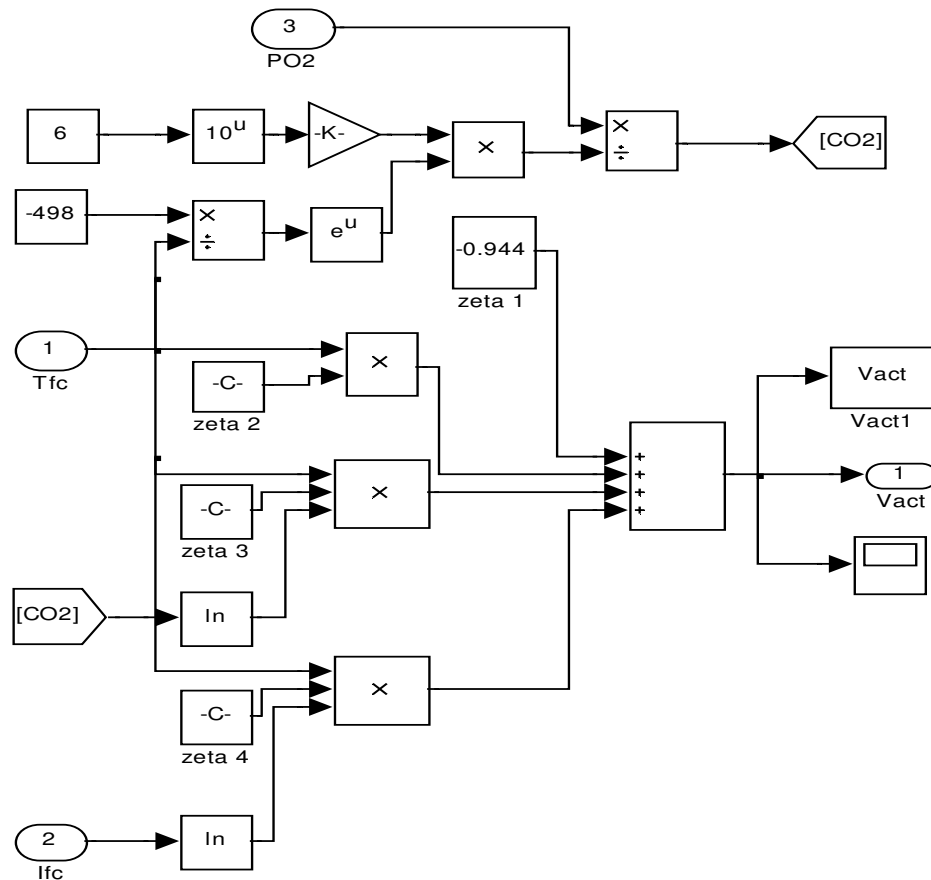


Figure 3.1: Simulink block diagram of activation overvoltage

3.4 Ohmic Losses

Ohmic losses are caused by two types of resistivity: the ionic resistivity of the electrolyte membrane towards the ion conduction and the electronic resistivity which is the resistance of both electrode materials and interconnections of bipolar plates towards the flow of electrons [1]. The electronic resistivity depends on the materials of electrodes and bipolar plates, and it is considered to be approximately constant, particularly over a temperature range 50 °C to 90 °C of PEM fuel cell operation, and hence can be ignored. Ionic resistivity is more complicated and is not constant over operating temperatures, because the resistance of the electrolyte to the conduction of ions depends on many factors, including material characteristics of the membrane, water content and its distribution in the membrane, fuel cell temperature, and drawn current from the fuel cell [40].

Theoretically, for PEM fuel cell, the flow of electrons is equal to the flow of ions. Therefore, the voltage drop due to ohmic losses is defined as the sum of electronic and ionic resistance losses.

$$V_{ohm} = -I \cdot (R_{ions} + R_{electrons}) \quad (3.3)$$

Where, I is the current drawn from fuel cell in ampere (A), R_{ions} and $R_{electrons}$ are the ionic and electronic resistivity in ohm (Ω), respectively. By ignoring electronic resistivity in order to determine the impact of membrane resistivity on the output voltage of the PEM fuel cell, Equation (3.3) becomes:

$$V_{ohm} = -I \cdot R_{ions} \quad (3.4)$$

The negative sign in Equation (3.4) represents a loss. Mann et al. and Wang and Wang [40, 52] developed an empirical model of ionic resistivity of the membrane R_{ions} as a

function to the membrane specific resistivity R_m (ohm.cm), membrane active area of the fuel cell A_{fc} (cm²), and thickness of the membrane L (cm).

$$R_{ions} = \frac{R_m \cdot L}{A_{fc}} \quad (3.5)$$

Where, R_m is a function of the cell temperature in kelvin (K), the current drawn from the fuel cell in ampere (A), membrane active area, and λ which is a semi-empirical variable, represents water content in the membrane. The value of R_m is not unique; it changes from one membrane to another based on the membrane dimensions and membrane preparation procedure.

$$R_m = \frac{181.6 \left[1 + 0.03 \left(\frac{I}{A_{fc}} \right) + 0.062 \left(\frac{T}{303} \right)^2 \cdot \left(\frac{I}{A_{fc}} \right)^{2.5} \right]}{\left[\lambda - 0.634 - 3 \left(\frac{I}{A_{fc}} \right) \right] \cdot \exp \left[4.18 \left(\frac{T - 303}{T} \right) \right]} \quad (3.6)$$

The parameter λ represents the number of water molecules per sulfonic group in the structure of the membrane (H₂O/SO₃⁻H⁺). At an ambient temperature of 30 °C and under the condition of equilibrium of saturated water vapour, the measured value of λ is 14 water molecules per sulfonic group [42]. The value of λ is influenced by: membrane fabrication processes, operation time (i.e. time being in service), cell relative humidity, and the stoichiometric ratio of the supplied gases [40].

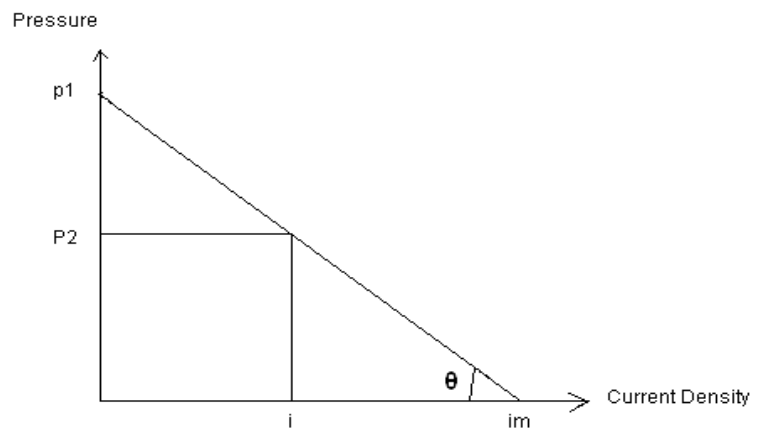
Values of λ are calculated equal to zero for a dry membrane, 14 for saturated, and 23 for supersaturated membrane. A higher temperature would dry the membrane and increase its resistivity to ionic conduction and hence increase the ohmic losses, unless water is added to the reactant gases to increase the water content in the electrolyte membrane [42, 52]. The implementation of ohmic overvoltage in Simulink is shown in Figure 3.2.

4. Diffusion characteristics of other components such as the gas diffusion layer and the electrodes.
5. Efficient recirculation of air around the cathode in order to remove the extra water.

At higher currents, if the flow rates of the reactant and fuel become insufficient to meet the requirements of the reaction rate, it leads to a decline in the concentration of the reactant and the fuel, hence a drop in the cell voltage. The process of providing sufficient flow according to the reaction rate is a design and operational challenge. Oxygen starvation occurs when the partial pressure of oxygen falls below a critical level at any location in the air channel of the cathode, this leads to a rapid drop in the cell voltage, which in severe cases can cause hot spots or burn the surface of membrane [2]. In order to determine the impact of drawn current upon the concentration losses, it is presumed that the drawn current density i ($A.cm^{-2}$) from the fuel cell cannot exceed the maximum current density i_m of the cell, and the gases cannot be supplied higher than the predesigned maximum flow rate. If P_1 is the pressure when the current density is zero (no current drawn), and by assuming that at maximum current density i_m , the pressure in the anode and cathode will fall linearly down to zero and the voltage will consequently drop sharply to zero as well, then the pressure P_2 at any current density i can be determined as given below [1]:

$$\tan \theta = \frac{P_1}{i_m} = \frac{P_2}{i_m - i}$$

$$\frac{P_2}{P_1} = \frac{i_m - i}{i_m} = 1 - \frac{i}{i_m}$$



By adopting the equation of open circuit voltage for a PEM fuel cell given by Larminie and Dicks [1], if the pressures for the hydrogen, oxygen, and the produced water are changed from P_1 to P_2 , then the voltage of the PEM fuel cell will change by the amount of ΔV , as given in the equations below:

$$V_{con} = \Delta V_{hydrogen} + \Delta V_{oxygen} + \Delta V_{water} \quad (3.7)$$

$$\Delta V_{hydrogen} = \frac{R \cdot T}{2F} \cdot \ln\left(\frac{P_{2,H}}{P_{1,H}}\right) \quad (3.8)$$

$$\Delta V_{oxygen} = \frac{R \cdot T}{4F} \cdot \ln\left(\frac{P_{2,O}}{P_{1,O}}\right) \quad (3.9)$$

$$\Delta V_{water} = \frac{R \cdot T}{2F} \cdot \ln\left(\frac{P_{2,H_2O}}{P_{1,H_2O}}\right) \quad (3.10)$$

Where, V_{con} is the voltage drop due to concentration losses, R is the universal gas constant (8.31441 kJ/kmol.K), T is the temperature in kelvin (K), and F is Faraday's constant (96485 coulombs/mol). By considering water pressure to be unity, and substitution of (3.8) and (3.9) in (3.7), yields Equation (3.11) after rearrangement, which describes the impact of concentration losses upon the output voltage of a hydrogen-oxygen PEM fuel cell when useful current is drawn from it.

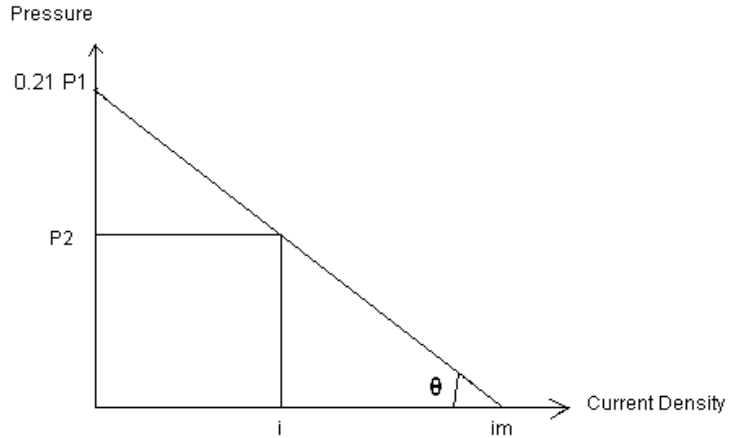
$$V_{con} = \frac{R \cdot T}{2F} \cdot \ln\left(1 - \frac{i}{i_m}\right) + \frac{R \cdot T}{4F} \cdot \ln\left(1 - \frac{i}{i_m}\right) = \frac{3R \cdot T}{4F} \cdot \ln\left(1 - \frac{i}{i_m}\right) \quad (3.11)$$

In the case of a fuel cell that is supplied with fresh air rather than pure oxygen, which is the most common, and in order to simplify our calculations, it is assumed that at maximum current density i_m , the partial pressure of oxygen in the cathode will fall

linearly down to zero and the voltage will drop sharply to zero as well. Air contains 21% oxygen, and the remaining 79% of the gasses do not contribute towards the reaction and will residue in the cathode chamber, hence the partial pressure of oxygen in the cathode at zero current drawn from the fuel cell is $P_{O_2} = 0.21 P_{air} = 0.21 P_1$. Then, the pressure P_2 at any current density i will be as given below:

$$\tan \theta = \frac{0.21 P_1}{i_m} = \frac{P_2}{i_m - i}$$

$$\frac{P_2}{P_1} = 0.21 * \left(1 - \frac{i}{i_m} \right)$$



By substituting the above in Equation (3.9) and by considering water pressure to be unity and rearranging for air, this yields Equation (3.12) which describes the impact of concentration losses upon the output voltage of a hydrogen-air PEM fuel cell when useful current is drawn from it, and it can be noticed that the concentration losses in the case of using fresh air instead of pure oxygen are remarkably higher.

$$V_{con} = \frac{R.T}{2F} \cdot \ln \left(1 - \frac{i}{i_m} \right) + \frac{R.T}{4F} \cdot \ln \left(0.21 * \left(1 - \frac{i}{i_m} \right) \right) = \frac{3R.T}{4F} \cdot \ln \left(1 - \frac{i}{i_m} \right) - \left(1.5607 * \left(\frac{R.T}{4F} \right) \right)$$

$$V_{con} = \frac{3R.T}{4F} \cdot \left(\ln \left(1 - \frac{i}{i_m} \right) - 0.5203 \right) \quad (3.12)$$

The implementation of concentration overvoltage in Simulink is shown in Figure 3.3.

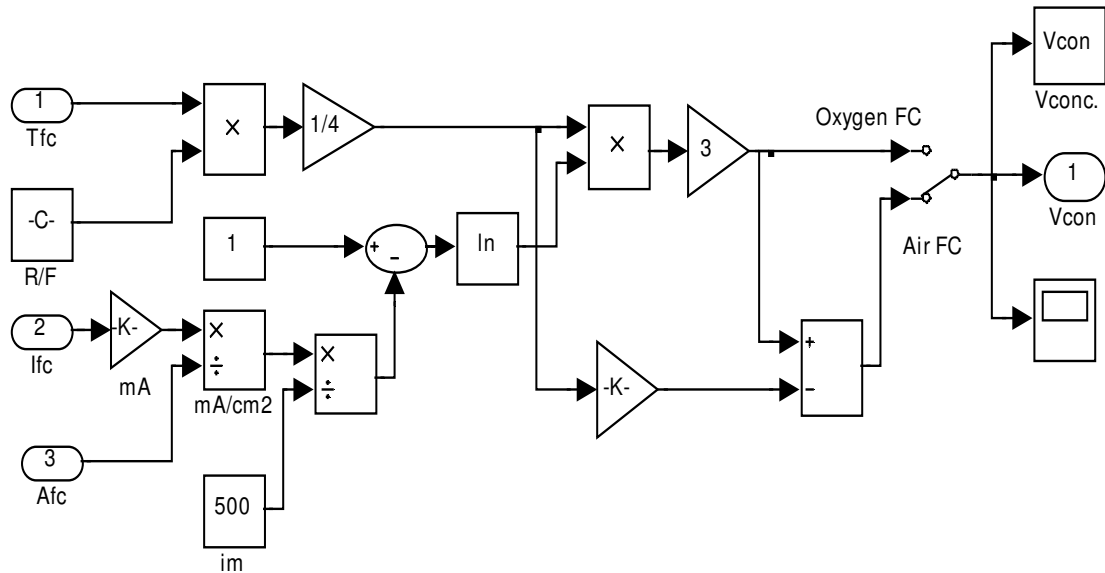


Figure 3.3: Simulink block diagram of concentration overvoltage

3.6 Total Losses of PEM Fuel Cell

The output voltage of a PEM fuel cell is subject to various losses which can be expressed by the equation below [1]:

$$V_{fc} = n * (V_{oc} + V_{act} + V_{ohm} + V_{con}) \quad (3.13)$$

Where, n is the number of cells connected in series in the stack, V_{OC} represents the open circuit voltage of the PEM fuel cell as it has been derived previously for a liquid state of water produced by the fuel cell and given by Saleh et al. [79]:

$$V_{oc} = 1.228 - (0.85 * 10^{-3} * (T - 298.15)) + (4.3086 * 10^{-5} * T * \ln(P_{H_2} * (P_{O_2})^{1/2})) \quad (3.14)$$

The implementation in Simulink for the open circuit voltage as given in Equation (3.14) is shown in Figure 3.4. While Figure 3.5 shows the fuel cell voltage model as given in Equation (3.13) for a single PEM fuel cell.

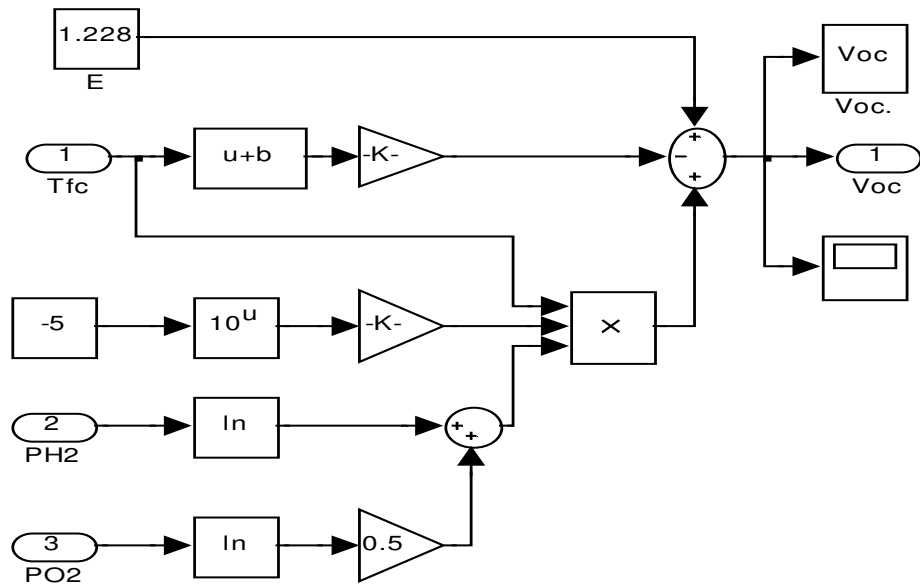


Figure 3.4: Simulink block diagram of open circuit voltage for a PEM fuel cell

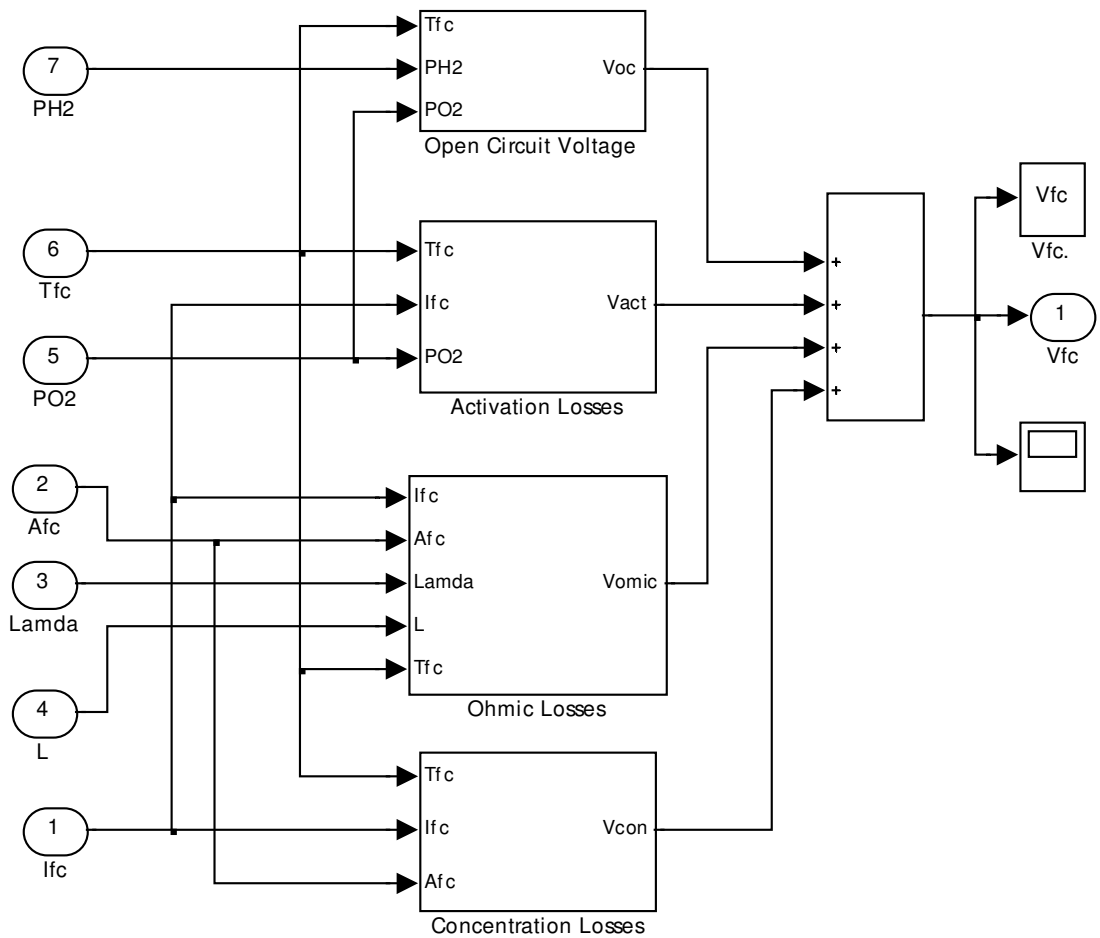


Figure 3.5: Simulink block diagram of voltage model for a single PEM fuel cell

3.7 Summary

In this chapter, the major variables and parameters related to the potential losses of the PEM fuel cell were identified, and their influence upon the operation, and hence, the performance of the PEM fuel cell. Impacts of load current, pressure and concentration of oxygen, cell temperature, level of water content in the electrolyte membrane, thickness of the membrane and the membrane active area on the performance and output power of the fuel cell stack were determined. Also, a modified equation was derived to determine the impact of using air to supply a PEM fuel cell instead of pure oxygen upon the concentration losses and the output voltage when useful current is drawn from it.

For a PEM fuel cell, the exchange current density at the cathode electrode is much smaller than its value at the anode electrode; sometimes 10^5 times smaller. Therefore, activation loss at the cathode is higher when compared with activation loss at the anode which can be ignored. Hence, a cathode's exchange current density is the most vital factor affecting activation losses.

The electronic resistivity depends on the materials of electrodes and bipolar plates, and it is considered to be approximately constant, particularly over a temperature range 50°C to 90°C of PEM fuel cell operation, and hence can be ignored. While, ionic resistivity is more complicated and is not constant over operating temperatures, because the resistance of the electrolyte to the conduction of ions depends on many factors, including material characteristics of the membrane, water content and its distribution in the membrane, fuel cell temperature, and drawn current from the fuel cell.

The failure in maintaining the required mass flow rate of reactant and fuel to reach the electrode interface will lead to a drop in the concentrations and consequently cause drop in the cell voltage.

In the next chapter, the major thermodynamic variables and parameters involved in the operation of a PEM fuel cell will be modelled. The impact of influencing environmental conditions during fuel cell operation will be considered, along with the incorporation of the effects of different dynamic conditions, such as changes in the dynamical properties of the fluids in the supply-return manifolds, and inside the anodes and cathodes of the PEM fuel cell stack will be determined and modelled.

Chapter Four: Mathematical Modelling of Gases Flow in the PEM Fuel Cell

4.1 Introduction

The flow rate of fuel along with that of air/oxygen needed for reaction, and temperature are the most vital dynamic properties of the PEM fuel cell, and prediction of the transient dynamics will help in analysing the behaviour of the system at the design stage and developing a reliable and efficient control strategy [11].

Yuan et al. [45] determined the impacts of operating parameters such as operating pressure, cell temperature, relative humidity of reactant gases, and air stoichiometric ratio on the performance of PEM fuel cells operating under steady-state conditions for a three-dimensional multi-phase fuel cell model. While, del Real et al. [46] attempted to predict the steady and transient responses for a dynamic model of a 1.2 kW PEM fuel cell due to load changes associated with the impacts of water flooding and purging hydrogen.

Yousef et al. [48] proposed a zero-dimensional lumped model of PEM fuel cells to determine the impacts of various operating and design parameters, such as input temperature, pressure, stoichiometric ratio, thickness of membrane and gas diffusion layer on the performance of the fuel cell. While, Pasricha and Shaw [50] proposed the impact of temperature on the performance of a fuel cell in the simple dynamic electrical model of a PEM fuel cell.

Golbert and Lewin [5] developed a time dependent model of a fuel cell to consider the heat transfer between the fuel cell body, gas channels, and the cooling water, with determining the condensation and evaporation rates. Also, they modelled the water content, water dragged through the membrane, and water at the cathode.

The stack of PEM fuel cells must be operated with other components in order to form an integrated fuel cell power system. These components are mainly divided into four systems as reported by Pukrushpan et al. [80].

- Hydrogen supply system.
- Air supply system.
- Cooling system.
- Humidification system.

A fuel cell stack model can be sub-divided into five interacting sub-models:

- Stack voltage model.
- Manifold flow model.
- Cathode flow model.
- Membrane hydration model.
- Anode flow model.

The stack voltage model was presented in Chapter Three, while other four sub-models will be modelled and presented in the following sections of this chapter.

4.2 System Description and Assumptions

In this research, a commercially available 1 kW Horizon (H-1000) fuel cell stack is adopted as an experimental device, which was designed by the manufacturer to be a self-humidified fuel cell stack. Therefore, water will not be added to the streams of supplied hydrogen and air in order to humidify the fuel cells [81].

In order to maintain flow rate and pressure of hydrogen and air within the desired level, hydrogen and air must be replenished via hydrogen-air supply systems. A hydrogen supply system consists of a tank of pressurised pure hydrogen, an inlet flow control valve, and an outlet purge valve. While an air supply system consists of air supply fans, and the connections of main supply manifolds. Figure 4.1 shows the mechanical components and flow variables associated with the Horizon (H-1000) fuel cells stack system at sea level operation.

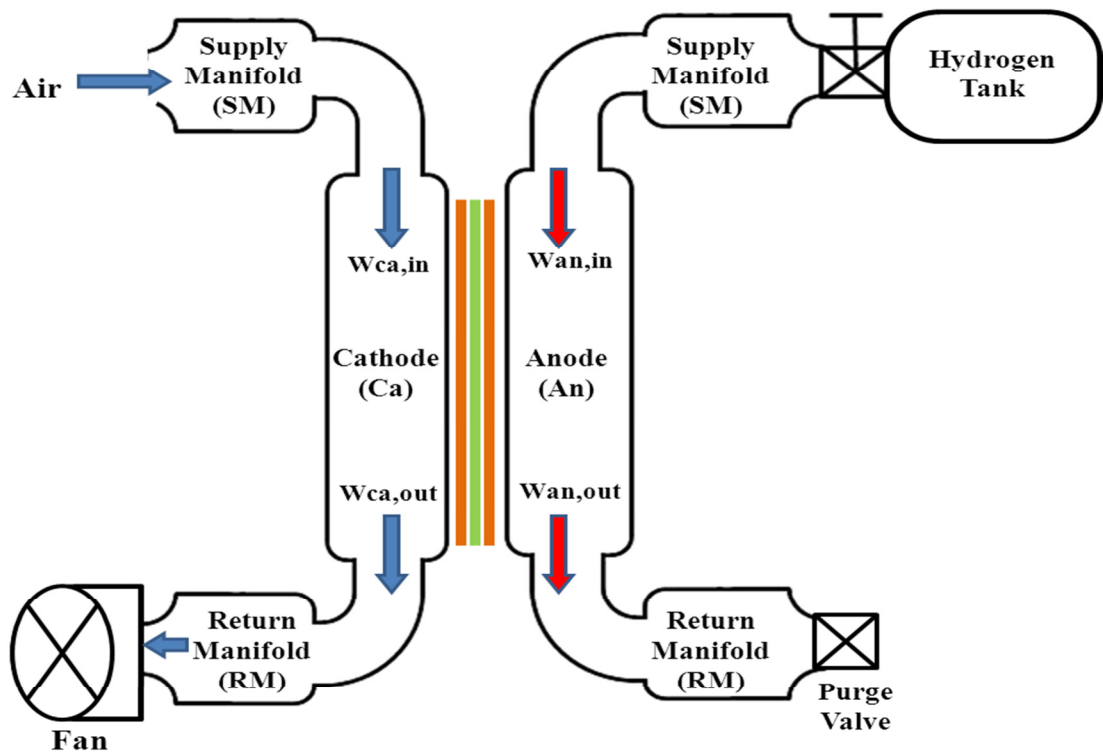


Figure 4.1: Mechanical components and flow variables associated with the Horizon fuel cells stack system (H-1000) at sea level operation

The Horizon fuel cell stack system (H-1000) is designed to have four fans installed at the exit outlet of the return manifolds of cathodes. Hence, fans are configured as a ducted inlet-free outlet, working as suction devices at the outlet of the return manifolds of cathodes [81]. For the Horizon (H-1000) fuel cell stack system, the rotational speed of four axial fans and the frequency of purging for the outlet hydrogen valve are

controlled by an inbuilt stack's controller, in order to maintain enough operational pressure at the cathode and anode, and also to provide a sufficient flow of air and hydrogen leading to maintaining a certain level of stack temperature and retaining the continuity of the electrochemical reaction.

Pukrushpan et al. [2] reported that the flow control valve of hydrogen must be controlled simultaneously in order to maintain a sufficient flow of hydrogen, and also to keep the minimum pressure difference across the membrane. This could be implemented by using a high gain proportional controller in order to keep the pressure in the anode tracking the pressure in the cathode.

It is assumed that all the gases inside the stack of fuel cells will behave as an ideal gas; also the properties of gases leaving the specific volume are the same as those inside that volume. The dimensions of the Horizon (H-1000) fuel cell stack are relatively small, hence, the distances between the supply-return manifolds and anodes-cathodes of the fuel cell are small, therefore it is assumed the impact of heat radiation or conduction between anodes-cathodes and supply-return manifolds are very small and can be ignored. Hence, the temperature of gases in the anodes-cathodes and also along the supply-return manifolds will be uniform and equal to the stack temperature. Moreover, because of the small size of the stack, it is assumed that the flow of gases within any cross sections in the stack will have approximately zero flow fractions.

The dynamic behaviour of the PEM fuel cell associated with the variations in temperature and heat dissipation of the stack are noticeably slower than the dynamics associated with the changes in pressures or flow rates of the reactants as reported by Pukrushpan et al. [2]. However, this research mainly focuses on the dynamic behaviour of the PEM fuel cell associated with changes in pressures or flow rates of the reactants, hence the slower dynamics associated with variations in temperature and heat dissipation are neglected. Therefore, it has been assumed that the average stack

temperature and relative humidity inside the cathode and anode are well regulated and maintained for all stages of modelling, analysis and control design.

The rate of changes in mass flow inside the stack system are governed by mass conservation principles, while the rate of changes in the pressures are governed by energy conservation principles [2, 82]. The values of the parameters used in our model are either drawn from the freely available literature or determined based on the dimensions and properties of the Horizon (H-1000) fuel cell stack system, as presented in Appendix A.

4.3 Air Fan Flow Calculations

The rotational speed of the fan has a significant impact upon the generated air flow and the performance of the fan [83, 84]. The governing equations of pressure rise and flow rate of supply air can be determined based on the pressure-flow performance curve for the axial fan model (Delta FFB-0912-EHE) installed in the Horizon (H-1000) fuel cell stack as presented in Figure A.1 in Appendix A. The pressure-flow performance has been regenerated with an approximation in terms of (kPa) and (m^3/min) as presented in Figure 4.2. Equation (4.1) determines the relationship between the rise in the pressure and the flow rate of air through the fan.

$$\Delta P_f = \begin{cases} -6.0W_f + 16.9 & 0 \leq W_f \leq 1.5 \\ -1.6W_f + 10.3 & 1.5 < W_f \leq 1.75 \\ 7.5 & 1.75 < W_f \leq 2.25 \\ -4.0W_f + 16.5 & 2.25 < W_f \leq 2.5 \\ -10.484W_f + 32.71 & 2.5 < W_f \leq 3.12 \end{cases} \quad (4.1)$$

Where, W_f represents the air flow rate through the fan (m^3/min), while ΔP_f represents the rise in the pressure (kPa) of air generated by the fan, which represents the velocity (or dynamic) pressure at the fan outlet corresponding to its kinetic energy. Velocity pressure is always positive in the direction of airflow which represents the pressure required to accelerate the air from zero velocity to a certain value. Total pressure of air stream (P_t) is the algebraic sum of the fan static pressure (P_{sf}) and velocity pressure, as defined by a simplified Bernoulli's theorem [85].

$$P_t = P_{sf} + \Delta P_f \quad (4.2)$$

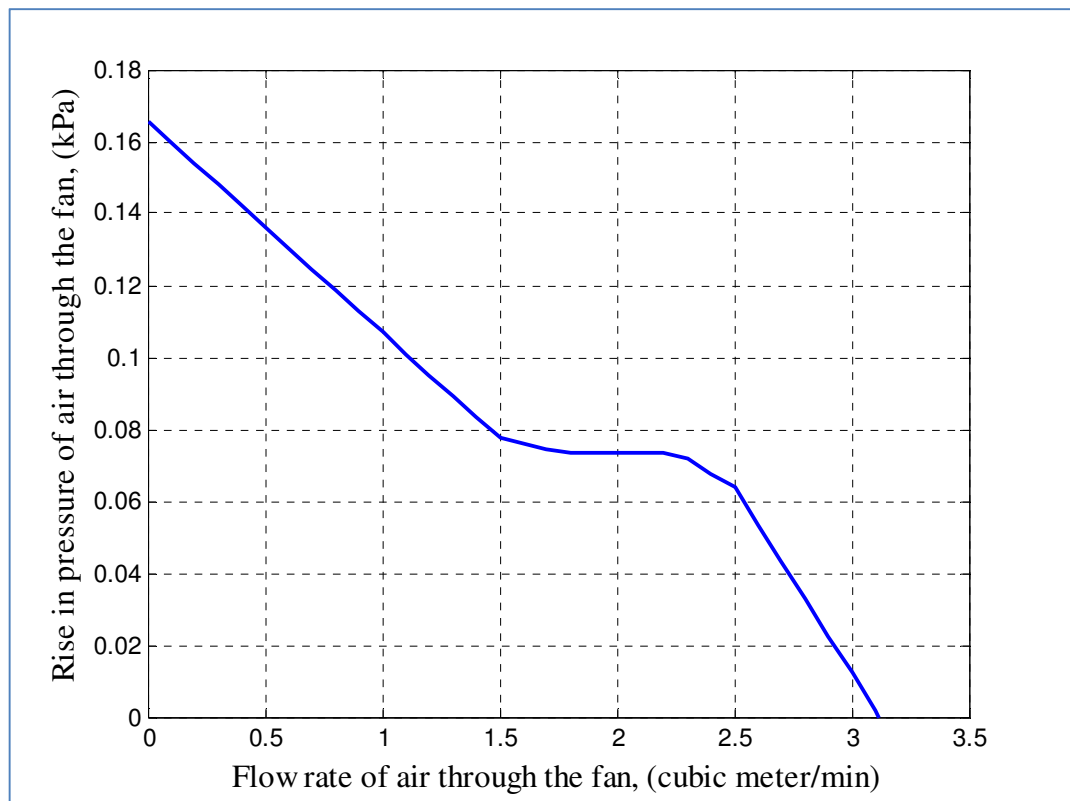


Figure 4.2: Pressure-flow performance curve for the axial fan used by Horizon (H-1000) fuel cell stack

In order to get the desired value of air flow rate inside the fuel cell stack, the pressure of supplied air to the supply manifold of the cathode will be equivalent to the sum of the

ambient pressure of air at sea level (101.325 kPa) and ΔP_f of the axial fans, as designed for the Horizon fuel cell stack (H-1000), as given below:

$$P_{sm,in,ca} = 101.325 + \Delta P_f \quad (4.3)$$

The output power for the fuel cell stack, with respect to the flow rates of the supply of hydrogen and air, is given in the user manual of the Horizon fuel cell stack, as shown in Figures A.2 and A.3 in Appendix A. Table 4.1 presents the values of the output voltages and currents, and the flow rates of the supplied hydrogen and air to the fuel cell stack [81, 86].

From Table 4.1, hydrogen flow rates (L/min) and air flow rates (m³/min) with respect to fuel cell current in ampere (A) for the Horizon (H-1000) fuel cell stack are drawn in Figures 4.3 and 4.4 respectively. By finding the slopes of the lines, the linear relation between the values of flow rates with respect to the current of the fuel cell stack can be determined, as given in the Equations (4.4) and (4.5) below:

$$\text{Hydrogen Flow (L/min)} = \begin{cases} (0.628 * I) + 0.082 & 1 \leq I \leq 6 \\ (0.57143 * I) + 0.4215 & 6 < I \leq 20 \end{cases} \quad (4.4)$$

$$\text{Air Flow (m}^3\text{/min)} = \begin{cases} (0.218 * I) + 0.019 & 1 \leq I \leq 2 \\ (0.17 * I) + 0.115 & 2 < I \leq 3 \\ (0.0758 * I) + 0.3976 & 3 < I \leq 8 \\ (0.07025 * I) + 0.442 & 8 < I \leq 12 \\ (0.060125 * I) + 0.5635 & 12 < I \leq 20 \end{cases} \quad (4.5)$$

Table 4.1: Output power of Horizon (H-1000) fuel cell stack with respect to the flow rates of supply hydrogen and air				
Output Current (Ampere), A	Output Voltage (Volt),V	Output Power (Watt), W	H₂ Flow (L/min)	Air Flow (m³/min)
1	63.5	63.5	0.71	0.237
2	61	122	1.37	0.455
3	59.5	178.5	2.01	0.625
4	58.5	234	2.63	0.703
5	57.5	287.5	3.23	0.778
6	57	342	3.85	0.855
7	56.5	395.5	4.45	0.930
8	56	448	5.04	1.004
9	55.5	499.5	5.62	1.076
10	55	550	6.19	1.147
11	54.5	599.5	6.74	1.217
12	54	648	7.29	1.285
13	53.5	695.5	7.82	1.352
14	53	742	8.35	1.417
15	52.5	787.5	8.86	1.481
16	52	832	9.48	1.544
17	51	867	10.01	1.593
18	50.5	909	10.64	1.652
19	50	950	11.25	1.710
20	49.5	990	11.85	1.766
21	48.5	1018.5	12.28	1.806

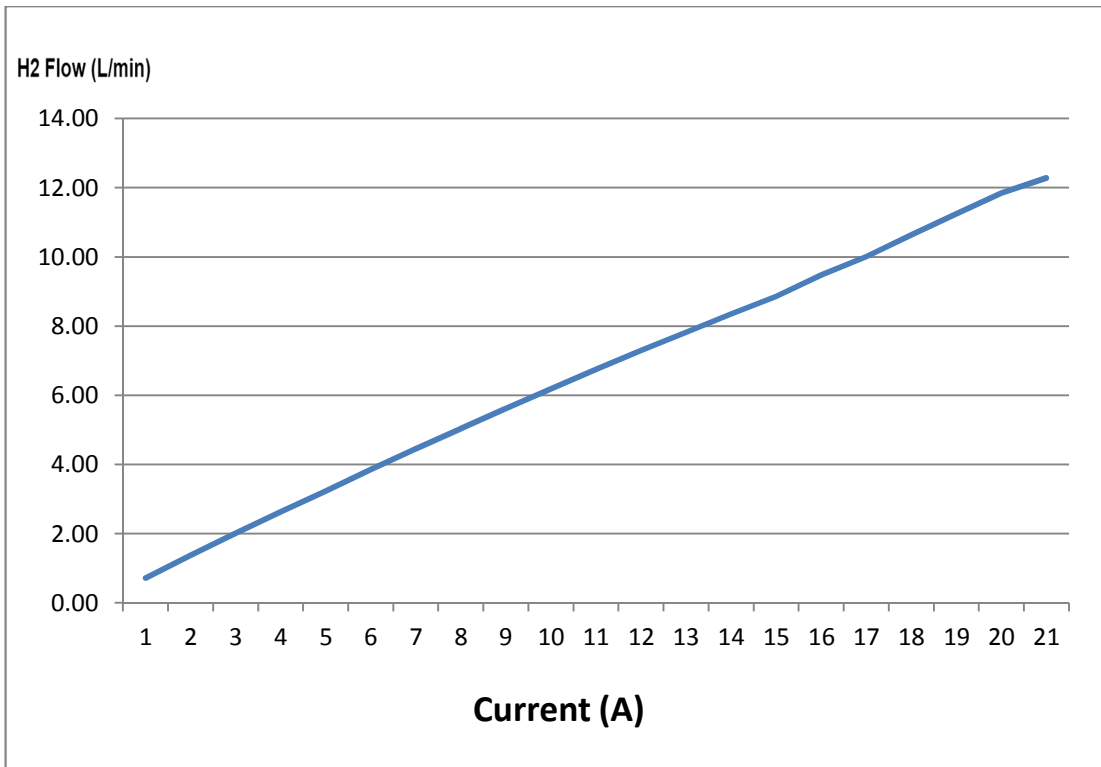


Figure 4.3: Hydrogen flow rate with respect to current for the Horizon (H-1000) stack

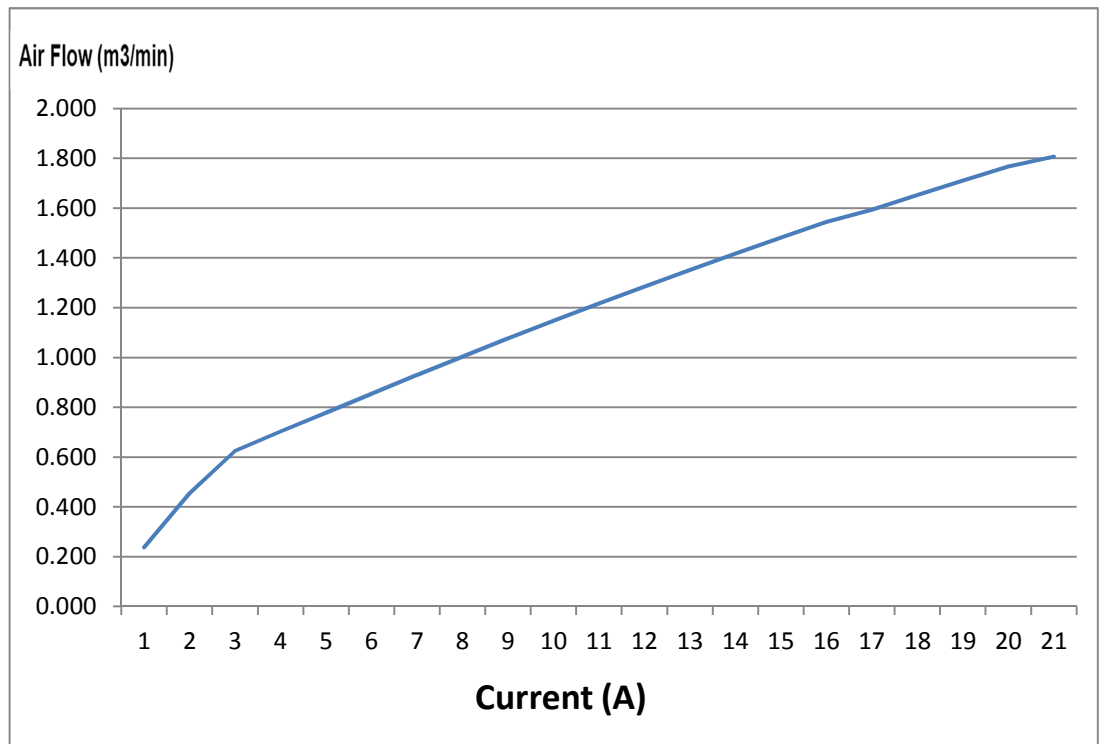


Figure 4.4: Air flow rate with respect to the current for the Horizon (H-1000) stack

The implementation in Simulink for Equations (4.1) and (4.3), which represent the pressure of the air at the supply manifold of the cathode, based on the supplied air flow by fans, is shown in Figure 4.5. While Figures 4.6 and 4.7 represent the implementation in Simulink for Equations (4.4) and (4.5), respectively, which represent the required flow rates of supplied hydrogen and air to the fuel cell stack, based on fuel cell stack current demand.

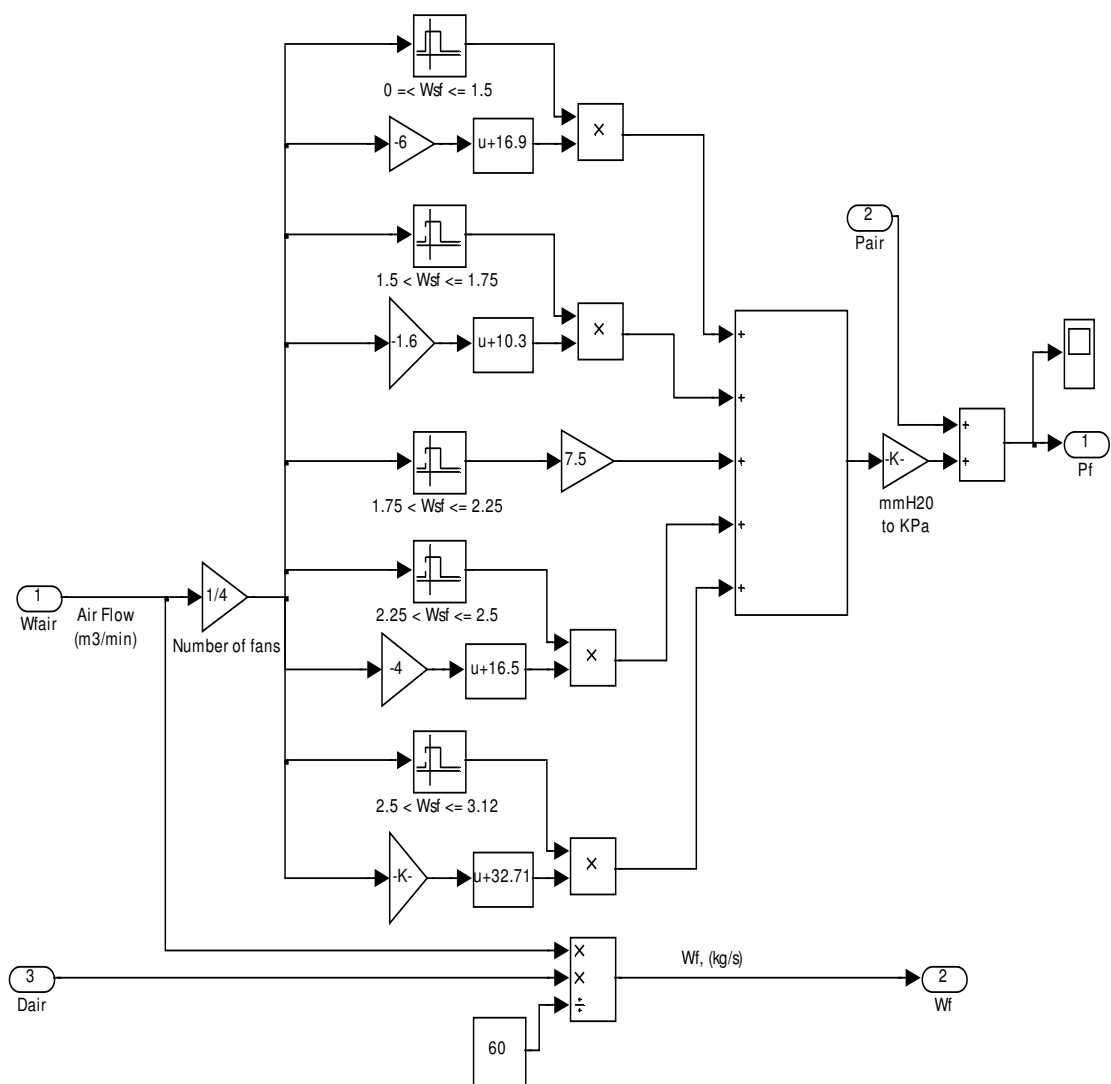


Figure 4.5: Simulink block diagram of the pressure of air at the supply manifold of cathode

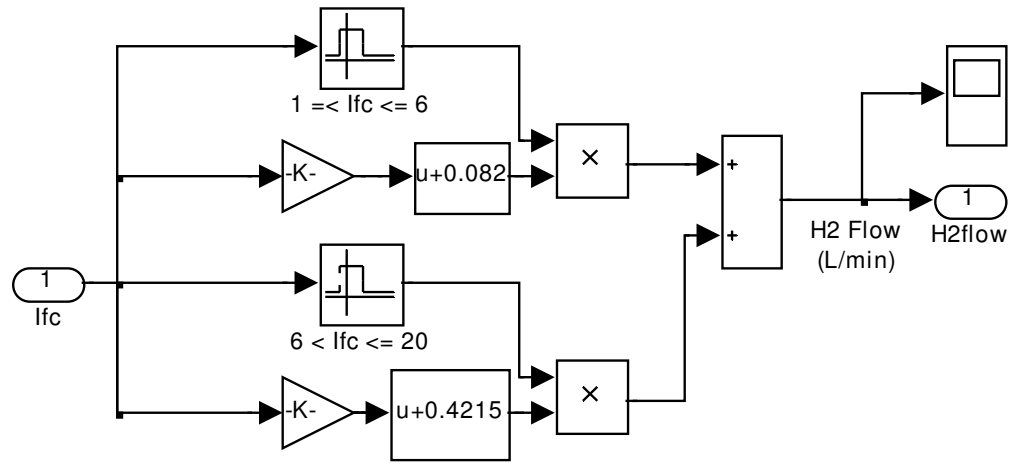


Figure 4.6: Simulink block diagram of the required supply hydrogen to the fuel cell stack

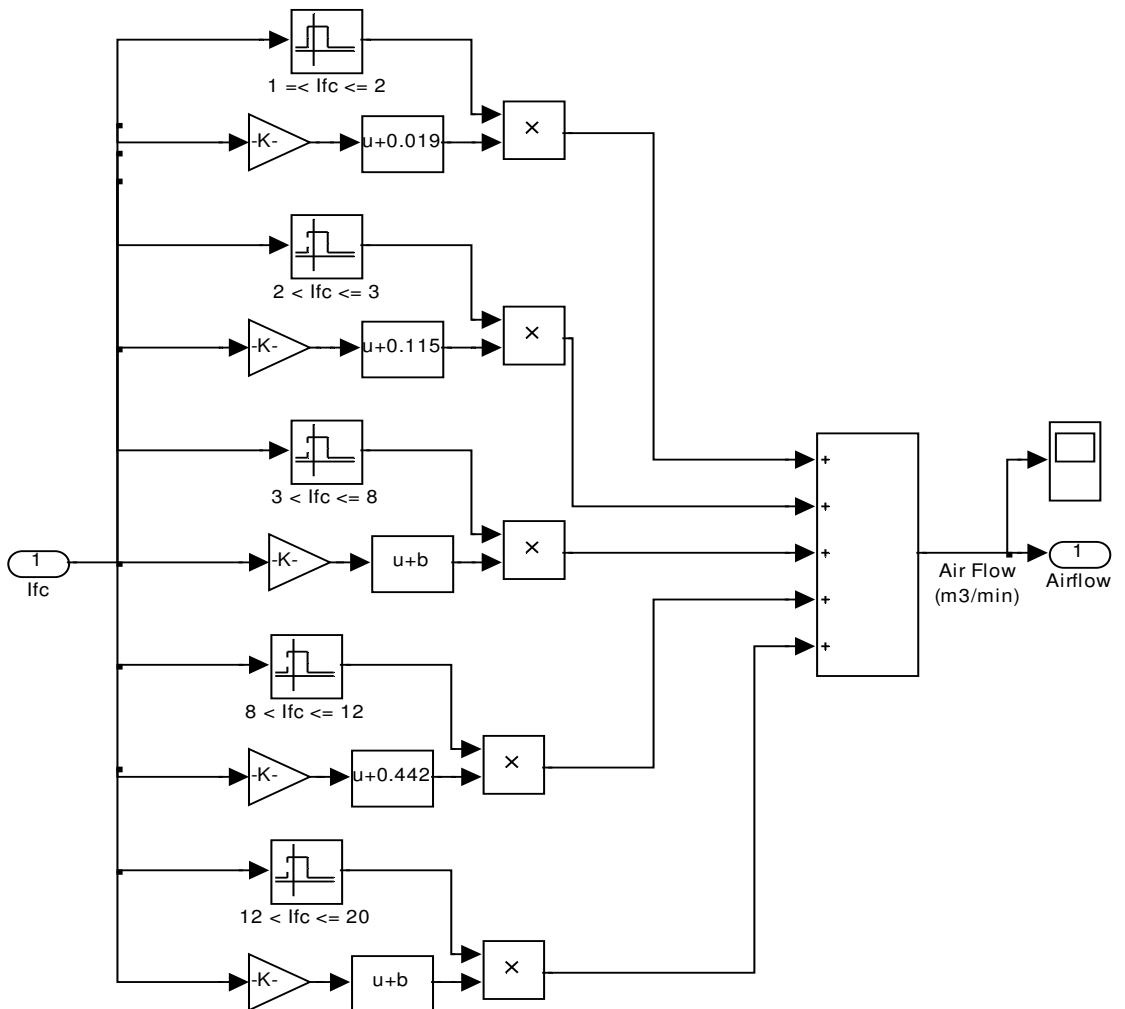


Figure 4.7: Simulink block diagram of the required supply air to the fuel cell stack

4.4 Thermodynamic Properties of Gases Flow in the PEM Fuel Cell

In thermodynamics, when the flow system is specified to be in a steady state, there are no changes in the properties of the flowing fluid through any section of the entire flow passage. When the flow system is described to be in steady flow, there will be no change in the mass flow rate through all cross sectional areas of the flow passage, hence the mass flow rate is assumed as a constant, irrespective of changes in direction or elevation of the flow or in the cross sectional area of the flow system [87].

$$W = \rho_1 \cdot A_1 \cdot v_1 = \rho_2 \cdot A_2 \cdot v_2 = \dots = \rho_x \cdot A_x \cdot v_x \quad (4.6)$$

Where, W is the mass flow rate (kg/s), ρ is the density (kg/m³), A is the flow area (m²), and v is the velocity of the fluid (m/s). Static properties of the fluid represent the properties of the fluid when there is no relative motion between the fluid and the measuring device. High velocity fluid may produce a significant change in the static properties of the fluid. For high velocity flows, if the potential energy of the fluid is negligible; hence the summation of the static enthalpy and kinetic energy represents stagnation enthalpy (h°), which represents the total energy (kJ/kg) of the flowing fluid per unit mass [88].

The properties of the fluid when its velocity is brought to rest (i.e. zero velocity) adiabatically and in an isentropic manner are called stagnation properties. During the isentropic stagnation process, the kinetic energy of the fluid undergoes enthalpy, which results in an increase in the pressure and temperature of the fluid. If the entropy of the fluid remains constant and the fluid flows with approximately zero fraction, then its enthalpy can be expressed as given below [87, 88]:

$$h^\circ = c_p \cdot T^\circ = c_p \cdot T + \frac{v^2}{2} = h + \frac{v^2}{2} \quad (4.7)$$

$$c_p = \frac{k}{k-1} \cdot R_s \quad (4.8)$$

Where c_p is the specific heat of the fluid (kJ/kg.K), and R_s is the specific constant of the fluid. For an ideal gas ($dh = c_p \cdot dT$), $h^\circ - h = c_p \cdot (T^\circ - T)$. With a datum temperature of 0K, yields with ($h = c_p \cdot T$) [87]. For a steady state flow of fluid flowing adiabatically through a flow system with a constant passage flow area, where there are no heat or work interactions and no changes in the potential energy or elevation of the fluid, the stagnation enthalpy of the fluid remains constant during a steady-state flow process ($h_1^\circ = h_2^\circ$).

$$h_1^\circ = h_1 + \frac{v_1^2}{2} = h_2 + \frac{v_2^2}{2} = h_2^\circ \quad (4.9)$$

When the flowing fluid is brought to a complete stop; then stagnation enthalpy at state 2 will be equal to the fluid static enthalpy at this state, as given below:

$$h_1 + \frac{v_1^2}{2} = h_2 = h_2^\circ \quad (4.10)$$

The density of the fluid varies as it moves down toward the downstream side of the flow system, from the definition of stagnation properties, total temperature (stagnation temperature T°), total pressure (stagnation pressure P°), and total density (stagnation density ρ°) of the fluid at a certain point can be determined, as given below [87, 88]:

$$T^\circ = T + \frac{v^2}{2 c_p} \quad (4.11)$$

$$P^\circ = P + \frac{\rho \cdot v^2}{2} \quad (4.12)$$

$$\rho^\circ = \rho \cdot \left(\frac{T^\circ}{T} \right)^{1/(k-1)} \quad (4.13)$$

$$\frac{P^\circ}{P} = \left(\frac{T^\circ}{T} \right)^{k/(k-1)} \quad (4.14)$$

Where, T , P , and ρ represent static properties of temperature, pressure and density of the fluid respectively; and T° , P° , and ρ° represent the properties of temperature, pressure, and density of the fluid under an isentropic stagnation state. k is the constant of specific heat ratio (c_p/c_v) for air at temperature 15 °C which is equal to 1.4 for dry air and 1.409 for hydrogen. The term $(v^2/2c_p)$ is the dynamic temperature of the fluid which is equivalent to the temperature rise during such a process. For low-speed flows, the static temperature and stagnation temperature are approximately the same [88].

In case of fluid that flows through a continuous flow system having a non-consistent passage area, such as diffuser or nozzle, due to high rates of flow through the system, there will be no significant heat transfer between the fluid and the surroundings, and the flow may be considered to be adiabatic. Also if it is assumed that the flow is frictionless with negligible elevation impact, then the flow can be considered to be isentropic. Hence, under these conditions, the stagnation enthalpy will remain constant along the flow passage, as presented in Equation (4.15) below [87].

$$h_1^\circ = h_2^\circ = \dots = h_x^\circ = \text{Constant} \quad (4.15)$$

The change in the flow area of the nozzle will change the pressure of the fluid and hence flow velocity. If the flow is assumed to be steady and unidirectional, and the gas is assumed to behave in an adiabatic and isentropic manner, stagnation enthalpy will remain constant at any point through the nozzle. Then, the velocity of the fluid at any point in the nozzle is determined below [87]:

$$v = \sqrt{2(h^\circ - h)} = \sqrt{2c_p \cdot (T^\circ - T)} \quad (4.16)$$

Substituting Equations (4.8) and (4.14) in Equation (4.16) and rearranging, yields the following:

$$v = \sqrt{2 \left(\frac{k}{k-1} \right) \cdot R_s \cdot T^\circ \cdot \left[1 - \left(\frac{P}{P^\circ} \right)^{(k-1)/k} \right]} \quad (4.17)$$

Since the flow of the fluid is assumed to be adiabatic and isentropic, and the stagnation enthalpy remains constant, the stagnation temperature and pressure will remain constant as well. Thus, the velocity of the fluid in Equation (4.17) can be determined in terms of initial stagnation temperature and pressure. For a steady flow flowing through a constant passage area with constant temperature, then Equation (4.6) above can be represented as:

$$\rho_1 \cdot v_1 = \rho_2 \cdot v_2 \quad (4.18)$$

However, the density of ideal gas can be determined as given in Equation (A.2) in Appendix A, yielding the following:

$$\rho = \frac{P}{R_s \cdot T}$$

$$\rho_1 \cdot v_1 = \rho_2 \cdot v_2 = \frac{P_1}{R_s \cdot T} \cdot v_1 = \frac{P_2}{R_s \cdot T} \cdot v_2$$

$$P_1 \cdot v_1 = P_2 \cdot v_2 \quad (4.19)$$

Due to the lack of experimental data and the difficulties in measuring the variation of pressures, densities, and temperatures of the flowing gases in the supply-return

manifolds, anodes, and cathodes of the fuel cell stack, gases are assumed to behave as an ideal gas with a constant specific heat and zero flow fractions. Moreover, and particularly in the supply-return manifolds of the stack, gases are assumed to be subject to the isentropic stagnation state. Equations (4.11), (4.12), (4.13), (4.17), and (4.19) will be used to determine the pressure, temperature, and velocity of gas leaving the supply manifold of the anode and cathode of the fuel cell stack. While under an assumption of steady flow, the mass flow rate of gas entering the supply manifold is assumed to be equal to the mass flow rate of gas leaving it.

4.4.1 Cathode Flow Model

The dimensions of the Horizon fuel cell stack (H-1000) are relatively small and the distances between the supply-return manifolds and anodes-cathodes of the fuel cells are small as well. Hence, it is assumed that the multiple cathodes in the stack are all lumped as one stack cathode volume, which represents the sum of volumes of each individual cathode volume in the stack. And the supply manifold of the cathode (s_m) lumps all the volumes of passages and connections between the inlet of air and the cathodes, while the return manifold (r_m) lumps all the volumes of passages and connections between the cathodes of fuel cells and the exit of air of the fuel cell stack.

The flow rate of supplied air to the manifold of cathode $W_{sm,in,ca}$ is equal to W_f , while the pressure of supplied air $P_{sm,in,ca}$ is equal to $(101.325 + \Delta P_f)$, as determined in Equations (4.1) and (4.3) above. The temperature of air exiting the supply manifold of the cathode is assumed to be equal to the temperature of the supplied air, which is equal to the ambient temperature. While the temperature of the air at any cross section in the cathode is assumed to be equal to the exit air of the cathode, which is considered to be equal to the stack temperature T_{st} .

The flow rate of gas passing through a nozzle is a function of the upstream and downstream pressure of the nozzle. Thus, the mass flow rate of fluid between two volumes can be determined by using a linearized nozzle equation given in Pukrushpan et al. and Grujicic et al. [80, 82]. Hence, the mass flow rate of air flowing between the exit of the supply manifold and the cathode is determined as given in Equation (4.20):

$$W_{sm,out,ca} = K_{sm,out,ca} \cdot (P_{sm,out,ca} - P_{ca,in}) \quad (4.20)$$

Where, $P_{ca,in}$ is the pressure of air entering the cathode, and $W_{sm,out,ca}$ is assumed to be equal to $W_{sm,in,ca}$ under a condition of steady flow. $K_{sm,out,ca}$ is the nozzle constant of the supply manifold outlet ($\text{kg}\cdot\text{s}^{-1}/\text{kPa}$) which represents the ratio of mass flow rate of air to the pressure. The value of $K_{sm,out,ca}$ for the Horizon (H-1000) fuel cell stack is determined and presented in Appendix A. The mass of a mixture of gases is equal to the sum of masses of individual components in the mixture [88]. The principle of mass conservation states that the rate of change of fluid mass inside the volume is equal to the net rate of fluid mass flowing into the volume. Hence, the rate of change in the mass of air inside the cathode of the fuel cell is determined as given below [32]:

$$\frac{dm_{ca}}{dt} = \frac{dm_{O_2}}{dt} + \frac{dm_{N_2}}{dt} + \frac{dm_{w,ca}}{dt} \quad (4.21)$$

$$\frac{dm_{O_2}}{dt} = W_{O_2,in} - W_{O_2,out} - W_{O_2,rct} \quad (4.22)$$

$$\frac{dm_{N_2}}{dt} = W_{N_2,in} - W_{N_2,out} \quad (4.23)$$

$$\frac{dm_{w,ca}}{dt} = W_{w,gen} - W_{w,mbr} - W_{w,out} \quad (4.24)$$

Where, m_{ca} represents the mass of gases inside the cathode (kg), m_{O_2} , m_{N_2} , and m_w represent mass of oxygen, nitrogen, and water vapour, respectively, in the cathode, $W_{w,gen}$ represents the mass flow rate of produced water as a result of electrochemical reaction, $W_{O_2,rcf}$ represents the mass flow rate of reacted oxygen in the cathode, and $W_{w,mbr}$ represents the mass flow rate of water vapour across the electrolyte membrane. The mass flow rate of air entering the cathode and the mass flow rate of air exiting the cathode are determined by the equations given below:

$$W_{ca,in} = W_{O_2,in} + W_{N_2,in} \quad (4.25)$$

$$W_{ca,out} = W_{O_2,out} + W_{N_2,out} + W_{w,out} \quad (4.26)$$

Substituting Equations (4.22), (4.23), (4.24), (4.25), and (4.26) in Equation (4.21) and rearranging, yields the following:

$$\frac{dm_{ca}}{dt} = W_{ca,in} - W_{ca,out} - W_{O_2,rcf} + W_{w,gen} - W_{w,mbr} \quad (4.27)$$

Using ideal gas law, under constant T and V :

$$\frac{dP}{dt} = \frac{R \cdot T}{V} \cdot \frac{dm/dt}{M} = \frac{R \cdot T}{V} \cdot \frac{W}{M} \quad (4.28)$$

Where, M represents the molar mass of gas (kg/kmol), and W represents the mass flow rate of flowing gas (kg/s).

$$\frac{dP_{ca}}{dt} = \frac{R \cdot T_{st}}{V_{ca}} \cdot \left(\frac{W_{ca,in}}{M_{air,in}} - \frac{W_{ca,out}}{M_{ca,out}} - \frac{W_{O_2,rcf}}{M_{O_2}} + \frac{W_{w,gen} - W_{w,mbr}}{M_w} \right) \quad (4.29)$$

$$\frac{dP_{ca}}{dt} = \frac{dP_{ca,in}}{dt} - \frac{dP_{ca,out}}{dt} + \frac{R \cdot T_{st}}{V_{ca}} \cdot \left(\frac{W_{w,gen} - W_{w,mbr}}{M_w} - \frac{W_{O_2,rcf}}{M_{O_2}} \right) \quad (4.30)$$

Where, M_{air} , M_{O_2} , and M_w represent the molar mass (kg/kmol) of air, oxygen, and water vapour respectively, R is the universal gas constant, V_{ca} is the volume of the cathode (m^3), and $W_{w,mbr}$ represents the mass flow rate of water vapour across the membrane. The mass flow rate of reacted oxygen $W_{O_2,rct}$ and produced water in the cathode $W_{w,gen}$ are determined by Larminie and Dicks [1]:

$$W_{O_2,rct} = M_{O_2} \cdot \frac{n \cdot I_{st}}{4F} \quad (4.31)$$

$$W_{w,gen} = M_w \cdot \frac{n \cdot I_{st}}{2F} \quad (4.32)$$

Where, molar mass of oxygen is $32 \cdot 10^{-3}$ kg/mol, molar mass of water is $18.02 \cdot 10^{-3}$ kg/mol, n is the number of cells in the stack, I_{st} is the current drawn from the stack in ampere (A), and F is Faraday's constant. For a steady flow, the rate of change in the mass of flowing fluid through a specific area would be zero (i.e. $dm/dt = 0$), hence $dP/dt = 0$ [89], then by taking the Laplace transform for Equation (4.30) above and rearranging, yields the following:

$$P_{ca,out} = P_{ca,in} + \frac{R \cdot T_{st}}{V_{ca}} \cdot \left(\frac{m_{w,gen} - m_{w,mbr}}{M_w} - \frac{m_{O_2,rct}}{M_{O_2}} \right) \quad (4.33)$$

From Equations (4.31) and (4.32), if at any specific second of time, the mass flow rate (kg/s) of reacted oxygen $W_{O_2,rct}$ and produced water in the cathode are equal to the mass of that component m (kg) at that time, it can be substituted in Equation (4.33) above, to determine the value of air pressure at the exit of the cathode. Since it is assumed that the multiple cathodes in the stack are all lumped as one stack cathode volume, and the flow of air supplied to the cathode mainly consists of 21% oxygen and 79% nitrogen, the

partial pressure of oxygen in the cathode is assumed to be approximately equal to 21% of the average sum of input and output air pressure of the cathode, as determined below:

$$P_{O_2} = 0.21 \left(\frac{P_{ca,in} + P_{ca,out}}{2} \right) \quad (4.34)$$

The implementation in Simulink for the mass flow rate of reacted oxygen and produced water in the cathode of the fuel cell stack, as presented in Equations (4.31) and (4.32) are shown in Figure 4.8. And the implementation in Simulink for the flow of air and partial pressure of oxygen in the cathode of the fuel cell stack are shown in Figure 4.9.

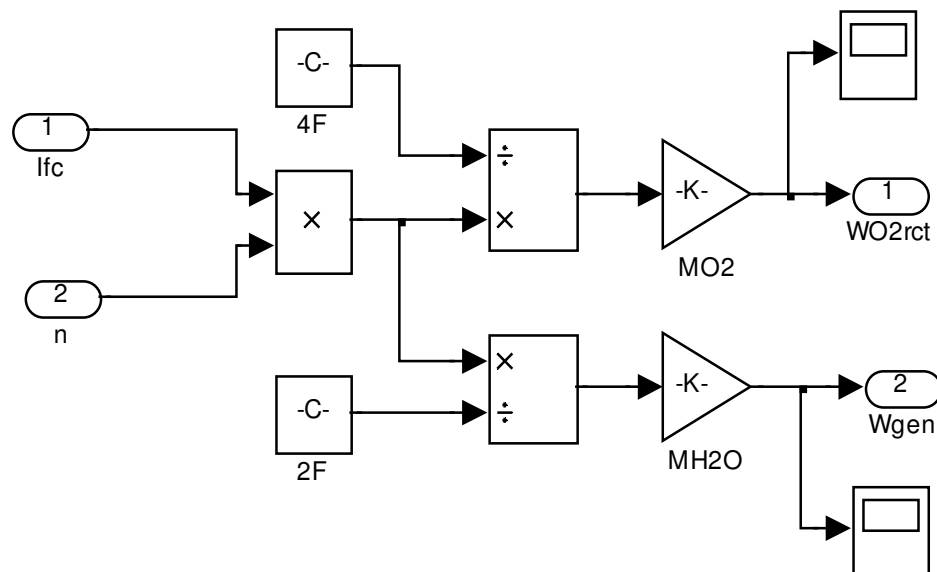


Figure 4.8: Simulink block diagram of the mass flow rate of reacted oxygen and produced water in the cathode of the fuel cell stack

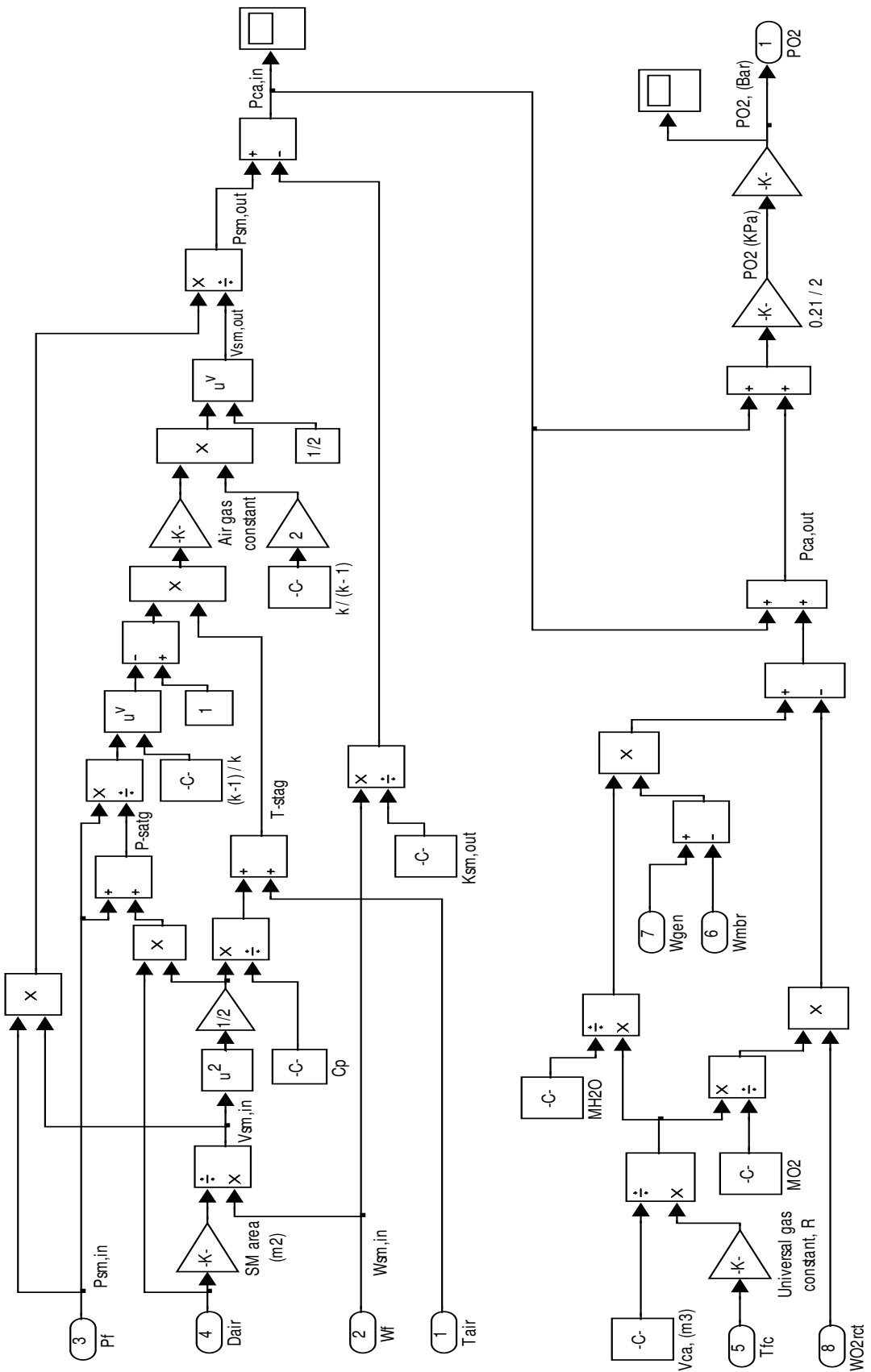


Figure 4.9: Simulink block diagram of the flow of air and partial pressure of oxygen in the cathode of the fuel cell stack

4.4.2 Membrane Hydration Model

Water content in the membrane and the mass flow rate of water across the membrane are assumed to be uniform over the two sides of membrane; the mass flow rate of water vapour across the membrane is given by Pukrushpan et al. [2, 80]:

$$W_{w,mbr} = M_w \cdot A_{fc} \cdot n \cdot \left(\left(n_d \cdot \frac{i}{F} \right) - \left(D_w \cdot \frac{\phi_{ca} - \phi_{an}}{L} \right) \right) \quad (4.35)$$

Where, A_{fc} is the membrane active area of the fuel cell (cm^2), n is the number of cells in the stack, F is Faraday's constant, i is the current density of the fuel cell (i.e. $i = I_{st} / A_{fc}$) in (mA/cm^2), n_d is the electro-osmotic drag coefficient which represents the number of water molecules dragged with each proton of hydrogen transported from anode to the cathode side of the fuel cell, D_w is the diffusion coefficient, ϕ_{ca} and ϕ_{an} represent the relative humidity in the cathode and anode respectively, and L is the thickness of the membrane (cm). The difference in relative humidity between the cathode and anode leads to back diffusion of water molecules from cathode to anode, as presented in the second term of Equation (4.35), and the coefficients D_w and n_d are functions to the membrane water content λ .

Pukrushpan et al. [80] reported that the value of water content in the electrolyte membrane varies between 0 and 14, which is equivalent to the relative humidity of 0 to 100%, respectively. The electro-osmotic drag coefficient n_d is determined by empirical Equation (4.36) below:

$$n_d = 0.0029 \lambda^2 + 0.05 \lambda - (3.4 \times 10^{-19}) \quad (4.36)$$

Mann et al. [40] reported that water content in the membrane is influenced by the procedure of membrane preparation, age of the membrane (i.e. time in service), relative humidity and membrane water activity, and stoichiometric ratio of the supplies gases.

The amount of water content λ is determined in Wang and Wang and Springer et al. [42, 52] as presented below:

$$\lambda = \begin{cases} 0.043 + 17.81 a - 39.85 a^2 + 36.0 a^3 & \text{for } 0 < a \leq 1 \\ 14 + 1.4 (a - 1) & \text{for } 1 < a \leq 3 \end{cases} \quad (4.37)$$

$$a = \frac{C_w \cdot R \cdot T}{P_{sat}} \quad (4.38)$$

Where, a represents the water activity in the membrane, C_w is the molar concentration of water in the electrolyte membrane (kmol/m^3), R is the universal gas constant, T is the temperature in kelvin (K), and P_{sat} is the saturation pressure of water vapour (kPa). Since it has been assumed that the temperature and relative humidity are constant, λ is constant as well and its value will be presumed to be equal to 7.0 which represents the moist status of the membrane. Moreover the impact of back diffusion of water will be ignored, and Equation (4.35) can be re-presented as in Equation (4.39):

$$W_{w,mbr} = \frac{M_w \cdot n \cdot n_d}{F} \cdot I_{st} \quad (4.39)$$

The implementation in Simulink for the mass flow rate of water vapour across the membrane of the fuel cell as presented in Equations (4.36) and (4.39) is shown in Figure 4.10.

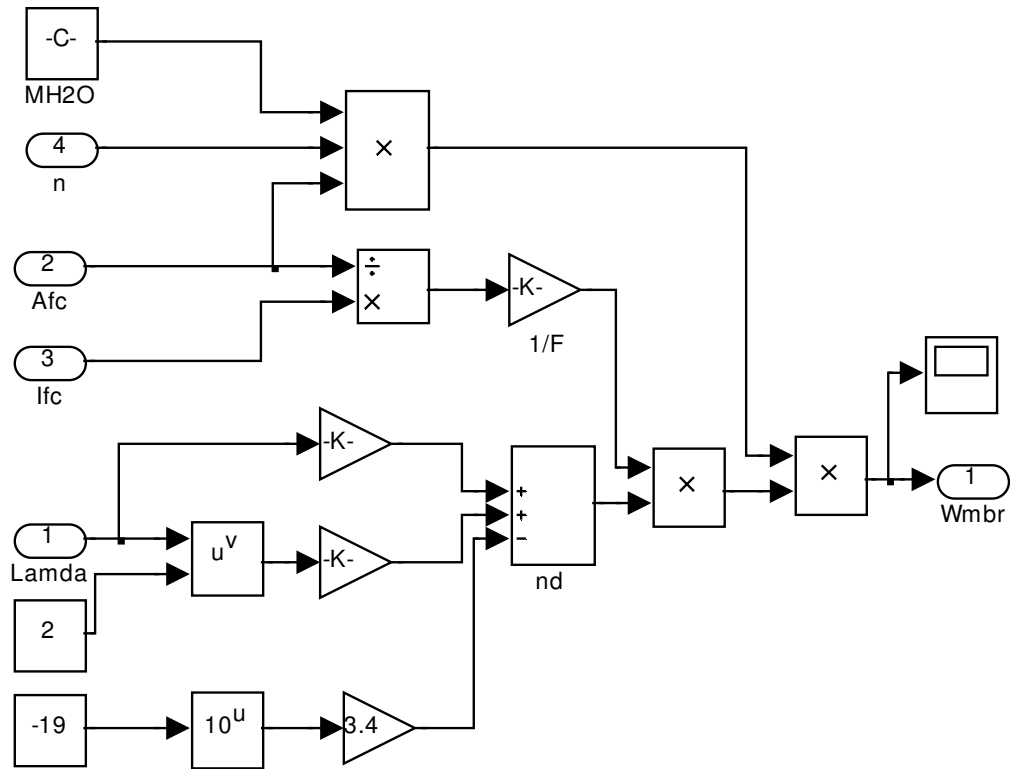


Figure 4.10: Simulink block diagram for the mass flow rate of water vapour across the membrane of the fuel cell stack

4.4.3 Anode Flow Model

Since the distances between the supply-return manifolds and anodes-cathodes of the fuel cell stack are small, it is assumed that multiple anodes are all lumped as one stack anode volume, which represents the sum of volumes of each individual anode volume in the stack. And the supply manifold (s_m) of the anode lumps all the volumes of passages and connections between the hydrogen supply outlet and the anodes, while the return manifold (r_m) lumps all the volumes of passages and connections between the anode exit outlet and the exit outlet of hydrogen of the stack. Hence, the pressure of hydrogen entering the supply manifold of anode $P_{s_m, in, an}$ is equal to the pressure of the main supply hydrogen by the pressure regulator valve which is 55 kPa. It is also assumed that the impact of back diffusion of water molecules from the cathode to anode is null. Thus, an anode chamber will be occupied by hydrogen gas only.

Mass flow rate between two volumes can be determined via using a linearized nozzle equation [80, 82], then the mass flow rate of hydrogen at the exit of the supply manifold of the anode is determined by Equation (4.40):

$$W_{sm,out,an} = K_{sm,out,an} \cdot (P_{sm,out,an} - P_{an,in}) \quad (4.40)$$

Where, $P_{an,in}$ is the pressure of hydrogen entering the anode, and $W_{sm,out,an}$ is assumed to be equal to $W_{sm,in,an}$ under a condition of steady flow. $K_{sm,out,an}$ represents the nozzle constant of the supply manifold outlet of the anode ($\text{kg}\cdot\text{s}^{-1}/\text{kPa}$), which represents the ratio of mass flow rate of hydrogen to the pressure. The value of $K_{sm,out,an}$ for the Horizon (H-1000) fuel cell stack is determined and presented in Appendix A. The rate of change in the mass of hydrogen inside the anode of the fuel cell is determined as given below:

$$\frac{dm_{an}}{dt} = W_{an,in} - W_{an,out} - W_{H2,rct} \quad (4.41)$$

Where, $W_{an,in}$ and $W_{an,out}$ represent the mass flow rate of hydrogen entering and leaving the anode, while $W_{H2,rct}$ represents the mass flow rate of the reacted hydrogen as a result of the electrochemical reaction, as determined by Larminie and Dicks [1]:

$$W_{H2,rct} = M_{H2} \cdot \frac{n \cdot I_{st}}{2F} \quad (4.42)$$

Where, M_{H2} represents the molar mass of pure hydrogen (kg/kmol), n is the number of cells in the stack, and I_{st} is the current drawn from the stack in ampere (A), and F is Faraday's constant. For a steady flow, the rate of change in the mass of flowing hydrogen through any specific area in the anode would be zero (i.e. $dm_{H2}/dt = 0$) [89], then Equation (4.41) can be represented as given in the following equation:

$$W_{an,out} = W_{an,in} - W_{H2,rct} \quad (4.43)$$

Substituting Equation (4.43) in Equation (4.28), and rearranging, yields the following:

$$\frac{dP_{an,out}}{dt} = \frac{dP_{an,in}}{dt} - \frac{R \cdot T_{st}}{V_{an} \cdot M_{H2}} \cdot W_{H2,rct} \quad (4.44)$$

Taking the Laplace transform for Equation (4.44), yields the following:

$$P_{an,out} = P_{an,in} - \frac{R \cdot T_{st}}{V_{an} \cdot M_{H2}} \cdot m_{H2,rct} \quad (4.45)$$

Where, R is the universal gas constant, and V_{an} is the volume of the anode (m^3). From Equation (4.42), if at any specific second of time, the mass flow rate (kg/s) of reacted hydrogen $W_{H2,rct}$ in the anode is equal to the mass of that component m (kg) at that time, it can be substituted in Equation (4.45) above, to determine the value of gas pressure at the exit of the anode. Since it is assumed that the multiple anodes in the stack are all lumped as one stack anode volume, the pressure of hydrogen in the anode is assumed to be approximately equal to the average sum of the input and output anode pressure, as determined below:

$$P_{H2} = \frac{P_{an,in} + P_{an,out}}{2} \quad (4.46)$$

A flow of hydrogen is necessary to be regulated to maintain a minimum pressure difference between anode and cathode, and also to provide sufficient hydrogen to the reaction. A purge valve at the exit outlet of the return manifold of the anode is important to keep the internal pressure of hydrogen inside the anode of the fuel cell at the appropriate level, also to flush the anodes from residual unreacted hydrogen and any traces of formed water [8]. However, the flow rate of hydrogen can be controlled based

on the feedback pressure difference between the cathode and anode as presented by Pukrushpan et al. [90].

The implementation in Simulink for the mass flow rate of reacted hydrogen in the anode of the fuel cell stack, as presented in Equation (4.42), is shown in Figure 4.11. And the implementation in Simulink for the flow and pressure of hydrogen in the anode of the fuel cell stack is shown in Figure 4.12. While Figure 4.13 presents the implementation in Simulink of the integration and connections of all electrical and thermodynamic sub-models for the entire developed model of the PEM fuel cell stack system.

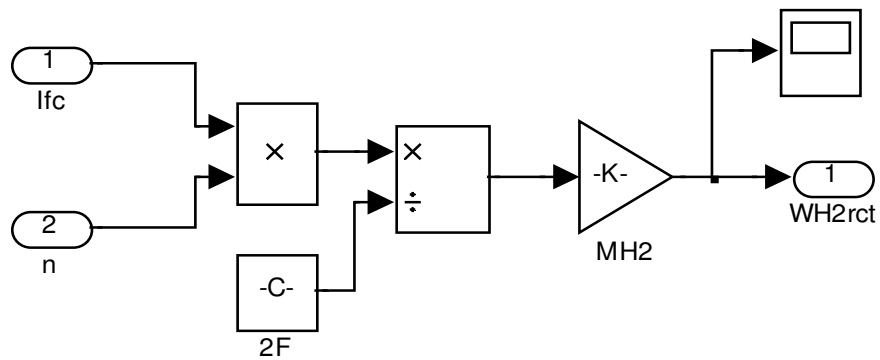


Figure 4.11: Simulink block diagram of the mass flow rate of reacted hydrogen in the anode of the fuel cell stack

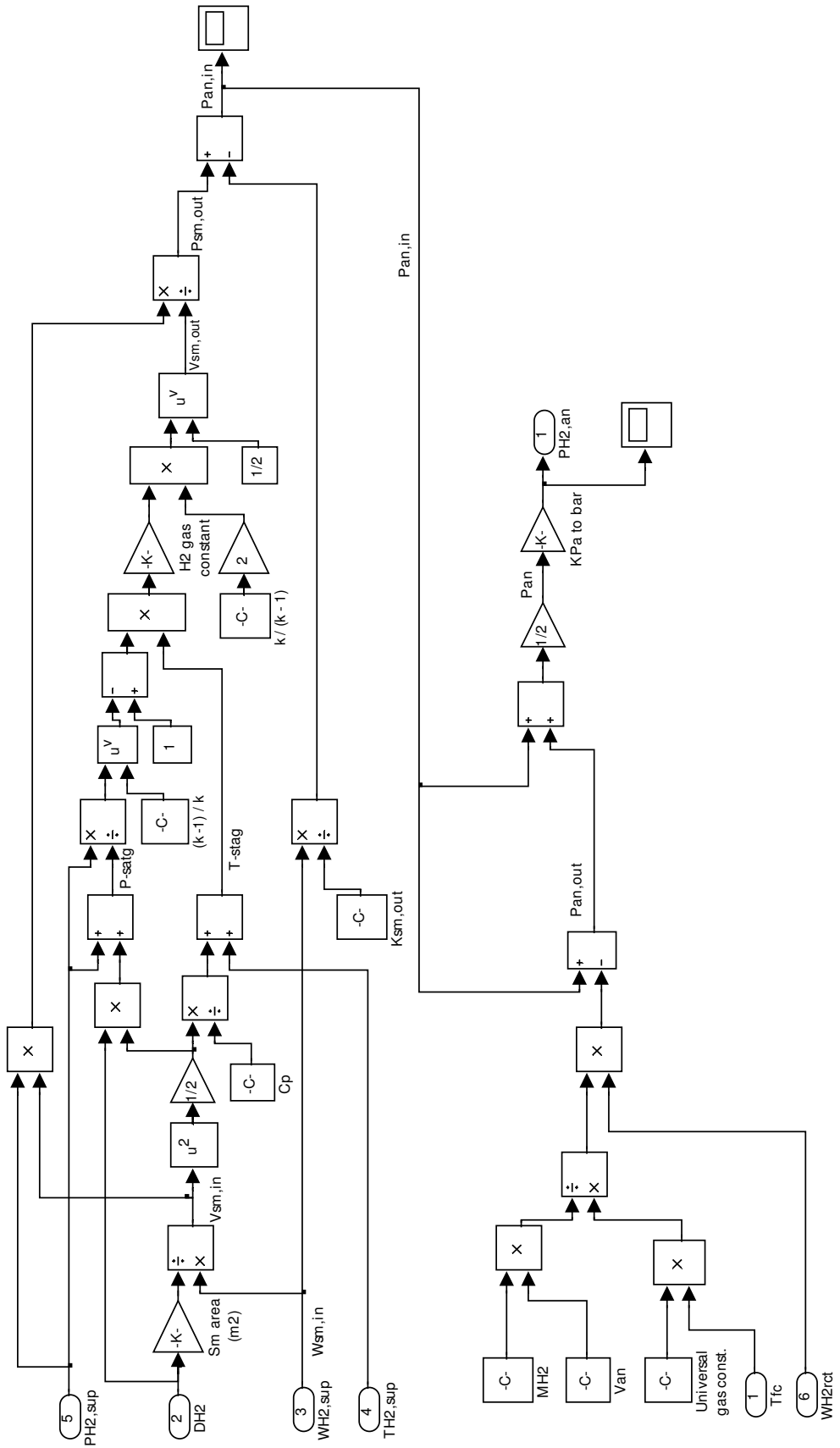


Figure 4.12: Simulink block diagram of the flow and pressure of hydrogen in the anode of the fuel cell stack

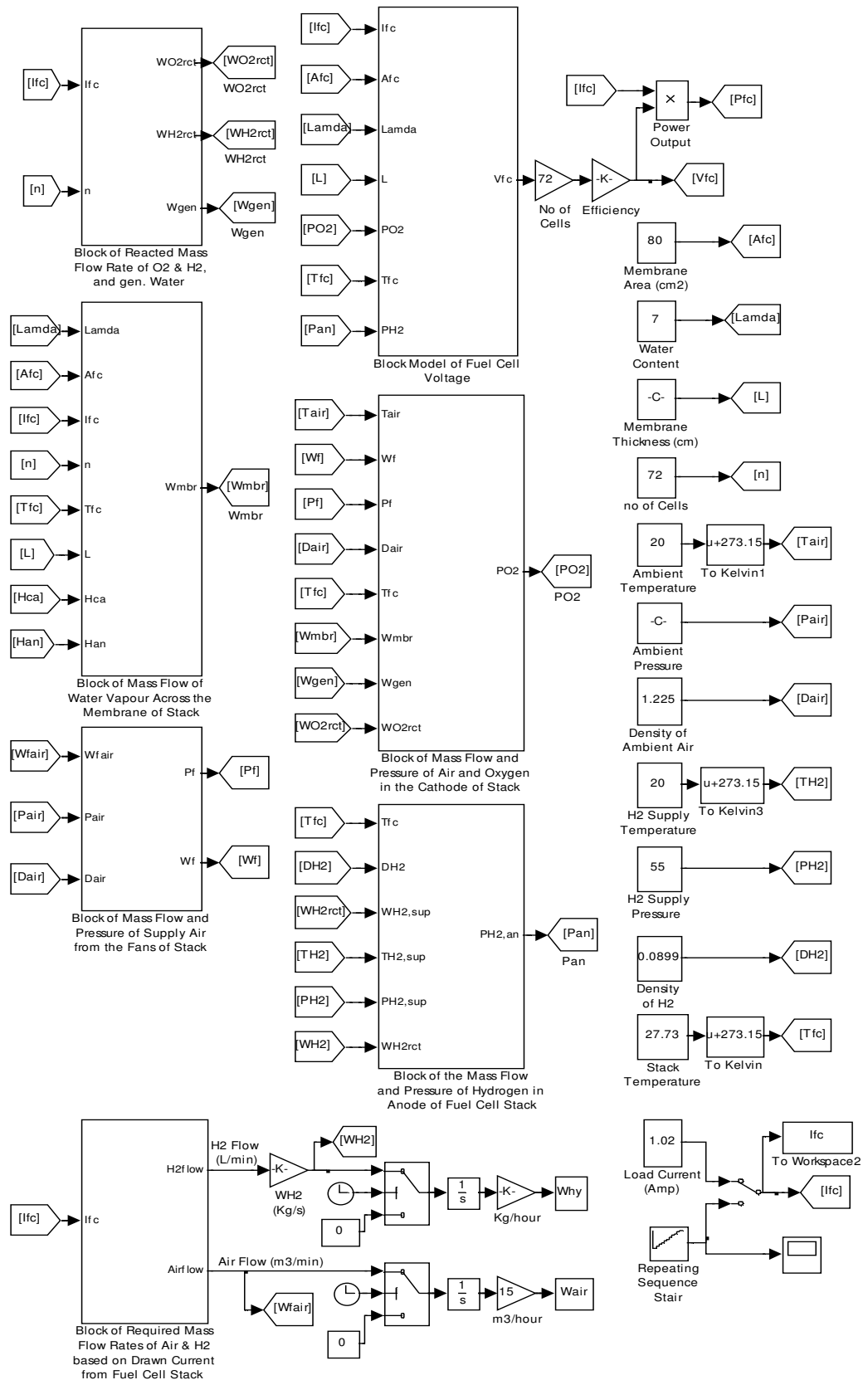


Figure 4.13: Simulink block diagram of the integration and connections of all electrical and thermodynamic sub-models for the entire developed model of the PEM fuel cells

4.5 Summary

This research mainly focuses on the dynamic behaviour of the PEM fuel cell associated with changes in pressures or flow rates of the reactants, hence the slower dynamics associated with variations in temperature and heat dissipation are neglected. Also the impact of heat radiation or conduction between anodes-cathodes and supply-return manifolds are very small and can be ignored. Hence, the temperature of gases in the anodes-cathodes and also along the supply-return manifolds will be uniform and equal to the stack temperature, and the average stack temperature and relative humidity inside the cathode and anode are well regulated and maintained for all stages of testing and analysis.

Also, the water content in the electrolyte membrane and the mass flow rate of water across the membrane are assumed to be uniform over the two sides of membrane, and the impact of back diffusion of water molecules from cathode to anode is ignored.

It was assumed that all the gases inside the stack of the PEM fuel cells will behave as an ideal gas; also the properties of gases leaving the specific volume are the same as those inside that volume.

The dimensions of the Horizon (H-1000) fuel cell stack are relatively small and the distances between the supply-return manifolds and anodes-cathodes of the fuel cell are small, thus it was assumed that the multiple volumes for a particular part of the fuel cell stack (i.e. cathodes, anodes, supply manifolds, and return manifolds) are all lumped as one stack volume for the same particular part. Moreover, because of the small size of the stack, it was assumed that the flow of gases within any cross sections in the stack will have approximately zero flow fractions.

Therefore, the developed mathematical model of PEM fuel cell stack is described to be zero-dimensional, as the dimensions have no impact on changing the properties of the flowing fluids and hence no impact on the performance of the entire system.

The proposed model in this research presents a simplified zero-dimensional mathematical model of a self-humidifying 1 kW PEM fuel cell, developed by modelling the major electric and thermodynamic variables and parameters involved in the operation of the PEM fuel cell. The model considers the impact of environmental conditions during fuel cell operation, and incorporates the effects of different dynamic conditions, such as changes in the dynamical properties of the fluids in the supply-return manifolds and inside the anodes and cathodes of the fuel cell stack, and also properties such as pressure, temperature and flow rates.

The proposed developed model can determine the impact of load current, changes in the pressure and temperature of the surroundings, changes in the temperature; pressures and flow rates of the fluids in the supply-return manifolds and inside the anodes and cathodes, stack operating temperature, water vapour across the membrane, relative humidity in the cathodes and anodes, water content in the electrolyte membrane, thickness of the membrane and the size of membrane active area, and the volume of the cathode and anode on the steady state performance and output power of the fuel cell stack. The usage of pure oxygen or fresh air is considered as well.

The proposed developed model in this research can be used by interested researchers as a generic model and simulation platform for a self-humidifying small-sized PEM fuel cell, with an output power varying from 50 W to 1 kW. Moreover, extrapolation to higher powers is also possible; where the dimensions of the supply-return manifolds, cathodes, and anodes need to be resized in order to capacitate the increase in the mass flow rates of fuel and reactant necessary to produce power higher than 1kW from the fuel cell stack.

The mathematical equations were modelled by using Matlab-Simulink tools in order to simulate the operation of the developed model with a commercially available 1 kW Horizon (H-1000) PEM fuel cell stack.

In the next chapter, the developed mathematical model will be simulated and tuned with a 1 kW Horizon (H-1000) PEM fuel cell stack, which is used as an experimental device in order to validate and tune the developed mathematical model with the output results of the test.

Chapter Five: Model Validation of the PEM Fuel Cell and Controller Design

5.1 Experimental Procedure and Validation of the Developed PEM Fuel Cell Model

The developed mathematical model relating to the PEM fuel cell in Chapters 3 and 4 will be simulated using parameters of the commercially available 1 kW Horizon (H-1000) PEM fuel cell stack, which is used as an experimental device in order to validate and tune the developed model with the output results of the tested stack.

Matlab-Simulink is used to simulate the developed model with operating conditions similar to the real operating conditions of the tested Horizon (H-1000) PEM fuel cell stack in the laboratory.

Also, different values of tuning efficiency are adopted for the developed model, in order to find the best tuning value, which enables the developed model to perform and produce a steady state output voltages and currents close to the output voltages and currents of the tested stack. Moreover, in order to get the most accurate real data outputs, the test of the PEM fuel cell stack is repeated several times on different occasions, in order to achieve a minimum deviation between the output voltages of the tested stack and output voltages of the developed model, also a closeness in the behaviour and steady state performance between the tested stack and the developed model.

The Horizon fuel cell stack (H-1000) is designed by the manufacturer to be a self-humidified fuel cell stack, consisting of 72 cells with cell active area of 80 cm^2 and

stack rated power of 1 kW with a maximum output of 43.2 V at 24 A, the hydrogen inlet pressure is 0.45-0.55 bar, and the maximum stack operating temperature is 65 °C. The fuel cell stack has four fans installed at the exit outlet of the return manifolds of cathodes. Hence, fans are configured as a ducted inlet-free outlet, working as suction devices at the outlet of the return manifolds of cathodes. The rotational speed of the four axial fans and the frequency of purging for the outlet hydrogen valve every 10 seconds are controlled by an inbuilt stack's controller, in order to maintain enough operational pressure at the cathode and anode, and also to provide a sufficient flow of air and hydrogen leading to maintaining a certain level of stack temperature and retaining the continuity of the electrochemical reaction. Also, the controller provides a protection shutdown for the stack at 30 A over current and 36 V low voltage operation [81].

An AttoPilot 50V/90A, DC voltage-current sensor with 2 analog outputs is used to measure the output voltages and currents from the stack via stepping down the detected voltage and current at a ratio of (63.69 mV/1V), and (36.6 mV/1A).

A USB interface data acquisition (NI USB-6008) with 8 analog inputs and 2 analog outputs ports is used to capture the real time currents and voltages, while LabVIEW v13.0 software is used for the purpose of data recording and analysis, with the sampling frequency set on 1 Hz.

SkyRC *i*-Meter operates for a maximum input voltage and current of 60 V and 100 A is used to manually measure the output voltages and currents from the fuel cell stack. And DC-DC Converter (Mean Well SD-1000L-24) with an input range of 19 V to 72 V and output of 24 V, with 40 A maximum current, is installed between the fuel cell stack and the BLDC motor in order to stabilise and maintain the output voltage.

A three phases, 14 poles, brushless DC Motor BLDC (KMS Quantum 4130/07) is used as an attached load to the Horizon fuel cell stack. The motor operates at supply voltage

of 18.5-29.6 V, with a maximum continuous current of 40 A and a maximum efficiency higher than 90%, and the ratio of rotational speed (rpm) to the supply voltage is 360/V. Al's Hobbies Professional analogue-digital servo tester is used to adjust the rotational speed of the BLDC motor and its propeller via generating a PWM signal to the electronic speed controller (ESC) in order to increase-decrease the current drawn from the fuel cell stack.

A pressure reduce valve (Swagelok) is used to maintain the supply pressure of hydrogen to the stack at 55 kPa. A temperature and humidity data-logger (KTH-300 Kistock), integrated with thermo-hygrometry (TH) probe sensor, is used to measure the temperature of the exit air from the stack.

The stack of Horizon PEM fuel cells has four extractor fan outlets, and TH sensors are mounted at each fan outlet in an attempt to obtain an accurate estimate of temperature. The stack temperature is determined by taking the average of the sums of temperature readings for these four TH sensors.

Figure 5.1 shows the block diagram configuration and bench layout of the Horizon (H-1000) fuel cell stack configured with measuring and controlling devices and the BLDC motor load during the testing process carried out in the laboratory. The defined values of variables and constants for the operational parameters involved in the simulation of the developed mathematical model for the PEM fuel cell stack are presented in Table 5.1.

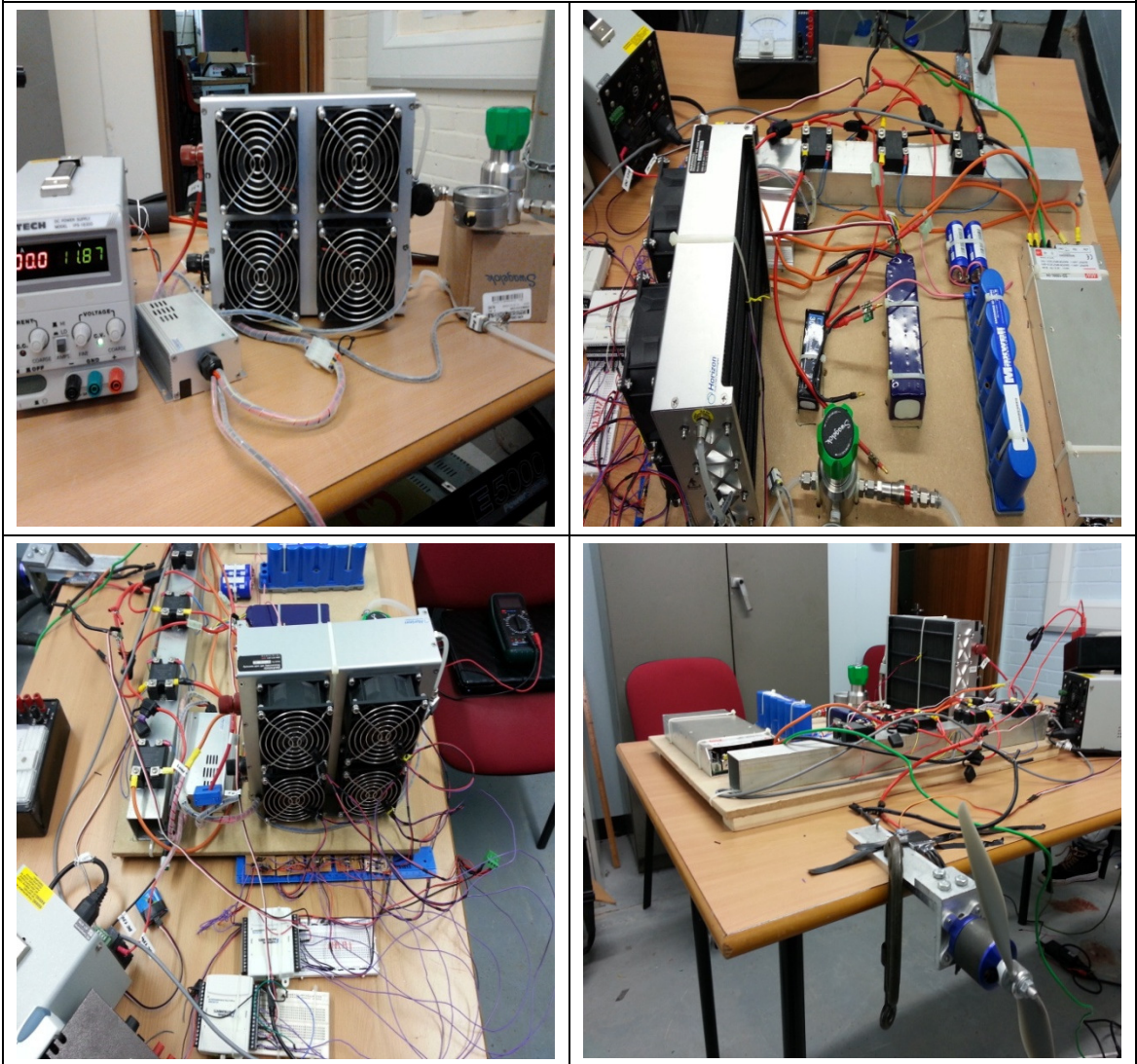
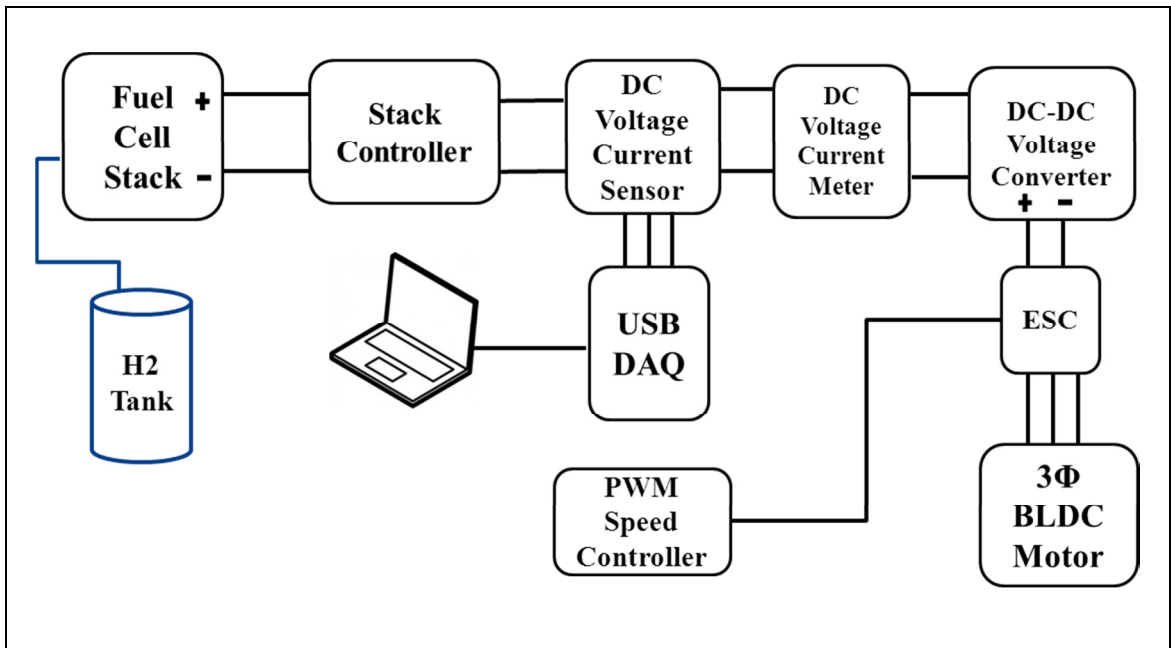


Figure 5.1: Block diagram configuration and bench layout of Horizon (H-1000) fuel cell stack configured with measuring and controlling devices, and a BLDC motor load

Table 5.1: Defined values of variables and constants for the operational parameters involved in the developed model of PEM fuel cell stack	
Variables and Constants	Defined Values
Number of cells in the stack (n)	72
Active area of electrolyte membrane (A_{fc})	80 cm ²
Water content in electrolyte membrane (λ)	7
Membrane thickness (L)	$25 * 10^{-4}$ cm
Maximum current density (i_m)	500 mA/cm ²
Temperature of supply air and hydrogen	Ambient Temperature
Ambient pressure	101.325 kPa
Ambient air density	1.225 kg/m ³
Pressure of supply hydrogen	55 kPa
Density of supply hydrogen	0.0899 kg/m ³

5.1.1 First Test

The Horizon (H-1000) PEM fuel cell stack is tested under atmospheric pressure and 23°C ambient temperature. The stack is operated for about 25 minutes under different levels of load current varying from 1 to 17 A in steps of 1 A, with an approximate holding time of one and a half minutes. One TH sensor is installed at the exit outlet of the fan in order to measure the temperature of the stack.

The developed mathematical model of the PEM fuel cell is simulated with an ambient temperature, stack temperature, and drawn current similar to the real operating

conditions of the tested Horizon (H-1000) PEM fuel cell stack in the laboratory, and the measured readings and the results of the simulation are presented in Table B.1 in Appendix B.

Different values of tuning efficiency (83%, 84%, 85%, and 86%) are adopted for the developed model of the PEM fuel cell. It was found that the best tuning value for the developed model, which enables the model to perform and produce output voltages close to the steady state output voltages of the tested stack, was at 84% with a 0.78 V average deviation between the output voltages of the tested stack and output voltages of the developed model, as shown in Table B.1 in the Appendix B. The output voltages for the tested Horizon (H-1000) fuel cell stack and the developed model are shown in Figure 5.2.

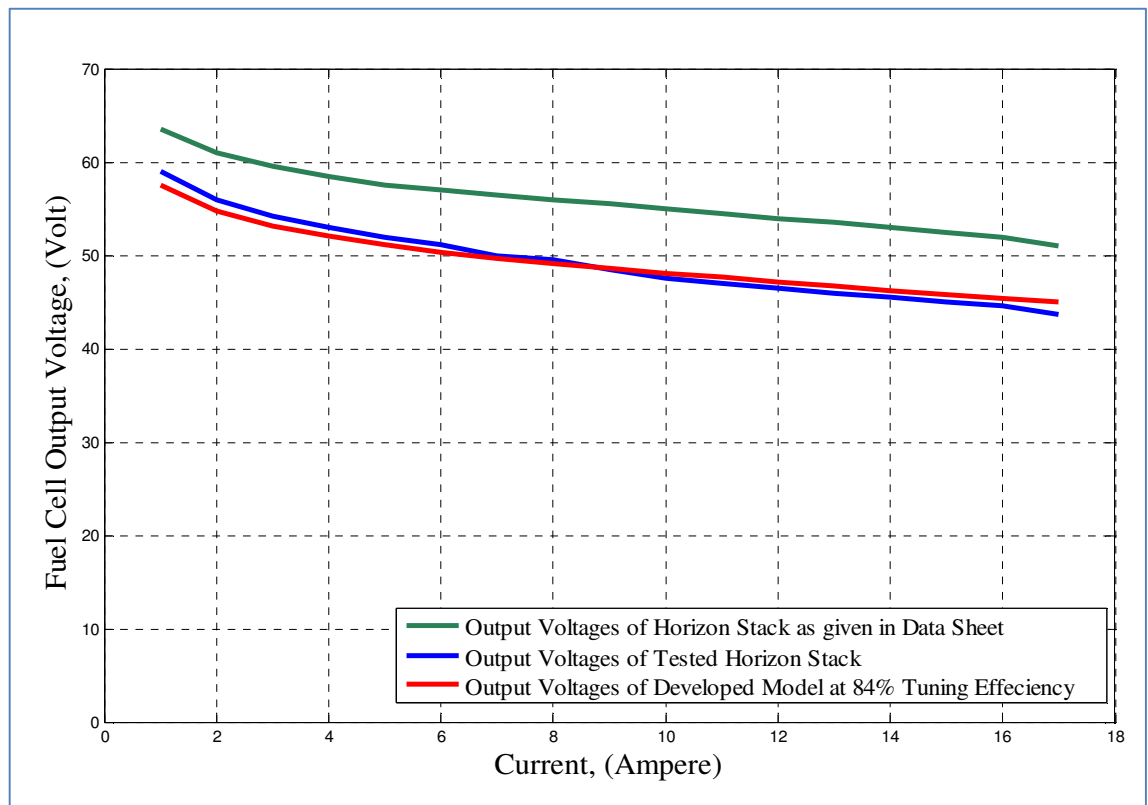


Figure 5.2: Output voltages for the Horizon (H-1000) fuel cell stack and mathematical developed model of the PEM fuel cell under various drawn load currents

The green line represents the output voltages as given in the data sheet of the 1 kW Horizon (H-1000) PEM fuel cell stack, for operating conditions defined at sea level and 25 °C ambient temperature. The blue line represents the steady state output voltages of the tested stack for about 25 minutes continuous operation at 23 °C ambient temperature, under different levels of load current varying from 1 to 17 A in steps of 1 A, with an approximate holding time of one and a half minutes. The red line represents the output voltages of the mathematical developed model based on operating conditions similar to the real operating conditions of the tested Horizon (H-1000) PEM fuel cell stack in the laboratory, with 84% model tuning efficiency.

It is clear that the performance and output voltages of the mathematical model developed for the PEM fuel cell is fairly close to the steady state performance and output voltages of the tested Horizon stack operated under varied levels of load current and stack temperature, which provides initial satisfaction about the validity of the proposed developed model in this research.

5.1.2 Second Test

The Horizon (H-1000) PEM fuel cell stack is tested under atmospheric pressure and 18°C ambient temperature. The stack is operated for about 38 minutes under different levels of current load varying from 0 to 25 A, with an approximate holding time of two minutes. Four TH sensors are installed at the exit outlets of four fans in order to obtain an accurate estimate of temperature. The impact of drawn load current and operational duration upon the temperature of the Horizon (H-1000) fuel cell stack are measured and presented in Table B.2 in Appendix B, while Figures 5.3, 5.4, and 5.5 reveal these impacts.

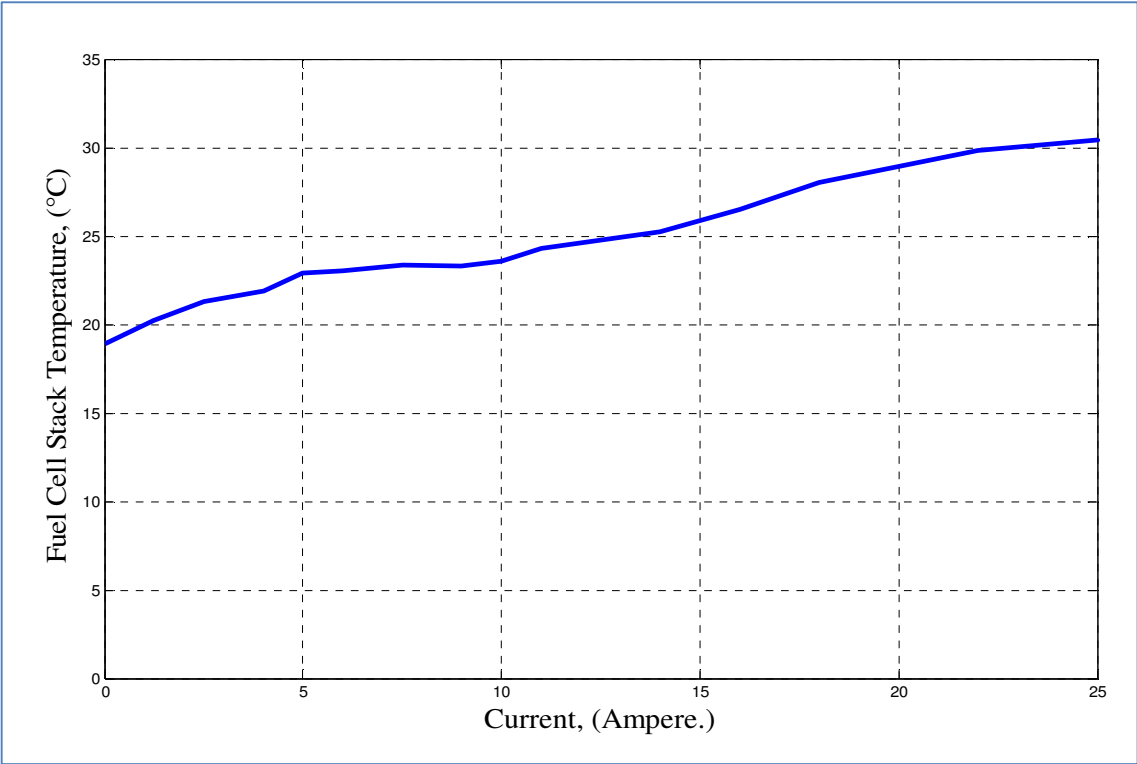


Figure 5.3: Impact of drawn load current on the temperature of the Horizon (H-1000) fuel cell stack

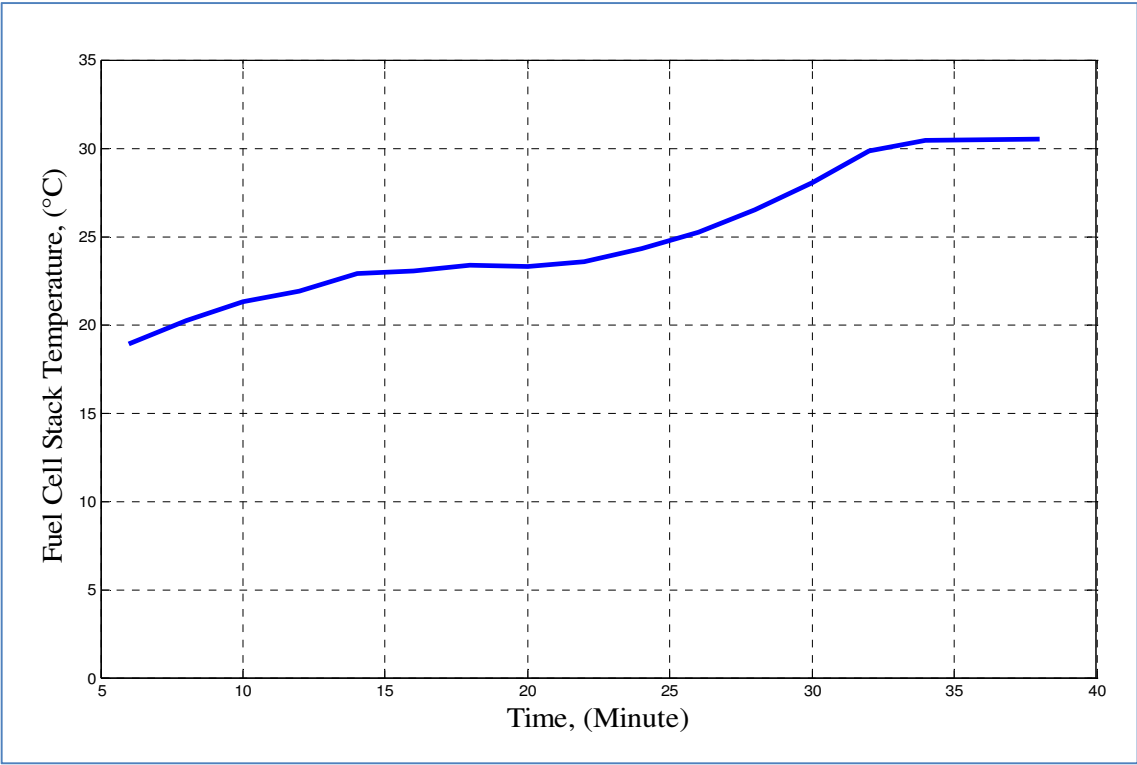


Figure 5.4: Impact of operational duration at varied load current on the temperature of the Horizon (H-1000) fuel cell stack

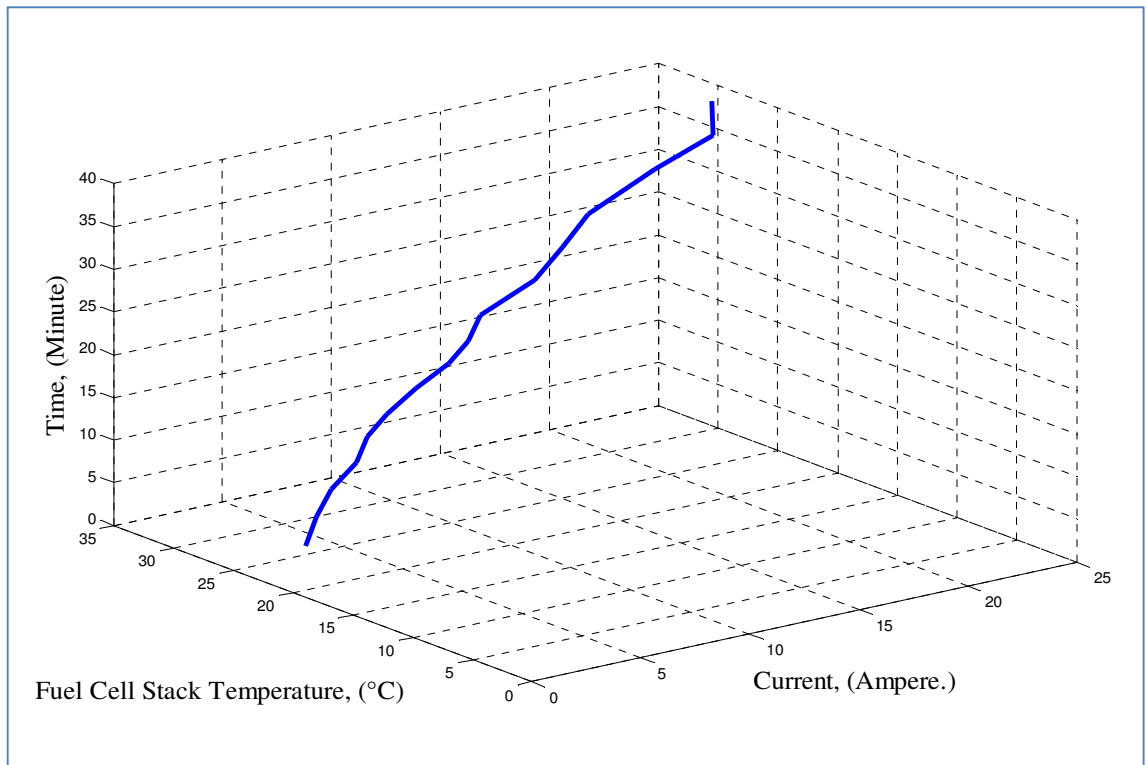


Figure 5.5: Impact of drawn load current and operational duration on the temperature of the Horizon (H-1000) fuel cell stack

5.1.3 Third Test

The Horizon (H-1000) PEM fuel cell stack is tested under atmospheric pressure and 20°C ambient temperature. The stack is operated for about 43 minutes under different levels of current load varying from 1 to 20 A, with an approximate holding time of three minutes. Data acquisition is set to capture and record the output voltages and drawn currents from the stack every 30 seconds, and four TH sensors are installed at the exit outlets of four fans in order to obtain an accurate estimate of temperature. Figure 5.6 shows the output voltages and drawn currents for the tested Horizon (H-1000) fuel cell stack, while Figure 5.7 shows the average voltages for each level of drawn current.

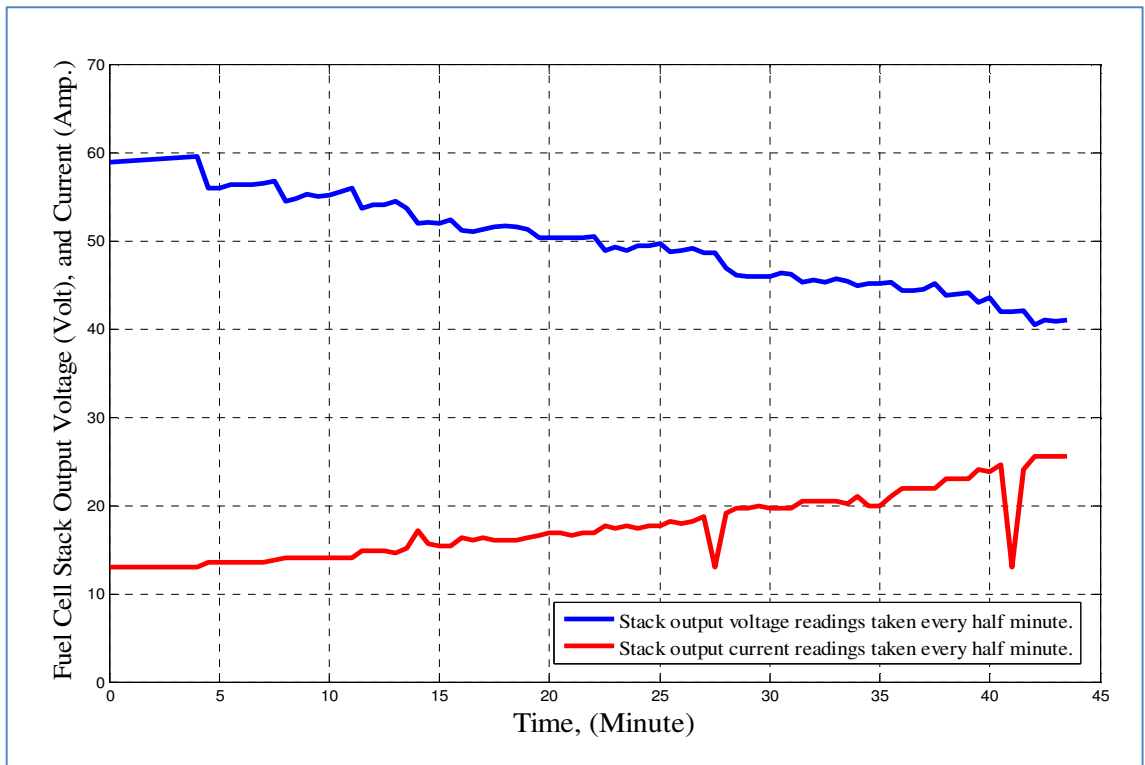


Figure 5.6: Output voltages and drawn currents for the Horizon (H-1000) fuel cell stack

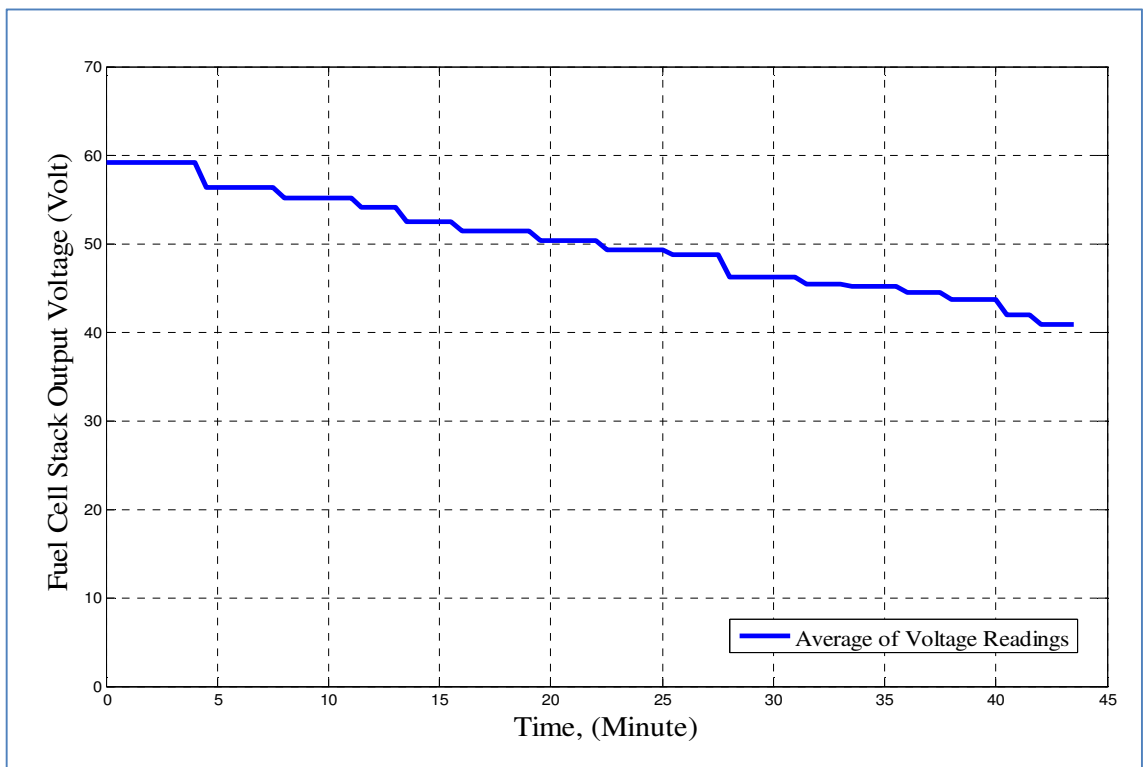


Figure 5.7: Average of output voltages for each level of drawn current from the Horizon (H-1000) fuel cell stack

The developed mathematical model of the PEM fuel cell is simulated with an ambient temperature, stack temperature, and drawn current similar to the real operating conditions of the tested Horizon (H-1000) PEM fuel cell stack in the laboratory, and the measured readings and the results of the simulation are presented in Table B.3 in Appendix B.

Different values of tuning efficiency (83%, 84%, 85%, and 86%) are adopted for the developed model of the PEM fuel cell. It was found that the best tuning value for the developed model, which enables the model to perform and produce output voltages close to the steady state output voltages of the tested stack, was at 85% with a 1.44 V average deviation between the output voltages of the tested stack and output voltages of the developed model, as shown in Table B.3 in the Appendix B. Figure 5.8 presents the output voltages for the tested stack under varied load currents and stack temperatures, and the output voltages for the developed model at 85% tuning efficiency; under varied load currents; for both varied stack temperatures and constant average stack temperature (27.73 °C). The impact of drawn currents and operational duration upon the temperature of the Horizon fuel cell stack are shown in Figures 5.9, 5.10, and 5.11, respectively.

It can be noticed from Figure 5.8, that for the developed PEM fuel cell model at 85% tuning efficiency, there are very small variations between the output voltages of the model at varied stack temperatures (represented by the red line) and the output voltages of the model at a constant average stack temperature of 27.73 °C (represented by the green line). Hence, the values of 85% tuning efficiency and 27.73 °C average stack temperature will be adopted for any further simulations for the developed mathematical model of the PEM fuel cell in this research.

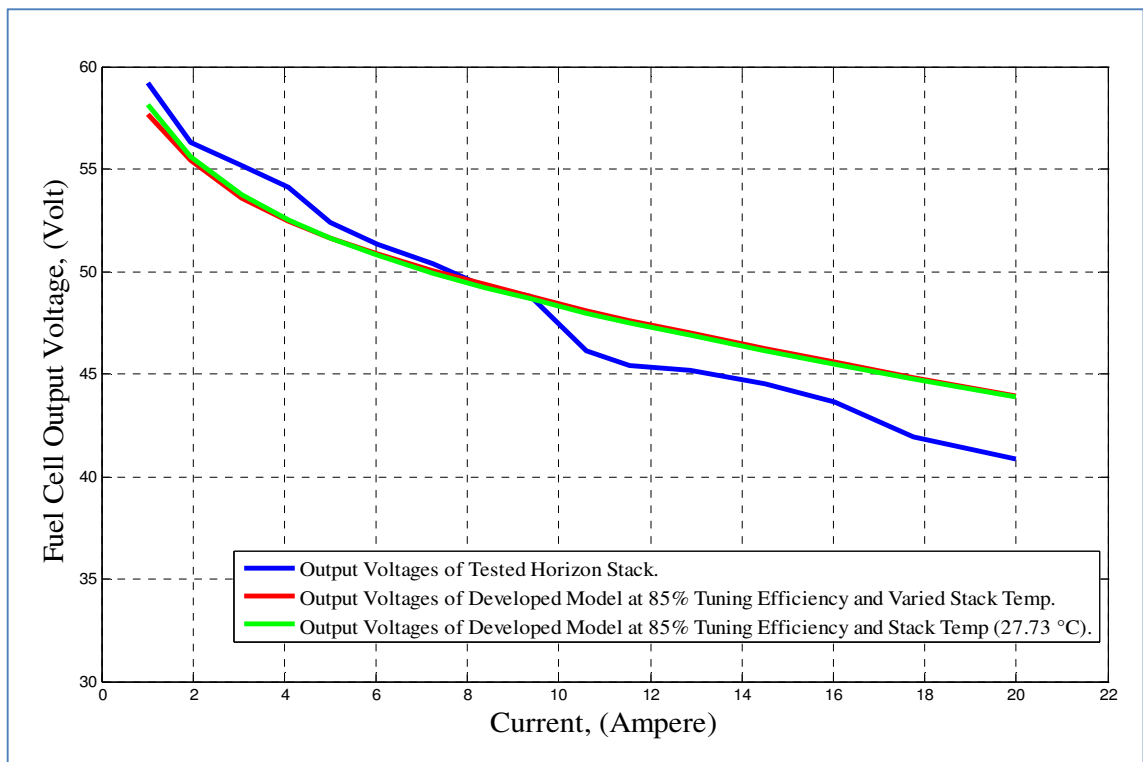


Figure 5.8: Output voltages of Horizon fuel cell stack test, and developed model of PEM fuel cell, under varied load currents and stack temperatures, and 85% tuning efficiency

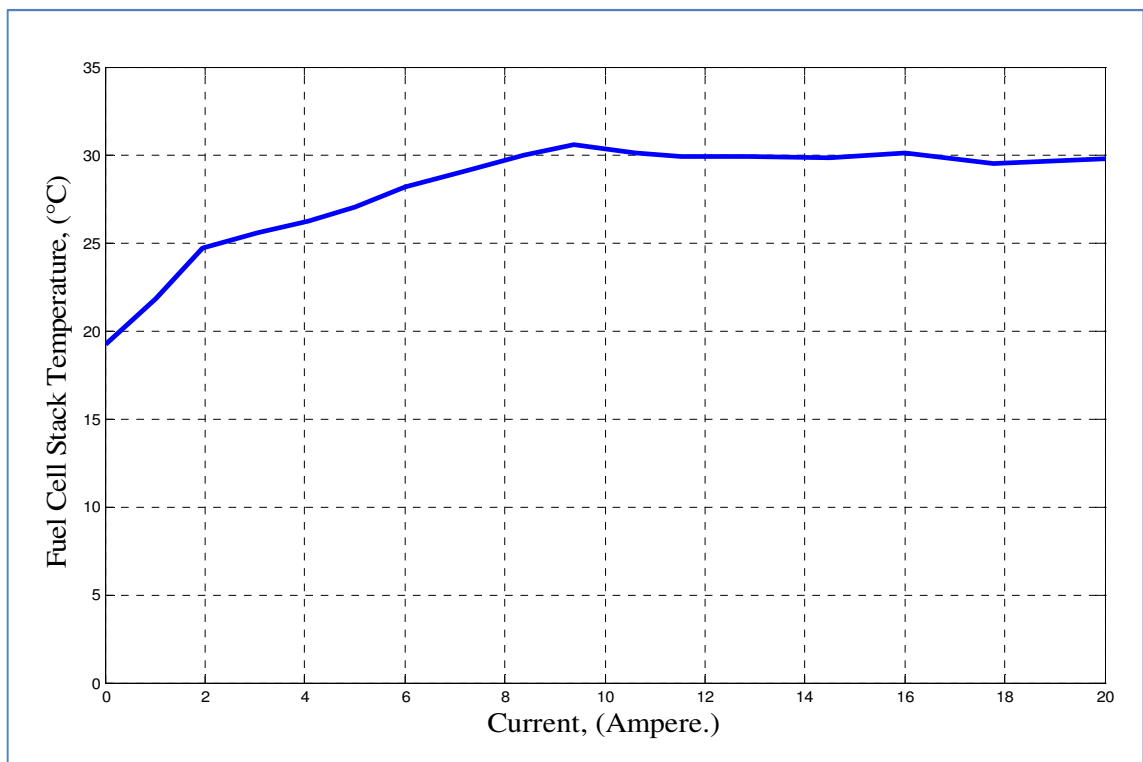


Figure 5.9: Impact of drawn current on the temperature of the Horizon (H-1000) stack

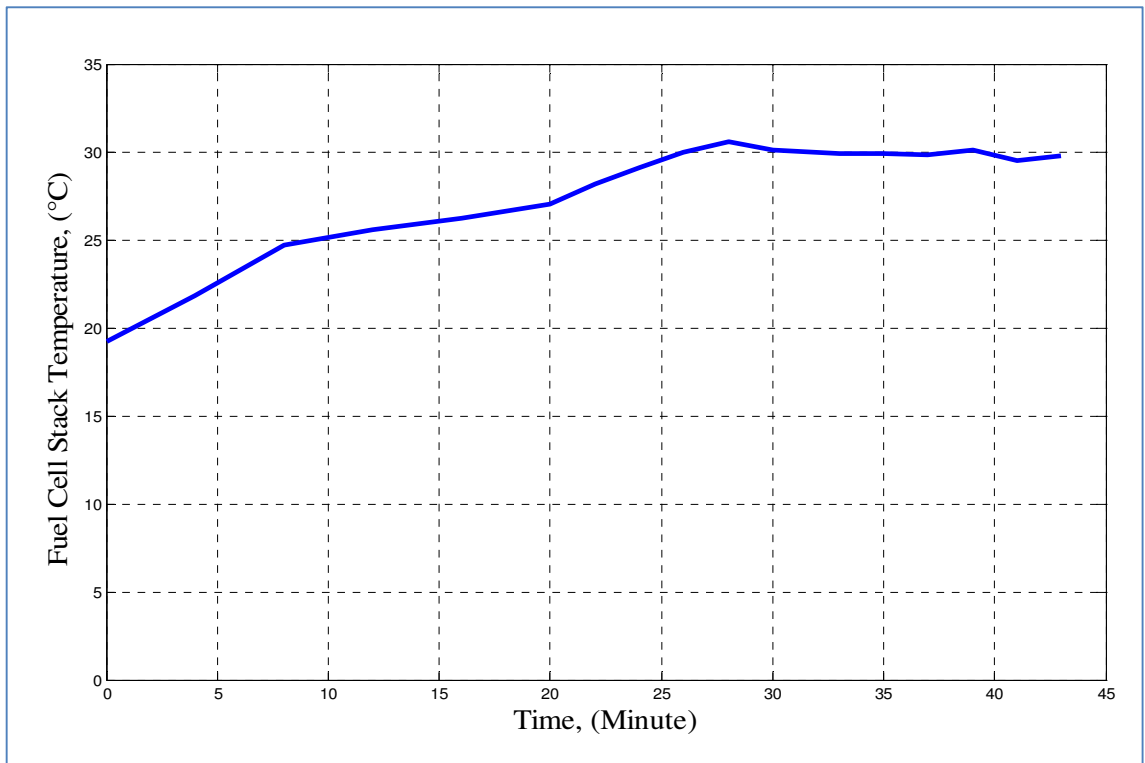


Figure 5.10: Impact of operational duration at varied load current on the temperature of the Horizon (H-1000) fuel cell stack

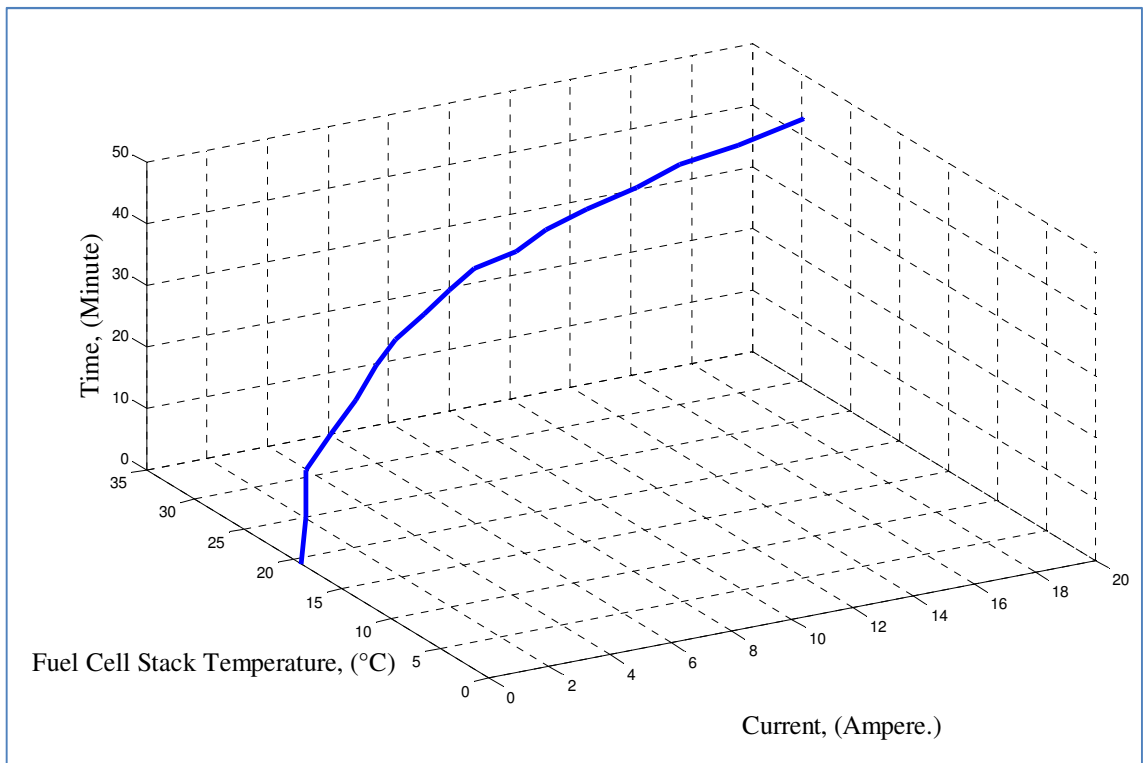


Figure 5.11: Impact of drawn current and operational duration on the temperature of the Horizon (H-1000) fuel cell stack

5.1.4 Fourth Test

The Horizon (H-1000) PEM fuel cell stack is tested under atmospheric pressure and 21.5°C ambient temperature. The test begins after leaving the fuel cell stack for about one hour from the last running test in order to refresh and rest the stack. The stack is operated for about 32 minutes, under constant load current of 9.08 A. Four TH sensors are installed at the exit outlets of four fans in order to obtain an accurate estimate of temperature, and readings are captured every two minutes. The impact of constant drawn load current and operational duration upon the temperature of the Horizon fuel cell stack are measured and presented in Table B.4 in Appendix B, Figure 5.12 visually represents this impact.

The output voltages for the tested Horizon fuel cell stack and the developed model of PEM fuel cell under the impact of constant drawn current 9.08 A and varied operating temperature are as shown in Figure 5.13. Where, the output voltages of the tested stack are almost stable around 51.6 V, and the fluctuations in the stack output are as a result of the drop in the pressure of hydrogen in the anode chambers of the Horizon PEM fuel cell stack, due to a frequent breathing process triggered by the hydrogen purging valve. While the output voltages of the developed model of PEM fuel cell are almost stable around 49-49.5 V, due to the variations in the operating temperature of the stack.

It is clear from the results presented for the tested Horizon (H-1000) fuel cell stack, as shown in the Figures (5.3, 5.4, 5.5, 5.9, 5.10, and 5.11), that the stack's temperature has a tendency to increase with operating time and drawn current. The temperature of the stack is maintained around 30 °C even if operational time is increased or there are further increases in the drawn current. This is due to the stack controller, which works to suppress any increase in the stack's temperature above 30 °C by pumping more air to the cathode, in order to maintain the operating temperature of the stack around a certain operating temperature.

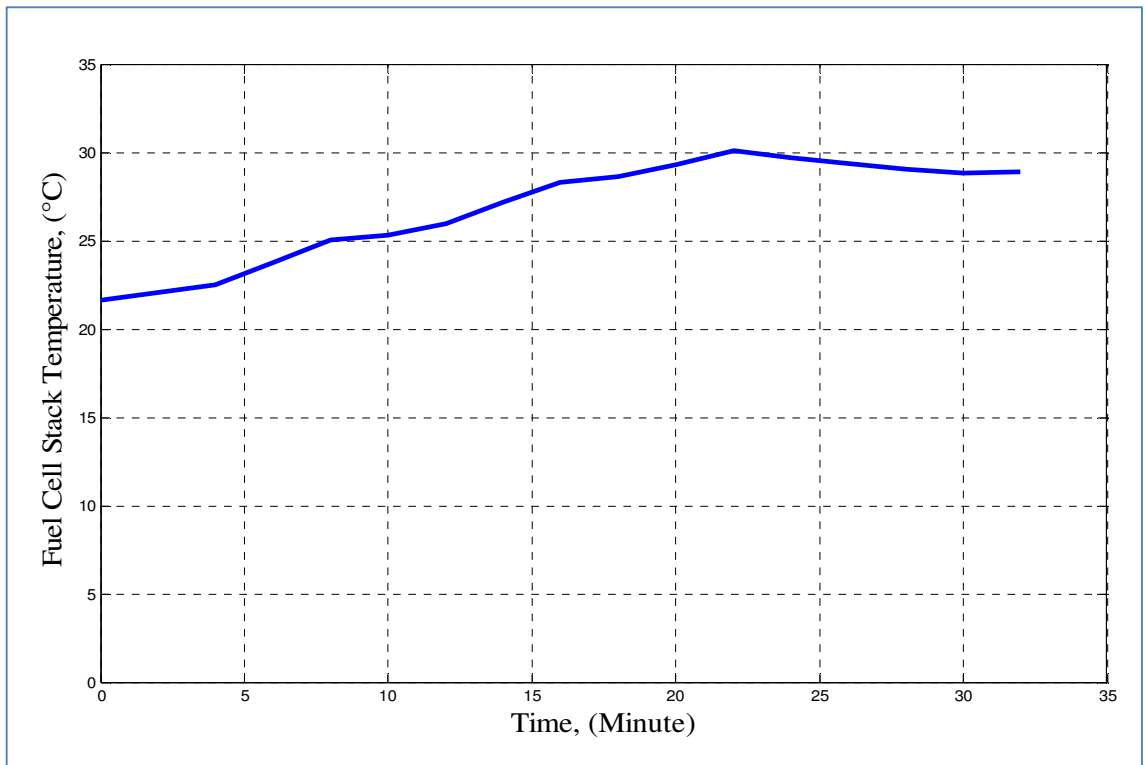


Figure 5.12: Impact of constant drawn load current and operational duration on the temperature of the Horizon (H-1000) fuel cell stack

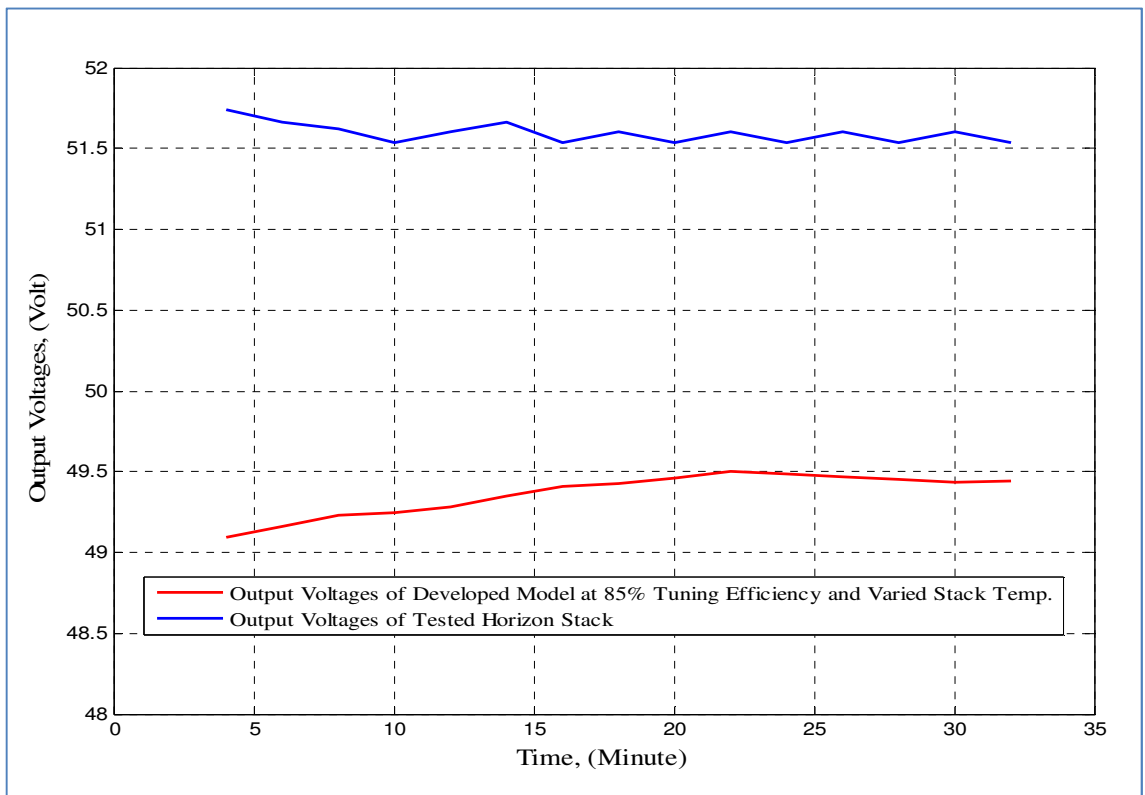


Figure 5.13: Output voltages for Horizon (H-1000) stack and the developed model of PEM fuel cell under the impact of constant drawn current and varied operating temperature

Kim and Kwon [24] adopted a 100 W Horizon PEM fuel cell stack as a prime source of power for a small unmanned aircraft. The test results and the performance evaluation obtained from continuously operating the stack for about 5 hours under 50 W of constant load showed that the temperature of the stack increases from 22 °C to 35 °C during the first 30 minutes of the stack's operation, while the stack's temperature is maintained below 35 °C for the rest hours of the test.

These observations and the closeness in the steady state performance and output voltages between the developed model of the PEM fuel cell in this research and the tested 1 kW Horizon (H-1000) PEM fuel cell stack, provide sufficient confidence in the validity and accuracy of the developed model, this is based on choosing the right tuning efficiency, which offers a minimum deviation between the output voltages of the tested stack and the developed model. The proposed developed model in this research can be used by the interested researchers as a generic model and simulation platform for a self-humidifying small-sized PEM fuel cell with an output power varying from 50 W to 1 kW. Moreover, extrapolation to higher powers is also possible; where the dimensions of the supply-return manifolds, cathodes, and anodes need to be resized in order to capacitate the increase in the mass flow rates of fuel and reactant necessary to produce power higher than 1 kW from the fuel cell stack.

5.2 PID Controller for Air and Hydrogen Supply

A proportional-integral-derivative (PID) controller is widely used in terms of commercial applications [91]. A PID controller was used to regulate the output voltage at a certain set point via controlling the flow rate of hydrogen and oxygen for a hybrid power-plant system of a 240 W PEM fuel cell stack used for a C-130 Hercules aircraft, as reported by Radmanesh et al. [6]. A proportional controller adjusts the speed, the

integral part the steady state error, and the derivative part the stability and the dynamic response [92].

Chen and Khaligh [66] used a proportional-integral (PI) controller to control the flow of currents between the load, fuel cell/electrolyser stack, solar photovoltaic panel, and the rechargeable batteries for a hybrid energy storage system, in order to extend the endurance of the UAS.

In this research, a PID controller is adopted to control the flow of fuel and air supplied to the PEM fuel cell stack, based on determining the current of the fuel cell stack with respect to the change in the demand current of the connected load. In order to determine the performance of the PID controller due to the change in the load demand, the following strategy was adopted:

1. The simulation of the PEM fuel cell model was started from time zero up to the first second, based on the initial value of the current equalling 1 A, with the output voltage equal to 58.2 V.
2. After the first second, the load demand was increased to 2 A and the power required to 111 W, resulting in an output voltage from the PEM fuel cell equal to 55.5 V.
3. The simulation lasted for four seconds further, in order to achieve five seconds of model simulation.
4. A mechanical adjustment delay of 200 ms corresponds to an arbitrary mechanical delay of flow valve adjustment.

It is observed that PID controller must be tuned between a zero and one second response interval, any settings for a time response higher than one second must be avoided as this will cause a delay in the response of the developed model of the PEM fuel cell to the power demand, as shown in Figure 5.14, for a PID controller with time response setting at 1.35 second, and integral value of 1.4763.

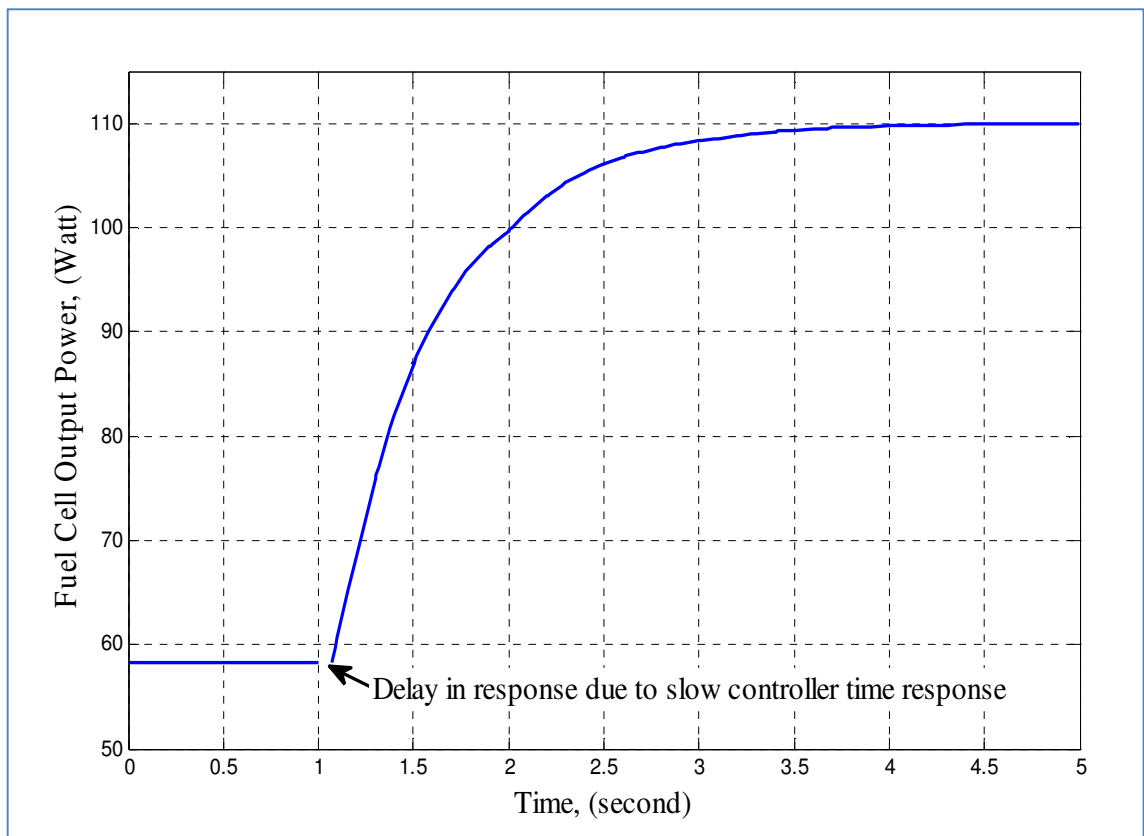


Figure 5.14: Response of developed PEM fuel cell model to the power demand for PID controller with time response setting at 1.35 second and integral value (1.4763)

The responses of the PID controller and time settings are tuned for seven different settings, by adjusting the response time of the controller via using the Auto-Tune function of the PID settings, which automatically determines the values of proportional, integral, and derivative settings, as presented below:

1. Zero delay response: Integral controller with setting response time 0.981 second, at integral value 2.038. The system response reaches outputs of 1.9 A and 105.8 W after 0.94 second, and reaches 2 A and 110.947 W after 2.62 seconds.
2. Fast response-1: Integral controller with setting response time 0.895 second, at integral value 2.2345. The system response reaches outputs of 1.9 A and 105.8 W after 0.7 second, and reaches 2 A and 110.947 W after 2.456 seconds.

3. Fast response-2: Integral controller with setting response time 0.78 second, at integral value 2.5655. The system response reaches outputs of 1.9 A and 105.8 W after 0.51 second, and reaches 2 A and 110.947 W after 2.373 seconds.
4. Fast response-3: PI controller with setting response time 0.679 second, at proportional value 0.0655, and integral value 2.9393. The system response reaches outputs of 1.9 A and 105.84 W after 0.41 second, and reaches 2 A and 110.947 W after 2.36 seconds.
5. Fast response-4: PI controller with setting response time 0.565 second, at proportional value 0.1837, and integral value 3.48112. The system response reaches outputs of 1.9 A and 105.8 W after 0.288 second, and reaches 2 A and 110.943 W after 2.24 seconds.
6. Overshoot-1: PID controller with setting response time 0.47 second, at proportional value 0.38513, integral value 3.7623, and derivative -0.02962. The system response reaches outputs of 1.9 A and 105.75 W at 0.178 second, and reaches 2 A and 110.5W at 2.18 seconds.
7. Overshoot-2, PID controller with setting response time 0.373 second, at proportional value 0.694, integral value 3.6508, and derivative -0.065. The system response reaches outputs of 1.9 A and 105.8 W at 0.139 second, then jumps to 2.15A and 119 W at 0.2 second, and settled on 2 A and 110.9 W at 2.75 seconds.

The output responses of the simulation of the developed PEM fuel cell model for various PID settings are presented in Figures 5.15 and 5.16, respectively. Table 5.2 presents the amount of air and hydrogen that needs to be supplied to the developed model of the PEM fuel cell stack in order to deliver the required level of power for a current load varying from 1 A to 2 A, with different PID controller settings. However, these settings apply only to the developed PEM fuel cell model based on the Horizon (H-1000) stack; other PEM stacks may have different tuning parameters.

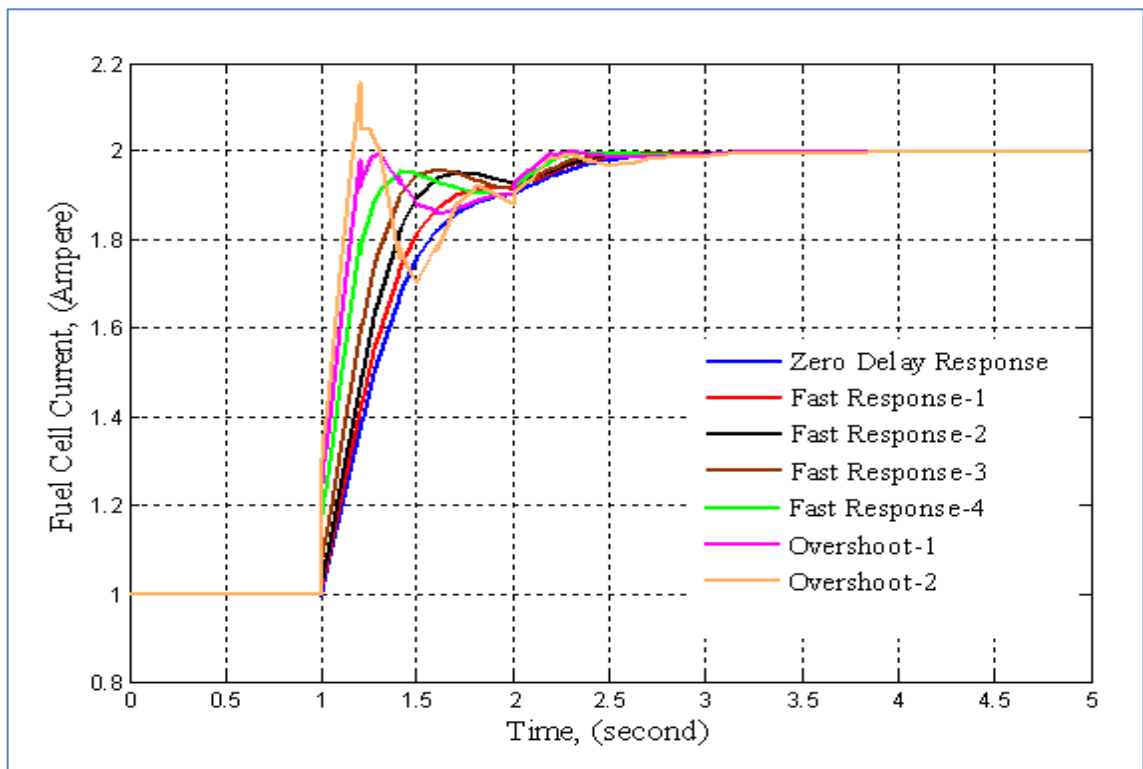


Figure 5.15: Responses of the developed PEM fuel cell model to the current demand varying from 1 A to 2 A, for PID controller with various time response settings

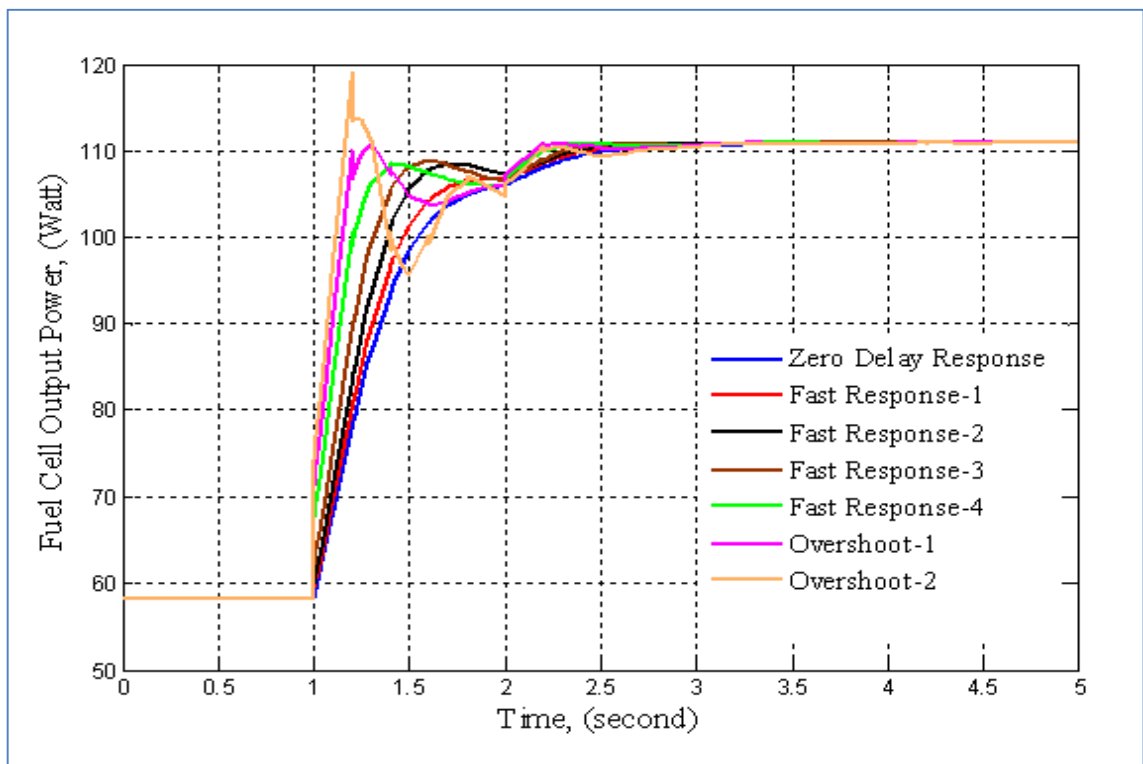


Figure 5.16: Responses of the developed PEM fuel cell model to the power demand varying from 58.2 W to 111 W, for PID controller with various time response settings

Table 5.2: Supply air and hydrogen to the developed model of PEM fuel cell stack with current demand varies from 1 A at (58.2 W) to 2 A at (111 W), for various PID response tuning settings				
Type of Controller	Response Time (sec.)	Response Type	Supply Air m ³ /hour	Supply Hydrogen Kg/hour
Integral	0.981	Zero delay	26.0234	0.0069
Integral	0.895	Fast response-1	26.1837	0.0069
Integral	0.78	Fast response-2	26.3700	0.0070
PI	0.679	Fast response-3	26.5198	0.0070
PI	0.565	Fast response-4	26.6924	0.0071
PID	0.47	Overshoot-1	26.7577	0.0071
PID	0.373	Overshoot-2	26.6843	0.0071

It is clear that reducing the time response of the PID controller leads to improving the overall response of the system. But, for Overshoot-2, the system starts to take a longer time to settle in comparison with Overshoot-1, as shown above in Figures 5.15 and 5.16, respectively.

From above results and settings, it can be concluded that the fast response-3 setting for the PI controller provides the most adequate trade-off choice between fast response and hydrogen-air consumption, in comparison with other settings. Therefore, this setting is going to be considered in optimising the consumption of air and hydrogen for the developed model of the PEM fuel cell used for the proposed UAS operation in this research.

Figure 5.17 presents the Simulink block diagram of the proposed PID controller for the developed model of the PEM fuel cell stack system. While Figure 5.18 presents a Simulink block integration between the PID controller and the entire developed model of the PEM fuel cell stack system.

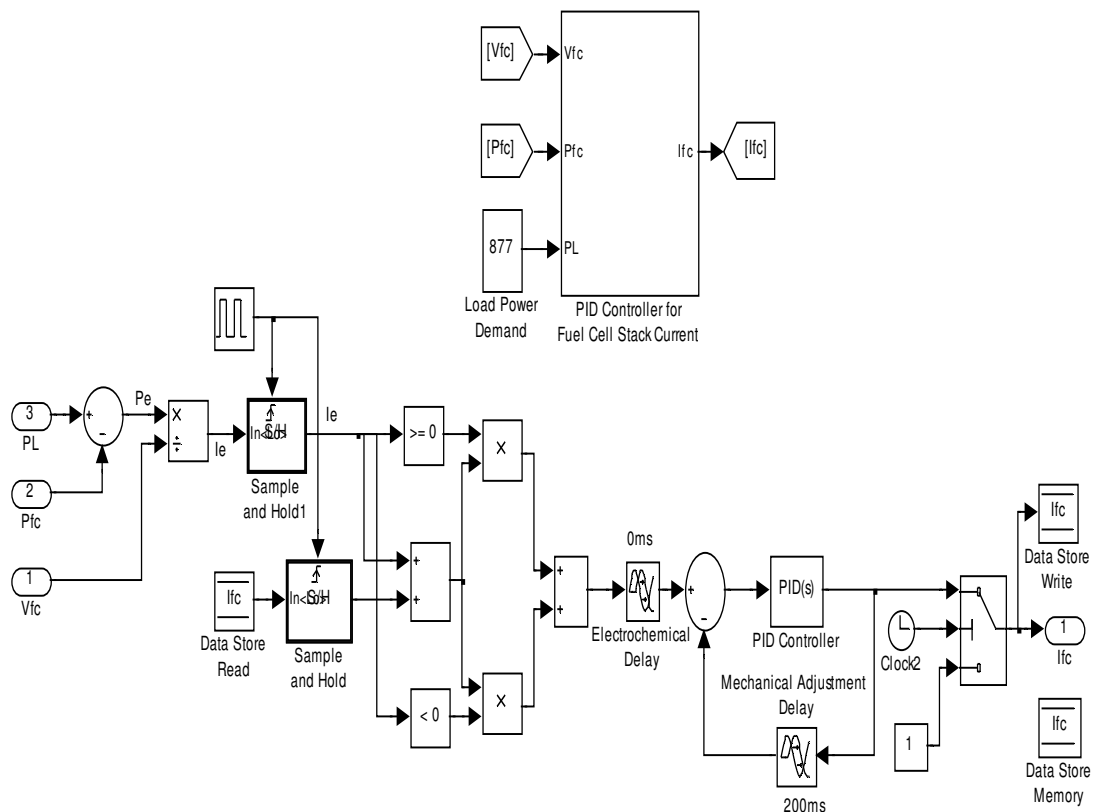


Figure 5.17: Simulink block diagram of the PID controller for the developed model of the PEM fuel cell stack system

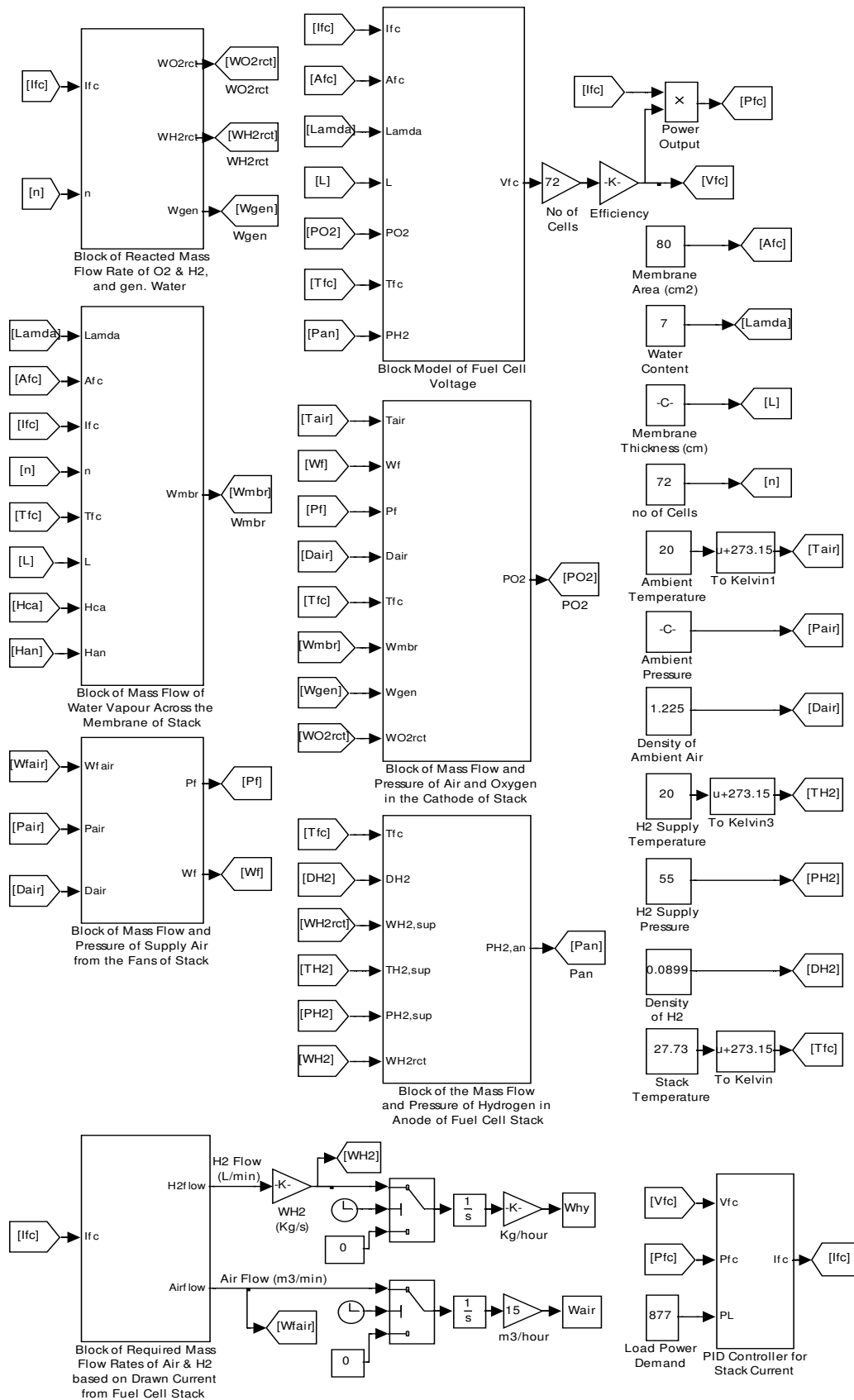


Figure 5.18: Simulink block integration between the PID controller and the entire developed model of the PEM fuel cell stack system

5.3 Summary

The mathematical model of the PEM fuel cell developed in Chapters 3 and 4 was simulated with a 1 kW Horizon (H-1000) PEM fuel cell stack, which was used as an experimental device to validate and tune the developed model with the output results of the tested stack.

The Horizon stack was tested and operated under varied levels of load current and stack temperatures, and the tests were repeated several times on different occasions in order to capture the most accurate real data output. The results obtained from the tested Horizon (H-1000) stack, and the simulations of the developed model of the PEM fuel cell show a close match in the steady state outputs and performance. Moreover, it has been noticed that for the simulated model at a tuning efficiency of 85% and 27.73 °C average stack temperature, there was a closeness in the performance and output voltages between the developed model and the tested stack, which provides sufficient confidence in the validity and accuracy of the developed model.

It is clear from the results presented for the tested Horizon (H-1000) fuel cell stack; that the stack's temperature has a tendency to increase with operating time and drawn current. The temperature of the stack was maintained around 30 °C, irrespective of extended operation or further increases in the drawn current.

Different settings of the PID controller were investigated in terms of optimising the consumption of air and hydrogen and getting a faster time response of the controller, and it was concluded that a proportional-integral (PI) controller with time response of 0.679 second at a proportional value of 0.0655, and integral value of 2.9393, provides the most adequate trade-off choice between fast response and hydrogen-air consumption, in comparison with other settings. Therefore, this setting is going to be used in optimising the consumption of air and hydrogen for the developed PEM fuel cell model used for the proposed UAS operation in the next chapters of this research.

However, these settings apply only to the developed PEM fuel cell model based on the Horizon (H-1000) stack; other PEM stacks may have different tuning parameters. In the next chapter, the implications of high altitudes upon the performance and operation of the PEM fuel cell will be investigated.

Chapter Six: Implications of High Altitudes on the Operation of PEM Fuel Cell Based UAS

6.1 Introduction

For high altitude long endurance (HALE) unmanned aircraft systems where a fuel cell operates as the prime source of power, the operation and performance of a PEM fuel cell at different altitudes is vitally important. In particular, for long journeys and at high altitude, wind turbulence and unexpected variations in the load demand make it necessary to find a stable and robust controller which can optimise and provide a fast and sufficient flow of hydrogen and air to the reaction of the fuel cell. This is one of the critical objectives in controlling a PEM fuel cell for UAS applications.

Bégot et al. [27] reported that it is a complicated task to start-up and operate the fuel cell stack with sub-zero ambient temperatures, as the water produced in the cathode can turn to ice which can block the passage of the reactant from reaching the reaction interface. The frozen water can change the conductive properties of the electrodes, membrane and in worst cases can damage the membrane. It has been found that the formation of ice will reduce the active surface of the electrode-catalytic layer which leads to a reduction in the rate of the electrochemical reaction, causing a high drop in fuel cell output power. At a high altitude of 11 km (~36,000 ft.), atmospheric temperature and pressure are approximately -56 °C and 0.227 bar, while air density is around 0.365 kg/m³, these are severe conditions for a fuel cell to operate. Also, published experimental data for such operating conditions are very limited [93].

It has been reported that Cessna and Boeing tested a 1.2 kW Ballard Nexa PEM fuel cell system at pressure of altitudes up to 5000 ft. (1524 m); they showed a drop of 25% in net power from 1300 W at sea level to 970 W at 5000 ft. Another test on a Ballard system was carried out by the U.S. Environmental Protection Agency for altitudes up to 7400 ft. (~2256 m) showing a decline in net power by 24% compared with sea level operation. While another stack manufacturer reported that between altitudes of 1000 ft. and 10,000 ft., the power output of the fuel cell stack drops by 1.5% per 1000 ft., for a fuel cell using fresh air extracted directly from the atmosphere. However, predicting performance of a fuel cell for altitudes higher than 10,000 ft. might be different to the predicted values for lower altitudes. Therefore, further studies are needed to accurately determine the impact of high altitude conditions on both the performance of the fuel cell stack and its power output, which are vital for the design requirements of fuel cell systems in aerospace applications [93].

6.2 Implications of High Altitudes on the Performance of the PEM Fuel Cell

In the last few years, small numbers of successful flight tests of light unmanned aircraft systems powered by fuel cells have been reported. However, most of these tests were restricted to short duration low altitude flights [28].

A PEM fuel cell for UAS applications needs careful water management, particularly for low temperature high altitude environment operations. Also, controlling the fuel cell temperature is a vital issue particularly at high current demand, as it needs a significant volume of air to cool down the stack, which otherwise increases the parasitic losses of the system. However, if heat transfer from the stack system to the environment and vice versa is managed and controlled effectively by using proper thermal insulation to

maintain the power system within the operational temperature boundaries, thereby reducing the amount of cooling air required, which improves the system efficiency [10]. At high cruise altitudes of UAS-based fuel cells, where the temperature and pressure are very low, air needs to be compressed in order to raise its pressure to an acceptable operational pressure level, also fuel and air must be heated up before being supplied to the stack in order to avoid excessive stack cooling and hence thermal stress caused by cold streams [10].

A water cooling system can be used to maintain stack temperature, but it is not appropriate for UAS applications, as it needs a coolant tank, pump and heat exchanger, which leads to an increase in the size, weight and complexity of the entire system. Therefore, an air cooling system could be considered as an adequate alternative option for cooling fuel cell stack [7].

Kim and Kwon [24] proposed that in order to provide a sufficient flow of air for the power system of the UAS, the fuel cell stack must be located in the front part of the fuselage to directly receive the flow of air through its intake, which is used to feed the cathodes and to cool down the entire system.

Dollmayer et al. [94] proposed a 700 kW fuel cell system as an alternative source of power to the combined generator and auxiliary power units in the conventional aircraft. Different fuel cell operations are proposed using ram air from the ambient atmosphere with two air temperatures (-24 °C and -57 °C), and cabin exhaust air at 22 °C. The fuel cell system consists of a solid oxide fuel cell stack (SOFC), two heat exchangers working to warm up the stream of air before supplying it to the cathode, an auto thermal fuel reformer that uses heated air to warm the stream of hydrogen up to 25 °C before supply it to the anode, a gas turbine with generator, a condenser for excess water recovery, and an afterburner that works to burn the exhaust air and the hydrogen leaving the cathode and anode of the stack. It has been found that using cabin exhaust air at

22°C instead of ram air to supply the fuel cell is more efficient in reducing fuel consumption.

Bégot et al. [27] estimated the impact of low temperature on the performance of a PEM fuel cell at start up and during different stages of operation via testing and characterising a fuel cell placed in a plastic housing climatic chamber to eliminate heat exchange with the ambient. A mix of non-conductive water with ethylene glycol is used to cool down the temperature of the environment inside the climate chamber and the surroundings of the fuel cell stack assembly to the level of sub-zero temperatures. An electric heater combined with heat exchanger and pump work to warm the fuel cell stack assembly in order to reach to the desired test temperature and also to return the stack temperature to the normal operational temperature. At the beginning of the test, the surrounding temperature inside the climatic chamber was set close to 15 °C, the temperature of the inlet gases (hydrogen and air) were maintained between 60 °C and 65 °C with 90% relative humidity along the two and a half hour test duration. Then, the temperature of the surroundings inside the chamber was reduced at a rate of 5 °C down to -34 °C. It was found that at -34 °C, and particularly at high load currents 50-75 A, the thermal energy produced by the stack is sufficient to maintain the temperature of the stack and the flowing gases inside it at approximately 60 °C, while the temperature of the inlet gases declined from 65 °C to 55 °C, due to the impact of heat exchange with the low temperature environment inside the chamber. The stack power output was approximately constant over the test duration with a slight decline in the power delivered by the stack in comparison with normal stack operation at a 15 °C ambient temperature, which might be due to the temperature constraints applied on the whole system inside the climatic chamber. The authors recommended that all system components must be selected in accordance with proper functionality at low temperatures. Efficient insulation should be applied to prevent heat exchange between

the fuel cell stack system and the surroundings, also by using a highly efficient and reliable heating management system it is possible to ensure no freezing water occurs inside the fuel cell stack or in the attached supply pipes or components. Also, it was noticed that a fuel cell assembly stack has a non-homogenous temperature distribution, as the temperature in the centre of the stack is higher than its ends particularly in a cold operation environment, typically for the aircraft with a high cruise altitude [27].

Pratt et al. [93] investigated the impact of ambient pressure and oxygen concentration on the performance of the PEM fuel cell. In order to simulate the variations in atmospheric conditions from sea level to altitude of 53,500 ft. (16,307 m), the stack of 23 cells was placed inside a vacuum chamber. This provides a pressure variation margin for atmospheric pressure down to 7.2 kPa (0.072 bar) by using a controlled vacuum pump capable of maintaining a continuous level of desired pressure inside the chamber equivalent to the altitude air pressure; the chamber is thermally insulated from the normal ambient surroundings. The cathode of the fuel cell stack is passive (i.e. no mechanical fans or blowers are installed to provide air to the cathode channel); hence the air flow through the cathode is controlled by the flow suction of the vacuum pump. The anode of the cell is dead-ended which means that all the hydrogen entering the anode is consumed by the fuel cell reaction, and the pressure of hydrogen inside the anode is almost constant. Air is cooled to the desired temperature which simulates the same air temperature at certain altitude before being supplied to the insulated chamber, while the relative humidity of the inlet air is manually controlled to achieve variations between 15% and 70%. The fuel cell stack was subjected to two different air pressures and three different air flow rates. It was reported that the impact of reducing the pressure and temperature of supplied air to the cathode on the output voltages of the fuel cell stack was significantly higher than the impact of reducing air flow rates. Moreover,

the impact of reducing air flow rates at low pressure-temperature was higher than its effect at a standard pressure-temperature of ~1 bar and 22 °C [93].

However, several deficiencies and constraints are evident in the experiments and analysis carried out by Pratt et al. [93]. The conducted experiments proposed to cover conditions that simulate altitudes up to approximately 16,307 m, but not enough data was collected at those very low-pressure conditions to allow extending the data analysis to this altitude. Experimental limitations did not allow testing the fuel cell under conditions of high flow rate of air with low pressure-temperature, which limited the tests and accordingly its results went up to 10,668 m only. Also, the test was carried under very low drawn current (less than 1 A), hence the results of the experiments did not reflect the right performance of stack under a rated drawn current, which reflects the impact of concentration losses on the output power of the stack.

6.3 Impact of High Altitude on the Air Consumption of the PEM Fuel Cell

The earth's lower atmosphere, known as the homosphere, which extends from sea level to 80-100 km, and consists of three layers: troposphere is lowest layer, the stratosphere layer extends above the troposphere, and the mesosphere layer is above the stratosphere. Within the homosphere, the main highly concentrated gases are nitrogen 78%, oxygen 21%, and the remaining 1% is composed of different types of gases such as argon, water vapour, carbon dioxide, methane, ozone, in addition to traces of inert gases such as neon, helium, and xenon. Within the homosphere, nitrogen and oxygen are considered as fixed gases where their concentrations are consistent and well mixed at any given altitude [95].

In earth's atmosphere, air density, pressure, and temperature vary with altitude, latitude, longitude, and the season. Air density and pressure decrease exponentially with increasing altitude, the highest air density and pressure are at sea level [95].

Within the troposphere and up to the height of the tropopause at 11 km (36,089 ft.), temperature decreases with the increase in altitude at a constant rate of $-6.5 \text{ }^\circ\text{C}/\text{km}$ (or $-1.98 \text{ }^\circ\text{C}/1000 \text{ ft.}$). In the model of international standard atmosphere (ISA), air is considered as a perfect gas within the troposphere, therefore, temperature and pressure of air at a certain altitude is given by the following [95, 96]:

$$T = T_o - ((6.5 + 273.15) * h) = 288.15 - \left(279.65 * \frac{h}{1000} \right) \quad (6.1)$$

Where, h is the altitude in metres, T_o is the temperature of the air at sea level in Kelvin which is equal to 288.15 K ($15 \text{ }^\circ\text{C}$).

$$P = P_o \cdot \left(1 - \left(0.0065 * \frac{h}{288.15} \right) \right)^{5.2561} \quad (6.2)$$

Where, P_o is the pressure of air at sea level which is equal to 101.325 kPa. Using ideal gas law, the density of dry air ρ (kg/m^3) at any altitude can be determined as a function of pressure and temperature [97].

$$\rho = \frac{P}{R_s \cdot T} \quad (6.3)$$

Where, R_s is specific gas constant for dry air ($R_s = 287 \text{ J}/\text{kg}\cdot\text{K}$), and T is absolute temperature in kelvin (K). At sea level, the air density ρ_o is $1.225 \text{ kg}/\text{m}^3$. Relative density of air at certain altitude (RD) is defined as the ratio of the density of air at this altitude ρ to the density of air at sea level ρ_o [95, 96].

$$RD = \frac{\rho}{\rho_o} = e^{-\frac{g_o \cdot h}{R_s \cdot T}} \quad (6.4)$$

Where, g_o equals to 9.81 m/s^2 , for a PEM fuel cell supplied with pure oxygen, the total mass flow rate of the reacted oxygen per second (W_{O_2}) is determined in Equation (4.31) in Chapter Four.

$$W_{O_2} = M_{O_2} \cdot \frac{n \cdot I_{st}}{4F} = 8 * \frac{n \cdot I_{st}}{F} \quad (6.5)$$

Where, n is the number of cells in the stack, M_{O_2} is the molar mass of oxygen (32 g/mol), I_{st} is the drawn current from the fuel cell stack in ampere (A), and F is Faraday's constant (96485 Coulombs/mol).

In the case where the PEM fuel cell is supplied with fresh air, with molar proportion of oxygen to air is 0.21 [97]. Then, at sea level, the mass flow rate of contributed existing air at the reaction interface of the cathode can be determined as given in Equation (6.6):

$$W_{air} = \frac{W_{O_2}}{0.21} = 38.1 * \frac{n \cdot I_{st}}{F} \quad (6.6)$$

At any given altitude, the mass flow rate of the contributed existing air at the reaction interface of the cathode can be determined as given in Equation (6.7) below:

$$W_{air,altitude} = \frac{W_{air}}{RD} \quad (6.7)$$

Based on the mathematical model of the PEM fuel cell developed and validated previously in Chapters Three to Five of this research, a Horizon (H-1000) PEM fuel cell stack consisting of 72 cells, with a maximum current of 20 A, using Equations (6.5) and (6.6) to determine the mass flow rate of contributed existing air at the reaction interface of the cathode at sea level, is found to be equal to 0.569 g/second.

If at high altitudes the PEM fuel cell is going to be supplied by fresh air extracted from the atmosphere, Equations (6.1), (6.2), (6.3), and (6.4) can be used to determine the relative density of air at certain attitudes. Then, using Equation (6.7) it is possible to determine the mass flow rate of the required air at the reaction interface of the cathode to produce a maximum 20 A current output at various altitudes, as shown in Figure 6.1.

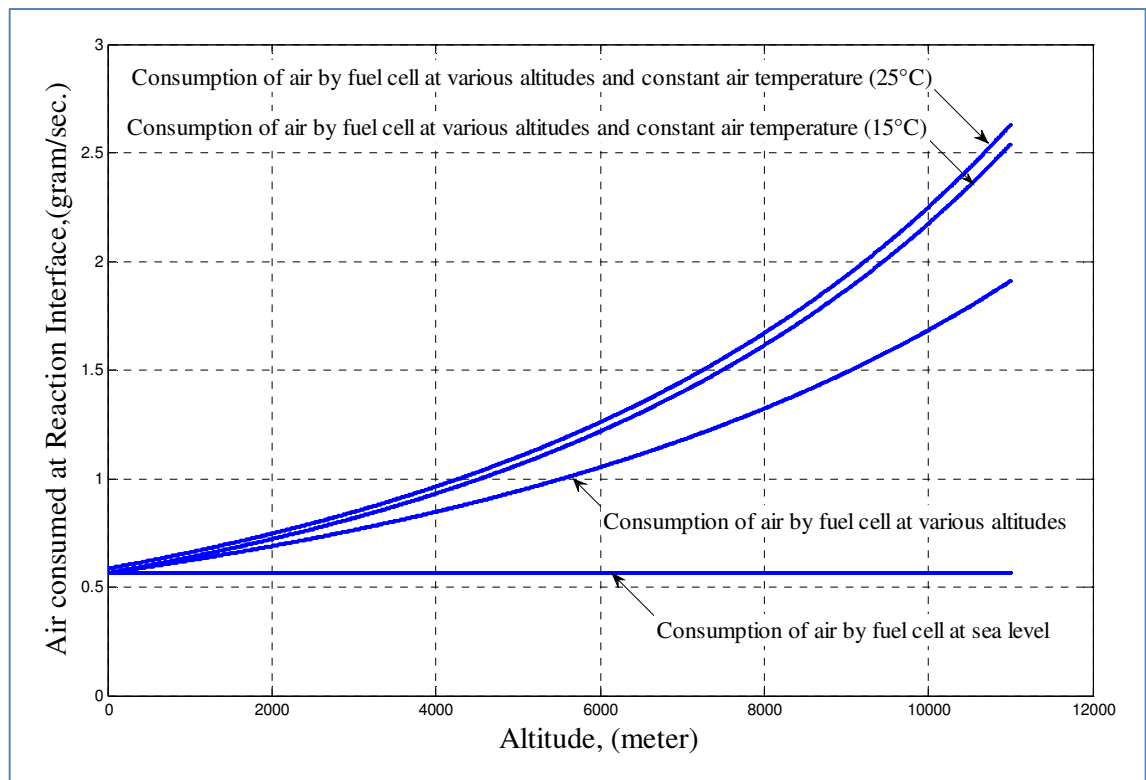


Figure 6.1: Impact of high altitudes on the mass flow rates of consumed air at the reaction interface for a PEM fuel cell stack being supplied by fresh air

It is clear that the mass flow rate of necessary consumed air at the reaction interface is increased exponentially with altitude increase. Theoretically, the ratio of the mass flow rate of consumed air at the reaction interface at an altitude of 10 km to the consumed air sea level is equal to $(1.69/0.569 = 2.97)$. Thus, the mass flow rate of contributed air in the reaction of the PEM fuel cell must be increased by 297% in order to produce the same level of output current at sea level. Yields with more power will be consumed by a

compressor to raise the flow rate of the supplied air. Such a compressor requires a significant fraction of the generated power, and contributes to increasing the total aircraft weight, which is very difficult to afford in a small UAS [28].

In fact, at an altitude of 10 km, the temperature of the air is equal to $-50\text{ }^{\circ}\text{C}$ and a fuel cell stack does not operate at such low temperature levels, unless special measures are applied to warm the air to $15\text{ }^{\circ}\text{C}$ before supplying it to the stack. It is assumed that at high altitudes, the PEM fuel cell is going to be supplied by fresh air from the atmosphere, after warming to $15\text{ }^{\circ}\text{C}$. Similarly, the mass flow rate of required air at the reaction interface of the cathode to produce the maximum current at various altitudes, (at $15\text{ }^{\circ}\text{C}$ constant temperature air supply to the fuel cell stack) can be determined and depicted in Figure 6.1.

Therefore, at an altitude of 10 km, at $15\text{ }^{\circ}\text{C}$ constant temperature air supply to the fuel cell stack, the mass flow rate of necessary consumed air at the reaction interface is 2.18 g/second, and the ratio of mass flow rate of consumed air at the reaction interface to consumed air at sea level is equal to $(2.18/0.569 = 3.83)$. Thus, the mass flow rate of contributed air in the reaction of the PEM fuel cell must be increased by 383% in order to produce the same level of output current at sea level.

It is clear that maintaining the temperature of the supplied air to the PEM fuel cell stack at $15\text{ }^{\circ}\text{C}$ for high altitude operations has an impact of increasing the mass flow rate of supplied air to the reaction interface, which leads to more power being consumed by the compressor to raise the flow rate of air.

Dollmayer et al. [94] reported, with regard to the proposed 700 kW solid oxide fuel cell system for aircraft applications, that supply streams of air and hydrogen must be warmed up to $25\text{ }^{\circ}\text{C}$ before supplying it to the fuel cell stack. Also, using cabin exhaust ($22\text{ }^{\circ}\text{C}$) air instead of ram air to supply the fuel cell is more efficient in reducing fuel consumption.

Based on the proposed developed model of a PEM fuel cell and PID controller, the amounts of hydrogen and air required to be supplied to the fuel cell stack, in order to produce a maximum power output of 877 W at 20 A current at different altitudes, where the air is assumed to be extracted from the surrounding ambient under conditions of maintaining hydrogen temperature at 15 °C and stack temperature at 27.73 °C, are presented in Table 6.1.

While looking at the performance of the fuel cell system model, it became clear that due to drops in the pressure, temperature and density of ambient air at 300 m altitude, the system stalled. While warming air up to 15 °C or 20 °C before supplying it to the fuel cell system lead to an increase the density of the air, which extended the operation of the fuel cell system up to 400 m altitude, as presented in Tables 6.2 and 6.3, respectively. Moreover raising the temperature of the hydrogen and air before supplying it to the fuel cell system would reduce the rate of consumption.

Table 6.1: Supply of hydrogen and air to the fuel cell stack based on developed model of PEM fuel cell and PID controller at different altitudes under conditions of fixed hydrogen temperature at 15 °C, constant stack temperature at 27.73 °C, and maximum power output of stack at 877 W at 20 A current					
Altitude (km)	Ambient Air Pressure (kPa)	Ambient Air Temperature (°C)	Ambient Air Density (kg/m ³)	Supplied Air (m ³ /hour)	Supplied Hydrogen (g/hour)
0	101.325	15.00	1.225	97.859	57.20
0.1	100.120	14.35	1.213	97.899	57.23
0.2	98.945	13.70	1.202	97.942	57.27
0.3	97.772	13.05	1.190	System Stalled	

Table 6.2: Supply of hydrogen and air to the fuel cell stack based on developed model of PEM fuel cell and PID controller at different altitudes under conditions of fixed hydrogen and ambient air temperature at 15 °C, constant stack temperature at 27.73°C, and maximum power output of stack at 877 W at 20 A current				
Altitude (km)	Ambient Air Pressure (kPa)	Air Density After Warming (kg/m ³)	Supplied Air (m ³ /hour)	Supplied Hydrogen (g/hour)
0	101.325	1.2250	97.859	57.20
0.1	100.120	1.2107	97.897	57.23
0.2	98.945	1.1965	97.934	57.26
0.3	97.772	1.1823	97.971	57.29
0.4	96.611	1.1682	System Stalled	

Table 6.3: Supply of hydrogen and air to the fuel cell stack based on developed model of PEM fuel cell and PID controller at different altitudes under conditions of fixed hydrogen and ambient air temperature at 20 °C, constant stack temperature at 27.73°C, and maximum power output of stack at 877 W at 20 A current				
Altitude (km)	Ambient Air Pressure (kPa)	Air Density After Warming (kg/m ³)	Supplied Air (m ³ /hour)	Supplied Hydrogen (g/hour)
0	101.325	1.204	97.847	57.19
0.1	100.120	1.190	97.884	57.22
0.2	98.945	1.176	97.920	57.25
0.3	97.772	1.162	97.958	57.28
0.4	96.611	1.148	System Stalled	

It has been reported in the literature that at high altitudes, where the temperature, pressure and density of air are very low, compressed air and hydrogen can be used to supply the fuel cells with a sustainable source of air or oxygen. Also, fuel and air must be heated up before being supplied to the stack, in order to avoid excessive stack cooling and hence thermal stress caused by cold streams [10, 93].

In this research, and for high altitude model simulation and design consideration, it will be considered that the air supply to the manifold of cathodes is not going to be supplied from the available air extracted from the atmosphere. Alternatively, air will be supplied by a pressurised tank of dry air connected to the supply manifold of cathodes. Moreover, due to the drop in atmospheric pressure and temperature, it is necessary to maintain the operational environment of the stack, such as pressure, temperature and air humidity as close as possible to conditions at sea level. Therefore, the stack of fuel cells will be considered to be located inside a sealant thermally isolated chamber with an internal ambient pressure and temperature equal to 1atm and 15 °C, respectively.

However, a certain amount of unreacted air and hydrogen will leave the stack of the fuel cells associated with water in the form of vapour or liquid, as a result of electrochemical reactions. These residual fluids will accumulate inside the sealant chamber. This will present another operational problem; hence, the air inside the chamber needs to be refreshed in order to maintain a certain operational temperature, relative humidity and pressure approximately close to sea level conditions.

At high altitudes, the pressure inside the chamber containing the fuel cell stack will be higher than altitude pressures. Therefore, any attempt to drain the chamber via opening the drain valve will create a high flow of air at the exit outlet of the chamber as a result of a great pressure difference between the chamber and external atmosphere. This will create a sudden and rapid increment in the flow of air entering the stack which may lead to a spike in the output voltage of the fuel cells; hence, instability in the operation and performance of the stack, and further unnecessary consumption in the usage of air. Also, this may damage the electrolyte membrane due to pressure differences.

The difference between the internal and external pressure of the main stack chamber can be eliminated by either installing a series of sequential settling drain chambers at the exit outlet of the main stack chamber, which can drain the contents (i.e. accumulated

gases) of the main stack chamber slowly and sequentially, or by recycling the internal accumulated gases inside the main chamber after a process of refining and gas separating ending with recompressing air and hydrogen again to their storage cylinders, however this option will add more complexity, weight and cost to the entire system.

Figure 6.2 shows the mechanical components and flow variables associated with the proposed model of a fuel cell stack system operating at high altitudes. The hydrogen and air supply system consists of tanks of pressurised dry air and pure hydrogen, inlet pressure regulator valves (PRV), a hydrogen purging valve, drain tank, and connection pipes between the components.

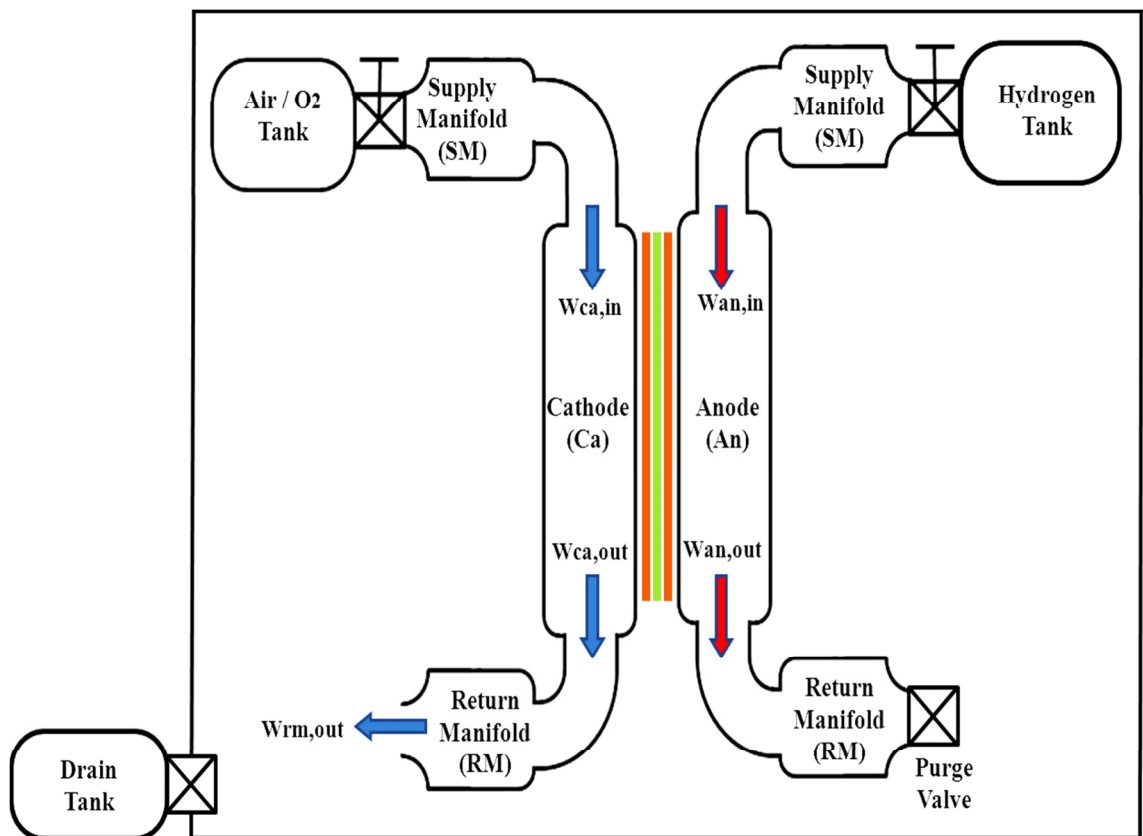


Figure 6.2: Mechanical components and flow variables associated with proposed model of fuel cells stack system operating at high altitudes

6.4 Summary

The impacts of high altitudes upon the operation and consumption of air were determined in order to establish how to maintain a certain level of delivered power to the load. Also, the implications associated with operating a PEM fuel cell stack at high altitudes were considered and different technical solutions proposed.

It has been proven that warming the extracted air from the atmosphere at high altitudes (~10 km) in order to feed the stack must be avoided, as this increases the flow of supplied air to the cathode by about 400% in comparison with the flow at sea level, in order to overcome the drop in the density of air at high altitudes and to produce consistent stable power from the stack, which would add more complexity, weight and cost to the system.

It is clear that due to the drops in the pressure, temperature and density of the ambient air at 300 m altitude, the fuel cell stack system is stalled. While warming air up to 15 °C or 20 °C before supplying it to the fuel cell system lead to an increase the density of the air, which extended the operation of the fuel cell system up to 400 m altitude. Moreover raising the temperature of the hydrogen and air before supplying it to the fuel cell system would reduce the rate of consumption.

In the next chapter, different types of hydrogen fuel will be investigated in order to choose the appropriate type of hydrogen to be used for UAS applications that can offer low cost and weight, and low complexity to the entire system. Also, the maximum static thrust required to be produced by the propulsion system, in order to accelerate the airplane to take-off, will be determined based on the generating capacity of the power supply system.

Chapter Seven: Static Thrust for Unmanned Aircraft Systems

7.1 Introduction

High altitude long endurance (HALE) unmanned aircraft systems are typically designed to fly at altitudes between 15 and 20 km, cruising at low speeds and circling the area of interest. They play a vital role in providing high-resolution surveillance due to their closeness to the earth. A HALE UAS needs to have a lightweight, high lift-low drag, low power consumption, and highly efficient propulsion and power system, in order to increase the mission endurance. Eliminating the mechanical couplings between the propulsion system and the power generation system would lead to enhancing the overall efficiency of the system and hence extending its endurance, as the privilege of deploying a fuel cell power system in comparison with turbo jet and combustion engines [10, 73].

Flight endurance is an important factor in improving the performance of the mission; higher energy density and efficiency of the power supply system are very important in increasing flight endurance of the UAS [7].

Due to the low efficiency of gas turbines and reciprocating engines, particularly for small scale UAS, batteries are used as a secondary power source. The energy density (i.e. energy capacity per unit volume or weight) of the available batteries is too low to power a small UAS to have long endurance. A Lithium polymer battery can provide energy of 200 W-hr/kg, which can offer an endurance of 60-90 minutes for a small

UAS. A hydrogen fuel cell system has high energy density and is more efficient in extending the endurance of a UAS in comparison with lithium batteries, hence can be considered an ideal power alternative to existing batteries [7, 24, 53].

The UAS consumes more power during take-off and climb than in cruise mode. Combining fuel cells and rechargeable batteries in a configuration of hybrid propulsion systems offers a significant increase in the UAS endurance, where the fuel cell is normally used for the cruise flight, while the auxiliary batteries provide the additional power required for taking-off, climbing, and the increase in power demand of transient loads [7, 68]. The duration of maximum power produced from the batteries during the take-off and climb is much shorter than the cruising phase, where the fuel cell can recharge the batteries [9].

The power supply system of the UAS is categorised as having a fuel cell power-plant and fuel cell subsystem. The fuel cell power-plant consists of the fuel cell stack, air and hydrogen supply and regulation systems, and a cooling system. The fuel cell subsystem consists of electrical distribution bus and power management system. The power supply system provides power to the propulsion system through the DC bus voltage. The propulsion system consists of an electric motor, a motor controller, and the propeller [22, 26].

The power generated from the PEM fuel cell power system is determined according to the size of the fuel cell stack, while the energy capacity is determined according to the storage capacity of the hydrogen and oxygen vessels [31]. However, in the case of a fixed size of hydrogen tank, the endurance of the aircraft is limited by the efficiency of the propulsion system and the power-plant system [26].

7.2 Hydrogen Fuel for UAS Applications

Hydrogen is considered an ideal fuel for fuel cell operation, as it offers a benefit of excluding any unnecessary processes of pre-reforming or pre-treatment [10]. Hydrogen can provide specific energy about three times higher than hydrocarbon fuel. Hence, fuel mass will approximately be reduced to one third in comparison with the same given mission and payload using hydrocarbon fuel [72, 98].

Hydrogen generated by different processes is used to feed the fuel cell power-plant for UAS applications, this includes chemical hydrates, low pressure liquid hydrogen, and high pressurised hydrogen gas [22]. Metal hydrides are too heavy to satisfy the energy density requirement, which adds extra weight to the system, while storage of hydrogen in solid or slush forms could lead to minor savings in the weight and volume of the storage tank, but on the other hand needs excessive energy to sub cool the hydrogen fuel [7, 98].

Liquid hydrogen could be the alternative choice, but liquid hydrogen needs to be cooled and stored below 20 kelvin (-253 °C). A storage tank must be insulated to eliminate the evaporating of liquid hydrogen to gas form; also the rate of evaporated hydrogen must be monitored and controlled. Thus, storage of hydrogen in liquid form requires careful procedures to balance between the mechanical and thermal requirements of the design, which would lead to increases in the weight, cost and complexity of the system. Also, the process of liquefying hydrogen gas requires complicated cryogenic equipment which consumes high power [10, 21, 99]. However, the low density of liquid hydrogen needs a storage volume that is approximately four times bigger than a tank of hydrocarbon fuel that is used for the same mission and payload [98]. Moreover, most of the commercial available liquid hydrogen fuel is produced from natural gas, which leads to a release of carbon dioxide in the environment [100].

Leachman et al. [99] investigated different techniques for generating a sufficient flow of hydrogen gas from liquid hydrogen for a long endurance UAS operation for different flying phases, including take-off, cruise and landing. To force hydrogen to flow out of its storage tank, the pressure inside the storage tank needs to be raised (i.e. pressurise the tank). An electric heater can be used to vaporise a certain volume of liquid hydrogen, which leads to consuming further power and hence more power losses. An external pressurisation tank of helium gas works to elevate the internal pressure of the liquid hydrogen tank, but this will add extra mass and volume to the total fuelling system, sometimes more than 20% which is equivalent to the payload weight for the high altitude long endurance UAS design.

The design and development of light, durable and efficient insulated tanks for liquid hydrogen storage is considered to be a technical challenge, particularly for aircraft applications, as it needs to eliminate the heat conduction process between the tank and the surroundings, consequently leading to losing a certain amount of hydrogen as a result of venting the tank to lower the elevated pressure [98].

The high energy density of the chemical hydride makes it a reliable source of hydrogen, a sodium borohydride solution is characterised as stable, non-toxic and non-flammable, and has a hydrogen production capacity of 10.8 wt.%. The technique for generating hydrogen from a chemical hydride requires a chemical hydride solution cartridge, a micro pump, a catalytic reactor, a gas-liquid separator and a dehumidifier. The process needs to be controlled which adds cost and complexity to the entire system. However, this technique involves different complications such as instability in hydrogen generation due to clogging in the flow channel and internal pressure fluctuations [7].

Seo et al. [61] adopted an advanced ammonia borane-based hydrogen (NH_3BH_3) power pack to continuously drive an unmanned aircraft system, using a 200 W PEM fuel cell stack. The development of a continuous hydrogen generator using ammonia borane fuel

causes several complications, for example, continuous supply of solid ammonia borane, the purification process of hydrogen containing gaseous by-products, and discharging of liquid-solid residual materials from the reactor.

Huang et al. [69] developed a design model of a 300 W PEM fuel cell stack integrated with a sodium borohydride (NaBH_4) based hydrogen generator. It was reported that the performance and power output of the fuel cell using hydrogen extracted from the NaBH_4 hydrogen generator, and that provided from a conventional pressurised hydrogen cylinder, is approximately the same.

Semiz et al. [59] reported that that rate of hydrogen production depends mainly on the catalytic activity of the catalyst rather than the concentration of the sodium borohydride solution. However, there is a threshold catalyst concentration for the maximum available reaction rate; hence, increasing the concentration of the catalyst above this threshold will not add any contribution to the rate of hydrogen production.

Most fuel-cell-based UAS depend on an on-board compressed hydrogen cylinder or chemical hydride system to produce hydrogen for fuel cell operation [68]. Compressed hydrogen gas is a common storage method which needs safety procedures for the refilling process [24].

However, as it has been presented above, whether using chemical hydride or liquid hydrogen as a source of hydrogen gas, special requirements are needed to manage and control the process of hydrogen generation, which adds more cost, complexity and weight to the power system of the UAS. Therefore, compressed hydrogen will be considered as the source of hydrogen supplied to the fuel-cell-based UAS in this research.

7.3 Calculation of Required Thrust

In UAS missions, the highest power consumption occurs during take-off and the climb to the designated cruising altitude, while the lowest power consumption occurs during descent. The longest time and highest energy consumptions are during the cruising stage. At constant altitude where the weight of the aircraft is equal to the lift and the thrust is equal to the drag. The calculations of power requirements for cruising involve a thrust calculation related to the efficiency of the propulsion system, which depends on propeller diameter, changes in the direction of air flow and its velocity, and density of air [10].

The dimension of the propeller plays a significant role in determining the required power to be drawn by the motor from the power supply system. A bigger propeller requires higher power to turn it and hence more current needs to be drawn from the power supply [53].

In the design of the propeller driven airplane, static thrust is a vital element to be determined, in order to successfully select the appropriate propeller and motor. Static thrust represents the maximum thrust produced by the propeller while the airplane is located in a stationary position on the ground (zero velocity), and this thrust will decrease with forward velocity [101].

The power delivered by the motor to the propeller (P_d) in terms of propeller rotational speed, propeller constant, and propeller power factor is empirically calculated as given in Equation (7.1) below [102]:

$$P_d = \text{Propeller Constant} * [\text{rpm}]^{\text{power factor}} \quad (7.1)$$

Where, power is in watts, and rpm is in thousands. The required thrust produced by the propeller can be determined by Equation (7.2) given below [103]:

$$T = 2\rho \cdot A \cdot v \cdot w \quad (7.2)$$

Where, ρ is the density of the air (kg/m^3), A is the rotational area of the propeller ($A = \pi \cdot r^2$), v is the velocity of the stream air through the propeller (m/s), and w is the propeller induced velocity (m/s) which represents the velocity of the stream air accelerated by the propeller. Velocity of the stream air through the propeller can be determined by Equation (7.3):

$$v = V_o + w \quad (7.3)$$

Where, V_o is the velocity of the free-stream air far ahead from the propeller (m/s). While, the induced velocity through the propeller can be found by substituting Equation (7.3) in Equation (7.2) above, yielding the following:

$$w = \frac{1}{2} \left(-V_o + \sqrt{V_o^2 + \left(\frac{2T}{\rho \cdot A} \right)} \right) \quad (7.4)$$

The necessary power required by the propeller (P_r) which is equal to the product of thrust and the velocity of air through the propeller shown as follows [103]:

$$P_r = T \cdot v = T \cdot (V_o + w) \quad (7.5)$$

The part of the equation ($T \cdot V_o$) represents the useful power of the propeller, while the part ($T \cdot w$) represents the induced power of the propeller. For a static case (i.e. the airplane is located in a stationary position on the ground) where V_o is zero, by substituting in Equations (7.4) and (7.5) above, the induced velocity and induced power of the propeller is produced, as given in Equations (7.6) and (7.7), respectively:

$$w = \sqrt{\frac{T_s}{2\rho \cdot A}} \quad (7.6)$$

$$P_i = \frac{T_s^{3/2}}{\sqrt{2\rho \cdot A}} \quad (7.7)$$

Hence, by rearranging Equation (7.7), the static thrust (T_s) can be determined as given in Equation (7.8) below [103]:

$$T_s = \left(2\rho \cdot A \cdot P_i^2\right)^{1/3} \quad (7.8)$$

For a given ρ and A as constant, a maximum static thrust (T_{sm}) is achieved when the induced power by the propeller (P_i) reaches its maximum (i.e. equal to the total power delivered by the motor P_d). Thus, the maximum static thrust produced by the propeller can be represented as given below:

$$T_{sm} = \left(2\rho \cdot A \cdot P_d^2\right)^{1/3} \quad (7.9)$$

However, not all of the electrical DC power supplied to the motor (P_s), which represents the power drawn from the fuel cell stack, will be fully converted to the mechanical work to drive the propeller; part of this power is dissipated by the inefficiency of the motor. The electrical efficiency of the motor is determined as the ratio between the output to input power, as given in Equation (7.10), below:

$$\eta_m = \frac{P_d}{P_s} \quad (7.10)$$

Where, η_m is the efficiency of the motor, power is in watts (equivalent to N.m/s) and in terms of horse power (1 hp = 746 W).

For the BLDC motor (KMS Quantum 4130/07) used in the experiment, with a DC input supply voltage of 24 V, maximum efficiency (> 90%), and RPM rating of 360/V (8640 rpm at 24 V), the recommended propellers for this motor are (15" x 08"), (15" x 10"),

and (16" x 10"), with average propeller constants being 1.258, 1.773, and 2.23, respectively for 3.08 power factor, as given by Aircraft R/C Electric Aircraft and Gliders datasheet and the RC Model Centre [104, 105].

Using Equations (7.1), (7.9), and (7.10) to determine the maximum static thrust produced by the propeller for the specific BLDC motor, two values for static thrust to weight ratio (T/W) (0.2 and 0.4) will be used in this research so as to offer different operational scenarios for the UAS applications – also assuming that maximum efficiency of the BLDC motor is 95%.

First Option: For propeller size 15" x 08", with an average propeller constant of 1.258 and 3.08 power factor.

$$P_d = 1.258 * (8.640)^{3.08} = 964 \text{ W}$$

$$P_s = \frac{964}{0.95} = 1015 \text{ W}$$

$$T_{sm} = \left(2 * 1.225 * (0.381/2)^2 * \pi * (964)^2 \right)^{1/3} = 63.8 \text{ N}$$

For a static thrust to weight ratio of 0.4, the maximum permitted mass of the UAS must not exceed 16.28 kg, as determined below:

$$Weight = \frac{63.8}{0.4} = 159.5 \text{ N}$$

$$Mass = \frac{159.5}{9.8} = 16.28 \text{ kg}$$

For a static thrust to weight ratio of 0.2, the maximum permitted mass of the UAS must not exceed 32.55 kg, as determined below:

$$Weight = \frac{63.8}{0.2} = 319 \text{ N}$$

$$Mass = \frac{319}{9.8} = 32.55 \text{ kg}$$

Second Option: For propeller size 15" x 10", with an average propeller constant of 1.773 and 3.08 power factor.

$$P_d = 1.773 * (8.640)^{3.08} = 1359 \text{ W}$$

$$P_s = \frac{1359}{0.95} = 1430 \text{ W}$$

$$T_{sm} = \left(2 * 1.225 * (0.381/2)^2 * \pi * (1359)^2 \right)^{1/3} = 80.2 \text{ N}$$

For a static thrust to weight ratio of 0.4, the maximum permitted mass of the UAS must not exceed 20.46 kg, as determined below:

$$Weight = \frac{80.2}{0.4} = 200.5 \text{ N}$$

$$Mass = \frac{200.5}{9.8} = 20.46 \text{ kg}$$

For a static thrust to weight ratio of 0.2, the maximum permitted mass of the UAS must not exceed 40.92 kg, as determined below:

$$Weight = \frac{80.2}{0.2} = 401 \text{ N}$$

$$Mass = \frac{401}{9.8} = 40.92 \text{ kg}$$

Third Option: For propeller size 16" x 10", with an average propeller constant of 2.23 and 3.08 power factor.

$$P_d = 2.23 * (8.640)^{3.08} = 1709 \text{ W}$$

$$P_s = \frac{1709}{0.95} = 1799 \text{ W}$$

$$T_{sm} = \left(2 * 1.225 * (0.4064/2)^2 * \pi * (1709)^2 \right)^{1/3} = 97.55 \text{ N}$$

For a static thrust to weight ratio of 0.4, the maximum permitted mass of the UAS must not exceed 24.89 kg, as determined below:

$$Weight = \frac{97.55}{0.4} = 243.875 \text{ N}$$

$$Mass = \frac{243.875}{9.8} = 24.89 \text{ kg}$$

For a static thrust to weight ratio of 0.2, the maximum permitted mass of the UAS must not exceed 49.77 kg, as determined below:

$$Weight = \frac{97.55}{0.2} = 487.75 \text{ N}$$

$$Mass = \frac{487.75}{9.8} = 49.77 \text{ kg}$$

The calculations presented above for the power delivered to the BLDC motor and the maximum static thrust produced by the propeller, and consequently the maximum permitted mass of the UAS, for two values of static thrust to weight ratio (0.2 and 0.4), and for three different sizes of propeller, are as presented in Table 7.1.

Bradley et al. [26] reported that for their designed power-plant for an unmanned powered aircraft, that the specified static thrust to weight ratio is 0.165 which provides 26.52 N static thrust, for the total mass of the aircraft of 16.4 kg.

As it has been presented above, that for the BLDC motor (KMS Quantum 4130/07) used in the experiment, with a rated DC supply voltage of 24 V, and RPM rating of 360/V. Thus, the rotational speed of the motor can vary from 360 rpm at 1 V supply voltage to 8,640 rpm at 24 V.

The power drawn by the BLDC motor and the maximum static thrust produced by the propeller, and consequently maximum permitted mass of the UAS, for three different sizes of propeller and for two values of static thrust to weight ratio (0.2 and 0.4), with respect to the rotational speed of the propeller varying between 360 to 8,640 rpm are as presented in Figures 7.1, 7.2, 7.3 and 7.4, respectively. The results indicate that a bigger propeller offers higher thrust, hence increasing the permitted weight of the UAS and the

payload, but a bigger propeller also increases the magnitude of power drawn from the power system.

Table 7.1: Calculations of the power supplied to and produced from the BLDC motor, maximum static thrust produced, and maximum permitted mass of the UAS					
Propeller Size, (inch)	Power Supplied to the Motor, (W)	Power Delivered by Motor to Propeller, (W)	Maximum Static Thrust Produced, (N)	Maximum Permitted Mass of UAS, (kg)	
				at T/W (0.4)	at T/W (0.2)
15" x 08"	1,015	964	63.8	16.28	32.55
15" x 10"	1,430	1,359	80.2	20.46	40.92
16" x 10"	1,799	1,709	97.55	24.89	49.77

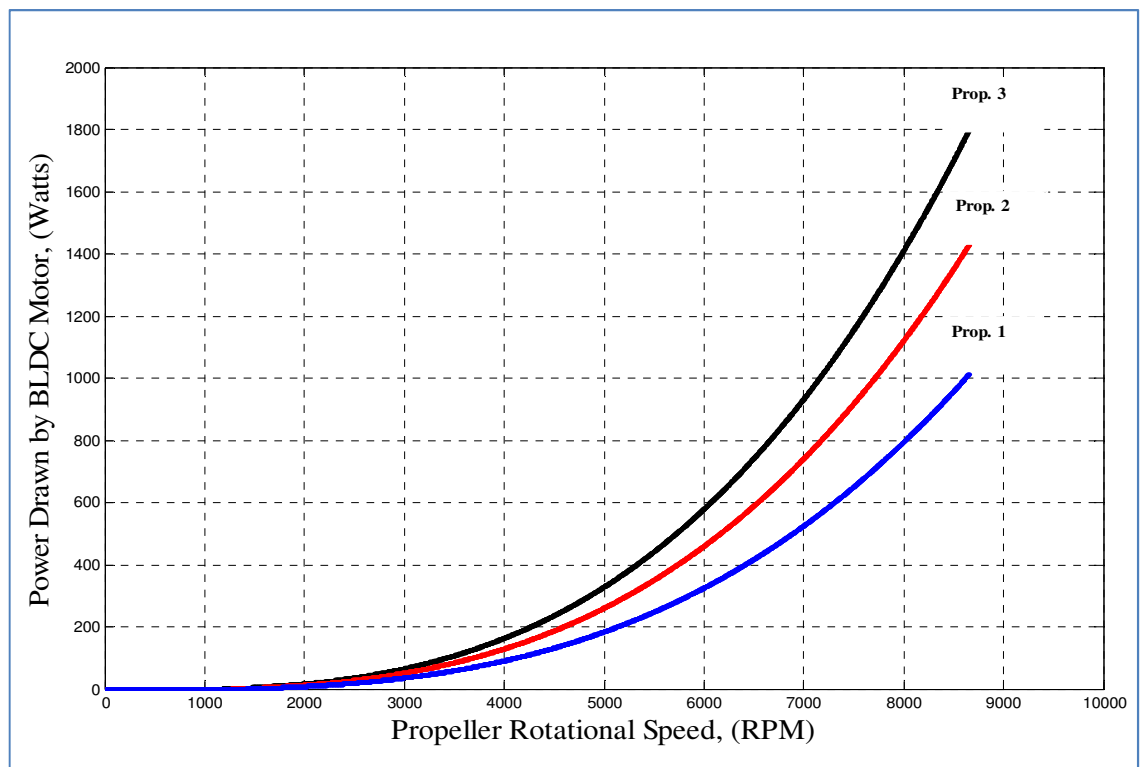


Figure 7.1: Power drawn by the BLDC motor with respect to the rotational speed of the propeller for three different sizes of propeller

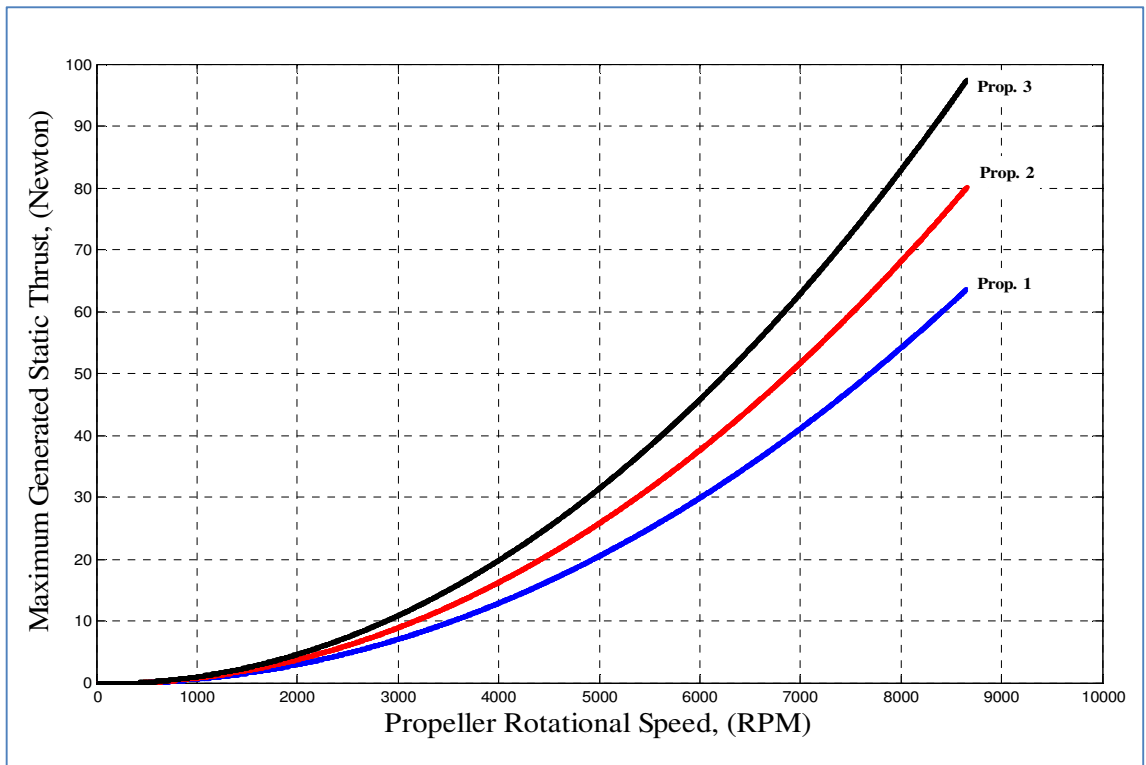


Figure 7.2: Maximum static thrust with respect to the rotational speed of the propeller for three different sizes of propeller

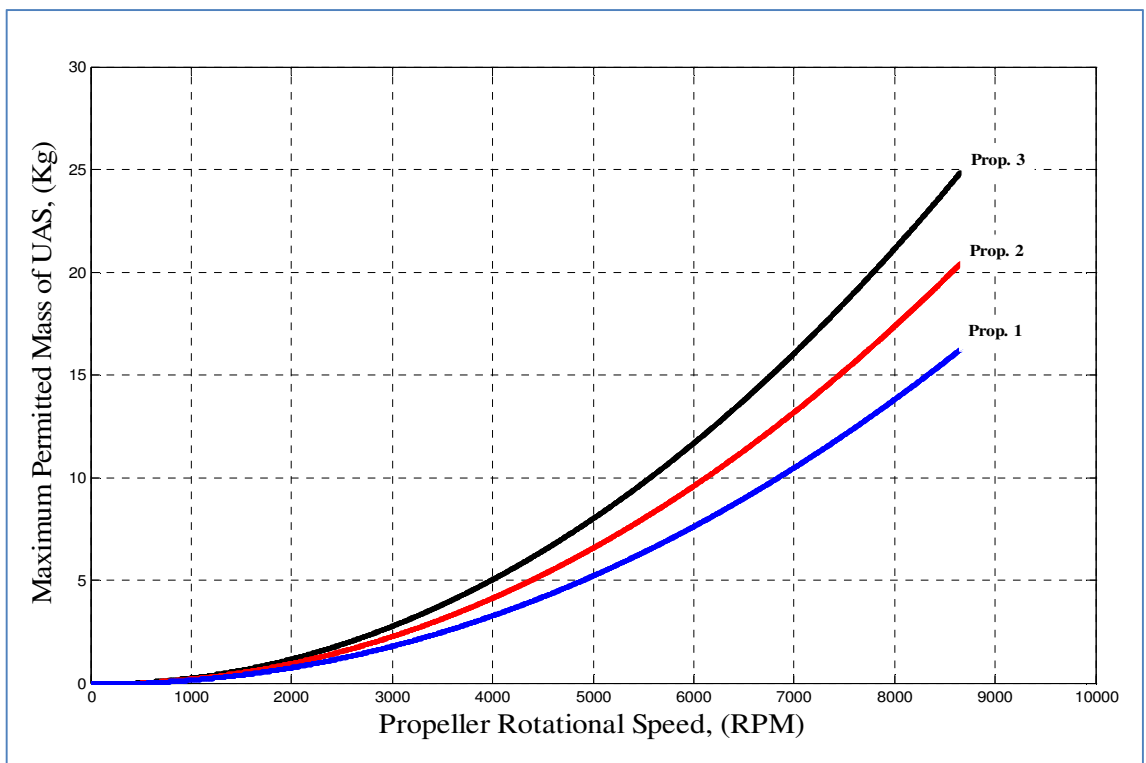


Figure 7.3: Maximum permitted mass of the UAS with respect to the rotational speed of the propeller for three different sizes of propeller, at 0.4 static thrust to weight ratio

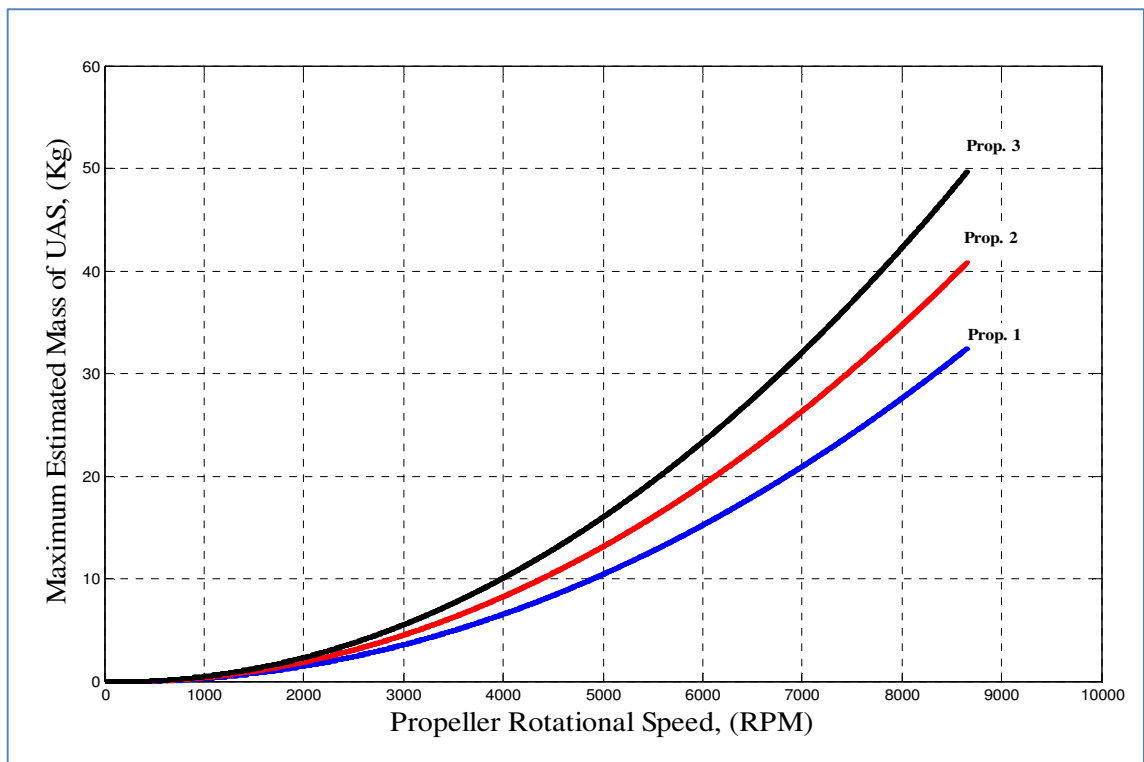


Figure 7.4: Maximum permitted mass of the UAS with respect to the rotational speed of the propeller for three different sizes of propeller, at 0.2 static thrust to weight ratio

It is clear from the results that the best option for the adopted Horizon (H-1000) fuel cell stack and the (KMS Quantum 4130/07) BLDC motor in this research is to use a propeller size of 15" x 8". The maximum power drawn by the BLDC motor from the power supply system is approximately 1 kW at maximum rotational speed of the propeller (8,640 rpm), which is within the maximum power production capacity of the fuel cell stack. Also, the maximum permitted mass of the UAS was increased from 16.28 kg for 0.4 static thrust to weight ratio of the UAS to 32.55 kg for 0.2 static thrust to weight ratio of the UAS. Thus, determining the value of the static thrust to weight ratio is very important in extending the maximum permitted total mass of the UAS.

7.4 Summary

In this chapter, different types of hydrogen fuel for UAS applications were considered, in order to choose the appropriate type of hydrogen source to be used for the UAS applications which can offer low cost and weight, and low complexity of the entire system.

It has been concluded that whether using chemical hydride or liquid hydrogen as a source of hydrogen gas, special requirements are needed to manage and control the process of hydrogen generation, which adds more cost, complexity and weight to the power system of the UAS, hence compressed hydrogen gas was considered to be the best source of hydrogen supplied to the fuel-cell-based UAS in this research.

The maximum static thrust required to be produced by the propulsion system in order to accelerate the airplane was determined based on the capacity of the power system, also different sizes of propellers were examined in order to find the appropriate propeller which draws power from the BLDC motor based on the maximum production capacity of the fuel cell stack power system, hence the maximum weight of the UAS is determined accordingly. Also two values for static thrust to weight ratio 0.2 and 0.4 were adopted in order to offer different operational scenarios for the UAS applications.

It is clear from the results that a bigger propeller offers higher thrust and hence increases the permitted weight of the UAS and the payload, but a bigger propeller will increase the magnitude of power drawn from the power system.

The best option for the fuel cell stack and BLDC motor used in this research was propeller sized 15" x 8". The maximum power drawn by the BLDC motor from the power supply system is approximately 1 kW at maximum propeller rotational speed (8,640 rpm), which is within the maximum power production capacity of the fuel cell stack. The maximum permitted mass and static thrust to weight ratio of the UAS were

considered and it was established that the value of the static thrust to weight ratio is very important in extending the maximum permitted total mass of the UAS.

In the next chapter, pressure vessel design will be presented and investigated for different types of stainless steel materials, in order to determine the weight and size of the hydrogen and air pressure vessels.

Chapter Eight: Pressure Vessel Design and Power Plant Mass Estimation Based UAS

8.1 Introduction

Materials that have properties such as high strength, high stiffness, high fracture toughness, low density, and low permeability to hydrogen molecules are ideally recommended for the design and construction of hydrogen storing tanks [98]. Lowering the mass of fuel tank will reduce power consumption; hence increase the endurance of the flight and the payload of the UAS [72].

In pressure vessel fabrication, composite materials are widely used due to their higher strength to weight ratios [72]. High storage density of hydrogen or oxygen would be achieved by a composite of ultra-light vessel materials such as polymer liners [31]. However, aluminium is the most recommended material among metals that fulfil the recommendations of NASA for tank fabrication for flight applications [100].

Romeo et al. [73] reported that hydrogen and oxygen in a pressurised form could be stored in pressure vessels mounted inside the wing of the plane. The weight and size of the storage tanks need to be optimised to reduce the power required by the flight.

Verstraete et al. [98] proposed in his work, a preliminary design model of 1.2 bar cryogenic liquid hydrogen tanks developed for small regional and large long-range subsonic aircraft. Two different insulation techniques, multi-layer insulations and low-density foam materials, are used in order to trade-off between the weight and the dimensions of the designed tanks, and consequently dimensions and overall weight of the fuselage.

Adam and Leachman [72] developed and fabricated a light-weight storage tank for liquid hydrogen for a PEM fuel cell power system integrated and designed for a small UAS (< 25 kg). The fuel tank consists of a cylindrical shape cryogenic vessel placed inside an outer vessel, while an insulating blanket made from multi-layer insulation is used to wrap the inner vessel to reduce radiation heat loss. Aluminium (6061-T6) material is used to construct the inner and outer vessels, the total mass of the two vessels is 6.3 kg, excluding the insulation materials.

Radmanesh et al. [6] reported that storing hydrogen in the form of highly pressurised gas is the cheapest method, due to developments in composite materials that offer storing pressure up to 800 bar. However, pressurised hydrogen gas is usually stored in steel tanks with a pressure range between 200 and 300 bar.

Furrutter and Meyer [53] used a light aluminium vessel weighing 0.255 kg filled with 30 bar of pressurised hydrogen, enough to supply hydrogen for a continuous nine minutes flying time, using a 100 W Horizon PEM fuel cell power-plant system placed in a small-scale fixed wing UAS, in order to provide enough power to maintain steady and stable flying level with 13 m/s maximum flight velocity, for a total mass of UAS of 5.3 kg.

Romeo et al. [73] proposed a parametric analysis to determine the impact of internal pressure and in-flight loads upon the size of the hydrogen pressure vessel, in order to reduce the weight of the vessel and to examine the safety margins between the applied pressure and the burst pressure, so as to fulfil the safety regulation requirements for a composite materials pressure vessel filled with 100 bar pressurised hydrogen mounted inside the wing of a UAS for a high altitude long endurance mission.

Bradley et al. [26] proposed using a 310 bar compressed hydrogen tank providing a storage volume capacity of 0.192 m³ (i.e. before compression) for a 500 W, 32-cell self-humidified PEM fuel cell as a main and only source of power for an unmanned powered

aircraft. To overcome the problem of very low power to weight ratio, the entire proposed fuel cell powered aircraft was designed to be operated at low speed, stable altitude flight level with slow manoeuvring, with a maximum flying altitude up to 30 m, for less than three minutes total flying time. However, the proposed integrated power fuel cell aircraft system was designed without consideration to the payload or endurance requirements. Total mass of the combined power-plant and the propulsion system was about 9.4 kg, which accounted for about 57% of the 16.4 kg total mass of the UAS.

Barbir et al. [31] reported that oxygen storage is the only option for space applications.

However, most of the research literature focuses on the design of hydrogen vessels for low altitude and low speed UAS applications, and for supplying air extracted directly from the surroundings, hence no oxygen pressure vessel has been used in the application. At a high altitude of 11 km (~36,000 ft.), atmospheric temperature and pressure are approximately -56 °C and 0.227 bar, air density is around 0.365 kg/m³, these are severe conditions for a fuel cell to operate. Also, published experimental data for such operating conditions are very limited [93]. Therefore, air or oxygen pressure vessel becomes a most vital issue relating to providing sufficient oxygen to the fuel cell power system.

Moreover, using pure oxygen instead of air to feed the fuel cell stack leads to an increase in the cell output voltage; as the pressure and diffusion rates of pure oxygen in the cathodes is higher than the partial pressure and diffusion rates of oxygen in the mixture of nitrogen-oxygen of air. However, using pure oxygen is critical, as the entire system requires certain procedures in terms of maintenance and safety. Operating a fuel cell stack with air requires a pumping device such as a blower or a compressor, resulting in further parasitic losses. Thus, the decision of whether to use pure oxygen or air is a debatable choice based on the application [31].

8.2 Pressure Vessel Design

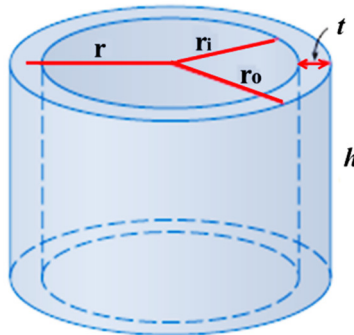
A cylindrical shell with hemispherical ends is frequently used in the pressure vessel design, as a hemispherical ends shell is more efficient than a flat-ended shell in enduring equivalent pressure [72]. The stresses in the cylindrical shell with two closed-ends under internal uniform pressure P can be determined under conditions of static equilibrium, as given in Equations (8.1), (8.2), and (8.3), respectively [106].

$$\sigma_L = \frac{P \cdot r}{2t} \quad (8.1)$$

$$\sigma_t = \frac{p \cdot r}{t} \quad (8.2)$$

Where, σ_L is stress in the longitudinal direction (i.e. the stress in the direction of closed-ends), σ_t is tangential stress which represents the stress applied on the curvature surface of the cylinder, t is the thickness of the shell, and r is the radius of the cylinder. Tangential stress can be expressed in terms of internal radius r_i of the cylinder, as presented in Equation (8.3).

$$\sigma_t = \frac{p}{t}(r_i + 0.5t) \quad (8.3)$$



Minimum shell thickness (in inches) is determined by using Equations (8.4) and (8.5), as given by Bednar and Chuse [106, 107]:

$$t = \frac{P \cdot r_i}{(\sigma_t - 0.5P)} \quad (8.4)$$

$$t = \frac{P \cdot r_i}{(S \cdot E) - 0.6P} \quad (8.5)$$

Where, E represents the weld joint efficiency code, S is the allowable code stress of the metal (in psi), r_i is the internal radius (in inches), and P is the internal pressure (in psi).

Where, Equation (8.5) is valid for a thin shell with thickness (t) less than ($1/2 r_i$) or P less than ($0.385 S.E$). According to the weld joint efficiency code, E has a value of 1.0 for fully radiographed (100% joint efficiency), 0.85 for spot-radiographed, and 0.7 for not radiographed [107].

For a cylindrical shell vessel under uniform external pressure, the thin wall of the vessel collapses at a stress much lower than the yield strength, as a result of instability of the shell. The instability of the shell is governed by many factors such as: properties of the materials used in manufacturing the vessel, operating temperature, shell thickness, unsupported length, and outside diameter. The behaviour of a thin wall shell under the impact of external pressure will differ according to the cylinder length. Pressure where the shell collapses is defined as collapse or critical pressure (P_c) [106].

A short cylindrical shell collapses by the impact of plastic yielding stress alone at high stresses close to the yield strength of the metal. Hence, the ordinary tangential shell stress given above in Equation (8.2) can be used to determine the critical pressure, as given in Equation (8.6) [106]:

$$P_c = \frac{S_y \cdot t}{r_o} \quad (8.6)$$

Where, S_y represents the yield stress of the metal (in psi), t is the shell thickness (in inches), and r_o is the outside radius of the shell (in inches) and ($r_o = r_i + t$). However,

long and intermediate cylinder lengths are not going to be considered in this research, as these types of cylinders are out of the scope of this research application.

A yield stress point is defined as the point up to which deformations occurring in the material are fully recovered upon the removal of the applied load (i.e. the material returns to its original status before being loaded), this region is called the elastic region. Most ductile materials, such as steel, experience plastic deformation especially when the applied load exceeds the yield stress point, and hence the material will not completely return to its original condition after removing the applied load.

8.3 Dimensions and Weight of Pressure Vessel

The volume of a cylindrical shell with inner radius r_i , outer radius r_o , and height h can be determined by subtracting the volume of the inner cylinder from the volume of the outer cylinder.

$$V_{cyl} = \pi \cdot r_o^2 \cdot h - \pi \cdot r_i^2 \cdot h = \pi \cdot h \cdot (r_o^2 - r_i^2) \quad (8.7)$$

Where, the difference between the outer radius and inner radius represents the thickness of the shell ($r_o - r_i = t$). Similarly, the volume of two hemispherical ends of the shell can be calculated as follows:

$$V_{sph} = \frac{4}{3} \pi \cdot (r_o^3 - r_i^3) \quad (8.8)$$

Hence, the volume (V_{shell}) and the mass (M_{shell}) for the shell of a pressure vessel with cylindrical shape and hemispherical ends can be calculated as given in Equations (8.9) and (8.10), respectively.

$$V_{shell} = \pi \cdot h \cdot (r_o^2 - r_i^2) + \frac{4}{3} \pi \cdot (r_o^3 - r_i^3) \quad (8.9)$$

$$M_{shell} = V_{shell} \cdot \rho_m \quad (8.10)$$

Where, ρ_m is the density of the material (g/cm^3) used in manufacturing the shell. The overall height of the shell (h_{shell}) can be determined as given in Equation (8.11):

$$h_{shell} = h + 2 r_o \quad (8.11)$$

The volume of the gas inside the cylindrical shell with hemispherical ends can be determined as given in Equation (8.12):

$$V_{gas} = \pi \cdot r_i^2 \cdot \left(h + \frac{4}{3} r_i \right) \quad (8.12)$$

The implementation of the above equations for a pressure vessel design in Matlab-Simulink are presented in Figures 8.1 and 8.2, representing the Simulink tools and blocks diagram configuration of the pressure vessel design developed in this research. This offers a generic weight estimation mechanism that enables the designer to estimate the size and weight of storage vessels by taking into the consideration the power capacity of fuel cell stack and the flight endurance, and hence determining the overall weight of the UAS, which is a key requirement in the preliminary aircraft design phase.

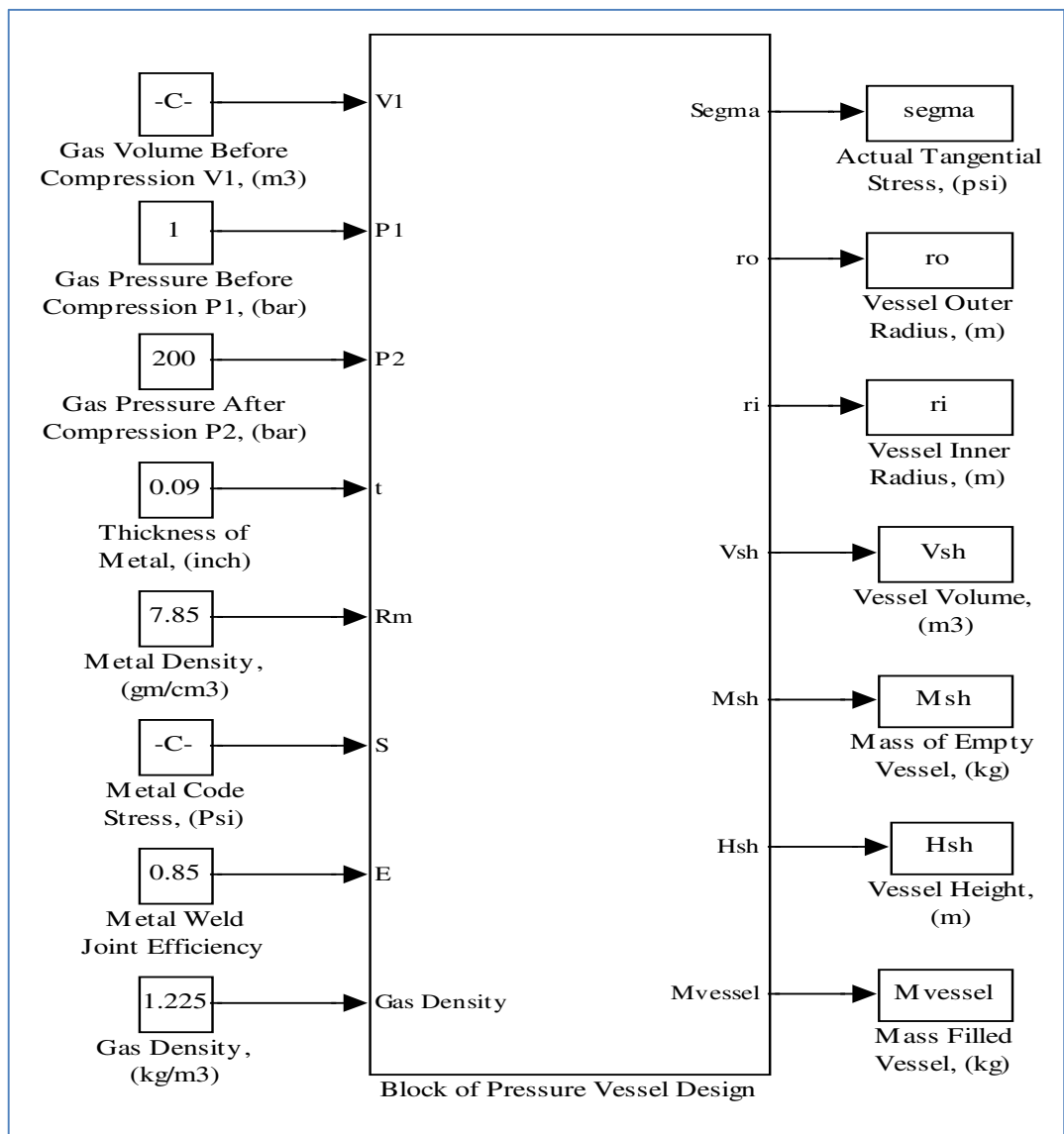


Figure 8.1: Simulink block tools of pressure vessel design

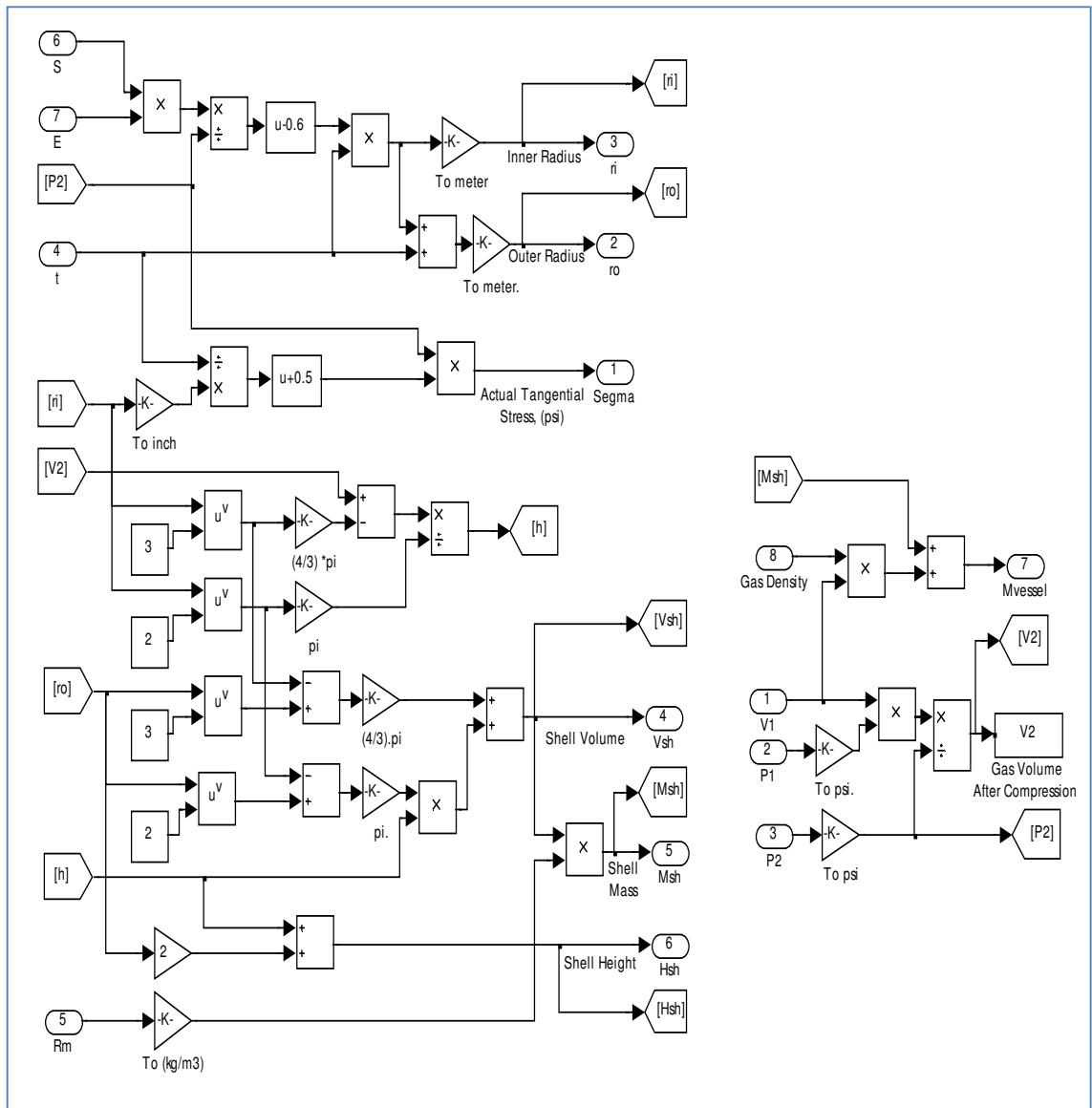


Figure 8.2: Simulink block diagram configuration of pressure vessel design

8.4 Hydrogen and Air-Oxygen Pressure Vessels

Based on the flow rates of supply hydrogen and air for the Horizon (H-1000) fuel cell stack, as presented in Table 4.1, in Chapter Four above, at 20 A current and power of 990 W, the flow of supplied air is 1.766 m³/min equal to 105.96 m³/hour, and the flow of supplied hydrogen is 11.85 L/min which equals 0.711 m³/hour (0.064 kg/hour).

Based on the developed model of the PEM fuel cell stack, at 20 A current and power of 877 W, the flow of supplied air is 119.948 kg/hour equal to 97.9162 m³/hour, and the flow of supplied hydrogen is 0.05725 kg/hour which equals 0.6368 m³/hour.

Where, at standard temperature and pressure, the density of dry air is 1.225 kg/m^3 , the density of oxygen is 1.429 kg/m^3 , the ratio of oxygen to air is 21%, and the density of hydrogen is 0.0899 kg/m^3 . The mass flow rates of reacted oxygen and hydrogen are given in Chapter Four above using Equations (4.31) and (4.42), respectively. For a fuel cell stack consisting of 72 cells, and drawn current is 20 A.

$$\text{Mass Flow of Supplied O}_2 = 97.9162 * 0.21 = 20.5624 \text{ m}^3/\text{hour} = 29.384 \text{ kg/hour}$$

$$W_{O_2, rct} = MO_2 \cdot \frac{n \cdot I_{st}}{4F} = \frac{32 * 72 * 20}{4 * 96485} = 0.1194 \text{ g/s} = 0.43 \text{ kg/hour} = 0.3 \text{ m}^3/\text{hour}$$

$$W_{H_2, rct} = MH_2 \cdot \frac{n \cdot I_{st}}{2F} = \frac{2.02 * 72 * 20}{2 * 96485} = 0.015 \text{ g/s} = 0.054 \text{ kg/hour} = 0.6 \text{ m}^3/\text{hour}$$

A PEM fuel cell is commonly supplied with hydrogen and oxygen at a level higher than the level of reaction rate in order to prevent starvation. The ratio of mass flow rate of supplied gas to the mass flow rate of reacted gas, defined as the utilisation factor μ , is given in Equation (8.13) below [35]:

$$\mu = \frac{\text{Mass flow rate of supplied gas}}{\text{Mass flow rate of reacted gas}} \quad (8.13)$$

$$\mu_{O_2} = \frac{\text{Mass flow of supplied Oxygen}}{\text{Mass flow of reacted Oxygen}} = \frac{20.5624}{0.3} = 68.5 \approx 68$$

$$\mu_{H_2} = \frac{\text{Mass flow of supplied Hydrogen}}{\text{Mass flow of reacted Hydrogen}} = \frac{0.6368}{0.6} = 1.06$$

It is clear that the amount of supplied oxygen or air is 68 times higher than the reacted amount required to produce 20 A of current, which means more air is being pumped to the fuel cell stack, this can be referred to the design of the Horizon fuel

cell stack (H-1000), in order to keep a high level of air flowing inside the stack, yielding a maintained low stack temperature.

It has been reported in the literature that in order to ensure a faster and better response against sudden changes in the load demand, a high utilisation factor needs to be applied. Hence, starvation occurs at the level of higher current drawn from the fuel cell, and this will enable the fuel cell to respond faster to the load changes. But, this will lead to extra hydrogen and air not going to be used in the reaction, which leads to more losses. Therefore, a compromise between the utilisation factor and the size of the gas storage must be considered [35, 56].

Barbir et al. [31] reported that using pure oxygen instead of air to feed the fuel cell stack leads to an increase in the cell output voltage; this is due to the fact that pressure and diffusion rates of pure oxygen in the cathodes is higher than the partial pressure and diffusion rate of oxygen in the nitrogen-oxygen mixture of air. However, the use of pure oxygen is a serious undertaking, as the entire system requires certain procedures in terms of maintenance and safety. Operating a fuel cell stack with air requires a pumping device such as a blower or a compressor, resulting in further parasitic losses. Thus, the decision of whether to use pure oxygen or air is a debatable choice based on the application.

Shih et al. [54] reported that there is a significant increase of up to 32% for the maximum power drawn from a fuel cell stack fed by pure oxygen, in comparison with a stack fed by atmospheric air.

Bégot et al. [27] recommended setting the stoichiometry rates of supplied hydrogen and air to the PEM fuel cell stack of about 1.5 and 2.5, respectively, with 90% relative humidity for a fuel cell stack operating under sub-zero ambient temperature conditions. While the air compressor is controlled to maintain the supplied air to the stack at 2.5 stoichiometric ratio [20].

In this research, three scenarios will be adopted to determine the size and weight of pressure vessels required to supply air or oxygen to the fuel cell stack for high altitude operations. Moreover, three different types of stainless steel metals are adopted in the design of the pressure vessels in order to find an appropriate metal that provides low size and weight advantages. However, the stainless steel materials are chosen based on their specifications in offering high yield strength, high stress resistance, high corrosion resistance, and their availability in a decent range of thicknesses, also their suitability in storing high pressurised gases for aerospace and industrial applications.

First Metal: AK 2205 Duplex Stainless Steel

AK Steel 2205 Duplex Stainless Steel has specifications of high corrosion resistance, high strength and high stress resistance, and low thermal expansion. These specifications make this type of steel highly suitable for applications like heat exchangers, pressure vessels, tanks and pipes, and oil field equipment. 2205 duplex stainless is manufactured and supplied with a standard thickness (0.25 - 2.29 mm), with mechanical properties of 0.2% yield strength equal to 621 MPa (90,069.5 psi) at typical room temperature, and material density about 7.85 g/cm³ [108].

For pressure vessel design calculations using AK Steel 2205 Duplex Stainless Steel, it is assumed that the weld joint efficiency code ($E = 0.85$), and the allowable code stress of the metal ($S = 90,069.5$ psi).

Second Metal: AK 15-5 PH Stainless Steel

AK Steel 15-5 PH Stainless Steel provides high strength, good corrosion resistance, and good stress resistance in transverse and longitudinal directions, this type of steel is widely used in petrochemical, chemical and aerospace applications. 15-5 PH stainless steel is manufactured and supplied in original condition of class-A, which is prepared for immediate use by consumers. There are eight standard heat treatments applied on the

class-A stainless steel to provide a wide range of properties in order to meet the requirements of specific customer applications. 15-5 PH stainless steel class-A is supplied with standard thickness (0.38 - 3.18 mm), with maximum 0.2% yield strength acceptable for material specification equal to 1103 MPa (159,979 psi), and material density about 7.78 g/cm³ [109].

For pressure vessel design calculations using AK Steel 15-5 PH Stainless Steel, it is assumed that the weld joint efficiency code ($E = 0.85$), and the allowable code stress of the metal ($S = 159,979$ psi).

Third Metal: AK 440A Stainless Steel

AK Steel 440A Stainless Steel in hardened and stress relieved conditions provides high strength and corrosion resistance, this type of steel is widely used in dental and surgical instruments, and manufacturing of crushing machines. 440A stainless steel is manufactured and supplied with standard thickness (0.25 - 3.68 mm), with maximum 0.2 % yield strength mechanical properties equal to 1655 MPa (240,040.4 psi), and material density about 7.74 g/cm³ [110].

For pressure vessel design calculations using AK Steel 440A Stainless Steel, it is assumed that the weld joint efficiency code ($E = 0.85$), and the allowable code stress of the metal ($S = 240,040.4$ psi).

However, all calculations related to the design of pressure vessels and power-plant mass estimations in the following sections of this chapter will be determined based on the developed model of the PEM fuel cell stack and the Simulink tools of pressure vessel design developed in this research.

8.4.1 First Scenario: Pressure Vessel for Compressed Air

At sea level, based on the developed model of a PEM fuel cell stack, for one hour's operation of the stack at a maximum current of 20 A, and power 877 W, the required

supply of air is 119.948 kg/hour (which is equal to 97.9162 m³/hour), under 1atm ambient pressure. Using Equation (A.3) in Appendix A, to determine the volume of air under compression, assuming P₁=1atm = 1.01317 bar = 14.504 psi, V₁ = 97.9162 m³, and assuming that air is going to be pressurised up to 200 bar (2,900.8 psi), the new volume of air is determined as given below:

$$V_2 = \frac{97.9162 * 14.504}{2,900.8} = 0.49 \text{ m}^3$$

BOC Industrial Gases UK [111] provides different sizes of cylindrical air vessels with a maximum filling pressure up to 200 bar, at 15 °C ambient temperature. A cylinder type N, for storing 8.85 m³ (10.85 kg) of air, with the vessel dimensions (D x H) of (23 cm x 146 cm), and a gross weight of 82 kg. The calculations of the air pressure vessel design are presented in Appendix C, Section C.1.

8.4.2 Second Scenario: Pressure Vessel for Compressed Oxygen

At sea level, based on the developed model of a PEM fuel cell stack, for one hour's operation of the stack at a maximum current of 20 A, and power of 877 W, the required supply of pure oxygen is 29.384 kg/hour (which is equal to 20.5624 m³/hour) under 1atm ambient pressure. Using Equation (A.3) in Appendix A, to determine the volume of oxygen under compression, assuming P₁= 1atm = 1.01317 bar = 14.504 psi, and V₁ = 20.5624 m³, and assuming that oxygen is going to be pressurised up to 230 bar (3,335.92 psi), the new volume of oxygen is determined as given below:

$$V_2 = \frac{20.5624 * 14.504}{3,335.92} = 0.09 \text{ m}^3$$

BOC Industrial Gases UK [112] provides different sizes of cylindrical oxygen vessels with the maximum filling pressures varying between 137 and 230 bar, at 15 °C ambient

temperature. A cylinder type W, for storing 11.09 m³ (15.85 kg) of oxygen, with the vessel dimensions (D x H) of (23 cm x 146 cm), and a gross weight of 80 kg.

The calculations of the oxygen pressure vessel design are presented in Appendix C, Section C.2. The dimensions and masses of air and oxygen cylindrical pressure vessels with two hemispherical ends for one hour's operation of a PEM fuel cell stack, at a maximum current of 20 A, power 877 W, and for different stainless steel materials are presented in Table 8.1 and Figures 8.3 and 8.4, respectively.

Table 8.1: Dimensions and masses of air and oxygen cylindrical pressure vessels with two hemispherical ends for one hour's operation of a PEM fuel cell stack, at a maximum current of 20 A, and power of 877 W								
	Pressure vessel cylinder filled by compressed air up to 200 bar to supply flow rate 97.9162 m ³ /hour equal to 119.948 kg/hour.				Pressure vessel cylinder filled by compressed O ₂ up to 230 bar to supply flow rate 20.5624 m ³ /hour equal to 29.384 kg/hour.			
	Dimensions of Vessel		Mass of Vessel (kg)		Dimensions of Vessel		Mass of Vessel (kg)	
Type of Stainless Steel	Height (m)	Diameter (cm)	Empty Vessel	Filled Vessel	Height (m)	Diameter (cm)	Empty Vessel	Filled Vessel
AK 2205 Duplex, thickness 2.29 mm	44.85	12.25	299.25	419.2	11.014	10.676	64.854	94.24
AK 15-5 PH, thickness 3.18 mm	7.306	30.07	169.04	289.0	1.8478	26.18	37.06	66.5
AK 440A, thickness 3.68 mm	2.547	52.07	117.63	237.6	0.7331	45.313	29.345	58.73

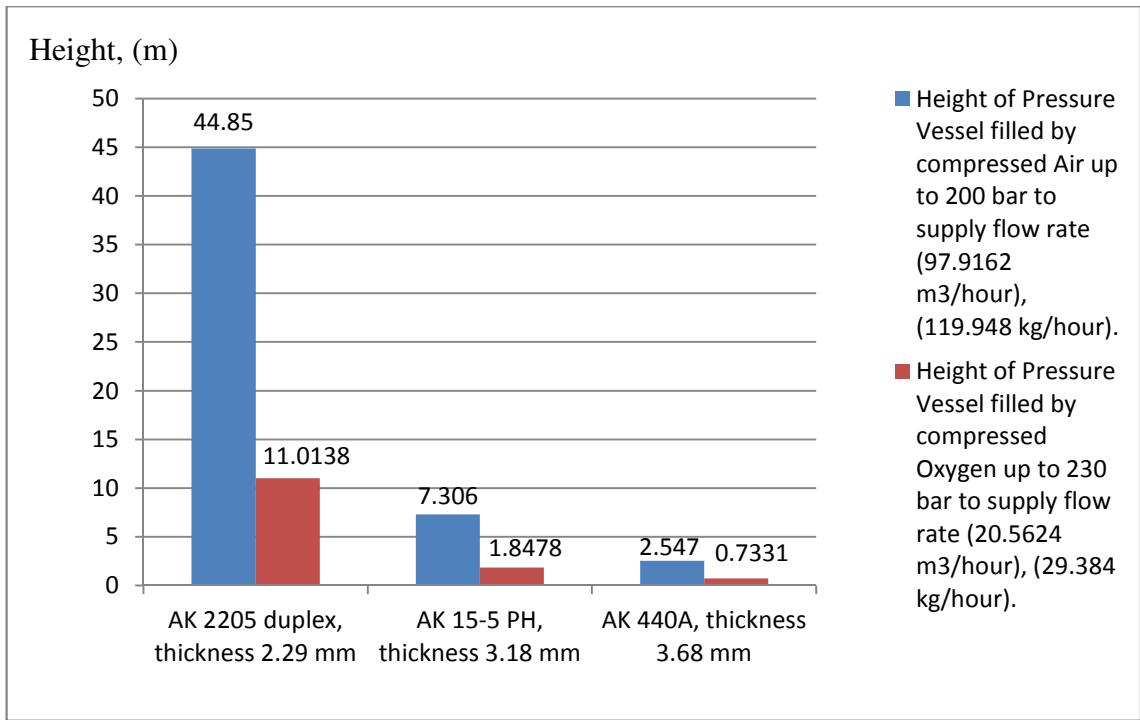


Figure 8.3: Heights of air and oxygen cylindrical pressure vessels for one hour's operation, at a maximum current of 20 A, and power of 877 W

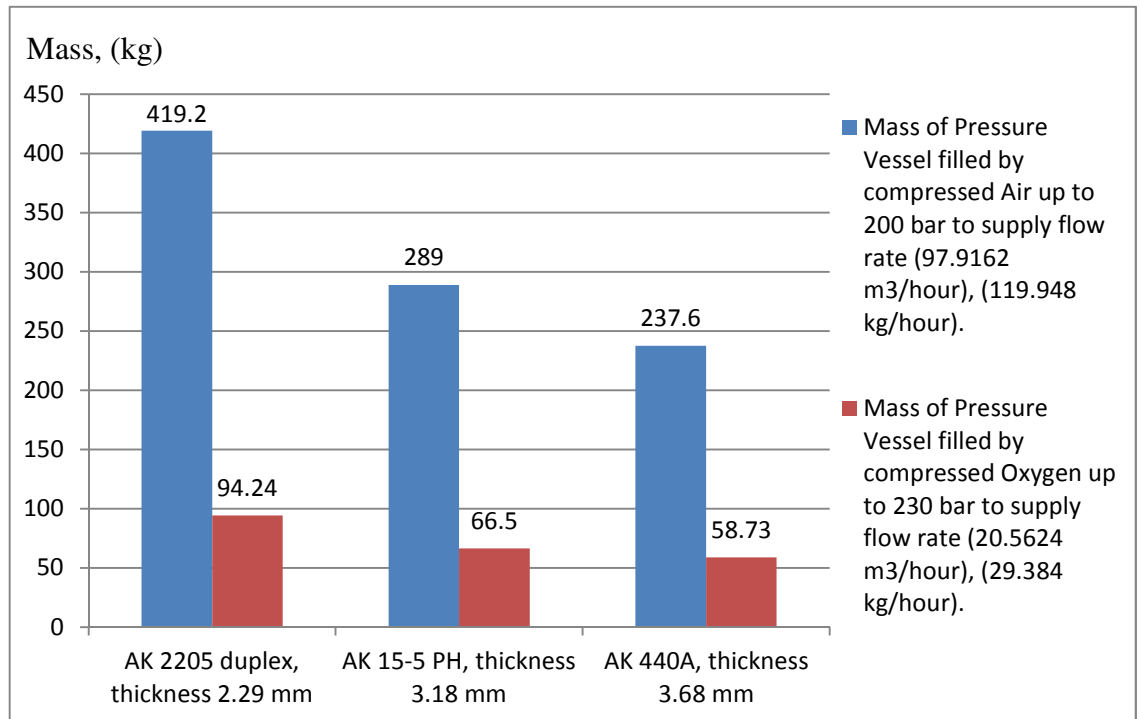


Figure 8.4: Masses of air and oxygen cylindrical pressure vessels for one hour's operation, at a maximum current of 20 A, and power of 877 W

In the case of air or oxygen, they are compressed up to 300 bar in an attempt to further reduce the size of the pressure vessel cylinder, Table 8.2 presents the dimensions and masses of cylindrical pressure vessel with two hemispherical ends for one hour's operation of a PEM fuel cell stack, at a maximum current of 20 A, and power of 877 W, with compression pressure up to 300 bar at 15 °C ambient temperature, as calculated by Simulink tools of pressure vessel design. It is clear that the impact of increasing the compression pressure of air or oxygen up to 300 bar would reduce the diameter of the vessel on the account of increasing the height with no significant impact on the whole mass of the vessel.

Table 8.2: Dimensions and masses of air and oxygen cylindrical pressure vessels with two hemispherical ends for one hour's operation of a PEM fuel cell stack, at a maximum current of 20 A, power of 877 W, and compression pressure up to 300 bar at 15 °C								
	Pressure vessel cylinder filled by compressed air to supply flow rate 97.9162 m ³ /hour equal to 119.948 kg/hour.				Pressure vessel cylinder filled by compressed oxygen to supply flow rate 20.5624 m ³ /hour equal to 29.384 kg/hour.			
	Dimensions of Vessel		Mass of Vessel, (kg)		Dimensions of Vessel		Mass of Vessel, (kg)	
Type of Stainless Steel	Height (m)	Diameter (cm)	Empty Vessel	Filled Vessel	Height (m)	Diameter (cm)	Empty Vessel	Filled Vessel
AK 2205 Duplex, thickness 2.29 mm	68.863	8.23	310.52	430.47	14.486	8.23	65.309	94.693
AK 15-5 PH, thickness 3.18 mm	11.006	20.14	169.44	289.39	2.368	20.14	36.412	65.796
AK 440A thickness 3.68 mm	3.70	34.81	113.94	233.89	0.8727	34.81	26.783	56.166

8.4.3 Third Scenario: Pressure Vessel for Limited Volume of Compressed Oxygen

The fuel cell stack is assumed to be supplied by pure oxygen with a mass flow rate sufficient to have a full reaction. It has been determined that 0.3 m³/hour of oxygen needs to be fully reacted in order to produce a 20 A current. In order to ensure that the cathodes of the stack are fully occupied with pure oxygen over the whole period of the operational time of the stack, the mass flow rate of supplied oxygen is assumed to be equal to 0.6 m³/hour, hence the utilisation factor is $\mu_{O_2} = 2$.

Pukrushpan et al. [2, 32] proposed in their works that an instantaneous limit of oxygen excess ratio which represents the ratio of supplied to reacted oxygen equal to $\mu_{O_2} = 2$, is the optimum rate to maintain the desired value of net power for the fuel cell stack.

However, managing the temperature of the stack is not the focus of this research, therefore any viable techniques, such as high-speed air pump or water flow heat exchanger can be used to maintain the temperature of the stack within the desired operational conditions.

At sea level, as it has been proposed above that for one hour's operation of stack consisting of 72 cells, and at load current of 20 A, the necessary proposed mass flow rate of supplied oxygen is assumed to be equal to 0.6 m³/hour (0.8574 kg/hour) under 1atm ambient pressure. Using Equation (A.3) in Appendix A, to determine the volume of oxygen under compression, assuming $P_1 = 1\text{atm} = 1.01317\text{ bar} = 14.504\text{ psi}$, and $V_1 = 0.6\text{ m}^3$, and assuming that oxygen is going to be pressurised up to 230 bar (3,335.92 psi), the new volume of oxygen is determined as given below:

$$V_2 = \frac{0.6 * 14.504}{3,335.92} = 2.609 * 10^{-3} \text{ m}^3 = 2,609 \text{ cm}^3$$

Using AK 2205 Duplex Stainless Steel, the calculations of the pressure vessel design are presented in Appendix C, Section C.3. The dimensions and masses of an oxygen

cylindrical pressure vessel with two hemispherical ends, using AK 2205 Duplex Stainless Steel with 2.29 mm metal thickness, for several hours of operation, at maximum current of 20 A, and power of 877 W, and for a limited volume of compressed oxygen up to 230 bar at 15 °C ambient temperature, are presented in Table 8.3 and Figure 8.5.

Table 8.3: Dimensions and masses of oxygen cylindrical pressure vessel with two hemispherical ends, using AK 2205 Duplex Stainless Steel with 2.29 mm metal thickness, for several hours of operation, at maximum current of 20 A, and power of 877W, and for a limited volume of compressed oxygen up to 230 bar at 15 °C							
	Before Compression at atmospheric pressure		After Compression up to 230 bar	Dimensions and Masses of Pressure Vessel			
Hours of operations	Volume (m ³)	Mass (kg)	Volume (cm ³)	Height (m)	Diameter (cm)	Mass of Empty Vessel (kg)	Mass of Filled Vessel (kg)
1	0.60	0.8574	2,609	0.357	10.68	2.09	2.95
2	1.20	1.715	5,217	0.677	10.68	3.98	5.7
3	1.80	2.5722	7,826	0.997	10.68	5.86	8.44
4	2.40	3.43	10,435	1.316	10.68	7.74	11.17
5	3.0	4.287	13,043	1.634	10.68	9.62	13.91

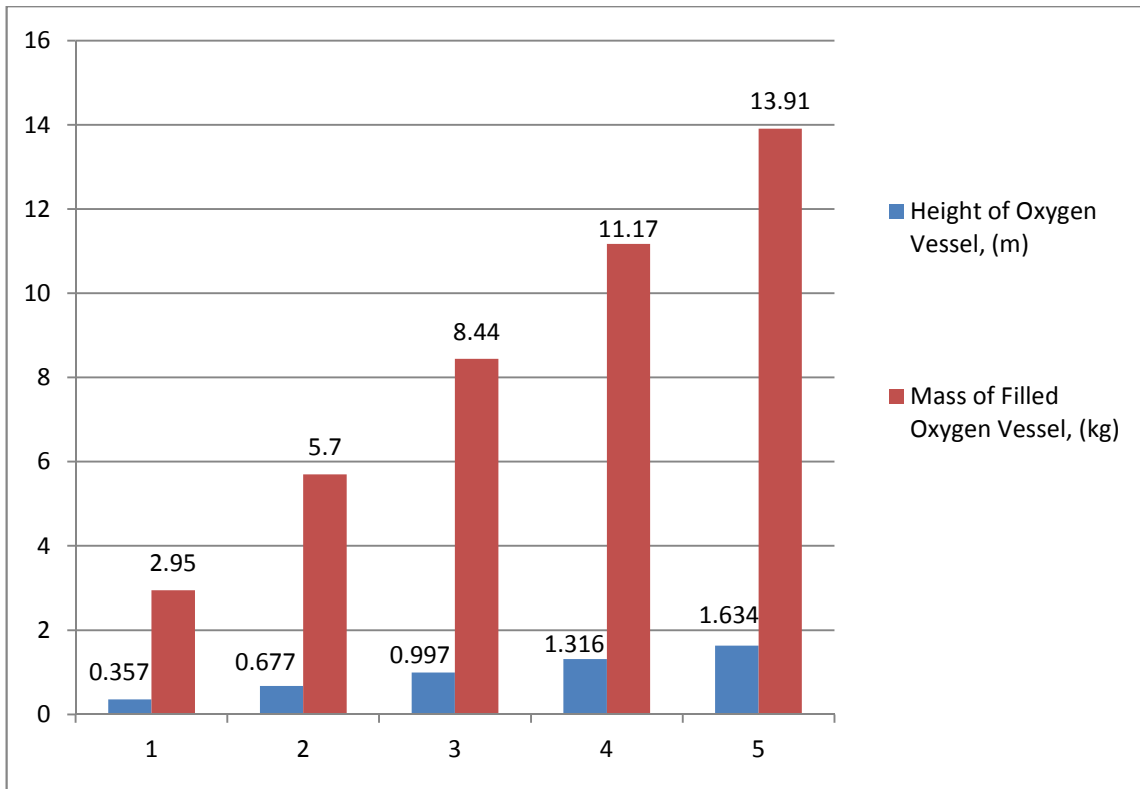


Figure 8.5: Heights and masses of oxygen cylindrical pressure vessel for several hours of operation, at maximum current of 20 A, and power of 877 W, and for a limited volume of compressed oxygen up to 230 bar

In the case where oxygen is compressed up to 300 bar in an attempt to further reduce the size of the pressure vessel cylinder, Table 8.4 presents the dimensions and masses of the oxygen cylindrical pressure vessel with two hemispherical ends, using AK 2205 Duplex Stainless Steel with 2.29 mm metal thickness, for several hours of operation, at maximum current of 20 A, and power of 877 W, for a limited volume of compressed oxygen up to 300 bar at 15 °C ambient temperature, as calculated by the Simulink tools of pressure vessel design. It is clear that the impact of increasing the compression pressure of oxygen up to 300 bar would reduce the diameter of the vessel on the account of increasing the height, with no significant impact on the whole mass of the vessel.

Table 8.4: Dimensions and masses of oxygen cylindrical pressure vessel with two hemispherical ends, using AK 2205 Duplex Stainless Steel with 2.29 mm metal thickness, for several hours of operation, at maximum current of 20 A, and power of 877W, for a limited volume of compressed oxygen up to 300 bar at 15 °C

Hours of operations	Before Compression at atmospheric pressure		After Compression up to 300 bar	Dimensions and Masses of Pressure Vessel			
	Volume (m ³)	Mass (kg)	Volume (cm ³)	Height (m)	Diameter (cm)	Mass of Empty Vessel (kg)	Mass of Filled Vessel (kg)
1	0.60	0.8574	2,000	0.4523	8.23	2.03	2.887
2	1.20	1.715	4,000	0.874	8.23	3.932	5.646
3	1.80	2.5722	6,000	1.296	8.23	5.8332	8.4053
4	2.40	3.43	8,000	1.7176	8.23	7.735	11.165
5	3.0	4.287	10,000	2.1394	8.23	9.637	13.924

8.4.4 Pressure Vessel for Compressed Hydrogen

At sea level, based on the developed model of a PEM fuel cell stack, for one hour's operation of the stack at a maximum current of 20 A, and power of 877 W, the required supply of hydrogen is 0.05725 kg/hour (which is equal to 0.637 m³/hour), under 0.55 bar of supply pressure of hydrogen. Using Equation (A.3) in Appendix A, to determine the volume of hydrogen under compression, assuming $P_1 = 0.55 \text{ bar} = 7.98 \text{ psi}$, and

$V_1 = 0.637 \text{ m}^3$, and assuming that hydrogen is going to be pressurised up to 175 bar (2,538.2 psi), the new volume of hydrogen is determined as given below:

$$V_2 = \frac{0.637 * 7.98}{2,538.2} = 0.002002 \text{ m}^3 = 2,002 \text{ cm}^3$$

BOC Industrial Gases UK [113] provides different sizes of cylindrical hydrogen vessels with a maximum filling pressure up to 175 bar, at 15 °C ambient temperature. Using AK 2205 Duplex Stainless Steel, the calculations of the hydrogen pressure vessel design are presented in Appendix C, Section C.4. The dimensions and masses of the hydrogen cylindrical pressure vessel with two hemispherical ends, using AK 2205 Duplex Stainless Steel with 2.29 mm metal thickness, for several hours of operation, at maximum current of 20 A, and power of 877 W, and for a limited volume of compressed hydrogen up to 175 bar at 15 °C ambient temperature are presented in Table 8.5 and Figure 8.6.

Table 8.5: Dimensions and masses of hydrogen cylindrical pressure vessel with two hemispherical ends, using AK 2205 Duplex Stainless Steel with 2.29 mm metal thickness, for several hours of operation, at maximum current of 20 A, and power of 877W, for a limited volume of compressed hydrogen up to 175 bar at 15 °C

Hours of operations	Before Compression at pressure of 0.55 bar		After Compression up to 175 bar	Dimensions and Masses of Pressure Vessel			
	Volume (m ³)	Mass (kg)	Volume (cm ³)	Height (m)	Diameter (cm)	Mass of Empty Vessel (kg)	Mass of Filled Vessel (kg)
1	0.637	0.05725	2,002	0.1892	13.98	1.45	1.5073
2	1.274	0.1145	4,004	0.3287	13.98	2.53	2.6445
3	1.911	0.1718	6,006	0.4682	13.98	3.6105	3.7823
4	2.548	0.2291	8,008	0.6078	13.98	4.692	4.9211
5	3.185	0.2864	10,01	0.7473	13.98	5.773	6.0593

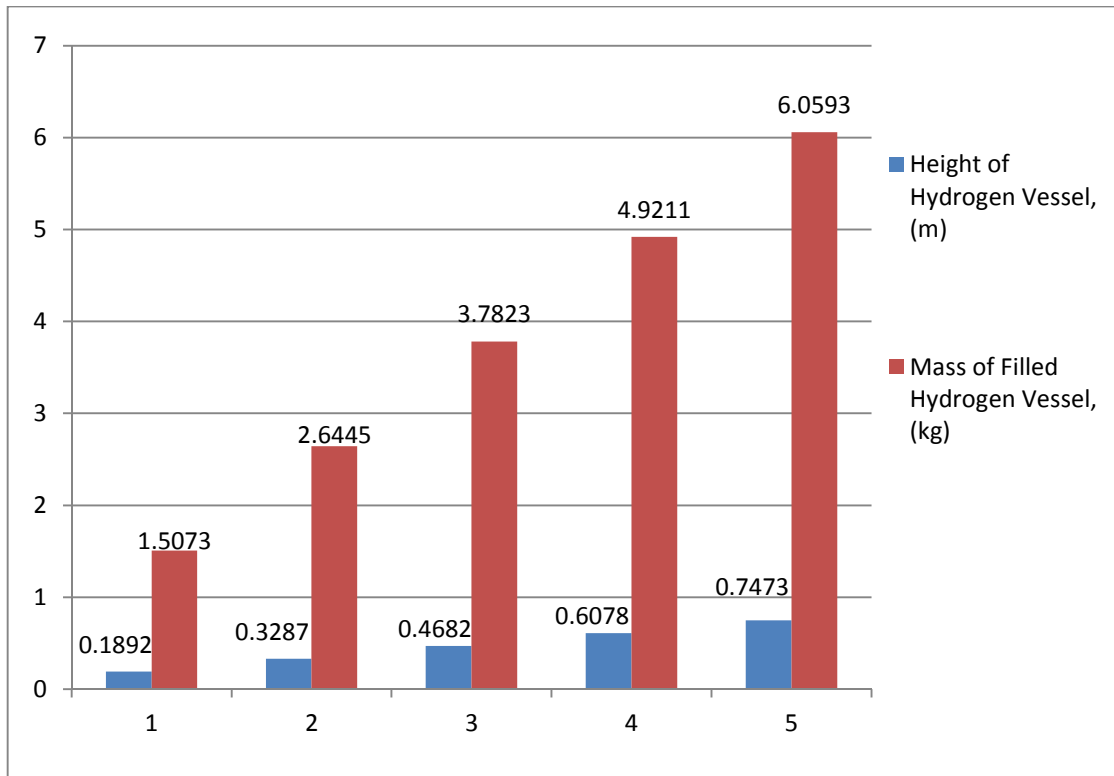


Figure 8.6: Heights and masses of hydrogen cylindrical pressure vessel for several hours of operation, at maximum current of 20 A, and power of 877 W, and for limited volume of compressed hydrogen up to 175 bar at 15 °C ambient temperature

In the case where hydrogen is compressed up to 300 bar in an attempt to further reduce the size of the pressure vessel cylinder, Table 8.6 presents the dimensions and masses of the hydrogen cylindrical pressure vessel with two hemispherical ends, using AK 2205 Duplex Stainless Steel with 2.29 mm metal thickness, for several hours of operation, at maximum current of 20 A, and power of 877 W, and for a limited volume of compressed hydrogen up to 300 bar at 15 °C ambient temperature, as calculated by the Simulink tools of pressure vessel design. It is clear that the impact of increasing the compression pressure of hydrogen up to 300 bar would reduce the diameter of the vessel on the account of increasing the height, with no significant impact on the whole mass of the vessel.

Table 8.6: Dimensions and masses of hydrogen cylindrical pressure vessel with two hemispherical ends, using AK 2205 Duplex Stainless Steel with 2.29 mm metal thickness, for several hours of operation, at maximum current of 20 A, and power of 877W, for a limited volume of hydrogen compressed up to 300 bar at 15 °C

Hours of operations	Before Compression at pressure of 0.55 bar		After Compression up to 300 bar	Dimensions and Masses of Pressure Vessel			
	Volume (m ³)	Mass (kg)	Volume (cm ³)	Height (m)	Diameter (cm)	Mass of Empty Vessel (kg)	Mass of Filled Vessel (kg)
1	0.637	0.05725	1,167.84	0.2768	8.23	1.238	1.2951
2	1.274	0.1145	2,335.67	0.523	8.23	2.3484	2.4629
3	1.911	0.1718	3,503.5	0.7693	8.23	3.459	3.6308
4	2.548	0.2291	4,671.34	1.016	8.23	4.57	4.799
5	3.185	0.2864	5,839.17	1.262	8.23	5.68	5.967

It is clear from the results obtained for the pressure vessels design presented above, that it is not possible by any means to use high flow rates of air (97.9162 m³/hour) or oxygen (20.5624 m³/hour), as presented in the first and second scenario, in order to supply the fuel cell stack, particularly for high altitude UAS applications, as it requires a great size and heavy mass of vessel to carry the compressed air or oxygen. Alternatively, using limited volumes and flow rates of hydrogen (0.637 m³/hour) and oxygen (0.6 m³/hour) in order to supply the fuel cell stack, as presented in the third

scenario can offer an optimum pressure vessel design in terms of lowering the size and weight of the vessel, hence saving more power and extending the endurance of the mission, and allowing further payload to be added for the same mission duration.

Figures 8.7 and 8.8 present the flow rates of supply hydrogen and oxygen based on the developed model of a PEM fuel cell stack, using limited volumes and flow rates of hydrogen ($0.637 \text{ m}^3/\text{hour}$) and oxygen of ($0.6 \text{ m}^3/\text{hour}$) under various current load demand and up to five hours of operation.

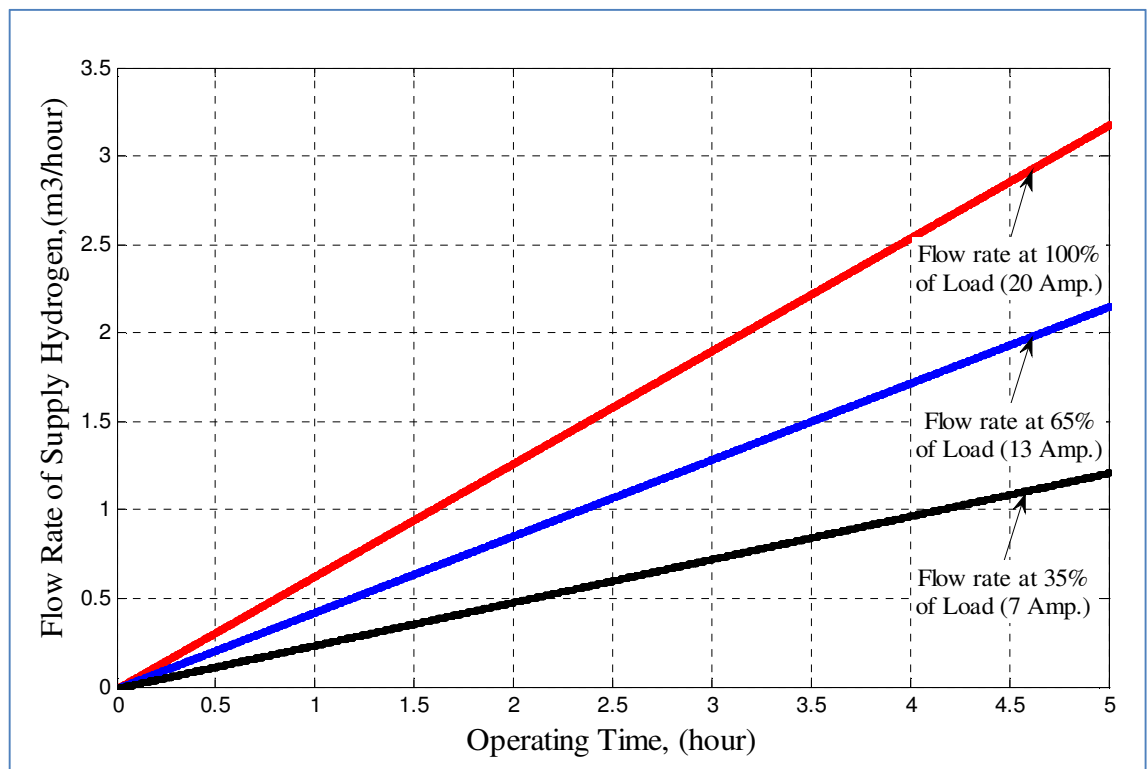


Figure 8.7: Flow rates of supply hydrogen based on the developed model of a PEM fuel cell stack, using limited flow rate of hydrogen ($0.637 \text{ m}^3/\text{hour}$), under various current load demand and up to five hours of operation

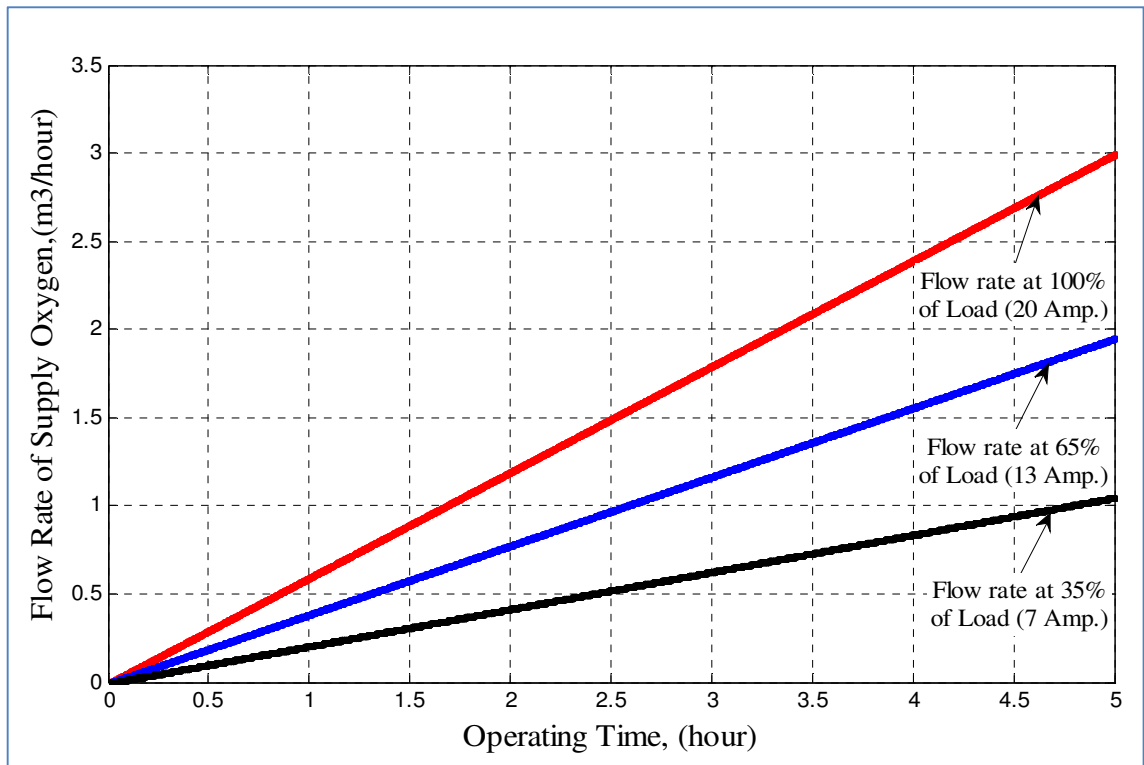


Figure 8.8: Flow rates of supply oxygen based on the developed model of a PEM fuel cell stack, using limited flow rate of oxygen ($0.6 \text{ m}^3/\text{hour}$), under various current load demand and up to five hours of operation

8.5 Power Plant Mass Estimation for a PEM Fuel-Cell-Based UAS

A power supply system of a UAS can be categorised into a fuel cell power-plant and a fuel cell subsystem. A fuel cell power-plant consists of the fuel cell stack, air and hydrogen supply and regulation systems, and a cooling system. A fuel cell subsystem consists of electrical distribution bus and power management system. The power supply system provides power to the propulsion system through the DC bus voltage. The propulsion system consists of an electric motor, motor controller, and the propeller [22, 26].

The power generated from the PEM fuel cell power system is determined according to the size of the fuel cell stack, while the energy capacity is determined according to the storage capacity of the hydrogen and oxygen vessels [31]. However, in the case of a

fixed size of hydrogen tank, the endurance of the aircraft is limited by the efficiency of the propulsion system and the power-plant system [26].

In UAS missions, the highest power consumption occurs during take-off and climb to the designated cruise altitude, while the lowest power consumption occurs during descent. The largest time and energy consumptions are during the cruise stage, at constant altitude where the weight of the aircraft is equal to the lift, and the thrust is equal to the drag [7, 10].

Kim et al. [7] reported that during take-off and flight manoeuvres, power will be supplied from both the fuel cell and batteries, while the fuel cell stack will supply steady power during the cruise mode. While, Adam and Leachman [72] reported that a mass flow rate of 0.07416 kg/hour (0.825 m³/hour) of hydrogen is sufficient to produce a 979W power output from the Horizon (H-1000) fuel cell stack during the take-off and climb phase for a small UAS (< 25 kg), while a mass flow rate of 0.03744 kg/hour (0.4165 m³/hour) of hydrogen is sufficient to produce power of 498 W for the cruise phase.

Seo et al. [61] reported a cruising speed of 59.8 km/hour for a small UAS (< 7.5 kg) using a 200 W PEM fuel cell stack to achieve a flying mission up to 200 m altitude for the 57 minute continuous flying test. While, Furrutter and Meyer [53] reported that at a steady and stable flying altitude, the maximum flight velocity is 46.8 km/hour for a small-scale fixed wing UAS using a 100 W Horizon PEM fuel cell power-plant system, and 5.3 kg total mass of UAS.

In this research, it is assumed that the UAS will need one hour to climb to the cruising altitude of 36,000 ft. (i.e. climbing speed is 11 km/hour) with maximum load current of 20 A (100% load current) drawn from the power supply system represented by the fuel cell stack. While during the cruising mode, the drawn current from the fuel cell stack will be assumed to be equal to 13 A (i.e. 65% of max. load). Also, the UAS is assumed

to spend 45 minutes descending and landing from the cruising altitude, with a drawn current from the fuel cell stack of 7 A (i.e. 35% of max. load). Based on the developed model of the PEM fuel cell stack and the Simulink tools of pressure vessel design, Table 8.7 presents the volumes of supplied oxygen and hydrogen according to the load demand and flying mode. While, Table 8.8 presents the volumes and masses of supply oxygen and hydrogen to the fuel cell stack according to the total flying hours.

Table 8.7: Volumes of supplied oxygen and hydrogen to the fuel cell stack according to the load demand and flying mode, based on the developed model of a PEM fuel cell stack and Simulink tools of pressure vessel design						
Flying Mode	Operating Time (minutes)	Fuel Cell Stack Current (A)	Current Load %	Fuel Cell Stack Output Power (W)	Volume of Supply Oxygen (m ³)	Volume of Supply Hydrogen (m ³)
Climbing	60	20.0	100	877.0	0.60	0.637
Cruising	60	13.0	65	609.0	0.391	0.4316
Landing	45	7.0	35	352.0	0.158	0.1825
Total Volumes of Supplied Gases					1.149	1.2511

Using the data given in Table 8.8 it is possible to determine the desired flying hours of the mission of the UAS, and using the results obtained from Tables 8.3 and 8.5 above, to estimate the total mass and sizes of the oxygen and hydrogen pressure vessels accordingly. Table 8.9 presents the design specifications for the oxygen and hydrogen pressure vessels according to the desired flying hours, based on the developed model of the PEM fuel cell stack and Simulink tools of pressure vessel design. While, the masses

of the items and components used in the design of the power-plant system and the propulsion system, associated with the estimated mass of the UAS frame structure and the carried payload for UAS applications, are presented in Table 8.10.

Table 8.8: Volumes and masses of supply oxygen and hydrogen to the fuel cell stack according to the total flying hours, based on the developed model of a PEM fuel cell stack and Simulink tools of pressure vessel design						
Total Flying Time (minute)	Total Flying Time (hour)	Cruising Time (hour)	Volume of Supply Oxygen (m ³)	Mass of Supply Oxygen (kg)	Volume of Supply Hydrogen (m ³)	Mass of Supply Hydrogen (kg)
135	2.25	0.5	0.9535	1.3626	1.0353	0.0931
165	2.75	1	1.149	1.6419	1.2511	0.1125
195	3.25	1.5	1.3445	1.9213	1.4669	0.1319
225	3.75	2	1.54	2.2007	1.6827	0.1513
255	4.25	2.5	1.7355	2.48	1.8985	0.1707
285	4.75	3	1.931	2.7594	2.1143	0.1901
315	5.25	3.5	2.1265	3.0388	2.3301	0.2095
345	5.75	4	2.322	3.3181	2.5459	0.2289
375	6.25	4.5	2.5175	3.5975	2.7617	0.2483
405	6.75	5	2.713	3.8769	2.9775	0.2677
435	7.25	5.5	2.9085	4.1562	3.1933	0.2871
465	7.75	6	3.104	4.4356	3.4091	0.3065

Table 8.9: Design specifications for the oxygen and hydrogen pressure vessels according to the desired flying hours, based on the developed model of a PEM fuel cell stack and Simulink tools of pressure vessel design

Total Flying Time (minute)	Total Flying Time (hour)	Cruising Time (hour)	Oxygen Pressure Vessel Design with Diameter (10.68 cm)		Hydrogen Pressure Vessel Design with Diameter (13.98 cm)		Levels of H ₂ /O ₂	Total Mass of Filled H ₂ /O ₂ Vessels (kg)
			Height (m)	Mass of Filled Vessel (kg)	Height, (m)	Mass of Filled Vessel (kg)		
135	2.25	0.5	0.677	5.7	0.3287	2.65	EFTA	8.35
165	2.75	1					FOL	
195	3.25	1.5	0.997	8.44	0.4682	3.7823	EFTA	12.23
225	3.75	2					EFTA	
255	4.25	2.5					FOL	
285	4.75	3	1.316	11.17	0.6078	4.9211	EFTA	16.1
315	5.25	3.5					EFTA	
345	5.75	4					FOL	
375	6.25	4.5	1.634	13.91	0.7473	6.0593	EFTA	20.0
405	6.75	5					EFTA	
435	7.25	5.5					FOL	

* EFTA: Extra Flying Time Available

* FOL: Fuel on Limit (for both hydrogen and oxygen)

Table 8.10: Masses of the items and components used in the design of the power-plant system and propulsion system with the estimated mass of the UAS frame structure and carried payload for UAS applications	
Item Description	Mass (kg)
Horizon (H-1000) PEM Stack with Controller	5.000
BLDC motor KMS Quantum 4130/07	0.396
Propeller (15" x 8")	0.2
DC-DC Converter (Mean Well SD-1000L-24)	1.94
Estimated mass of batteries, electronics and connections	0.5
Estimated mass of high speed air pump	0.5
Estimated mass of UAS frame structure	5.0
Estimated mass of payload	2.0
Total	15.536

As determined in Chapter Seven - Section 7.3, for 0.4 static thrust to weight ratio of a UAS, the maximum permitted mass of the UAS is 16.28 kg. While for 0.2 static thrust to weight ratio of a UAS, the maximum permitted mass of the UAS is 32.55 kg.

It is clear that adopting a static thrust to weight ratio of 0.4 must be avoided, as it offers low mass allowance for the whole UAS. For a maximum four hour cruising mission (345 minutes total flying time), the total mass of the whole UAS is estimated to be equal to $(16.1 + 15.536 = 31.636 \text{ kg})$ as given in Tables 8.9 and 8.10, respectively, which is less than the maximum permitted mass of a UAS having a 0.2 static thrust to weight ratio.

The developed model of a PEM fuel cell in this research, associated with estimations of the total masses of hydrogen and oxygen vessels and the mass of the propulsion system, can offer a maximum of 345 minutes of flying time for the UAS mission; this

is based on a Horizon (H-1000) PEM stack. A generic weight estimation mechanism could easily be inferred from the work. Furthermore, reducing the mass of the frame structure and the payload, and choosing light equipment to be carried on board would reduce the overall mass of the UAS, and reduction of aerodynamic drag will extend the flying mission, as the power requirement is reduced.

The design of the power-plant system and UAS frame structure may vary according to the type of mission in terms of cruising altitude, required flying hours, and the size and weight of the payload. Therefore, the designer must consider all these parameters during the design stage of the entire UAS.

8.6 Summary

In this chapter, the design of hydrogen and air-oxygen pressure vessels were investigated in order to determine the weight and size of the vessel based on mass flow rates of gases and power demand per operational hour, for high altitude UAS operation. Three scenarios were adopted in determining the size and weight of pressure vessels required to supply air or oxygen to the fuel cell stack, based on the governing equations of the pressure vessel design and the related mass estimation. Different types of stainless steel materials were used in the design of the pressure vessel in order to find an appropriate material that provides low size and weight advantages. Also, hydrogen pressure vessel design and mass estimation were also considered.

It is clear from the results obtained for the pressure vessel design presented above, that it is not possible by any means to use high flow rates of air ($97.9162 \text{ m}^3/\text{hour}$) or oxygen ($20.5624 \text{ m}^3/\text{hour}$), as presented in the first and second scenario, to supply the fuel cell stack, particularly for UAS applications as these require a high size and heavy mass of vessel to carry the compressed air or oxygen. Alternatively using limited volumes and flow rates of hydrogen ($0.637 \text{ m}^3/\text{hour}$) and oxygen ($0.6 \text{ m}^3/\text{hour}$), as

presented in the third scenario, can offer the optimum pressure vessel design in terms of lowering the size and weight of the vessel, hence reducing power consumption and extending the endurance of the mission, and allowing further payload to be added for the same mission duration.

The developed model of a PEM fuel cell in this research, associated with estimations of the total masses of hydrogen and oxygen vessels and the mass of the propulsion system, can offer a maximum 345 minutes of flying time for the UAS mission; this is based on a Horizon (H-1000) PEM stack. A generic weight estimation mechanism could easily be inferred from the work. Furthermore, by reducing the mass of the frame structure and the payload, and choosing light equipment to be carried on board it would be possible to reduce the overall mass of the UAS. Reduction of aerodynamic drag would also extend the flying mission, as the power requirement is reduced.

Simulink tools of pressure vessel design were developed and formed that can estimate and determine the overall weight of the UAS, based on determining the size and weight of the combined power-plant of a fuel cell stack with hydrogen and air/oxygen vessels and the propulsion system of the UAS for high altitude operation.

The design of the power-plant system and UAS frame structure may vary according to the type of the mission, in terms of cruising altitude, required flying hours, and the size and weight of the payload. Therefore, the designer must consider all these parameters during the design stage of the entire UAS.

In the next chapter, the final conclusion and possible future work relating to the research will be presented and discussed.

Chapter Nine: Conclusion and Future Work

9.1 Conclusion

This research presents a design of a PEM fuel cell power system for unmanned aircraft systems with an integrated approach that enables estimation of required power for high altitudes UAS operation which is then used to determine the size and weight of the combined power-plant of fuel cell stack with hydrogen and air/oxygen vessels and the propulsion system of the UAS. This approach takes into the consideration the power capacity of fuel cell stack and the flight endurance as two main factors in designing the size and weight of storage vessels, and hence determining the overall weight of the UAS, which is a key requirement in the preliminary aircraft design phase.

Although many of the fuel cell models are available in the literature, most of these models estimated the output voltage of a fuel cell for a particular set of operating conditions and some for limited dynamic variations. *The proposed model in this research presented a simplified zero-dimensional mathematical model for a self-humidifying 1 kW PEM fuel cell developed by modelling the major electric and thermodynamic variables and parameters involved in the operation of a PEM fuel cell.*

The major variables and parameters related to the potential losses of a PEM fuel cell were identified, and their influence upon the operation and performance of the PEM fuel cell, in Sections 3.2 to 3.5. *Also, a modified equation was derived and validated in order to determine the impact of using air to supply the PEM fuel cell, instead of*

using pure oxygen, on the concentration losses and the output voltage when useful current is drawn from it, as presented in Section 3.5.

The major thermodynamic variables and parameters involved in the operation of a PEM fuel cell, along with the effects of influencing environmental conditions during fuel cell operation, were considered. Incorporation of the effects of different dynamic conditions, such as changes in the dynamical properties of the fluids in the supply-return manifolds and inside the anodes and cathodes of the PEM fuel cell stack, were determined and modelled, in order to determine the pressures and concentrations of hydrogen and oxygen in the anode and cathode respectively. This yielded a determination of the output voltage of the PEM fuel cell stack, as presented in Section 4.4.

In particular, the following issues were considered: the impact and effects on the PEM fuel cell operation of load current, pressure and concentration of the oxygen and hydrogen in the cathode and anode of the fuel cell; changes in the pressure and temperature of the surroundings; stack operating temperature; relative humidity in the cathodes and anodes; water content in the electrolyte membrane; drag and diffusion of water molecules across the membrane; dimension of the membrane; and the volume of the cathode and anode.

The mathematical model of the PEM fuel cell developed in this research was simulated using Matlab-Simulink, and was validated against the commercially available 1 kW Horizon (H-1000) PEM fuel cell stack. The Horizon stack was tested and operated under varied levels of load current and stack temperature, and the tests repeated several times on different occasions in order to capture the most accurate real data output. *The results obtained from the tested Horizon (H-1000) stack, and the simulations of the developed model of the PEM fuel cell showed close matches in the output power and the steady state performance, which provides sufficient confidence in the validity and accuracy of the developed model of the PEM fuel cell, as presented in Section 5.1.*

Different settings of the PID controller were investigated in terms of optimising the consumption of air and hydrogen and getting a faster time response from the controller. It was concluded that a proportional-integral (PI) controller with time response 0.679 seconds, at proportional value 0.0655, and integral value 2.9393, provides the most adequate trade-off choice between fast response and optimising consumption of hydrogen and air, in comparison with other settings for the developed model of the PEM fuel cell used for the proposed UAS operation. These settings apply only to the developed PEM fuel cell model based on the Horizon (H-1000) stack; other PEM stacks may have different tuning parameters, as presented in Section 5.2.

The proposed developed model in this research can be used by interested researchers as a generic model and simulation platform for a self-humidifying small-sized PEM fuel cell with an output power varying from 50 W to 1 kW. Moreover, extrapolation to higher powers is also possible; where the dimensions of the supply-return manifolds, cathodes, and anodes need to be resized in order to capacitate the increase in the mass flow rates of fuel and reactant necessary to produce power higher than 1 kW from the fuel cell stack.

The impact of high altitudes on the operation and the consumption of air were determined in order to maintain a certain level of delivered power to the load. Also, the implications associated with operating the PEM fuel cell stack at high altitudes and different technical solutions were proposed. *It was proved that warming the extracted air from the atmosphere at high altitudes (~10 km) in order to feed the stack must be avoided, as this would increase the flow of supplied air to the cathode by about 400% in comparison with sea level, in order to overcome the drop in the density of air at high altitudes and to produce consistent stable power from the stack, which would add more complexity, weight and cost to the system, as presented in Chapter Six.*

Different types of hydrogen fuel for UAS applications were also investigated in order to choose the appropriate type of hydrogen to be used for UAS applications that can offer low cost and weight, and low complexity to the entire system. It was concluded that whether using chemical hydride or liquid hydrogen as a source of hydrogen gas, special requirements are needed to manage and control the process of hydrogen generation, which adds more cost, complexity and weight to the power system of a UAS. Thus, compressed hydrogen gas was considered to be the best source of supplied hydrogen to the fuel-cell-based UAS, as presented in Section 7.2.

The maximum static thrust that needs to be produced by the propulsion system in order to accelerate the airplane to commence take-off was determined based on the capacity of the power system. Also, different sizes of propellers were examined in order to find an appropriate propeller that draws power from the BLDC motor based on maximum production capacity of the fuel cell stack power system, hence the maximum weight of the UAS was determined accordingly. Also, two different values for static thrust to weight ratio were adopted, in order to offer different operational scenarios for the UAS applications, as presented in Section 7.3.

Pressure vessel designs for hydrogen and air-oxygen storing cylinders were investigated, in order to determine the weight and size of the vessel based on mass flow rates of gases and power demand per operational hour, for high altitude UAS operations. Three scenarios were adopted in determining the size and weight of the pressure vessels required to supply air or oxygen to the fuel cell stack, based on the governing equations of the pressure vessel design and the related mass estimation. Also, different types of stainless steel materials were used in the design of the pressure vessel so as to find an appropriate material that provides low size and weight advantages. Hydrogen pressure vessel design and mass estimation were also considered, as presented in Section 8.4.

It is clear from the results obtained for the pressure vessel design, as presented in Section 8.4, that it is not possible to use high flow rates of air (97.9162 m³/hour) or oxygen (20.5624 m³/hour) to supply the fuel cell stack, particularly for UAS applications, as it requires a large size and heavy mass of vessel to carry the compressed air or oxygen. Alternatively, using limited volumes and flow rates of hydrogen (0.637 m³/hour) and oxygen (0.6 m³/hour) can offer the optimum pressure vessel design, in terms of lowering the size and weight of the vessel, hence reducing power consumption and extending the endurance of the mission, and allowing further payload to be added for the same mission duration.

Simulink tools of pressure vessel design were developed and formed in this research to estimate and determine the overall weight of the UAS, based on determining the size and weight of the combined power-plant of fuel cell stack, with hydrogen and air/oxygen vessels, and the propulsion system of the UAS for high altitude operation, as presented in Section 8.4.

The developed model of a PEM fuel cell in this research, associated with estimations of the total masses of hydrogen and oxygen vessels and the mass of the propulsion system, can potentially extend the flying duration and altitude for more than five hours and a half, reaching up to 11 km altitude, for a UAS with an overall weight of 32 kg, including a payload capacity of 2 kg; this is based on a Horizon (H-1000) PEM stack. A generic weight estimation mechanism could easily be inferred from the work.

Furthermore, reducing the mass of the frame structure and the payload, and choosing light equipment to be carried on board would reduce the overall mass of the UAS. Furthermore, reduction of aerodynamic drag would extend the flying mission, as the power requirement is reduced, as presented in Section 8.5.

The design of the power-plant system and UAS frame structure may vary according to the type of mission, in terms of cruising altitude, required flying hours, and the size and

weight of the payload. Therefore, the designer must consider all these parameters during the design stage of the entire UAS.

9.2 Future Work

There are many areas that could be considered as a potential starting point for future work, in order to extend and develop this part of the research further.

1. The impact of water produced by the fuel cell in a vapour state and its impact on the open circuit voltage of a PEM fuel cell, and the impact of the two phases of water (vapour and liquid) in the gas diffusion layer and their impacts on the transport of gases and on the performance of the fuel cell, in particular when the pressure of water vapour has no unity value, needs further investigation.
2. The capacitance impact of the charged double layer on the electrochemical model, in order to determine the transient response of fuel cell voltage needs to be involved in the model of the PEM fuel cell in order to increase the accuracy of the PEM fuel cell model.
3. The impact of activation losses at the anode of the fuel cell and the electronic resistivity of the materials such as electrodes and bipolar plates on the output voltage of the PEM fuel cell, can be considered for further future investigation.
4. The dynamic model needs to be further developed in order to determine the impact of non-linearity. Especially of dropping behaviours of the gaseous pressure and its impacts on the concentration losses and output voltages of the PEM fuel cell.
5. Further work needs to be carried out in order to develop a thermal dynamic model to determine the impact of heat radiation or conduction between anodes-cathodes and supply-return manifolds, and to understand the impact of produced heat as a result of electrochemical reaction, and the friction impact of the

flowing reactants inside the fuel cell on the performance and power output of the PEM fuel cell stack.

6. Further investigations need to be carried out on the impact of non-uniform distribution of water content across the electrolyte membrane, and the variation of humidity levels between anode and cathode of the fuel cell stack, and the impact of back diffusion of water molecules from cathode to anode, in order to extend the simulation and the validation of the developed model for other applications.
7. The level of aging and degradation of the electrolyte membrane over the operating time and its impact on the performance of the fuel cell needs to be investigated further in the future.
8. Different control techniques, in terms of optimising the consumption of air and hydrogen and providing faster time responses, particularly at high altitude stack operation, could be investigated further.
9. The implications associated with operating a PEM fuel cell stack at high altitudes, such as insulation and draining issues, could be taken for further investigation in the future.
10. The impact of using limited volumes and flow rates of hydrogen and oxygen on the performance of the PEM fuel cell stack for high altitude UAS operations needs to be physically examined and investigated, so as to obtain further accurate calculations in terms of pressure vessel design, and consequently flying time estimation, with the possibility of adopting different operational scenarios.
11. Finally, the design and calculations of the pressure vessel and power-plant mass estimation were carried out based on the developed model for the PEM fuel cell, for approximately 1 kW maximum power output – the design could be extended

to develop and validate a power-plant system of up to 5 kW for high altitude UAS operations.

However, points (5, 9, 10, and 11) listed above, could be recommended as the most prioritise investigation issues for future work.

References

1. James Larminie and Andrew Dicks, *Fuel Cell Systems Explained*. Second ed. 2003: John Wiley & Sons Ltd.
2. Jay T. Pukrushpan, Anna G. Stefanopoulou, and Huei Peng, *Control of Fuel Cell Breathing*. IEEE Control Systems Magazine, 2004. **24**(2): p. 30-46.
3. M.Y. El-Sharkh, A. Rahman, M.S. Alam, et al., *A dynamic model for a stand-alone PEM fuel cell power plant for residential applications*. Journal of Power Sources, 2004. **138** (1-2): p. 199-204.
4. Jing QIU, Zhaoyang DONG, Junhua ZHAO, et al., *A low-carbon oriented probabilistic approach for transmission expansion planning*. Journal of Modern Power Systems and Clean Energy, 2015. **3**(1): p. 14-23.
5. Joshua Golbert and Daniel R. Lewin, *Model-based control of fuel cells: (1) Regulatory control*. Journal of Power Sources, 2004. **135**(1-2): p. 135-151.
6. Hamid Radmanesh, Seyed Saeid Heidari Yazdi, S. H. Fathi, et al., *Modelling and Simulation of Fuel Cell Dynamics for Electrical Energy Usage of Hercules Airplanes*. The Scientific World Journal, 2014. **2014**.
7. Kyunghwan Kim, Taegy Kim, Kiseong Lee, et al., *Fuel cell system with sodium borohydride as hydrogen source for unmanned aerial vehicles*. Journal of Power Sources, 2011. **196**(21): p. 9069-9075.
8. D. Verstraete, K. Lehmkuehler, A. Gong, et al., *Characterisation of a hybrid, fuel-cell-based propulsion system for small unmanned aircraft*. Journal of Power Sources, 2014. **250**: p. 204-211.
9. Akira Nishizawa, Josef Kallo, Olivier Garrot, et al., *Fuel cell and Li-ion battery direct hybridization system for aircraft applications*. Journal of Power Sources, 2013. **222**: p. 294-300.
10. P. Aguiar, D. J. L. Brett, and N. P. Brandon, *Solid oxide fuel cell/gas turbine hybrid system analysis for high-altitude long-endurance unmanned aerial vehicles*. International Journal of Hydrogen Energy, 2008. **33**(23): p. 7214-7223.

11. P. R. Pathapati, X. Xue, and J. Tang, *A new dynamic model for predicting transient phenomena in a PEM fuel cell system*. Journal of Renewable Energy, 2005. **130**(1): p. 1-22.
12. P. Rodatz, G. Paganelli, A. Sciarretta, et al., *Optimal power management of an experimental fuel cell/supercapacitor-powered hybrid vehicle*. Journal of Control Engineering Practice, 2005. **13**(1): p. 41-53.
13. Carlos Bordons, Alicia Arce, and Alejandro J. del Real. *Constrained Predictive Control Strategies for PEM fuel cells*. in *American Control Conference*. 2006. Minneapolis, Minnesota, USA. 2486-2491.
14. Sheng-Li Chen, A.B. Bocarsly, and J. Benziger, *Nafion-layered sulfonated polysulfone fuel cell membranes*. Journal of Power Sources, 2005. **152**: p. 27-33.
15. Yun Wang, Ken S. Chen, Jeffrey Mishler, et al., *A review of polymer electrolyte membrane fuel cells: technology, applications, and needs on fundamental research*. Applied Energy, 2011. **88**(4): p. 981-1007.
16. S. Litster and G. McLean, *Review PEM fuel cell electrodes*. Journal of Power Sources, 2004. **130**(1-2): p. 61-76.
17. Zhen Yang, Xiaofeng Peng, Buxuan Wang, et al., *Modeling of ion conductivity in Nafion membranes*. Frontiers of Energy and Power Engineering in China, 2007. **1**(1): p. 58-66.
18. Horizon Fuel Cell Technologies. "*H-SERIES 10W-5kW PEM STACK MODULES*". [cited 2015 December]; Available from: <http://www.horizonfuelcell.com/#!h-series-stacks/c52t>.
19. G. Correa, Fabio Borello, and Massimo Santarelli, *Sensitivity analysis of temperature uncertainty in an aircraft PEM fuel cell*. International Journal of Hydrogen Energy, 2011. **36**(22): p. 14745-14758.
20. Nieves Lapena-Rey, Jonay Mosquera, Elena Bataller, et al., *Environmentally friendly power sources for aerospace applications*. Journal of power sources, 2008. **181**(2): p. 353-362.
21. Amir S. Gohardani, Georgios Doulgeris, and Riti Singh, *Challenges of future aircraft propulsion: a review of distributed propulsion technology and its potential application for the all electric commercial aircraft*. Progress in Aerospace Sciences, 2011. **47**(5): p. 369-391.

22. Thomas H. Bradley, Blake A. Moffitt, Thomas F. Fuller, et al., *Comparison of design methods for fuel-cell-powered unmanned aerial vehicles*. Journal of Aircraft, 2009. **46**(6): p. 1945-1956.
23. A. Lucken, J. Brombach, and D. Schulz, *Design and protection of a high voltage DC onboard grid with integrated fuel cell system on more electric aircraft*, in *Electrical Systems for Aircraft, Railway and Ship Propulsion (ESARS)*. 2010, IEEE. p. 1-6.
24. Taegyu Kim and Sejin Kwon, *Design and development of a fuel cell-powered small unmanned aircraft*. International Journal of Hydrogen Energy, 2012. **37**(1): p. 615-622.
25. Unmanned Aerial Vehicle System Association. "UAV or UAS ?". [cited 01 Nov. 2015]; Available from: https://www.uavs.org/index.php?page=what_is.
26. Thomas H. Bradley, Blake A. Moffitt, Dimitri N. Mavris, et al., *Development and experimental characterization of a fuel cell powered aircraft*. Journal of Power Sources, 2007. **171**(2): p. 793-801.
27. Sylvie Bégot, Fabien Harel, Denis Candusso, et al., *Fuel cell climatic tests designed for new configured aircraft application*. Energy Conversion and Management, 2010. **51**(7): p. 1522-1535.
28. Jordi Renau, Antonio Lozano, Jorge Barroso, et al., *Use of fuel cell stacks to achieve high altitudes in light unmanned aerial vehicles*. International Journal of Hydrogen Energy, 2015.
29. B. Saeed and G. B. Gratton, *An evaluation of the historical issues associated with achieving non-helicopter V/STOL capability and the search for the flying car*. The Aeronautical Journal, 2010. **114**(1152): p. 91-102.
30. The MathWorks, Inc, *MATLAB and Simulink*, in www.mathworks.com. March 2010: USA.
31. Frano Barbir, Trent Molter, and Luke Dalton, *Efficiency and weight trade-off analysis of regenerative fuel cells as energy storage for aerospace applications*. International journal of hydrogen energy, 2005. **30**(4): p. 351-357.
32. Jay T. Pukrushpan, Anna G. Stefanopoulou, and Huei Peng. *Modeling and Control for PEM Fuel Cell Stack System*. in *Proceedings of American Control Conference*. 2002. 4, 3117-3122.

33. M. E. Schenck, JS Lai, and K. Stanton. *Fuel cell and power conditioning system interactions*. in *IEEE-APEC 2005*. 2005. Texas-USA. 1, 114 - 120.
34. Phatiphat Thounthong, St'ephane Ra'el, and Bernard Davat, *Test of a PEM fuel cell with low voltage static converter*. *Journal of Power Sources*, 2006. **153**(1): p. 145-150.
35. A. A. Abul-Hawa, M. S. Ebaid, F. S. Bhinder, et al. *Control strategy for polymer electrolyte membrane fuel cell systems*. in *Procs UKACC Int Conf Control 2006 Paper 94*. 2006. University of Strathclyde Publishing.
36. J.C. Amphlett, R.F. Mann, B.A. Peppley, et al., *A model predicting transient responses of proton exchange membrane fuel cells*. *Journal of Power Sources*, 1996. **61**(1-2): p. 183-188.
37. J.C. Amphlett, R.M. Baumert, R.F. Mann, et al., *Parametric modeling of the performance of a 5-kW proton-exchange membrane fuel cell stack*. *Journal of Power Sources*, 1994. **49**: p. 349-356.
38. J.C. Amphlett, R.M. Baumert, R.F. Mann, et al., *Performance Modeling of the Ballard Mark IV Solid Polymer Electrolyte Fuel Cell, I. Mechanistic Model Development*. *Journal of the Electrochemical Society*, 1995. **142**(1): p. 1-8.
39. J.C. Amphlett, R.M. Baumert, R.F. Mann, et al., *Performance Modeling of the Ballard Mark IV Solid Polymer Electrolyte Fuel Cell, II. Empirical Model Development*. *Journal of the Electrochemical Society*, 1995. **142**(1): p. 9-15.
40. Ronald F. Mann, John C. Amphlett, Michael A. I. Hooper, et al., *Development and application of a generalised steady-state electrochemical model for a PEM fuel cell*. *Journal of Power Sources*, 2000. **86**(1-2): p. 173-180
41. Carl Berger, *Handbook of Fuel Cell Technology*. 1986: Prentice-Hall, INC., Englewood Clifes.
42. T. E. Springer, T. A. Zawodzinski, and S. Gottesfeld, *Polymer Electrolyte Fuel Cell Model*. *Journal of Electrochem. Soc.*, 1991. **138**(8): p. 2334-2342.
43. Felix N. Büchi and Günther G. Scherer, *In-situ resistance measurements of Nafion® 117 membranes in polymer electrolyte fuel cells*. *Journal of Electroanalytical Chemistry*, 1996. **404**(1): p. 37-43.

44. R. Seyezhai and B. L. Mathur, *Mathematical Modeling of Proton Exchange Membrane Fuel Cell*. International Journal of Computer Applications, 2011. **20**(5): p. 0975-8887.
45. Wei Yuan, Yong Tang, Minqiang Pan, et al., *Model prediction of effects of operating parameters on proton exchange membrane fuel cell performance*. Renewable Energy, 2010. **35**(3): p. 656-666.
46. Alejandro J. del Real, Alicia Arce, and Carlos Bordons, *Development and experimental validation of a PEM fuel cell dynamic model*. Journal of power sources, 2007. **173**(1): p. 310–324.
47. Sang-Kyun Park and Song-Yul Choe, *Dynamic modeling and analysis of a 20-cell PEM fuel cell stack considering temperature and two-phase effects*. Journal of Power Sources, 2008. **179**(2): p. 660–672.
48. M. ELSayed Youssef, Khairia E. AL-Nadi, and Moataz H. Khalil, *Lumped model for proton exchange membrane fuel cell (PEMFC)*. International Journal of Electrochemical Science, 2010. **5**: p. 267-277.
49. Andrew Rowe and Xianguo Li, *Mathematical modeling of proton exchange membrane fuel cells*. Journal of Power Sources, 2001. **102**: p. 82-96.
50. Sandip Pasricha and Steven R. Shaw, *A Dynamic PEM Fuel Cell Model*. IEEE Transactions on Energy Conversion, 2006. **21**(2): p. 484-490.
51. Jung S. Yi and Trung V. Nguyen, *An Along-the-Channel Model for Proton Exchange Membrane Fuel Cells*. Journal of the Electrochemical Society 1998. **145**(4): p. 1149 -1159.
52. Yun Wang and Chao-Yang Wang, *Modeling Polymer Electrolyte Fuel Cells with Large Density and Velocity Changes*. Journal of The Electrochemical Society, 2005. **152**(2): p. A445-A453.
53. M. K. Furrutter and Johan Meyer, *Small fuel cell powering an unmanned aerial vehicle*, in *AFRICON, 2009. AFRICON'09*. 2009, IEEE. p. 1-6.
54. Nai-Chien Shih, Biing-Jyh Weng, Jiunn-Yih Lee, et al., *Development of a small fuel cell underwater vehicle*. International Journal of Hydrogen Energy, 2013. **38**(25): p. 11138-11143.

55. Phatiphat Thounthong, St'ephane Ra'el, and Bernard Davat, *Control strategy of fuel cell/supercapacitors hybrid power sources for electric vehicle*. Journal of Power Sources, 2006. **158**(1): p. 806–814.
56. K. H. Hauer, D. J. Friedmann, R. M. Moore, et al., *Dynamic Response of an Indirect-Menthol Fuel Cell Vehicle*, in *SAE 2000 World Congress, (2000-01-0370)*. 2000.
57. Jay. T. Pukrushpan, *Modeling and control of fuel cell systems and fuel processors*, in *Department of Mechanical Engineering*. 2003, The University of Michigan: Michigan.
58. A. Heinzl, J. Roes, and H. Brandt, *Increasing the electric efficiency of a fuel cell system by recirculating the anodic offgas*. Journal of Power Sources, 2005. **145**(2): p. 312-318.
59. Levent Semiz, Ramis Berkay Serin, Nurdan Demirci Sankir, et al., *Chemical hydride powered and air breathing PEMFC for UAVs*, in *International Conference on Renewable Energy Research and Applications (ICRERA)*. 2013, IEEE. p. 555-558.
60. Junzhi Zhang, Guidong Liu, Wensheng Yu, et al., *Adaptive control of the airflow of a PEM fuel cell system*. Journal of Power Sources, 2008. **179**(2): p. 649–659.
61. Jung-Eun Seo, Yujong Kim, Yongmin Kim, et al., *Portable ammonia-borane-based H₂ power-pack for unmanned aerial vehicles*. Journal of Power Sources, 2014. **254**: p. 329-337.
62. Trung Van Nguyen and Mack W. Knobbe, *A liquid water management strategy for PEM fuel cell stacks*. Journal of Power Sources, 2003. **114** (1): p. 70 -79.
63. Anthony D. Santamaria, John Bachman, and Jae Wan Park, *Design strategy for a polymer electrolyte membrane fuel cell flow-field capable of switching between parallel and interdigitated configurations*. International Journal of Hydrogen Energy, 2013. **38**(14): p. 5807-5812.
64. John J. Cooley, Peter Lindahl, Clarissa L. Zimmerman, et al., *Multi-converter System Design for Fuel Cell Buffering and Diagnostics under UAV Load Profiles*. IEEE Transactions on Power Electronics, 2014. **29**(6): p. 3232 - 3244.

65. Zhenhua Jiang, Lijun Gao, Mark J. Blackwelder, et al., *Design and experimental tests of control strategies for active hybrid fuel cell/battery power sources*. Journal of Power Sources, 2004. **130**(1-2): p. 163-171.
66. Hao Chen and Alireza Khaligh, *Hybrid energy storage system for unmanned aerial vehicle (UAV)*, in *IECON 2010-36th Annual Conference on IEEE Industrial Electronics Society*. 2010, IEEE. p. 2851-2856.
67. Z Zhong, H Huo, X Zhu, et al., *Adaptive maximum power point tracking control of fuel cell power plants*. Journal of Power Sources, 2008. **176**: p. 259-269.
68. E. Troncoso, N. Lapeña-Rey, and O. Valero, *Off-grid test results of a solar-powered hydrogen refuelling station for fuel cell powered Unmanned Aerial Vehicles*. International Journal of Hydrogen Energy, 2014. **39**: p. 11267-11278.
69. Zhen-Ming Huang, Ay Su, Che-Jung Hsu, et al., *A high-efficiency, compact design of open-cathode type PEMFCs with a hydrogen generation system*. Fuel, 2014. **122**: p. 76-81.
70. Dries Verstraete, Andrew Gong, Dylan D.-C. Lu, et al., *Experimental investigation of the role of the battery in the AeroStack hybrid, fuel-cell-based propulsion system for small unmanned aircraft systems*. International Journal of Hydrogen Energy, 2015. **40**(2): p. 1598–1606.
71. B. Omar, *Experimental Study Of Using A PEM Fuel Cell/battery Hybrid System To Power Small UAVs*. WIT Transactions on Ecology and the Environment, 2015. **206**: p. 273-284.
72. Patrick Adam and Jacob Leachman. *Design of a reconfigurable liquid hydrogen fuel tank for use in the Genii unmanned aerial vehicle*. in *ADVANCES IN CRYOGENIC ENGINEERING: Transactions of the Cryogenic Engineering Conference-CEC*. 2014. Vol. 1573, No1, p. 1299-1304. AIP Publishing.
73. Giulio Romeo, Francesco Danzi, Enrico Cestino, et al., *Design and Optimization of a Composite Vessel for Hydrogen Storage Subject to Internal Pressure and In-Flight Loads for UAVs*. International Journal of Aerospace Sciences, 2013. **2**(3): p. 124-137.
74. Perry J. Hardin and Ryan R. Jensen, *Small-scale unmanned aerial vehicles in environmental remote sensing: Challenges and opportunities*. GIScience & Remote Sensing, 2011. **48**(1): p. 99-111.

75. Jorge Barroso, Jordi Renau, Antonio Lozano, et al., *Experimental determination of the heat transfer coefficient for the optimal design of the cooling system of a PEM fuel cell placed inside the fuselage of an UAV*. Applied Thermal Engineering, 2015. **89**: p. 1-10.
76. M. J. Khan and M. T. Iqbal, *Dynamic modeling and simulation of a small wind-fuel cell hybrid energy system*. Journal of Renewable Energy, 2005. **30**(3): p. 421-439.
77. Sung Han Kim, Craig M. Miesse, Hee Bum Lee, et al., *Ultra compact direct hydrogen fuel cell prototype using a metal hydride hydrogen storage tank for a mobile phone*. Applied Energy, 2014. **134**: p. 382-391.
78. www.chem.umn.edu. "Platinum Catalyzed Reaction of Hydrogen and Oxygen". 2000 [cited 2011 23 January]; Available from: http://www.chem.umn.edu/services/lecturedemo/info/hydrogen_and_platinum.html.
79. Ibrahim M. M. Saleh, Rajnish K. Calay, and Ali Rashid, *Modelling and Examining Open Circuit Voltage for PEM Fuel Cell*. Journal of Electrical Engineering, 2013. **Volume 13. 3. 20**.
80. Jay T Pukrushpan, Huei Peng, and Anna G Stefanopoulou. *Simulation and analysis of transient fuel cell system performance based on a dynamic reactant flow model*. in *Proceedings of International Mechanical Engineering Congress & Exposition (IMECE 2002)*. 2002.
81. Horizon Fuel Cell Technology, *H-1000 Fuel Cell Stack-User Manual*, Horizon Fuel Cell Technology, 18 May 2011.
82. M Grujicic, K M Chittajallu, E H Law, et al., *Model-based control strategies in the dynamic interaction of air supply and fuel cell*. Proceedings of the Institution of Mechanical Engineers, vol. 218, Part A: Journal of Power and Energy, 2004. **218**(7): p. 487-499.
83. Eck, Dr.-Ing. Bruno, *Fans: Design and Operation of Centrifugal, Axial-Flow and Cross-Flow Fans*. first English edition ed. 1973: Pergamon Press.
84. U.S. Department of Energy - EERE, *Improving Fan System Performance - A Sourcebook for Industry*. Industrial energy efficiency sourcebooks. 1989, Washington, DC: Air Movement and Control Association International, Inc.

85. W. P. Jones, *Air Conditioning Engineering*. Fifth ed. 2001: Butterworth-Heinemann.
86. Horizon Fuel Cell Technology, *H-1000XP Fuel Cell Stack-User Manual*, Horizon Fuel Cell Technology, 11 Nov. 2011.
87. Jesse S. Doolittle and Francis J. Hale, *Thermodynamics For Engineers*. 1984: John Wiley & Sons, Inc.
88. Yunus A. Cengel and Michael A. Boles, *Thermodynamics: An Engineering Approach*. 6th ed. 2008, New York: McGraw-Hill, Inc.
89. G. K. Batchelor, *An introduction to fluid dynamics*. 1967: Cambridge University Press.
90. Jay T. Pukrushpan, Huei Peng, and Anna G. Stefanopoulou, *Control-Oriented Modeling and Analysis for Automotive Fuel Cell Systems*. *Journal of Dynamic Systems, Measurement, and Control - Transactions of the ASME*, 2004. **126**: p. 14-25.
91. K.K. Tan, S. Huang, and R. Ferdous, *Robust self-tuning PID controller for nonlinear systems*. *Journal of Process Control*, 2002. **12**(7): p. 753-761.
92. Roland S. Burns, *Advanced Control Engineering*. 2001: Butterworth-Heinemann.
93. Joseph W. Pratt, Jacob Brouwer, and G. Scott Samuelson, *Performance of proton exchange membrane fuel cell at high-altitude conditions*. *Journal of propulsion and power*, 2007. **23**(2): p. 437-444.
94. Jürgen Dollmayer, Nicola Bundschuh, and Udo B. Carl, *Fuel mass penalty due to generators and fuel cells as energy source of the all-electric aircraft*. *Aerospace science and technology*, 2006. **10**(8): p. 686-694.
95. Mark Z. Jacobson, *Fundamentals of Atmosphere Modeling*. Second ed. 2005: Cambridge University Press.
96. Mustafa Cavcar, *The International Standard Atmosphere (ISA)*, <http://home.anadolu.edu.tr/~mcavcar/common/ISAweb.pdf>.
97. Stephen R. Turns, *Thermodynamics: Concepts and Applications*. 2006: Cambridge University Press.

98. D. Verstraete, P. Hendrick, P. Pilidis, et al., *Hydrogen fuel tanks for subsonic transport aircraft*. International Journal of Hydrogen Energy, 2010. **35**(20): p. 11085-11098.
99. Jacob Leachman, Melissa Jean Street, and Teira Graham. *Catalytic pressurization of liquid hydrogen fuel tanks for unmanned aerial vehicles*. in *ADVANCES IN CRYOGENIC ENGINEERING: Transactions of the Cryogenic Engineering Conference-CEC*. 2012. (Volume 57): Vol. 1434, No 1, p. 1261-1267. AIP Publishing.
100. Gary L. Mills, Brian Buchholtz, and Al Olsen. *Design, fabrication and testing of a liquid hydrogen fuel tank for a long duration aircraft*. in *ADVANCES IN CRYOGENIC ENGINEERING: Transactions of the Cryogenic Engineering Conference-CEC*. 2012. (Volume 57): Vol. 1434, No1, p. 773-780. AIP Publishing.
101. John D. Anderson, Jr., *Introduction To Flight*. 3rd ed. 1989: McGraw-Hill Book Company.
102. Philip Connolly. "Air Craft Data Sheet - Hyperion Prop Talk". [cited 2014 08 June]; Available from: http://aircraft-world.com/prod_datasheets/hp/emeter/hp-proptalk.htm.
103. Barnes W. McCormick, *Aerodynamics Aeronautics, And Flight Mechanics*. 2nd ed. 1995: John Wiley & Sons, INC.
104. Air Craft R/C Electric Aircraft & Gliders. "Air Craft Data Sheet". [cited 2014 08 - June]; Available from: http://aircraft-world.com/prod_datasheets/hp/emeter/hp-propconstants.htm.
105. RC Model Centre. "KMS Quantum 4130/07 Bless Motor - Product Information". [cited 2015 29 June]; Available from: http://www.rcmodelcentre.co.uk/KMS-Quantum-4130/07-BLess-Motor/prod_5808.html?review=write.
106. Henry H. Bednar, *Pressure Vessel Design Handbook*. 2nd ed. 1986, FLORIDA: Krieger Publishing Company.
107. Robert Chuse, *Pressure Vessels: The ASME Code Simplified*. 5th ed. 1977: McGraw-Hill Company.

108. AK Steel Corporation. "2205 Duplex Stainless Steel". 2013 [cited 2014 18 May]; Available from: http://www.aksteel.com/pdf/markets_products/stainless/duplex/2205DuplexSS201312.pdf.
109. AK Steel Corporation. "15-5 PH Stainless Steel". 2014 [cited 2014 18 May]; Available from: http://www.aksteel.com/pdf/markets_products/stainless/precipitation/15-5 PH Stainless Steel 201404.pdf.
110. AK Steel Corporation. "440A Stainless Steel". 2014 [cited 2014 28 June]; Available from: http://www.aksteel.com/pdf/markets_products/stainless/ferritic/440A%20Stainless%20Steel%20DS%20201403.pdf.
111. BOC Industrial Gases UK. "*Compressed Air - Factsheet*". [cited 2014 05 July]; Available from: http://www.boconline.co.uk/internet.lg.lg.gbr/en/images/Compressed-Air-factsheet410_54561.pdf.
112. BOC Industrial Gases UK. "*Oxygen - Factsheet*". [cited 2014 05 July]; Available from: http://www.boconline.co.uk/internet.lg.lg.gbr/en/images/Oxygen-factsheet410_54571.pdf.
113. BOC Industrial Gases UK. "*Hydrogen - Factsheet*". [cited 2014 05 July]; Available from: http://www.boconline.co.uk/internet.lg.lg.gbr/en/images/Hydrogen-factsheet410_116758.pdf.
114. J. B. Jones and R. E. Dugan, *Engineering Thermodynamics*. 1996: Prentice-Hall International, Inc.
115. Delta Electronics, INC. "*Specification For Approval*". July 2005 [cited 2013 09 June]; Available from: [http://www.delta-america.com/Products/FanUploads/Specification/FFB0912EHE\(REV00\).pdf](http://www.delta-america.com/Products/FanUploads/Specification/FFB0912EHE(REV00).pdf).

Bibliography

Books & Thesis:

Culp, Principles of Energy Conversion. Second ed. 1991: McGraw-Hill, Inc.

Gordon Rogers and Mayhew, Engineering Thermodynamics: Work and Heat Transfer. 4th Edition ed. 1992: Longman Group.

Jacek F. Gieras and Wing, Permanent Magnet Motor Technology: Design and Applications. Second ed. 2002, New York: Marcel Dekker, INC.

John B. Heywood, Internal Combustion Engine Fundamentals. first ed. 1988: McGraw-Hill, Inc.

Mauro Graziani and Fornasiero, Renewable Resources And Renewable Energy: A Global Challenge. 2007: CRC Press, Taylor & Francis Group.

Roland S. Burns, Advanced Control Engineering. 2001: Butterworth-Heinemann.

Stefán Baldursson, BLDC Motor Modelling and Control - A Matlab®/Simulink® Implementation in Department of Energy and Environment, Electric Power Engineering. 2005, Chalmers University of Technology.

T.J.E. Miller, Brushless Permanent-Magnet and Reluctance Motor Drives. 1989: Clarendon Press. Oxford.

Journals & Proceedings:

Ardalan Vahidi, Stefanopoulou, and Peng. Model predictive control for starvation prevention in a hybrid fuel cell system. in Proceedings of the 2004 American Control Conference. 2004. USA. 1, 834-839.

Ardalan Vahidi, Stefanopoulou, and Peng, Current Management in a Hybrid Fuel Cell Power System: A Model-Predictive Control Approach. IEEE Transactions on Control Systems Technology, 2006. **14**(6): p. 1047 - 1057.

Cheng Bao, Ouyang, and Yi, Modeling and control of air stream and hydrogen flow with recirculation in a PEM fuel cell system-**I**. Control-oriented modeling. *International Journal of Hydrogen Energy*, 2006. **31**(13): p. 1879–1896.

Cheng Bao, Ouyang, and Yi, Modeling and control of air stream and hydrogen flow with recirculation in a PEM fuel cell system-**II**. Linear and adaptive nonlinear control. *International Journal of Hydrogen Energy*, 2006. **31**: p. 1897 – 1913.

Chris Yang, Srinivasan, Bocarsly, Tulyani, and Benziger, A comparison of physical properties and fuel cell performance of Nafion and zirconium phosphate/Nafion composite membranes. *Journal of Membrane Science*, 2004. **237**: p. 145–161.

David E. Moilanen, Piletic, and Fayer, Water Dynamics in Nafion Fuel Cell Membranes: the Effects of Confinement and Structural Changes on the Hydrogen Bond Network. *The journal of physical chemistry. C, Nanomaterials and interfaces*, 2007. **111**(25): p. 8884–8891.

Dennis E. Curtin, Lousenberg, Henry, Tangeman, and Tisack, Advanced materials for improved PEMFC performance and life. *Journal of Power Sources*, 2004. **131**(1-2): p. 41-48.

DL Gabriel, Meyer, and Plessis, Brushless DC motor characterisation and selection for a fixed wing UAV, in *IEEE AFRICON*. 2011: Zambia.

G. Correa, Santarelli, Borello, Cestino, and Romeo, Flight test validation of the dynamic model of a fuel cell system for ultra-light aircraft. *Proceedings of the Institution of Mechanical Engineers, Part G: Journal of Aerospace Engineering*, 2015. **229**(5): p. 917-932.

Gifford N. L., G., E., and J., Experimental Study of Low-Pressure Automotive Cooling Fan Aerodynamics Under Blocked Conditions, in *CSME 2006 Forum*. 2006: Calgary.

Jay T. Pukrushpan, Stefanopoulou, Varigonda, Pedersen, Ghosh, and Peng. Control of Natural Gas Catalytic Partial Oxidation for Hydrogen Generation in Fuel Cell Applications. in *IEEE Transaction of Control System Technology*. 2003. 13, 2030-2036.

K. D. Kreuer, On the development of proton conducting polymer membranes for hydrogen and methanol fuel cells. *Journal of Membrane Science*, 2001. **185**(1): p. 29-39.

L. Ghassemzadeh, Marrony, Barrera, Kreuer, Maier, and Müller, Chemical degradation of proton conducting perfluorosulfonic acid ionomer membranes studied by solid-state nuclear magnetic resonance spectroscopy. *Journal of Power Sources*, 2009. **186**(2): p. 334-338.

M. T. Iqbal, Modeling and control of a wind fuel cell hybrid energy system. *Journal of Renewable Energy*, 2003. **28**(2): p. 223–237.

M. Uzunoglu, Onar, and Alam, Dynamic Behavior of PEM FCPPs under various load conditions and voltage stability analysis for stand-alone residential applications. *Journal of Power Sources*, 2007. **168**: p. 240-250.

Patric Jannasch, Recent developments in high-temperature proton conducting polymer electrolyte membranes. *Journal of Current Opinion in Colloid & Interface Science*, 2003. **8**(1): p. 96-102.

S.A. Grigoriev, Porembsky, and Fateev, Pure hydrogen production by PEM electrolysis for hydrogen energy. *International Journal of Hydrogen Energy*, 2006. **31**(2): p. 171-175.

S.C. Morris, Good, and Foss, Velocity measurements in the wake of an automotive cooling fan. *Experimental Thermal and Fluid Science*, 1998. **17**: p. 100-106.

Yun Wang and Wang, Dynamics of polymer electrolyte fuel cells undergoing load changes. *Journal of Electrochimica Acta*, 2006. **51**: p. 3924-3933.

Appendices

Appendix A

According to the specifications of Horizon (H-1000) fuel cell stack, the dimensions of the stack are (26.7 x 21.6 x 8.0 cm), and the dimensions of assembled fuel cells are (21.6 x 19.6 x 4.0 cm). Therefore, the estimated volume of whole stack is approximately equal to 4,614 cm³, and the estimated volume for the assembly of 72 fuel cells is approximately equal to 1,693 cm³, which represents the total volume of anodes and cathodes. The difference between whole stack volume and total volume of anodes-cathodes represents the volume of the supply-return manifolds, which is approximately equal to 2,921 cm³. Thickness of electrolyte membrane is (25*10⁻⁴ cm), and thickness of assembly bipolar plates for anode-cathode is approximately 0.05 cm. And a maximum production capacity of current is 400-500 mA/cm² at 0.6 V/cell [81].

$$\text{Area of Single Fuel Cell} = 19.6 \times 4.0 = 78.4 \text{ cm}^2$$

$$\text{Area of Supply Manifolds of Cathodes} = 21.6 \times 19.6 = 423.4 \text{ cm}^2$$

$$\text{Area of Supply Manifolds of Anodes} = 19.6 \times 4.0 = 78.4 \text{ cm}^2$$

Volume of anodes and cathodes for a stack of 72 cells can be estimated from the dimensional properties of the stack, as determined below:

$$\text{Thickness of Singel Cell} = \frac{21.6}{72} = 0.3 \text{ cm}$$

$$\text{Thickness of Single (Anode-Cathode)} = 0.3 - 0.05 - 25 * 10^{-4} = 0.2475 \text{ cm}$$

$$\text{Volume of Single Anode} = \frac{0.2475 * 19.6 * 4}{2} = 9.702 \text{ cm}^3$$

$$\text{Volume of Stack Anode} = 9.702 * 72 \approx 699 \text{ cm}^3$$

Hence, volume of fuel cell stack cathode is 699 cm³. For Horizon (H-1000) fuel cell stack, in order to produce maximum current of 24 A at 43.2 V, a maximum flow rate of supplied hydrogen to the stack is 14 L/min at pressure 55 kPa, and maximum flow rate of supplied air is 1.95 m³/min at pressure of 1atm (101.325 kPa) and ambient temperature of 15 °C (288 K), for air density equals to 1.225 kg/m³ [81, 86].

The ideal gas law equation is given below [114]:

$$P \cdot V = N \cdot R \cdot T = \frac{m}{M} \cdot R \cdot T \quad (\text{A.1})$$

Where, P is the pressure (kPa), V is the volume of gas (m³), T is absolute temperature in kelvin (K), R is universal gas constant ($R = 8.31441 \text{ kPa}\cdot\text{m}^3/\text{kmol}\cdot\text{K}$), N is the number of moles which is the ratio of mass m in (kg) to the molar mass of gas M in (kg/kmol).

The term (R/M) represents the specific gas constant R_s in (kPa.m³/kg.K).

$$P = \frac{m}{V} \cdot R_s \cdot T = \rho \cdot R_s \cdot T \quad (\text{A.2})$$

Where, the term (m/V) is the density of gas ρ in (kg/m³). For two volumes of gas, the pressures of gas are defined as given below,

$$P_1 = \frac{m_1}{V_1} \cdot R_s \cdot T_1$$

$$P_2 = \frac{m_2}{V_2} \cdot R_s \cdot T_2$$

Under condition of constant temperature and for a fixed mass of gas, hence ($T_1 = T_2$ and $m_1 = m_2$) yields;

$$P_1 \cdot V_1 = P_2 \cdot V_2 \quad (\text{A.3})$$

Table A.1 shows the values of specific gas constant R_s for several gases. As it has been defined previously in Chapter Four, the constant $K_{sm,out}$ represents the nozzle constant of supply manifold outlet, which is the ratio of flow rate of gas (kg/s) to the pressure (kPa).

$$K_{sm,out} = \frac{W}{P}$$

Assuming that at any specific second of time, the mass flow rate W (kg/s) of hydrogen or air will be equal to the mass of that component m (kg) at that time. Then, by replacing m by W in the Equation (A.1) of ideal gas above yields;

$$P \cdot V = \frac{W}{M} \cdot R \cdot T$$

$$K_{sm,out} = \frac{W}{P} = \frac{M \cdot V}{R \cdot T} * C \quad (A.4)$$

Where, R is the universal gas constant ($R = 8.31441$ kPa.m³/kmol.K), T is standard temperature in kelvin (K), V is the volume (m³), M is the molar mass of gas (kg/kmol), and C is the correction constant which will be used to tune the flow rate of the gas in our model with the actual flow rate of Horizon (H-1000) fuel cell stack.

Since air flows from supply manifold to the cathode (i.e. flows between two different volumes) is going to occupy the volume of cathode, then by substituting the value of cathodes volume (as estimated above 699 cm³) in Equation (A.4) to estimate the value of the constant $K_{sm,out,ca}$ for Horizon (H-1000) fuel cell stack, at standard temperature 15°C (288 K), and for C equals to 100. Yielding the following:

$$K_{sm,out,ca} = \frac{M_{air} \cdot V_{ca}}{R \cdot T_{st}} * C = \frac{28.97 * 699 * 10^{-6}}{8.31447 * 288} * 100 = 8.457 * 10^{-4}$$

Similarly, by using Equation (A.4) to the determine the value of $K_{sm,out,an}$ for anode.

$$K_{sm,out,an} = \frac{M_{H2} \cdot V_{an}}{R \cdot T_{st}} * C = \frac{2.02 * 699 * 10^{-6}}{8.31447 * 288} * 100 = 0.59 * 10^{-4}$$

At standard temperature 15 °C, the constant of specific heat ratio ($k = c_p/c_v$) which is equal to 1.4 for dry air and 1.409 for hydrogen. The value of c_p is determined by the Equation (A.5) given below [114]:

$$c_p = \frac{k}{k-1} \cdot R_s \quad (A.5)$$

$$c_{p_{air}} = \frac{1.4}{1.4-1} * 0.287 = 1.0045, \text{ and } c_{p_{H2}} = \frac{1.409}{1.409-1} * 4.125 = 14.21$$

Table A.1: Values of specific gas constant for several gases		
Gas	Molar Mass M , (kg/kmol)	Specific Gas Constant R_s , (kPa.m ³ /kg.K)
Dry Air	28.97	0.287
Hydrogen, H ₂	2.016	4.125
Oxygen, O ₂	32.00	0.260
H ₂ O, (Vapour)	18.02	0.4614
Carbon dioxide CO ₂	44.01	0.1889
Nitrogen N ₂	28.01	0.297
Helium, He	4.004	2.077
Argon, Ar	39.94	0.208

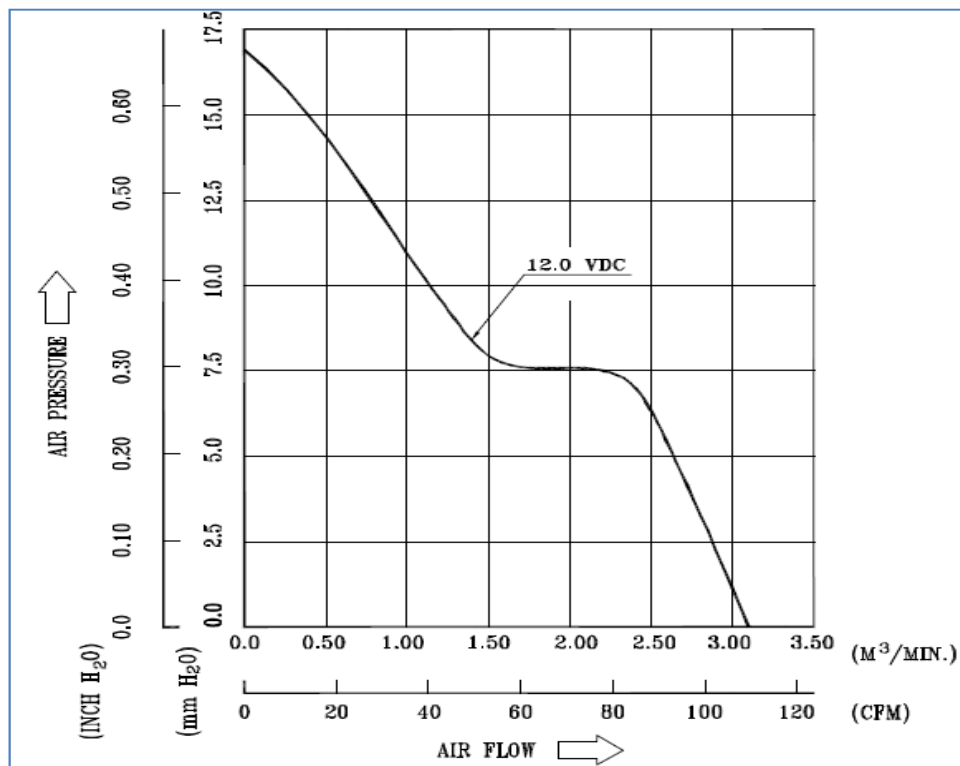


Figure A.1: Pressure-flow performance curve for Delta axial fan (cited from Delta Electronics [115])

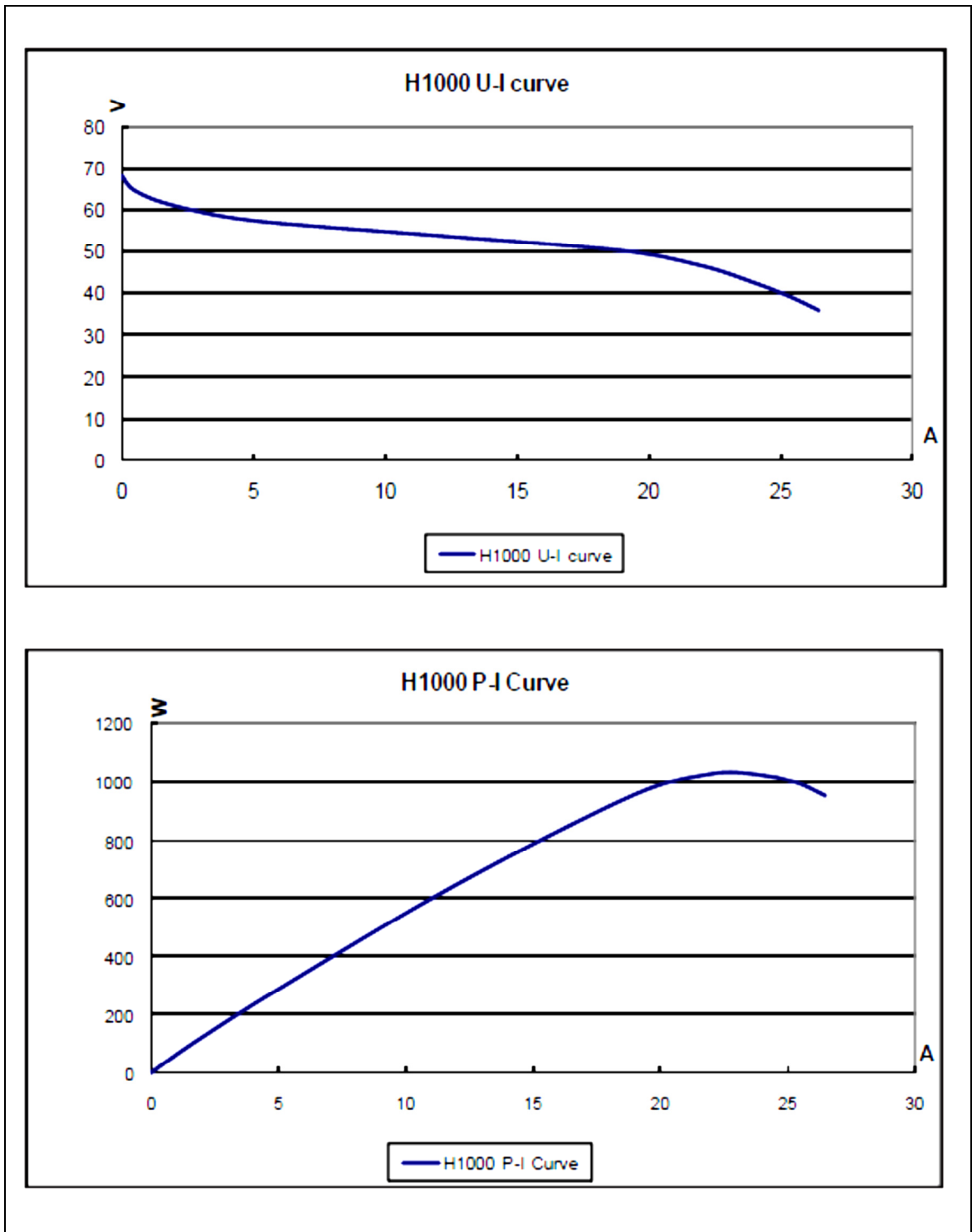


Figure A.2: Voltage-Current and Power-Current for Horizon (H-1000) fuel cell stack, (cited from [81])

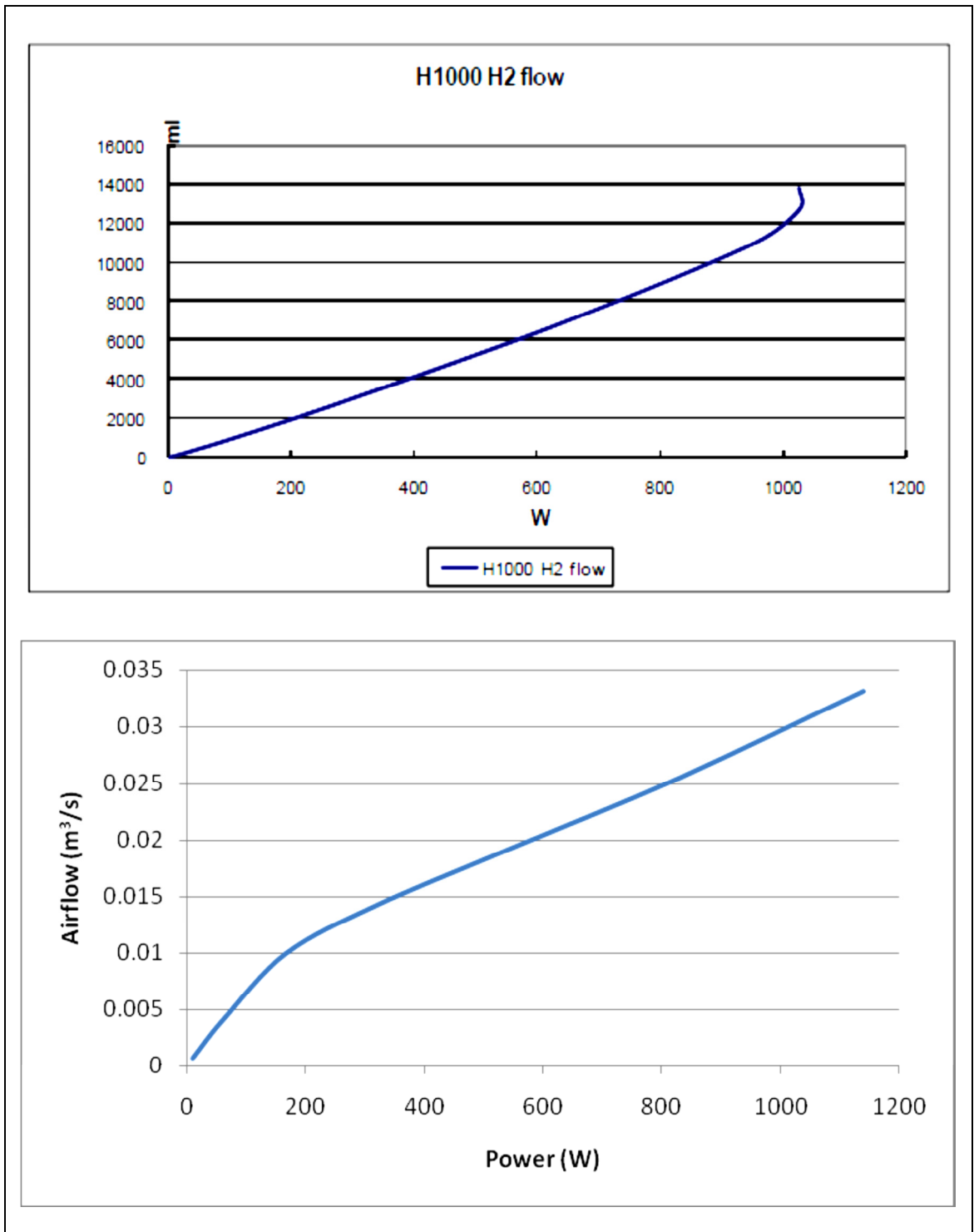


Figure A.3: Hydrogen and air flow rates for Horizon (H-1000) fuel cell stack, (cited from [81, 86])

Table B.2: Second test for Horizon (H-1000) fuel cell stack under different levels of varying current load						
Fuel cell stack test at 18°C ambient temperature		Temperature of exit air (°C) from the stack				
Operating Time (Minutes)	Current (A)	Outlet Fan-1	Outlet Fan-2	Outlet Fan-3	Outlet Fan-4	Average Stack Temperature
6.00	0.00	18.4	18.7	19	19.4	18.88
8.00	1.25	19.9	20.1	20.4	20.6	20.25
10.00	2.50	20.9	21.3	21.4	21.6	21.30
12.00	4.00	21.7	22	22	22	21.93
14.00	5.00	22.5	22.9	23	23.2	22.90
16.00	6.00	22.6	22.8	23.3	23.4	23.03
18.00	7.50	23.1	23.4	23.5	23.5	23.38
20.00	9.00	22.9	23.3	23.5	23.6	23.33
22.00	10.00	23.1	23.4	23.9	23.9	23.58
24.00	11.00	23.7	24.3	24.6	24.7	24.33
26.00	14.00	24.9	25.3	25.7	25.1	25.25
28.00	16.00	26.4	26.3	26.6	26.8	26.53
30.00	18.00	27.7	27.9	28.4	28.2	28.05
32.00	22.00	29.1	29.9	30.2	30.1	29.83
34.00	25.00	29.7	30.4	30.9	30.8	30.45
38.00	25.00	29.7	30.4	30.9	30.9	30.48

Table B.3: Output voltages for third test of Horizon (H-1000) fuel cell stack, and the developed model of PEM fuel cell with different model tuning efficiencies

Fuel cell stack test at 20°C ambient temperature			Fuel cell stack temperature (°C)							Output voltages (volt) of the developed PEM fuel cell model at different tuning efficiency					Deviation between Horizon fuel cell output voltages and the tuned developed model					
Operating Time (Minutes)	Load Current (A)	Output Voltage (V)	Outlet Fan-1	Outlet Fan-2	Outlet Fan-3	Outlet Fan-4	Average Temp.	0.83	0.84	0.85	0.86	AI Tuning Eff. (0.85) & Stack Temp. (27.73 °C)	0.83	0.84	0.85	0.86				
0.00	0.00	60.53	18.9	19.0	19.4	19.6	19.23	-	-	-	-	-	-	-	-	-				
4.00	1.02	59.18	21.5	21.7	22.0	22.2	21.85	56.31	56.99	57.66	58.34	58.12	2.87	2.19	1.52	0.84				
8.00	1.94	56.29	24.6	24.6	24.7	24.9	24.70	54.08	54.73	55.39	56.04	55.60	2.21	1.56	0.91	0.26				
12.00	3.06	55.17	25.3	25.5	25.7	25.9	25.60	52.33	52.96	53.59	54.22	53.73	2.84	2.21	1.58	0.95				
16.00	4.08	54.09	25.8	26.1	26.4	26.6	26.23	51.20	51.82	52.44	53.05	52.53	2.89	2.26	1.65	1.03				
20.00	5.00	52.42	26.6	26.8	27.3	27.4	27.03	50.39	51.00	51.61	52.21	51.65	2.03	1.42	0.82	0.21				
22.00	6.02	51.35	27.4	27.9	28.4	28.9	28.15	49.64	50.24	50.83	51.43	50.81	1.71	1.11	0.51	0.09				
24.00	7.25	50.39	28.4	29.0	29.4	29.5	29.08	48.83	49.42	50.01	50.60	49.93	1.56	0.97	0.38	0.21				
26.00	8.37	49.27	29.4	29.7	30.2	30.6	29.98	48.19	48.77	49.35	49.93	49.23	1.08	0.50	0.08	0.66				
28.00	9.39	48.79	29.8	30.4	30.9	31.3	30.60	47.64	48.21	48.79	49.36	48.64	1.15	0.58	0.00	0.57				
30.00	10.61	46.15	29.5	29.9	30.3	30.7	30.10	46.97	47.54	48.10	48.67	47.98	0.82	1.39	1.95	2.52				
33.00	11.53	45.43	29.7	29.9	29.9	30.0	29.88	46.50	47.06	47.62	48.18	47.51	1.07	1.63	2.19	2.75				
35.00	12.86	45.17	29.6	29.7	30.1	30.1	29.88	45.88	46.43	46.99	47.54	46.88	0.71	1.26	1.81	2.37				
37.00	14.50	44.51	29.1	29.5	30.1	30.6	29.83	45.15	45.70	46.24	46.79	46.14	0.64	1.19	1.73	2.28				
39.00	16.02	43.66	30.0	30.0	30.1	30.3	30.10	44.53	45.06	45.60	46.14	45.48	0.87	1.40	1.94	2.47				
41.00	17.76	41.92	29.3	29.3	29.6	29.8	29.50	43.79	44.32	44.84	45.37	44.76	1.87	2.40	2.92	3.45				
43.00	20.00	40.86	28.9	29.6	30.1	30.4	29.75	42.91	43.43	43.94	44.46	43.85	2.05	2.56	3.08	3.60				
												Average of Dev.					1.65	1.54	1.44	1.52

Table B.4: Fourth test of Horizon (H-1000) fuel cell stack and the developed model of PEM fuel cell, under impact of constant current load

Fuel Cell Stack Test		Exit Air Temperature (°C) of Stack					Output voltages (V) of developed PEMFC model at 85% tuning efficiency and different stack temperature	
Operating Minutes	Current (A)	Output Voltages (V)	Outlet Fan-1	Outlet Fan-2	Outlet Fan-3	Outlet Fan-4		Average Stack Temp.
0.00	0.00	60.53	21.5	21.7	21.7	21.7	21.65	-
4.00		51.74	22.2	22.3	22.6	22.9	22.50	49.0921
6.00		51.66	23.3	23.6	23.9	24.2	23.75	49.1608
8.00		51.62	24.7	24.9	25.1	25.4	25.03	49.2307
10.00		51.24	24.9	25.2	25.4	25.6	25.28	49.2444
12.00		51.60	25.6	25.9	26.1	26.3	25.98	49.283
14.00		51.66	26.7	26.7	27.3	27.9	27.15	49.346
16.00		51.54	27.6	28.0	28.5	29.0	28.28	49.4072
18.00	9.08	51.60	28.0	28.5	28.8	29.2	28.63	49.4261
20.00		51.54	28.6	29.0	29.5	30.1	29.30	49.4622
22.00		51.60	29.7	30.0	30.2	30.5	30.10	49.5052
24.00		51.54	29.3	29.6	29.8	30.1	29.70	49.4837
26.00		51.60	28.9	29.2	29.5	29.8	29.35	49.4649
28.00		51.54	28.5	28.9	29.3	29.5	29.05	49.4487
30.00		51.60	28.2	28.6	29.1	29.4	28.83	49.4369
32.00		51.54	28.4	28.7	29.0	29.4	28.88	49.4396

Appendix C

C.1 First Scenario: Pressure Vessel for Compressed Air

At sea level, based on developed model of PEM fuel cell stack for one hour operation of stack at maximum current of 20 A, and power 877 W, the required supply of air is (119.948 kg/hour) which is equal to (97.9162 m³/hour) under 1atm ambient pressure, and by using Equation (A.3) in appendix A.

$$P_1 \cdot V_1 = P_2 \cdot V_2$$

Assuming $P_1 = 1\text{atm} = 1.01317\text{ bar} = 14.504\text{ psi}$, and $V_1 = 97.9162\text{ m}^3$, and assuming that air is going to be pressurized up to 200 bar (2,900.8 psi) in order to reduce the volume of the storage vessel as it has been produced by BOC Industrial Gases UK [111].

$$V_2 = \frac{97.9162 * 14.504}{2,900.8} = 0.49\text{ m}^3$$

First Metal: AK 2205 Duplex Stainless Steel

Assuming that ($E = 0.85$), and ($S = 90,069.5\text{ psi}$), inner radius of the cylinder can be determined by using Equation (8.5) above, for material thickness equals to 2.29 mm (0.09 inch), and material density about 7.85 g/cm³.

$$r_i = \frac{((90,069.5 * 0.85) - (0.6 * 2,900.8)) * 0.09}{2,900.8} = 2.3214\text{ inch} = 5.9\text{ cm}$$

Hence actual stress inside the vessel can be determined by using Equation (8.3):

$$\sigma_t = \frac{p}{t}(r_i + 0.5t) = \frac{2,900.8}{0.09} * \left(2.3214 + \frac{0.09}{2}\right) = 76,271.7\text{ psi}$$

It is clear that actual internal stress caused by the pressurised air is lower than the maximum allowable stress of the shell material. The outer radius of the shell is:

$$r_o = r_i + t = 2.3214 + 0.09 = 2.4114\text{ inch} = 6.125\text{ cm}$$

Using Equation (8.6) above to determine the maximum external pressure that the vessel can handle under impact of uniform external pressure.

$$P_c = \frac{S_y \cdot t}{r_o} = \frac{90,069.5 * 0.09}{2.4114} = 3,36164 \text{ psi} = 231.8 \text{ bar}$$

Since the required vessel needs to carry a volume of 0.49 m³ of compressed air, then using Equation (8.12) above to determine the height (*h*) of the cylinder.

$$h = \frac{0.49 - \frac{4}{3} \pi \left(\frac{5.9}{100} \right)^3}{\pi \left(\frac{5.9}{100} \right)^2} = 44.728 \text{ m} = 4,472.8 \text{ cm}$$

Using Equations (8.9) and (8.10) above to determine the mass and volume of the shell for a cylindrical pressure vessel with hemispherical ends:

$$V_{shell} = \pi * 4,472.8 * \left[(6.125)^2 - (5.9)^2 \right] + \frac{4}{3} \pi \left[(6.125)^3 - (5.9)^3 \right] = 38,120.9 \text{ cm}^3$$

$$M_{shell} = 38,120.9 * 7.85 = 299,250 \text{ g} = 299.25 \text{ kg}$$

Total mass of filled cylinder of compressed air for one hour operation is (299.25 + 119.948 = 419.198 kg) (~ 419.2 kg). While, the overall height of the shell can be determined by using Equation (8.11):

$$h_{shell} = 4,472.8 + 2 * (6.125) = 4,485.05 \text{ cm} = 44.8505 \text{ m}$$

Second Metal: AK 15-5 PH Stainless Steel

Assuming that (*E* = 0.85), and (*S* = 159,979 psi), inner radius of the cylinder can be determined by using Equation (8.5) above, for material thickness equals to 3.18 mm (0.1252 inch), and material density about 7.78 g/cm³.

$$r_i = \frac{((159,979 * 0.85) - (0.6 * 2,900.8)) * 0.1252}{2,900.8} = 5.794 \text{ inch} = 14.7167 \text{ cm}$$

Hence actual stress inside the vessel can be determined by using Equation (8.3):

$$\sigma_t = \frac{P}{t} (r_i + 0.5t) = \frac{2,900.8}{0.1252} * \left(5.794 + \frac{0.1252}{2} \right) = 135,693.5 \text{ psi}$$

It is clear that actual internal stress caused by the pressurised air is lower than the maximum allowable stress of the shell material. The outer radius of the shell is:

$$r_o = r_i + t = 5.794 + 0.1252 = 5.9192 \text{ inch} = 15.035 \text{ cm}$$

Using Equation (8.6) above to determine the maximum external pressure that the vessel can handle under impact of uniform external pressure:

$$P_c = \frac{S_y \cdot t}{r_o} = \frac{159,979 * 0.1252}{5.9192} = 3,383.8 \text{ psi} = 233.3 \text{ bar}$$

The required vessel needs to carry a volume of 0.49 m³ of compressed air, then using Equation (8.12) above to determine the height (*h*) of the cylinder:

$$h = \frac{0.49 - \frac{4}{3} \pi \left(\frac{14.7167}{100} \right)^3}{\pi \left(\frac{14.7167}{100} \right)^2} = 7.0053 \text{ m} = 700.53 \text{ cm}$$

Using Equations (8.9) and (8.10) above to determine the mass and volume of the shell for a cylindrical pressure vessel with hemispherical ends:

$$V_{shell} = \pi * 700.53 * \left[(15.035)^2 - (14.7167)^2 \right] + \frac{4}{3} \pi \left[(15.035)^3 - (14.7167)^3 \right] = 21,726.5 \text{ cm}^3$$

$$M_{shell} = 21,726.5 * 7.78 = 169,040 \text{ g} = 169.04 \text{ kg}$$

Total mass of filled cylinder of compressed air for one hour operation is (169.04 + 119.948 = 288.988 kg) (~ 289 kg). While, the overall height of the shell can be determined by using Equation (8.11):

$$h_{shell} = 700.53 + 2 * (15.035) = 730.6 \text{ cm} = 7.306 \text{ m}$$

Third Metal: AK 440A Stainless Steel

Assuming that ($E = 0.85$), and ($S = 240,040.4$ psi), inner radius of the cylinder can be determined by using Equation (8.5) above, for material thickness equals to 3.68 mm (0.14489 inch), and material density about 7.74 g/cm^3 .

$$r_i = \frac{((240,040.4 * 0.85) - (0.6 * 2,900.8)) * 0.14489}{2,900.8} = 10.10424 \text{ inch} = 25.6648 \text{ cm}$$

Hence actual stress inside the vessel can be determined by using Equation (8.3):

$$\sigma_t = \frac{p}{t} (r_i + 0.5 t) = \frac{2,900.8}{0.14489} * \left(10.10424 + \frac{0.14489}{2} \right) = 203,744.4 \text{ psi}$$

It is clear that actual internal stress caused by the pressurised air is lower than the maximum allowable stress of the shell material. The outer radius of the shell is:

$$r_o = r_i + t = 10.10424 + 0.14489 = 10.24913 \text{ inch} = 26.0328 \text{ cm}$$

Using Equation (8.6) above to determine the maximum external pressure that the vessel can handle under impact of uniform external pressure:

$$P_c = \frac{S_y \cdot t}{r_o} = \frac{240,040.4 * 0.14489}{10.24913} = 3,393.4 \text{ psi} = 234 \text{ bar}$$

The required vessel needs to carry a volume of 0.49 m^3 of compressed air, then using equation (8.12) above to determine the height (h) of the cylinder:

$$h = \frac{0.49 - \frac{4}{3} \pi \left(\frac{25.6648}{100} \right)^3}{\pi \left(\frac{25.6648}{100} \right)^2} = 2.02575 \text{ m} = 202.575 \text{ cm}$$

Using equations (8.9) and (8.10) above to determine the mass and volume of the shell for a cylindrical pressure vessel with hemispherical ends:

$$\begin{aligned} V_{shell} &= \pi * 202.575 * \left[(26.0328)^2 - (25.6648)^2 \right] + \frac{4}{3} \pi \left[(26.0328)^3 - (25.6648)^3 \right] \\ &= 15,197.4 \text{ cm}^3 \end{aligned}$$

$$M_{shell} = 15,197.4 * 7.74 = 117,630 \text{ g} = 117.63 \text{ kg}$$

Total mass of filled cylinder of compressed air for one hour operation is (117.63 + 119.948 = 237.578 kg) (~ 237.6 kg). While, the overall height of the shell can be determined by using Equation (8.11):

$$h_{shell} = 202.575 + 2 * (26.0328) = 254.64 \text{ cm} = 2.5464 \text{ m}$$

C.2 Second Scenario: Pressure Vessel for Compressed Oxygen

At sea level, based on developed model of PEM fuel cell stack for one hour operation of stack at maximum current of 20 A, and power of 877 W, the required supply of pure oxygen is (29.384 kg/hour) which is equal to (20.5624 m³/hour) under 1atm ambient pressure, and by using Equation (A.3) in appendix A.

$$P_1 \cdot V_1 = P_2 \cdot V_2$$

Assuming $P_1 = 1 \text{ atm} = 1.01317 \text{ bar} = 14.504 \text{ psi}$, and $V_1 = 20.5624 \text{ m}^3$, and assuming that oxygen is going to be pressurized up to 230 bar (3,335.92 psi) in order to reduce the volume of the storage vessel as it has been produced by BOC Industrial Gases UK [112].

$$V_2 = \frac{20.5624 * 14.504}{3,335.92} = 0.09 \text{ m}^3$$

First Metal: AK 2205 Duplex Stainless Steel

Assuming that ($E = 0.85$), and ($S = 90,069.5 \text{ psi}$), inner radius of the cylinder can be determined by using Equation (8.5) above, for material thickness equals to 2.29 mm (0.09 inch), and material density about 7.85 g/cm³.

$$r_i = \frac{((90,069.5 * 0.85) - (0.6 * 3,335.92)) * 0.09}{3,335.92} = 2.0115 \text{ inch} = 5.10921 \text{ cm}$$

Hence actual stress inside the vessel can be determined by using Equation (8.3):

$$\sigma_t = \frac{p}{t} (r_i + 0.5 t) = \frac{3,335.92}{0.09} * \left(2.0115 + \frac{0.09}{2} \right) = 76,225.7 \text{ psi}$$

It is clear that actual internal stress caused by the pressurised oxygen is lower than the maximum allowable stress of the shell material. The outer radius of the shell is:

$$r_o = r_i + t = 2.0115 + 0.09 = 2.1015 \text{ inch} = 5.33781 \text{ cm}$$

Using Equation (8.6) above to determine the maximum external pressure that the vessel can handle under impact of uniform external pressure:

$$P_c = \frac{S_y \cdot t}{r_o} = \frac{90,069.5 * 0.09}{2.1015} = 3,857.4 \text{ psi} = 266 \text{ bar}$$

Since the required vessel needs to carry a volume of 0.09 m³ of oxygen, then using Equation (8.12) above to determine the height (*h*) of the cylinder:

$$h = \frac{0.09 - \frac{4}{3} \pi \left(\frac{5.10921}{100} \right)^3}{\pi \left(\frac{5.10921}{100} \right)^2} = 10.907 \text{ m} = 1,090.7 \text{ cm}$$

Using Equations (8.9) and (8.10) above to determine the mass and volume of the shell for a cylindrical pressure vessel with hemispherical ends:

$$V_{shell} = \pi * 1,090.7 * \left[(5.33781)^2 - (5.10921)^2 \right] + \frac{4}{3} \pi \left[(5.33781)^3 - (5.10921)^3 \right]$$

$$= 8,261.6 \text{ cm}^3$$

$$M_{shell} = 8,261.6 * 7.85 = 64,854 \text{ g} = 64.854 \text{ kg}$$

Total mass of filled cylinder of oxygen for one hour operation is (64.854 + 29.384 = 94.238 kg) (~ 94.24 kg). While, the overall height of the shell can be determined by using Equation (8.11):

$$h_{shell} = 1,090.7 + 2 * (5.33781) = 1,101.38 \text{ cm} = 11.0138 \text{ m}$$

Second Metal: AK 15-5 PH Stainless Steel

Assuming that (*E* = 0.85), and (*S* = 159,979 psi), inner radius of the cylinder can be determined by using Equation (8.5) above, for material thickness equals to 3.18 mm (0.1252 inch), and material density about 7.78 g/cm³.

$$r_i = \frac{((159,979 * 0.85) - (0.6 * 3,335.92)) * 0.12525}{3,335.92} = 5.02841 \text{ inch} = 12.7722 \text{ cm}$$

Hence actual stress inside the vessel can be determined by using Equation (8.3):

$$\sigma_t = \frac{p}{t} (r_i + 0.5t) = \frac{3,335.92}{0.1252} * \left(5.02841 + \frac{0.1252}{2} \right) = 135,648.6 \text{ psi}$$

It is clear that actual internal stress caused by the pressurised oxygen is lower than the maximum allowable stress of the shell material. The outer radius of the shell is:

$$r_o = r_i + t = 5.02841 + 0.1252 = 5.15361 \text{ inch} = 13.09 \text{ cm}$$

Using Equation (8.6) above to determine the maximum external pressure that the vessel can handle under impact of uniform external pressure:

$$P_c = \frac{S_y \cdot t}{r_o} = \frac{159,979 * 0.1252}{5.15361} = 3,886.5 \text{ psi} = 268 \text{ bar}$$

The required vessel needs to carry a volume of 0.09 m^3 of oxygen, then using Equation (8.12) above to determine the height (h) of the cylinder:

$$h = \frac{0.09 - \frac{4}{3} \pi \left(\frac{12.7722}{100} \right)^3}{\pi \left(\frac{12.7722}{100} \right)^2} = 1.586 \text{ m} = 158.6 \text{ cm}$$

Using Equations (8.9) and (8.10) above to determine the mass and volume of the shell for a cylindrical pressure vessel with hemispherical ends:

$$V_{shell} = \pi * 158.6 * \left[(13.09)^2 - (12.7722)^2 \right] + \frac{4}{3} \pi \left[(13.09)^3 - (12.7722)^3 \right] = 4,763 \text{ cm}^3$$

$$M_{shell} = 4,763 * 7.78 = 37,060 \text{ g} = 37.06 \text{ kg}$$

Total mass of filled cylinder of oxygen for one hour operation is $(37.06 + 29.384 = 66.444 \text{ kg})$ ($\sim 66.5 \text{ kg}$). While, the overall height of the shell can be determined by using Equation (8.11):

$$h_{shell} = 158.6 + 2 * (13.09) = 184.78 \text{ cm} = 1.8478 \text{ m}$$

Third Metal: AK 440A Stainless Steel

Assuming that ($E = 0.85$), and ($S = 240,040.4$ psi), inner radius of the cylinder can be determined by using Equation (8.5) above, for material thickness equals to 3.68 mm (0.14489 inch), and material density about 7.74 g/cm^3 .

$$r_i = \frac{((240,040.4 * 0.85) - (0.6 * 3,335.92)) * 0.14489}{3,335.92} = 8.775 \text{ inch} = 22.2885 \text{ cm}$$

Hence actual stress inside the vessel can be determined by using Equation (8.3):

$$\sigma_t = \frac{p}{t} (r_i + 0.5 t) = \frac{3,335.92}{0.14489} * \left(8.775 + \frac{0.14489}{2} \right) = 203,702 \text{ psi}$$

It is clear that actual internal stress caused by the pressurised oxygen is lower than the maximum allowable stress of the shell material. The outer radius of the shell is:

$$r_o = r_i + t = 8.775 + 0.14489 = 8.91989 \text{ inch} = 22.6566 \text{ cm}$$

Using Equation (8.6) above to determine the maximum external pressure that the vessel can handle under impact of uniform external pressure:

$$P_c = \frac{S_y \cdot t}{r_o} = \frac{240,040.4 * 0.14489}{8.91989} = 3,899 \text{ psi} = 268.8 \text{ bar}$$

The required vessel needs to carry a volume of 0.09 m^3 of oxygen, then using Equation (8.12) above to determine the height (h) of the cylinder:

$$h = \frac{0.09 - \frac{4}{3} \pi \left(\frac{22.2885}{100} \right)^3}{\pi \left(\frac{22.2885}{100} \right)^2} = 0.28 \text{ m} = 28 \text{ cm}$$

Using Equations (8.9) and (8.10) above to determine the mass and volume of the shell for a cylindrical pressure vessel with hemispherical ends:

$$V_{shell} = \pi * 28 * \left[(22.6566)^2 - (22.2885)^2 \right] + \frac{4}{3} \pi \left[(22.6566)^3 - (22.2885)^3 \right] = 3,791.4 \text{ cm}^3$$

$$M_{shell} = 3,791.4 * 7.74 = 29,345 \text{ g} = 29.345 \text{ kg}$$

Total mass of filled cylinder of oxygen for one hour operation is (29.345+ 29.384 = 58.729 kg) (~ 58.73 kg). While, the overall height of the shell can be determined by using Equation (8.11):

$$h_{shell} = 28 + 2 * (22.6566) = 73.313 \text{ cm} = 0.7331 \text{ m}$$

C.3 Third Scenario: Pressure Vessel for Limited volume of Compressed Oxygen

At sea level, as it has been proposed in (Section 8.4.3) that for one hour operation of stack consists of 72 cells, and at load current of 20 A, the necessary proposed mass flow rate of supplied oxygen is assumed to be equal to (0.6 m³/hour) (0.8574 kg/hour) under 1atm ambient pressure, and by using Equation (A.3) in appendix A.

$$P_1 \cdot V_1 = P_2 \cdot V_2$$

Assuming $P_1 = 1 \text{ atm} = 1.01317 \text{ bar} = 14.504 \text{ psi}$, and $V_1 = 0.6 \text{ m}^3$, and assuming that oxygen is going to be pressurized up to 230 bar (3,335.92 psi) in order to reduce the volume of the storage vessel as it has been produced by BOC Industrial Gases UK [112].

$$V_2 = \frac{0.6 * 14.504}{3,335.92} = 2.609 * 10^{-3} \text{ m}^3 = 2,609 \text{ cm}^3$$

Using AK 2205 Duplex Stainless Steel material, and assuming that ($E = 0.85$), and ($S = 90,069.5 \text{ psi}$), inner radius of the cylinder can be determined by using Equation (8.5) above, for material thickness equals to 2.29 mm (0.09 inch), and material density about 7.85 g/cm³.

$$r_i = \frac{((90,069.5 * 0.85) - (0.6 * 3,335.92)) * 0.09}{3,335.92} = 2.0115 \text{ inch} = 5.10921 \text{ cm}$$

Hence actual stress inside the vessel can be determined by using Equation (8.3):

$$\sigma_t = \frac{p}{t} (r_i + 0.5 t) = \frac{3,335.92}{0.09} * \left(2.0115 + \frac{0.09}{2} \right) = 76,225.7 \text{ psi}$$

It is clear that actual internal stress caused by the pressurised oxygen is lower than the maximum allowable stress of the shell material. The outer radius of the shell is:

$$r_o = r_i + t = 2.0115 + 0.09 = 2.1015 \text{ inch} = 5.33781 \text{ cm}$$

Using Equation (8.6) above to determine the maximum external pressure that the vessel can handle under impact of uniform external pressure:

$$P_c = \frac{S_y \cdot t}{r_o} = \frac{90,069.5 * 0.09}{2.1015} = 3,857.4 \text{ psi} = 266 \text{ bar}$$

Since the required vessel needs to carry a volume of (2,609 cm³) of oxygen, then using Equation (8.12) above to determine the height (*h*) of the cylinder:

$$h = \frac{(2.609 * 10^{-3}) - \frac{4}{3} \pi \left(\frac{5.10921}{100} \right)^3}{\pi \left(\frac{5.10921}{100} \right)^2} = 0.25 \text{ m} = 25 \text{ cm}$$

Using Equations (8.9) and (8.10) above to determine the mass and volume of the shell for a cylindrical pressure vessel with hemispherical ends:

$$V_{shell} = \pi * 25 * \left[(5.33781)^2 - (5.10921)^2 \right] + \frac{4}{3} \pi \left[(5.33781)^3 - (5.10921)^3 \right] = 265.962 \text{ cm}^3$$

$$M_{shell} = 265.962 * 7.85 = 2,090 \text{ g} = 2.09 \text{ kg}$$

Total mass of filled cylinder for limited amount of oxygen for one hour operation is (2.09 + 0.8574 = 2.9474 kg) (~ 2.95 kg). While, the overall height of the shell can be determined by using Equation (8.11):

$$h_{shell} = 25 + 2 * (5.33781) = 35.676 \text{ cm}$$

C.4 Pressure Vessel for Compressed Hydrogen

At sea level, based on developed model of PEM fuel cell stack for one hour operation of stack at maximum current of 20 A, and power 877 W, the required supply hydrogen is

(0.05725 kg/hour) which is equal to (0.637 m³/hour), under 0.55 bar of supply pressure of hydrogen, by using Equation (A.3) in appendix A.

$$P_1 \cdot V_1 = P_2 \cdot V_2$$

Assuming $P_1 = 0.55 \text{ bar} = 7.98 \text{ psi}$, and $V_1 = 0.637 \text{ m}^3$, and assuming that hydrogen is going to be pressured up to 175 bar (2,538.2 psi) in order to reduce the volume of the storage vessel as it has been produced by BOC Industrial Gases UK [113].

$$V_2 = \frac{0.637 * 7.98}{2,538.2} = 2.002 * 10^{-3} \text{ m}^3 = 2,002 \text{ cm}^3$$

Using AK 2205 Duplex Stainless Steel material, and assuming that ($E = 0.85$), and ($S = 90,069.5 \text{ psi}$), inner radius of the cylinder can be determined by using Equation (8.5) above, for material thickness equals to 2.29 mm (0.09 inch), and material density about 7.85 g/cm³.

$$r_i = \frac{((90,069.5 * 0.85) - (0.6 * 2,538.2)) * 0.09}{2,538.2} = 2.6607 \text{ inch} = 6.758 \text{ cm}$$

Hence actual stress inside the vessel can be determined by using Equation (8.3):

$$\sigma_t = \frac{p}{t} (r_i + 0.5 t) = \frac{2,538.2}{0.09} * \left(2.6607 + \frac{0.09}{2} \right) = 76,306.8 \text{ psi}$$

It is clear that actual internal stress caused by the pressurised hydrogen is lower than the maximum allowable stress of the shell material. The outer radius of the shell is:

$$r_o = r_i + t = 2.6607 + 0.09 = 2.7507 \text{ inch} = 6.9868 \text{ cm}$$

Using Equation (8.6) above to determine the maximum external pressure that the vessel can handle under impact of uniform external pressure:

$$P_c = \frac{S_y \cdot t}{r_o} = \frac{90,069.5 * 0.09}{2.7507} = 2,947 \text{ psi} = 203.2 \text{ bar}$$

Since the required vessel needs to carry a volume of 2,002 cm³ of hydrogen, then using Equation (8.12) above to determine the height (h) of the cylinder:

$$h = \frac{(2.002 * 10^{-3}) - \frac{4}{3} \pi \left(\frac{6.758}{100} \right)^3}{\pi \left(\frac{6.758}{100} \right)^2} = 0.04943 \text{ m} = 4.943 \text{ cm}$$

Using Equations (8.9) and (8.10) above to determine the mass and volume of the shell for a cylindrical pressure vessel with hemispherical ends:

$$V_{shell} = \pi * 4.943 * \left[(6.9868)^2 - (6.758)^2 \right] + \frac{4}{3} \pi \left[(6.9868)^3 - (6.758)^3 \right] = 184.643 \text{ cm}^3$$

$$M_{shell} = 184.643 * 7.85 = 1,450 \text{ g} = 1.45 \text{ kg}$$

Total mass of filled cylinder of hydrogen for one hour operation is $(1.45 + 0.05725 = 1.50725 \text{ kg})$ ($\sim 1.5 \text{ kg}$). While, the overall height of the shell can be determined by using Equation (8.11):

$$h_{shell} = 4.943 + 2 * (6.9868) = 18.9166 \text{ cm} \approx 19 \text{ cm}$$